INVERSE SIZE EXCLUSION CHROMATOGRAPHY (ISEC) AS PORE STRUCTURAL CHARACTERIZATION METHOD OF POROUS MEDIA IN PACKED COLUMNS AND AS IMPORTANT TOOL FOR THE DEVELOPMENT PROCESS OF BONDED POLY(METHACRYLATE) COATED SILICAS FOR THE REVERSED PHASED HPLC OF PROTEINS AND PEPTIDES

Dissertation zur Erlangung des Grades

"Doktor der Naturwissenschaften"

(Dr. rer. nat.)

vorgelegt dem Fachbereich Chemie und Pharmazie

der Johannes Gutenberg-Universität Mainz

von

Dipl.-Chem. Zöfre Bayram-Hahn

geboren in Wiesbaden

Mai 2007, Mainz

Compromise makes a good umbrella, but a poor roof.

James Russell Lowell (1819-1891)

1 ABSTRACT

In this work, an improved protocol for inverse size exclusion chromatography (ISEC) was established to assess important pore structural data of porous silicas as stationary phases in packed chromatographic columns. After the validity of the values generated by ISEC was checked by comparison with data obtained from traditional methods like nitrogen sorption at 77 K (Case Study A), the method could be successfully employed as valuable tool at the development of bonded poly(methacrylate)-coated silicas, while traditional methods generate partially incorrect pore structural information (Case Study B).

Case Study A: Two different mesoporous silicas were converted by a so-called pseudomorphical transition into ordered MCM-41-type silica while maintaining the particle size and shape. Although substantial changes occurred between the original and treated material with respect to bulk structure, specific surface area, average pore diameter and specific pore volume, the pore connectivity from ISEC as one of the essential parameters remained nearly the same which was reflected by the same course of the theoretical plate height vs. linear velocity curves of the original and treated silica.

Case Study B: In the development of bonded poly(methacrylate)-coated silicas for the reversed phase separation of peptides and proteins, ISEC was the only method to generate valid pore structural information of the polymer-coated materials. Valid values of the native silicas could also be gathered by conventional methods like nitrogen sorption measurements and mercury intrusion porosimetry, correlating well with ISEC-data showing that the mean pore size of the native materials was varied from 15 nm to 120 nm. Synthesis procedures were developed to obtain reproducibly covalently bonded poly(methacrylate) coatings with good thermal stability on different base materials, employing as well particulate media and monolithic materials. Various synthetic parameters like hydrophobicity, polymer load etc. were systematically varied to optimize selected chromatographic properties including a low denaturation potential for which a special testing method was developed based on the bioactivity of an enzyme after the chromatographic run. Mainly the ISEC-measurements showed a strong decrease of the pore size of the coated materials leading to the conclusion that medium-hydrophobic coatings with low carbon loads on macro porous silicas are best suited as compared to mesoporous silicas, exhibiting good mass transfer values and a very high adsorption capacity towards lysozyme.

2 GENERAL SCOPE

In view of a better characterization of chromatographic adsorbents and in order to further enhance their mass transfer properties we selected and further developed ISEC as a fully automated and standardized characterization procedure for HPLC columns employing polystyrenes in tetrahydrofuran as solute. Based on the pore network model (PNM) and parallel pore model (PPM) developed by Liapis and Grimes the method generates the following parameters: the number average and volume average pore size distribution and the pore connectivity of the material. As reference and for better comparison of the results the pore size distribution of all tested materials was also investigated in bulk by nitrogen sorption at 77 K employing as well standard BJH-method or NLDFT-method whenever it was applicable while mercury intrusion porosimetry was used as reference method for macroporous materials.

At a first attempt we tried to compare and to correlate pore structural data from ISEC and nitrogen sorption experiments to HPLC performance parameters (plate height, plate height vs. linear velocity curves) on ordered mesoporous silicas, which were obtained by a pseudomorphical treatment from amorphous mesoporous silicas by a complex and harsh dissolution and re-precipitation process. Furthermore a series of C18-coated silicas with small but distinct variations in their mean pore size and pore volume was investigated to check for correlations to HPLC performance parameters. The capability of ISEC to gather pore size data of stationary phase materials in different solvents was employed to check for swelling effects of bonded and highly cross-linked polymer coated silicas.

The major part of the Ph. D. thesis was to find and optimize synthesis conditions for the chemical bonding of poly(methacrylates) on mesoporous and macroporous silicas for the reversed phase separation of proteins.

Bonded polymer-coated silicas based on poly(methacrylates) are thought as an promising alternative to silanized silicas for the following reasons:

- the co-monomer composition allows one to adjust and to control the hydrophobic relative to the hydrophilic properties of the coating;
- the composition enables one to adapt the composition of the polymeric layer with respect to a minimum denaturation potential of the proteins at the surface;
- the polymer load, the linker density and other reaction parameters can be adjusted to achieve an optimum column performance, column mass loadability and high biorecovery.

The optimization process was based on statistical design experiments to obtain optimum information, employing as optimization criteria as well standard testing procedures for the chromatographic performance and also novel testing methods to check for the biocompatibility of the stationary phase materials in-column.

A series of mesoporous to macroporous particulate silicas and also monolithic silicas were chosen as base material for the coating procedure, which were checked before and after the coating for their pore structural parameters by means of ISEC and nitrogen sorption measurements and then thoroughly evaluated for their chromatographic behavior. These experiments generated valuable information for the prediction of suitable base materials and promising polymer coatings for the biocompatible separation of proteins and peptides by reversed phase HPLC.

3 INTRODUCTION AND BACKGROUND

3.1 Porous Silicas

3.1.1 Porous Amorphous Silicas

It was early recognized that spherical mesoporous silicas bear a high potential as adsorbents in High Performance Liquid Chromatography (HPLC). They can be manufactured by specific processes preferably as spherical particles in the µm size range providing a surface area of up to several hundred m^2/g and a specific pore volume of up to 1 ml/g.

The pore structure can be well controlled in the mesopore- as well as in the macropore size range depending on the synthesis procedure and adjusted to the separation of low molecular weight as well as to high molecular weight analytes.

They can be manufactured by specific processes as spherical particles in the µm size range.

All synthesis procedures generate particulate materials with a broad particle size distribution, which have be classed prior to the use as stationary phase materials. Only the addition of a porogen during the course of a modified Stöber synthesis[1,2] allows the production of porous spherical silica particles with small polydispersity and a maximum particle size of 2 µm, which represents the lower size limit for the usability in HPLC.

As the chromatographic process is carried out at elaborated pressures of up to several hundred bars, rigid, non-swellable skeleton materials are used such as silica, alumina, titanium dioxide or graphitic carbon.

Coupling of alkyl-silanes onto the surface of silica particles can easily modify the surface chemistry of silica providing optimum interaction with the desired analytes without affecting the pore system too much, which consists of highly interconnected pores in the desired mesopore-range. The pore system thus provides a nearly ideal pathway for the mobile phase to easily and fully penetrate the particles, so the target analytes can reach the surface. In combination with the large variety of commercially available alkyl-silanes, a huge variation of stationary phases with different surface chemistries for nearly all chromatographic tasks is accessible on the base of surface modified silica. This is the primary cause that today's chromatography is mainly dependent on silica based stationary phases.

In this work several types of commercially available HPLC grade silica were employed: LiChrospher Si300, Kromasil 300, Nucleosil 300 and Nucleosil 1000, respectively.

[1] C. Kaiser, PhD Thesis, Johannes Gutenberg University Mainz (1996)
[2] K.Unger, C. Kaiser, Deutsches Patent, DE 195 30 031, (1995/97)

Apart from those highly porous silicas were prepared according to the poly(ethoxysiloxane) procedure developed by Schick–Kalb[3,4] and further developed by Hauck[5,6].

3.1.2 Highly Porous Silica Beads by the PES Process

In 1973 Schick-Kalb[3,4] developed a method to prepare porous spherical silica particles by the stepwise condensation of poly(ethoxysiloxane) in acidic medium with hydrochloric acid as catalyst. An optimised procedure starts from pre-polymerised tetraethoxysilane (TES 40) which is in the first reaction step converted into poly(ethoxysilane) (PES) (see Figure 1). The next step is the condensation of PES in a heterogeneous phase in the presence of ammonia with vigorous stirring. The addition of a porogen like cyclohexane allows to adjust both the porosity and the pore size of the final particles in a wide range[5,6,7,8]. Boosting up the porosity by a factor of up to four is possible via this procedure and increases the mass transfer in a chromatographic run, but impairs on the other hand the mechanical stability of the particles drastically, even minor pressure makes the particles collapse.

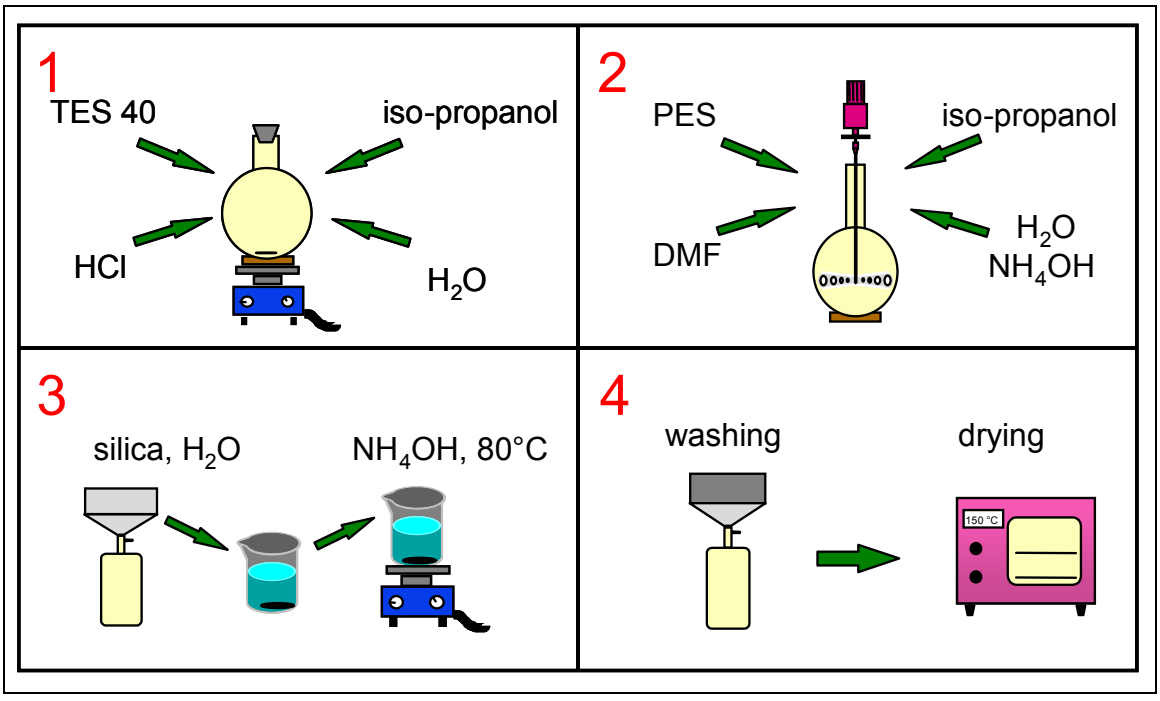

Figure 1: Schematic picture of the polyethoxysiloxane procedure.[8]

[3] K.K. Unger, P. Ringe, J. Schick-Kalb, B. Straube, Fresenius Z., Anal. Chem. 264 (1973) 267-272
[4] J. Schick-Kalb, K.-F. Krebs, K.K. Unger, J. Chromatogr. 83 (1973) 5-9
[5] H.E. Hauck, PhD Thesis, Technische Hochschule Darmstadt (1976)
[6] K. Unger, B. Scharf, J. of Colloid and Interface Sci. 55 (1976) 377-380
[7] B. Bidlingmaier, PhD Thesis, Johannes Gutenberg University Mainz (2001)
[8] C. du Fresne von Hohenesche, PhD Thesis, Johannes Gutenberg University Mainz (2002)

3.1.3 Ordered Mesoporous Silicas

In 1991 scientists from the Mobil Oil Corporation reported the synthesis of a new class of mesoporous alumosilicates via the condensation of silica precursors together with a cationic template respectively a tenside in the presence of a catalyst. The M41S family of materials exhibit defined pore systems with a diameter of around 3 nm[9,10,11], a high specific pore volume of up to 1.3 ml/g and a high surface area in the range of 1,500 m^2/g. Variation of the synthesis parameters allows to adjust the pore diameter in the range from 1.5 nm up to 10 nm[12,13,14,15]. The M41S family of materials is classified in three categories depending on their pore system which are represented by MCM-41, MCM-48 and MCM-50 (illustrated in Figure 2).

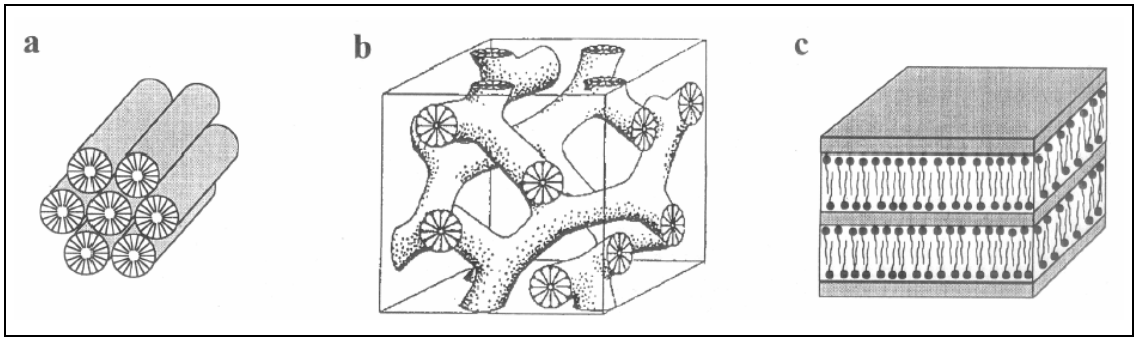

Figure 2: Pore system of M41S-class materials[16]: a) MCM-41, b) MCM-48, c) MCM-50

The MCM-41 exhibits straight channels, while the MCM-48 possesses a three dimensional pore system which is interconnected and the MCM-50 consists of lamellar layers. The extremely high surface area raised hope to be usable as stationary phases in HPLC[15,17,18]. But the use as stationary phase has special demands onto the morphology of the desired material: the particle shape should be more or less spherical and the particle size distribution should be narrow in the range of several micrometers. Furthermore, the material must be pressure stable to withstand the high pressure during the packing procedure and the chromatographic run. Last but not least, the pore system must be accessible for the analytes during a chromatographic run. Especially the last point favours MCM-48, because of its

[9] J.S. Beck, Mobil Oil, US Patent 5, 057, 296 (1991)
[10] J.S. Beck, J.C. Vartuli, W.J. Roth, M.E. Leonowicz, C.T. Kresge, K.D. Schmitt, C.T.-W. Chu, D.H. Olson, E.W. Sheppard, S.B. McCullen, J.B. Higgins, J.L. Schlenker, J.Am.Chem.Soc. 114 (1992) 10834-10843
[11] C.T. Kresge, M.E. Leonowicz, W.J. Roth, J.C. Beck, Nature 359 (1992) 710-712
[12] Q. Huo, D.I. Margolese, G.D. Stucky, Chem. Mater. 8 (1996) 1147-1160
[13] Q. Huo, D.I. Margolese, U. Ciesla, D.G. Demuth, P. Feng, T. Gier, P. Sieger, A. Firouzi, B.F. Chmelka, F. Schüth, G. Stucky, Chem. Mater. 6 (1994) 1176-1191
[14] A. Hahn, PhD Thesis, Johannes Gutenberg University Mainz (2003)
[15] Y.R. Ma, L.M. Qi, J.M. Ma, Y.Q. Yu, O. Liu, H.M. Cheng, Colloids Surf. A 229 (2003) 1-8
[16] C.A.Fyfe, G.Fu, J.Am.Chem.Soc. 117 (1995) 9709-9714
[17] M. Grün, A.A. Kurganov, S. Schacht, F. Schüth, K.K. Unger, J. Chrom. A 740 (1996) 1-9
[18] A. Kurganov, K. Unger, T. Issaeva, J. Chromatogr. A 753 (1996) 177-190

interconnected three-dimensional pore system. The straight channels in MCM-41 are not interconnected and even may behave as dead-end pores, which should result in low mass transfer kinetics. MCM-50 cannot be used because there was no successful removal of the template with preservation of the pore structure has been reported yet.

3.1.4 Hierarchically Structured Mesoporous Materials by Pseudomorphic Transformation

In 2002 Martin et al.[19] reported the successful isomorphic transformation of spherical porous amorphous silica with a broad pore size distribution into MCM-41 type material with well defined pores by a hydrothermal treatment – the so called Micelle-Templated Silicas (MTS). The specific alkaline reaction conditions, with the presence of surfactants – like cetyltrimethylammonium bromide (CTAB) – used for conventional MCM-41 synthesis preserved fully the original morphology. The resulting material is a hierarchically structured porous material, consisting of two different pore systems which are highly interwoven and interconnected, promising high mass transfer kinetics for adsorbents in liquid separations due to convective flow. The original pore system is partially conserved, while the MCM-41 pore system appears additionally and mainly increases the surface area of the material[20,21]. Therefore a high capacity for potentially adsorbed molecules can be expected.

During the course of the reaction, inside the particles a local dissolution of the silica occurs due the alkalinity of the reaction mixture. Afterwards a self assembly with the added surfactants occurs and finally the silica redeposits. After removal of the surfactant via calcination, well defined and highly ordered mesopores remain. The degree of transformation of the initial pore system mainly can be controlled via the synthesis time up to complete rearrangement.

The tailoring of the pore size can be achieved by the addition of 1,3,5-trimethyl benzene (TMB) or mixtures of TMB/decane.[22] Cylindrical pores in the range 6-10 nm can be achieved according to the following scheme:

[19] T. Martin, A. Galarneau, F. Di Renzo, F. Fajula, D. Plee, Angew. Chem. Int. Ed. 41 (2002) 2590-2592

[20] A. Lind, C. du Fresne von Hohenesche, J-H. Smatt, M. Linden, K. K. Unger, Microporous and Mesoporous Materials 66 (2003) 219-227

[21] T. Martin, A. Galarneau, F. Di Renzo, D. Brunel, F. Fajula, S. Heinisch, G. Cretier, J.-L. Rocca, Chem. Mater. 16 (2004) 1725-1731

[22] B. Lefèvre, A. Galarneau, J. Iapichella, C. Petitto, F. Di Renzo, F. Fajula, Z. Bayram-Hahn, R. Skudas, K. Unger, Chem. Mater. 17 (2005) 601-607

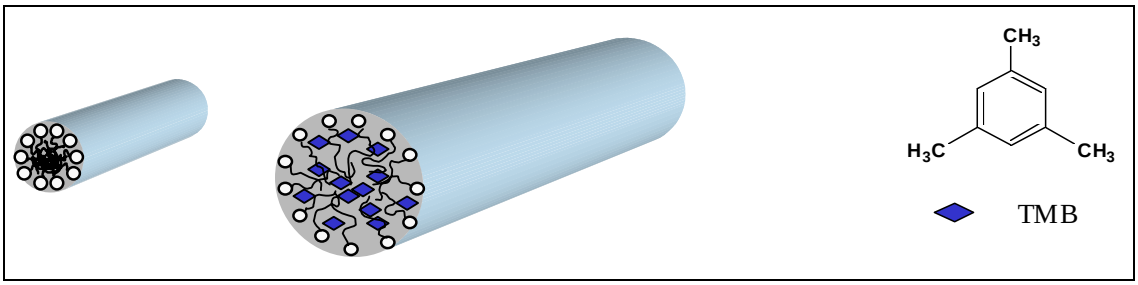

Figure 3: Principle of micelle enlargement by the addition of 1,3,5-trimethyl benzene (TMB)[23]

A typical reaction mixture has the following gel compositions: 1 SiO_2 / x C_{18}TAB / (x/4) NaI / 1.5x TMB / 3x C_{10} / y NaOH / 40 H_2O, with 0.075 < x < 0.1 and 0.3 < y < 0.4. As silica source any kind of porous material may be used.

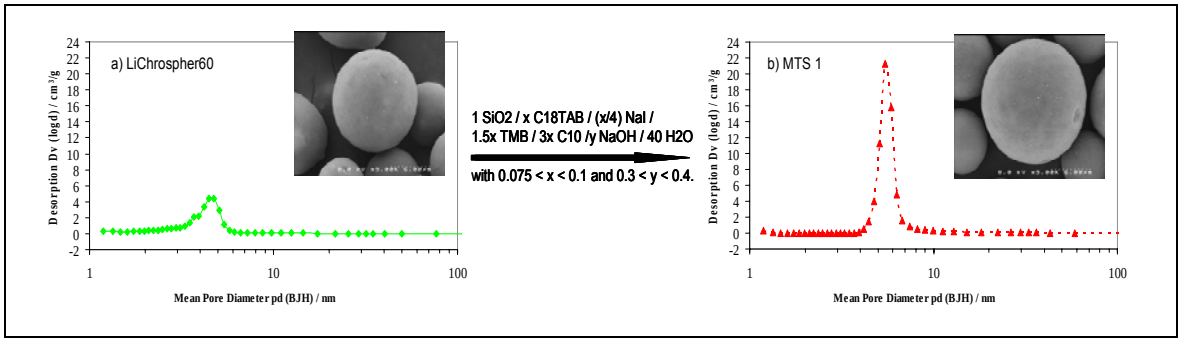

Figure 4: Pseudomorphic transformation – a) SEM image of silica precursor LiChrospher™ Si 60 and b) SEM image of MCM-41 type derivative MTS1

3.1.5 Monolithic Silica

Monolithic silica columns for chromatographic separations can be obtained via a procedure described by Nakanishi et al.[24,25,26]. The monolithic silica skeleton exhibits a bimodal pore size distribution (see Figure 5) with macropores in the range of several µm which generate the flow through the column and mesopores which are responsible for the high surface of the material. The base matter consists of an ultra pure silica with only small impurities of other metals (Na, Fe, Al < 10 ppm). After the preparation of these silica rods, they have to be covered with a chemical and mechanical stable PEEK-coating to be usable as HPLC-columns. Unlike the earlier introduced polymer based monolithic columns[27,28], the newly available silica based monolithic columns like Chromolith™ exhibit the same pressure stability like the usual silica based HPLC-columns. The pore structural parameters of

[23] Final Technical Report, 28 february 2005, EU-project G5RD-CT-2000-00317, Project No 317
[24] K. Nakanishi, J. Porous Mater. 4 (1997) 67-70
[25] K. Nakanishi, H. Minakuchi, N. Soga, N. Tanaka, J. Sol-Gel Sci. Tech. 8 (1997) 547-552
[26] K. Cabrera, G. Wieland, D. Lubda, K. Nakanishi, N. Soga, H. Minakuchi, K.K.Unger, Trends Anal. Chem. 17 (1998) 40-53
[27] C. Ericson, J.-L. Liao, K. Nakazato, S. Hjertén, J.Chromatogr. A 767 (1997) 33-41
[28] E.F. Hilder, F. Svec, J.M.J. Fréchet, J.Chromatogr. A 1044 (2004) 3-22

Chromoliths™ like porosity, pore size of mesopores and pore size of macropores are independently tuneable to a wide extend enabling excellent column efficiencies in combination with low backpressure.

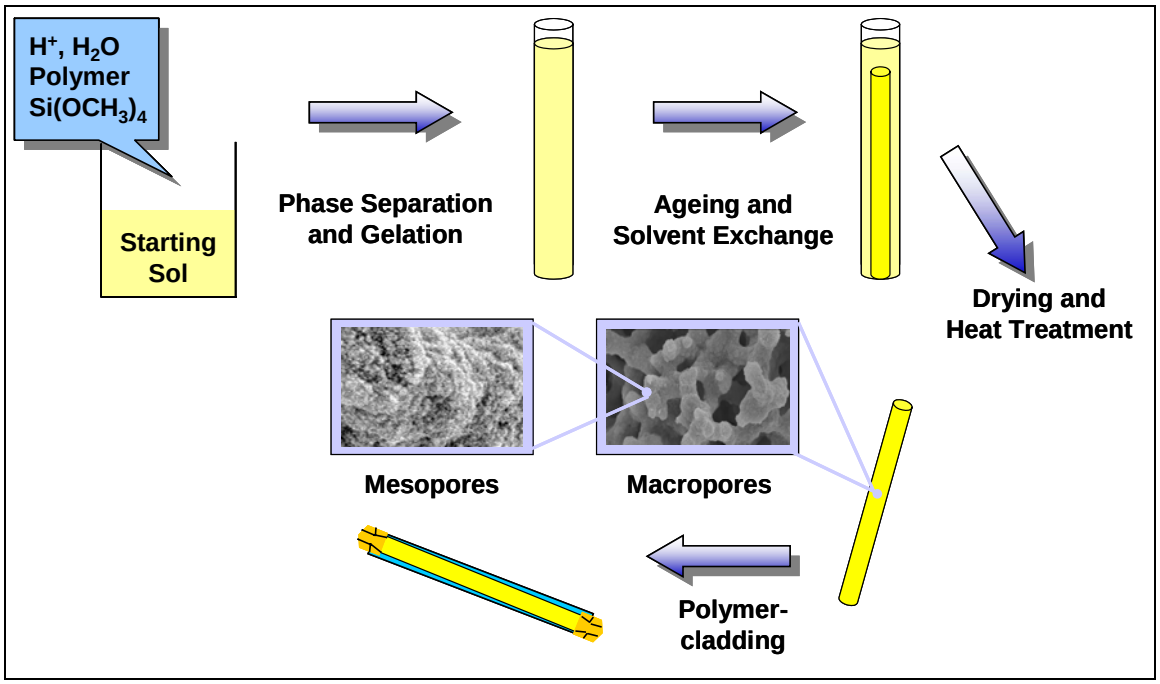

Figure 5: Principle of the synthesis and SEM images of monolithic silica.[8]

3.1.6 Surface Functionalization of Porous Silicas

Silica based stationary phases are commonly used in HPLC not only because of the extensive tuneability of their morphology and pore system or the excellent pressure stability of the skeleton, but even more for the various possibilities for applying different surface chemistries. As the surface of native silica possesses hydrophilic silanol groups it can be used as stationary phase in normal-phase high performance liquid chromatography (NP-HPLC). In the more commonly used reversed-phase HPLC (RP-HPLC), hydrophobic interactions between analytes and the stationary phase are the driving forces for the separation of the analytes. The retention of the analytes and the selectivity in the chromatographic process is mainly dependent of the specific surface area and the surface activity of the stationary phase. Commercially available chromatographic media possess surface areas in the range from 20 to 500 m^2/g and even more.

Two different principles are commonly employed to hydrophobically modify the silica surface. One approach is the coating with a polymer layer, for example via coupling of trichlorovinylsilane onto the silica surface followed by radical polymerization (polymer encapsulating[29]). The more frequently used approach is to couple reactive silanes with

[29] H. Engelhardt, H. Löw, W. Eberhardt, M. Mauss, Chromatographia 27 (1989) 535-543

hydrophilic ligands to the silanol groups on the silica surface[30]. The chromatographic properties of the final stationary phase are mainly dependent by the hydrophobic character and the type of the coating, but also by unreacted silanol groups. The main reason for the incomplete reaction of the silanol groups is the voluminous extension of the ligands. Remaining silanol groups are typically deactivated („endcapped“) via the reaction with small trifunctional silanes[31] containing reactive groups like -Cl, $-OCH_3$, $-OCH_2CH_3$, $-OCO-F_3$ or $–N(CH_3)_2$.

3.1.6.1 Functionalization with Silanes

N-alkylchlorosilanes or n-alkoxysilanes are the most often used modifiers for stationary phases for RP-HPLC. During the course of the reaction in the presence of catalytic reagents with the surface silanol groups, alcohols or hydrogen chloride are released. In general, the chain length of the ligands of the silanes is C4, C8 and C18 which represents the most often used modification for RP-HPLC.

In most cases, the modification of the silica particles results in a more or less dense monolayer of the alkylsilylgroups on the surface. Using di– or trifunctional silanes may result in much more complex surface chemistries. Especially in the presence of traces of water, polyfunctional silanes may interconnect with each other resulting in poorly defined and irreproducible polymer-like coatings[32].

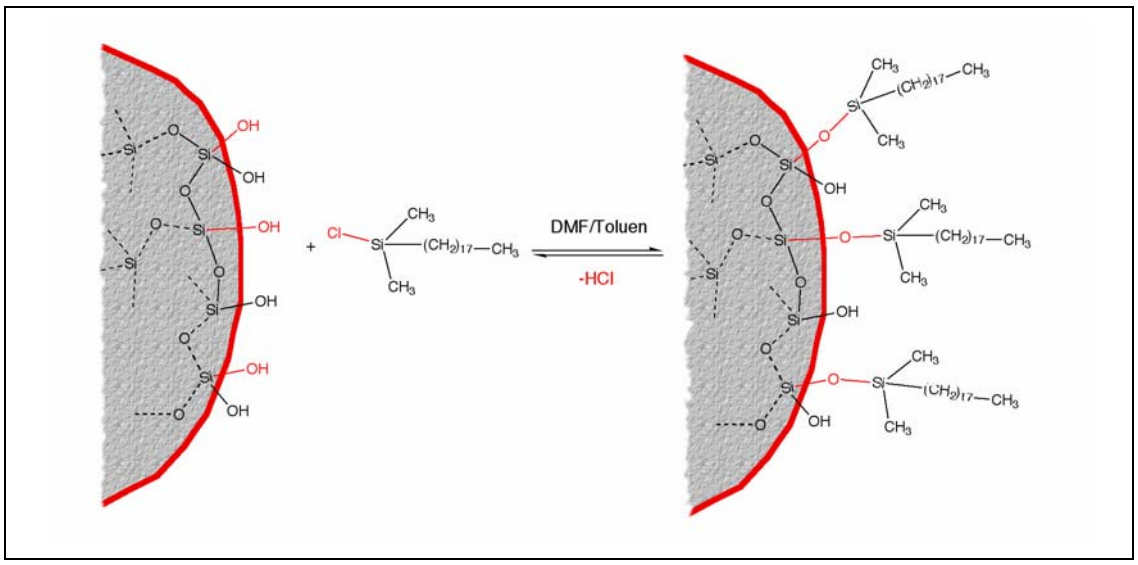

Figure 6: Reaction scheme of n-octadecyldimethylchlorosilane with the silica surface.[33]

[30] I. Halasz, I. Sebastian, Angew. Chem. Int. Ed. 8 (1969) 453

[31] J.J. Kirkland, J. Chromatogr. Sci. 9 (1971) 206-214

[32] K.K. Unger (Ed.), Packings and Stationary Phases in Chromatographic Techniques, N.Y., Marcel Dekker (1990)

[33] Z. Bayram-Hahn, Diploma thesis, Johannes Gutenberg University Mainz (2002)

The most often applied chromatographic method for the analytical separation of proteins and peptides is RP-HPLC[34,35]. However, this method is limited to the purification and separation of small peptides (< 50 amino acids). The high denaturation potential of the RP-HPLC is dependent of the hydrophobicity of the stationary phase and of the chromatographic conditions like pH, pressure or the contingent of the organic part of the mobile phase. Particularly enzymes loose their biological activity[36,37] during a chromatographic run, which prevents the use of this technique for the purification of biopolymers.

However, the chromatographic performance and the large variety of available modifications makes monomeric modified porous silica particles the most often used packing materials in modern RP-HPLC.

3.1.6.2 Functionalization by Polymers

Although micro particulate porous silica modified with alkylsilanes exhibit nearly ideal qualities for the use as stationary phase in HPLC, there is enough space for improvements. Especially the limited pH-stability of the monomeric modified silica based stationary phases is the major disadvantage of these materials. Attempts to produce pH-stable stationary phases are either based on shielding the silica skeleton via coating with a dense polymer layer[33,38,39] or switching to completely polymer based stationary phases[28] with totally porous, cross-linked polymer beads – or by using pH-stable inorganic particles like titanium dioxide.

Introducing polymer layers as interface of the stationary phase greatly extends the range of available surface properties for stationary phases in RP-HPLC. This allows a flexible tailoring of the hydrophobicity of the stationary phase. The major drawback for the extensive use of polymer coatings in HPLC are problems with the swelling of the polymer layer, limited pressure stability and in some cases insufficient reproducibility.

The core-shell principle with a silica core as skeleton and a polymer layer on the surface rises hope to offer the best of both worlds: the silica plays the roll of the pressure-stable and non-swellable backbone, protected by a dense polymer layer. By applying only thin polymer layers, the swelling effect should be negligible and the whole range of polymeric compositions may interact as interface for HPLC, improving remarkably the range of available stationary phases. In principle, they should exhibit enhanced reproducibility in

[34] M. Hanson, PhD Thesis, Johannes Gutenberg University Mainz (1992)
[35] K. Wagner, PhD Thesis, Johannes Gutenberg University Mainz (2001)
[36] K.D. Nugent, HPLC of Peptides and Proteins: Seperation, Analysis and Conformation, C.T. Mant, R.S. Hodges (Eds.), CRC Press, FL (1991) 279
[37] Z. Bayram-Hahn, PhD Thesis, Johannes Gutenberg University Mainz (2007)
[38] M. Hanson, K.K. Unger, G. Schomburg, J.Chromatogr. 517 (1990) 269-284
[39] G. Fischer, U. Skogsberg, S. Bachmann, H. Yüksel, S. Steinbrecher, E. Plies, K. Albert, Chem. Mater. 15 (2003) 4394-4400

comparison with fully polymeric materials. Two principles are employed for coating silica surfaces with polymer.

3.1.6.2.1 Non-Covalent Deposition

The rough surface of porous silica and the polar surface chemistry allows the easy and sufficient coating of silica particles with polymer via physisorption. Therefore this is the most often cited method in literature for the polymer coating of silica[32,33,38,41]. To achieve reproducible and stable polymer coatings, in a first step usually a well defined pre-synthesized polymer is adsorbed on the silica support. Due to the weak binding of the polymer onto the surface, an immobilisation procedure usually follows via cross-linking of the polymer-layer induced by peroxides[40,41,42], thermal treatments[43] or gamma-radiation[44,45].

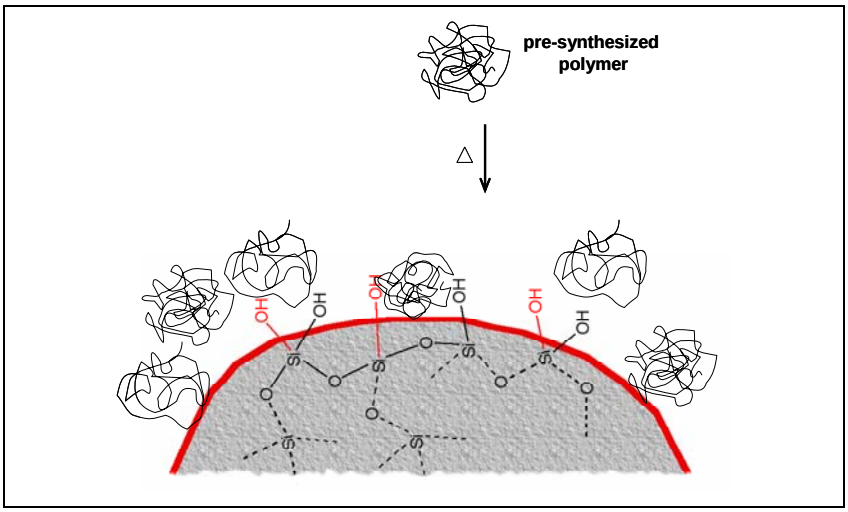

Figure 7: Schematic illustration of the physisorption process of polymers onto the silica surface.

In many cases, pre-synthesized polymers or oligomers with tenside-like structures are employed, enabling a thermodynamically driven self-assembly of the polymer chains on the surface[46], giving highly reproducible polymer coatings with well defined characteristics. The coating can easily be performed with any type of polymer, but as a matter of principle, the physisorption process is reversible. The hydrogen bonds between the polymer and the silanol groups can easily be broken by a good solvent. Therefore the polymer layer can be exchanged by other polymers or smaller molecules which compete with each other in the presence of good solvents[47]. Another problem of these non-covalent-bonded coatings is their

[40] G. Schomburg, Trends Anal.Chem 10 (1991) 163-169
[41] M. Hanson, K.K. Unger, Trends Anal.Chem. 11 (1992) 368-372
[42] Y. Mao, B.M. Fung, J.Chromatogr.A 790 (1997) 9-15
[43] L.M. Nyholm, K.E. Markides, J.Chromatogr.A 813 (1998) 11-20
[44] H. Figge, A. Deege, J. Köhler, G. Schomburg, J.Chromatogr. 351 (1986) 393-408
[45] I.C.S.F. Jardim, K.E. Collins, T.A. Anazawa, J.Chromatogr.A 849 (1999) 299-307
[46] A.L.R. Bug, M.E. Cates, S.A. Safran, T.A. Witten, J.Chem.Phys. 87 (1987) 1824-1833
[47] G.J. Fleer, M.A. Cohen-Stuart, J.M. Scheutjens, T. Cosgrove, B. Vincent, Polymeren at Interfaces,

poor thermal stability[48]. Because of the easy applicability of this technique on any polymer composition and its exquisite reproducibility, this technique is frequently used for the first evaluation steps of polymer coatings.

3.1.6.2.2 Covalent Binding: *grafting-to and grafting-from approaches*

To obtain much more robust polymer coatings, covalent bonds have to be established between the polymer layer and the silica surface. Three different approaches are established to produce chemisorbed polymer coatings on an inorganic support. The grafting-to method requires suitable immobilised groups on the surface[49,50] of the inorganic support. The co-polymerization of a living polymer chain[51] with these groups results in a chemisorbed polymer layer. Another route is via the polymerization of surface-bound vinyl groups with each other or via co-polymerization with suitable monomers[52,53], resulting in thin and nonflexible polymer coatings. The grafting-from method is launched from surface bound initiator groups which start the polymerization and results in a firmly bound polymer layer on the inorganic support material[54,55,56].

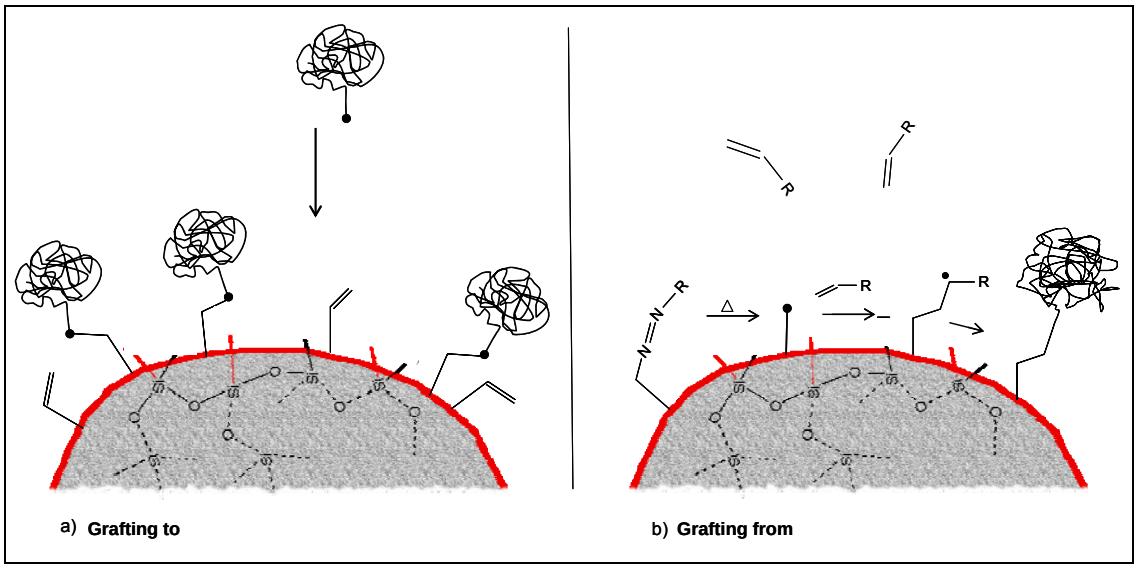

Figure 8: Reaction principles of polymer grafting methods – a) grafting to approach and b) grafting from approach

Chapman&Hall, London (1993)
[48] R. Zerushalmi, J. Klein, L. Fetters, Science 263 (1994) 793-795
[49] R. Jordan, K. Graf, K.K.Unger, Chem.Commun. 9 (1996) 1024-1025
[50] O. Prucker, C.A. Naumann, J. Rühe, W. Knoll, C.W. Frank, J.Am.Chem.Soc. 121 (1999) 8766-8770
[51] R. Hoene, K. Hamann, Angew.Chem. 84 (1972) 359
[52] R. Laible, K. Hamann, Adv.Colloid Interface Sci. 13 (1980) 65-71
[53] M. Chainberg, R. Parnas, Y. Cohen, J.Appl.Polym.Sci. 37 (1989) 2921-2931
[54] N. Ferry, R. Laible, K. Hamann, Angew.Makromol.Chem. 46 (1973) 81-109
[55] O. Prucker, J. Rühe, Macromolecules 31 (1998) 592-601
[56] B. Rückert, PhD Thesis, Johannes Gutenberg University Mainz (2002)

Grafting-to method

Living polymer chains may react with suitable termination groups on the surface of an inorganic support, resulting in a chemisorbed polymer coating. The reaction rate is driven by the gradient of the polymer concentration and restricted by the diffusion barrier of the interface between surface and polymer solution, which makes the reaction more and more unlikely while the reaction is proceeding. Therefore it is often reported, that this technique yields only a limited polymer density.[136] Another cutback is the often reported limited possibility for reproducibly obtaining thin homogeneous polymer layers. Usually, the full amount of polymer should get used up during the reaction. Therefore by knowing the surface area of the inorganic support material, the desired mean thickness of the polymer layer may be adjusted by applying the adequate amount of polymer solution.

Grafting-from method

Surface bound azo-initiator groups may start a radical polymerization in the presence of a monomer solution from the inorganic support. The method results in better reproducible and uniform polymer coatings compared to the grafting-to method. As the reaction is by an immobilized initiator respectively a growing polymer chain with highly mobile monomers in solution, there is virtually no diffusion barrier. Also, there is no sterical hindering for the monomer molecules to reach the growing polymer chain, which results in more dense coatings and possibly thicker polymer layers. By the addition of a cross-linker very stable polymer coatings can be obtained. The main problems are in creating a uniform layer of initiator groups on the surface of the support material. The optimization and fine-tuning of the reaction parameters plays the most important role in manufacturing reproducible polymer coatings. As a matter of principle of a radical polymerization, the mobile split-of part of the initiator groups may self-inhibit the polymerization, or start a polymerization in the monomer solution. This effect may be suppressed by choosing a suitable solute and by adjusting the monomer concentration.

3.2 Evaluation of the Pore System

The pore system of the stationary phase plays a very important role in the behaviour of a chromatographic system. If access of the analytes to the surface of the stationary phase is provided, or restricted is mainly depending on the characteristics of the pore system. The values for the pore size distribution, specific pore volume or pore connectivity are usually assessed via sorption measurements, intrusion techniques, radiation scattering techniques, pycnometry, calorimetric measurements or using inverse size-exclusion[57]. As all of these

[57] J. Rouquerol, D. Avnir, C. Fairbridge, D.H. Everett, M. Haynes, N. Pernicone, J.D.F. Ramsay, K.S.W. Sing, K.K. Unger, Recommendations for the Characterisation of Porous Solids, Pure & Appl.Chem. 66 (1994) 1739-1758

techniques are only indirect measurements of the desired values, certain assumptions regarding the pore shape and the mechanism of the pore filling during the measurement have to be made. Therefore, in many cases alternative pathways for the data treatment are available, giving more or less accurate values which may differ from each other and from method to method.

For obtaining a complete and reliable description of the pore system of a given material, very often several independent measuring techniques have to be applied and care must be taken in the interpretation of the obtained values for the characteristic data. In some cases, high resolution imaging techniques like transmission electron microscopy of reference samples may be used for judging which method describes the pore system best.

3.2.1 Transmission Electron Microscopy (TEM)

Electron microscopy is based on the quasi-elastic scattering of focussed monochromatic electrons. Applying for example 1 KV as acceleration voltage, the wavelength of the electrons is about 0.04 nm, allowing a spatial resolution of down to ca. 0.1 nm. In TEM-experiments, the sample is placed between the electron beam and the detector, which usually consists of a CCD-camera. Because of the strong interaction between electrons and dense matter, the electron beam can only investigate a very thin layer of the sample. Therefore, visualization of a sample is usually restricted to a few layers on the outer surface of a sample. By embedding a sample in an epoxy resin, it can be cut with a microtome in thin slices of about 40 nm. This may give an inside-view on the pore system of the particle as direct image. Due to the thickness of the slice and machine restrictions, the focus cannot be exactly defined. Therefore this method cannot generate fully valid data for the pore dimensions of the pore system but gives a good impression of the kind or nature of the pore system.

3.2.2 Mercury Intrusion Porosimetry

Mercury intrusion porosimetry[58] allows probing the pore system of bulk materials in a dry and evaporated state in a range between 360 µm to 3 nm[59] of mean pore diameter. The method utilizes the non-wetting nature of mercury towards most materials and the well defined surface tension of 484 MN/m^2 of this liquid. Additionally, this material features a very low vapour pressure at room temperature, which can be neglected in most data evaluations - although it is still high enough to exceed the MAC-tolerance at room temperature, when equilibrium is reached.

[58] S.J. Gregg, K.S.W. Sing, Adsorption, Surface Area and Porosity, 2nd Edition (1982) 173-194
[59] J. van Brakel, S. Modry, M. Svatá, Mercury Porosimetry: State of the Art in: Powder Technology 29 (1981) 1-12

The method is based on the principle, that the contact angle and the surface tension of a non-wetting liquid are independent from its pressure. Once the contact angle γ for liquid vs. sample and the surface tension γ are known, the pore can be probed by applying pressure p until the liquid penetrates the pore, see Figure 9.

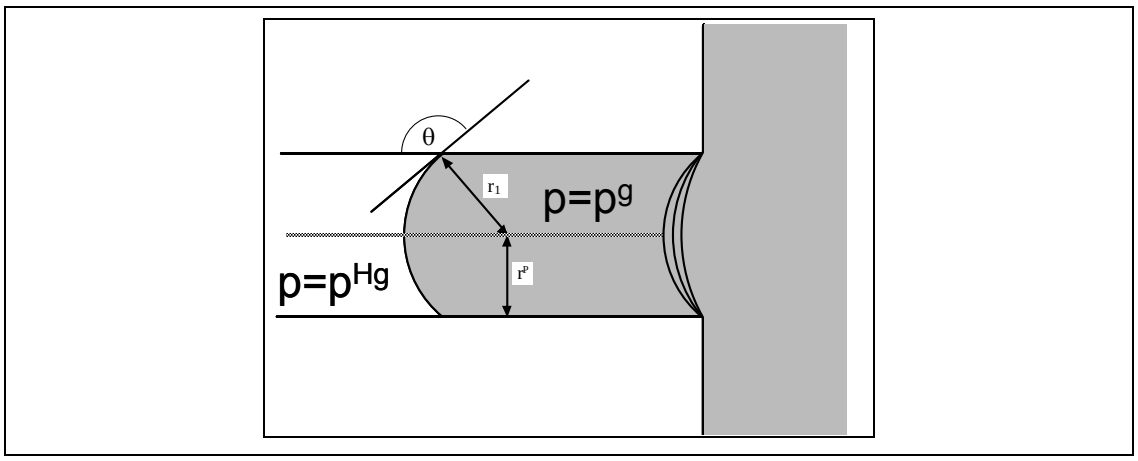

Figure 9: Principle of mercury intrusion porosimetry: a pore with the radius r can be penetrated by liquid mercury when the pressure p^g is reached.

To be more specific and in the case of mercury (Hg), the difference Δp between the applied pressure p^g and the vacuum pressure of mercury p^{Hg} has to be used. The contact angle is found in the literature, in most cases the contact angle for glass is used, which is between 135° up to 150°, depending on the source[60]. The pore radius r^P of a cylindrical tube is then determined via the Washburn-equation:

$$r^p = -\frac{2\gamma \cos\theta}{\Delta p};\ p^{Hg} - p^g = \Delta p \qquad [1]$$

Commercially mercury intrusion instruments measure volumetrically the amount of mercury at a given pressure v^p, up to the maximum pressure p_{max}, allowing to determine the specific surface area by mercury intrusion A_{Hg}:

$$A_{Hg} = -\frac{1}{\gamma \cos\theta} \int_0^{p_{max}} p\,dv^p \qquad [2]$$

The pore range of mercury intrusion instruments depends on the pressure range of the machine. A pressure range from 1 bar to 2,000 bar allows to cover a pore range from 7.5 µm to 7 nm. As the instruments start from vapour pressure, even larger pores and intra-particle space is covered by the method. Discrimination between intra-particle space and the pore system requires at least a factor of 10 between the sizes.

[60] H. Fischer, Bestimmung der Porenstruktur poröser Adsorbentien und Katalysatoren mit Hilfe der Quecksilberporosimetrie, Darmstadt (1974)

A general issue of the intrusion method is that the pore volume, which is only accessible via gateways with a smaller diameter, appears with the radius of these smaller pores – so-called bottle-neck pores – and cannot be completely emptied in the extrusion step. Furthermore, the contact angle in the extrusion step slightly differs from the one of the intrusion step, therefore all measurements exhibit a hysteresis between intrusion and extrusion curve, leaving a small amount of mercury in all probed samples.

While the method involves the application of large pressure upon the sample, pressure-induced deformation of the pore system must also be taken into account, which in the case of rigid inorganic materials usually appears at higher pressures and can be detected as a steep increase which ends in an x-axis parallel course of the curve.

3.2.3 Nitrogen Sorption at 77 K

The most commonly used method for the characterization of the pore properties of porous substances in bulk is the nitrogen sorption measurement at 77 K. The method generates values for the pore size distribution, the specific surface (a_s), specific pore volume (v_p) and mean pore diameter (p_d)[58].

The method is based on the measurement of nitrogen adsorption and desorption isotherms. The amount of adsorbed – respectively desorbed nitrogen x_a at a given relative pressure p/p_0 in relation to the dry sample mass is volumetrically determined. The measurement starts from an evaporated sample, where subsequently small amounts of nitrogen are dosed until the partial equilibrium pressure p stays constant. The procedure is stepwise repeated until the saturation pressure p_0 is reached. The volume of adsorbed nitrogen as a function of the partial equilibrium pressure represents the adsorption branch of the isotherm. Afterwards, the desorption branch of the isotherm is recorded.

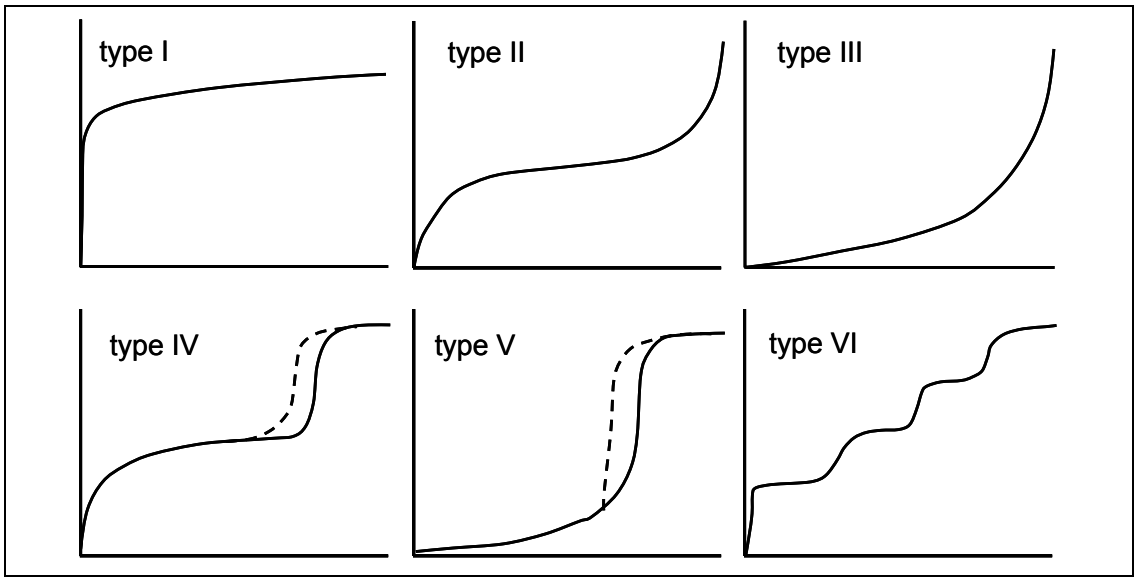

Figure 10: Classification of isotherms according to IUPAC.

According to IUPAC[61,62], porous materials are classified via the size of their pore system as micro-, meso- or macroporous materials (see Table 1). Brunauer, Deming, Deming and Teller[63] (BDDT) introduced in 1940 five types of characteristic isotherms, which were later completed by Sing giving the actual six types of isotherms[64]. Commonly used chromatographic media possess mainly mesopores, which are represented by an isotherm of type II (see Figure 10).

Table 1: IUPAC classification of pore systems according to pore diameter p_d.

micropores	mesopores	macropores
p_d < 2 nm	2 nm< p_d < 50 nm	p_d > 50 nm

The process of nitrogen adsorption is based on the formation of a layer of adsorbed nitrogen on the inner and outer surface of the sample material. At relative pressures between $0.05 < p/p_0 < 0.3$ the adsorbed nitrogen is building mono-, double- and multilayers. Above these values, condensation of nitrogen occurs in mesopores, which can be observed as strong increase in the value of adsorbed nitrogen. When the filling of the pores is complete, one can observe no further increase of the adsorbed volume of nitrogen until nearly $p=p_0$ is reached and condensation in the intraparticle space, respectively macropores occurs.

Mesoporous materials also exhibit a hysteresis between the adsorption and the desorption branch of the isotherm. This effect is commonly explained via a hindered emptying of the pores due to pore blocking or cavitation, where larger pores are accessible through smaller pores[65,66].

Different data treatment methods are available for the interpretation of the nitrogen adsorption-desorption isotherms to gather data about the pore system. Each method has specific models and assumptions, concerning the pore system or the nature of the surface and the interaction between surface and the adsorbed nitrogen. For adsorbents used as stationary phases, the commonly used methods are the ones to gain comparable data for the specific surface area and the pore size distribution of the material.

Information about the surface area of a material is commonly gained by the Brunauer-Emmett-Teller (BET) method[67]. This approach depends on the assumption, that the adsorbed nitrogen is in a quasi-liquid state and the probability to find a nitrogen molecule on

[61] IUPAC, Reporting physisorption data for gas/solid system, Pure Appl. Chem. 57 (1985) 603-619
[62] IUPAC, Manual of Symbols and Terminology, Appendix 2, part 1, Colloid and Surface
[63] S. Brunauer, L.S. Deming, W.S. Deming, E. Teller, J.Am.Chem.Soc**.** 62 (1940) 1723-1732
[64] IUPAC, Recommendations, Pure Appl, Chem. 66 (1994) 1739-1758
[65] P.T. Tanev, L.T. Vlaev, J. Colloid Interface Sci. 160 (1993) 110
[66] P.C. Ball, R. Evans, Langmuir 5 (1989) 714-723
[67] S. Brunauer, P.H. Emmet and E. Teller, J.Am.Chem.Soc. 60 (1938) 309-319

each place on the surface is equal, which is especially for inhomogeneous surfaces not necessarily the case. The method depends on the following BET equation:

$$1/(W((p_0/p)-1) = 1/ W_mC + (C-1)/W_mC\ p/p_0 \quad [3]$$

Where W is the mass of adsorbed gas at a relative pressure p_0 and W_m is the mass of a monolayer of adsorbate covering the surface. The term C (the BET C constant) is related to the energy of adsorption in the first adsorbed layer. A linear plot of $1/(W(p_0/p)-1)$ v_s p/p_0 of a minimum of three data points in the p/p_0 range of 0.05 to 0.35 generates the slope s as $S=(C-1)/W_mC$ and the intercept i as $i=1=/W_mC$. The determination of the weight of a monolayer is possible by using $W_m=1/(s+i)$. Finally this allows the determination of the total surface area s of the sample as:

$$S = W_mNA_{cs}/M \quad [4]$$

Where N is Avogadro's number, M is the molecular weight of the adsorbate. Nitrogen gives a hexagonal close-packed layer resulting in a cross-sectional area A_{cs} of 16.2 A^2.

The total pore volume can be derived from the amount of adsorbed nitrogen at a relative pressure p_0 as described by Gurwitsch[68]. The volume of nitrogen adsorbed V_{ads} has to be converted into the volume of fluid nitrogen V_{liq} via:

$$V_{liq} = p_0V_{ads}V_m/RT \quad [5]$$

Where V_m is the molar volume of liquid nitrogen, R is the gas constant and T is the ambient temperature. V_{liq} is assumed to be identical with the pore volume,

The average pore radius r_p can directly be derived from the BET surface area S and the pore volume. By assuming cylindrical pore geometry this can be expressed as:

$$r_p = 2V_{liq} / S \quad [6]$$

The pore size distribution of a material is commonly derived from the desorption branch of the isotherm assuming a parallel pore model with cylindrical pore geometry by a method introduced by Barrett, Joyner and Halenda[69] (BJH) in 1951 which is based on the Kelvin-equation:

[68] L.G. Gurwitsch, J.Phys.Chem.Soc. of Russia 47 (1915) 805
[69] E.P. Barrett, L.G. Joyner and P.P. Halenda, J.Amer.Chem.Soc. 73 (1951) 373-380

$$r_K = -2\,\gamma\,V_m / R\,T\,\ln(p/p_0) \quad [7]$$

Where γ is the surface tension of fluid nitrogen at its boiling point and r_K is the Kelvin radius of the pore. Using the appropriate values for nitrogen at 77 K the equation is reduced to:

$$r_K\,[\text{Å}] = 4.15 \log (p/p_0) \quad [8]$$

The Kelvin radius r_K is the radius of the pore in which condensation occurs at the relative pressure p/p_0. The actual pore radius r_P therefore is represented by the sum of the Kelvin radius and the thickness t of the adsorbed layer on the walls of the pore:

$$r_P = r_K + t \quad [9]$$

Starting from completely filled pores at p_1 with $p_1/p0 \approx 1$, the pore volume is represented with the inner capillary volume V_K by the following equation:

$$V_{p1} = V_{K1}\,(r_{p1}/r_{k1})^2 \quad [10]$$

Lowering the pressure to p_2 with $p_2 < p_1$, a liquid volume V_1 of nitrogen desorbs resulting in a reduced thickness Δt_1 of the adsorbed layer:

$$V_{p1} = V_1\,(r_{p1}/(r_{k1} + \Delta t_1/2))^2 \quad [11]$$

The next step is another lowering of the pressure to p_3 with $p_3 < p_2$, where the volume V_{p2} of desorbed nitrogen can be written as:

$$V_{p2} = (V_2 - V_{\Delta t2})(r_{p2}/(r_{k2} + \Delta t_2/2))^2 \quad [12]$$

$V_{\Delta t2}$ can be expressed as: $V_{\Delta t2} = \Delta t_2\,Ac_1$ where Ac_1 is the area exposed by the previously emptied pores. The representation of the expression for a stepwise desorption can be written as:

$$V_{\Delta t_n} = \Delta t_n \sum_{j-1}^{n-1} Ac_j \quad [13]$$

This will lead to an exact expression for calculating pore volumes at a given pressure p_n:

$$V_{p_n} = \left(\Delta V_n - \Delta t_n \sum_{j-1}^{n-1} Ac_j\right)\left(\frac{r_{p_n}}{r_{k_n} + \Delta t_n / 2}\right)^2 \quad [14]$$

The area A_p of an empty pore p is not constant, but varies with the dimension of the pore. Assuming cylindrical pore geometry the surface can be calculated as

$$A_p = 2\ V_p / r_p \qquad [15]$$

The cumulative summation ΣAc_j from A_p for each relative pressure decrement can then be computed to give the exact surface area at any step of the desorption process. By this method, the subsequent emptying of the pore system can be followed, generating the desorbed volume at any given pore radius which can then be interpreted as pore size distribution.

This method is derived from the assumption of the adsorption of a layer of fluid nitrogen on an even surface with a cylindrical pore system, with a constant value of the surface tension of the adsorbed nitrogen, which may not be completely true in the layers near the surface and when the building of layers is hindered.

Non-Local Density Functional Theory (NLDFT): recently discovered materials with well defined pore-structures like the M41S-family or the SBA-15 materials showed a distinct discrepancy between the pore size values generated by diffraction data or transmission electron microscopy and the values generated by the traditional procedures like BJH-method from nitrogen sorption experiments[22].

Furthermore the occurrence of the hysteresis in nitrogen sorption experiments was not reflected by the data treatment. Therefore a method was developed to overcome these problems, called "Non-Local Density Functional Theory (NLDFT)-method[70,71]. This procedure generates pore size values from nitrogen sorption experiments, which correlate well with diffraction data and furthermore reflects the hysteresis of the isotherm as important part of the experimental data[72].

The method is based on statistical mechanics employing Monte Carlo simulations and the non-local density functional theory (NLDFT) model of adsorption[73]. The modelling relys first of all on the knowledge of the interaction between nitrogen molecules in the fluidic phase and between the surface of the material and its validity, generating the mean field in density functional theory[74]. In the second modeling step an ensemble of interconnected pores is created with a well-defined and rigid geometry. Then grand-canonical Monte-Carlo simulations are run to simulate nitrogen sorption experiments at different relative pressures to generate the adsorption- and desorption isotherms[75]. Performing simulations with different pore size distributions generates the basis for the correlation between theory and experiment.

[70] Peter I. Ravikovitch, PhD Thesis, Yale University (1998)
[71] N. A. Seaton, J.P.R.B. Walton, N. Quirke, Carbon 27 (1989) 853-861
[72] L. Sarkisov and P. A. Monson, Langmuir, 16 (2000) 9857-9860
[73] A.V. Neimark, P.I. Ravikovitch, M. Grün, F. Schüth and K.K. Unger, J. Coll. Interface Sci. 207 (1998) 159-169
[74] Hyung-June Woo, L. Sarkisov, and P. A. Monson, Langmuir 17 (2001) 7472-7475
[75] L. Sarkisov and P. A. Monson, Langmuir 17 (2001) 7600-7604

First of all, the method explains well the appearence of hysteresis loops in nitrogen sorption experiments depending of the size and nature of the pore system[76] and therefore and of even more importance allows in the second step a more exact interpretation of nitrogen sorption data as both the adsorption and the desorption branch of the isotherm are used for the data treatment[77].

State-of-the-art commercially available software [ASWin ver. 1.5 from Quantachrome Instruments, Boynton Beach, Florida, USA] for nitrogen sorption instruments offers data treatment options by NLDFT-method based on a set of kernels for some typical interactions and pore geometries. After choosing a suitable type of pore geometry and interaction, for example in the case of native amorphous silicas of the type cylindrical pores and NLDFT equilibrium model, the software is then using a fitting algorithm to modify the pore size distribution in the model until the best fit of the experimental curve is reached, which is regarded as pore size distribution of the sample by NLDFT-method.

Right now, the NLDFT-method generates the most reliable results by means of pore structural values from nitrogen sorption data[78], especially if the investigated sample can be described with the kernels provided from the manufacturer. So far, native materials like silica, zeolites and carbons are well represented with various pore geometries in the software. Surface functionalized materials like C18-coated silicas are not represented at all and would need a large experimental effort for the correct data treatment by NLDFT-method. Furthermore, the NLDFT-method requires a rigid framework or rigid walls for building the pore system, and therefore the method is not applicable at its actual state for usual polymer-based materials, which are still capable of molecular moves at 77 K.

3.2.4 Inverse Size-Exclusion Chromatography (ISEC)

The investigation of the pore properties of chromatographic media should ideally be performed under similar conditions to those in the chromatographic applications. Unlike gas sorption, mercury intrusion or microscopic techniques, solute exclusion techniques are performed in liquid phase - and size-exclusion chromatography (SEC) is one of the modes of liquid chromatography. In SEC mode, the interactions between stationary phase and the analytes are suppressed by choosing appropriate conditions e.g. excellent solutes.

[76] Matthias Thommes, Bernd Smarsly, Matthijs Groenewolt, Peter I. Ravikovitch, Alexander V. Neimark, Langmuir 22 (2006) 756-764
[77] Peter I. Ravikovitch and Alexander V. Neimark, J. Phys. Chem. B 105 (29) (2001) 6817 – 6823
[78] U. Ciesla, M. Grün, T. Isajeva, A.A. Kurganov, A.V. Neimark, P. Ravikovitch, S. Schacht, F. Schüth and K.K. Unger, Access in Nanoporous Materials Part 4 (2002) 231-240

Therefore, the separation depends not on chemical interactions but only on the size of the analytes, in a kind of a physical sieving process[79,80,81] as an entropic effect.

Stationary phases usually exhibit a variety of different pore sizes. During the chromatographic run, analytes can access only pores larger than their own size, resulting in differences in the accessible volume depending on the size of the analyte: the smaller the probe molecule, the more volume is accessible. Therefore smaller analytes elute after larger ones, depending on the hydrodynamic volume of the molecules. Molecules, which are larger than the biggest pores are completely excluded from the pore system and therefore no difference can be observed in the exclusion volume for different kinds of probe molecules with sizes exceeding the exclusion limit of the sample material.

SEC is usually employed for the separation and the characterization of polymers, yielding the molecular size range of the investigated polymer. This is done via the comparison of the retention time of the sample and empirical size-exclusion calibration curves of well-defined polymer standards with known molecular dimensions. The correlation between the hydrodynamic dimensions of the analyte and the retention time gives direct information about the accessible void volume of the stationary phase, which consists of the intraparticle space of the packing material and the accessible pores.

Therefore – if interactions between the surface of the stationary phase and the analytes are suppressed – a relationship between the retention time and the hydrodynamic dimensions of the analytes can be derived to gather information about the pore system of the stationary phase. This technique is thus called inverse size-exclusion chromatography (ISEC) and was first employed by Aggerbrandt and Samuelson[82] in 1964 who used poly(ethyleneglycol) to assess the pore characteristics of cellulose fibres in swollen state. In 1978 Halasz and Martin[83] introduced ISEC to determine the pore size distribution of porous materials. Knox and Scott[84] proposed theoretical models for ISEC based on cylindrical pores up to complex agglomerates of spheres for the prediction of the pore size distribution from ISEC data. This allowed Gorbunov et al.[85] and Hagel et al.[86] to establish theoretical and practical procedures for the assessment of pore structural data via ISEC, generating values for the pore size distribution as well as for the external, internal and total porosity of packed columns. Both papers emphasize the use of a long series of well-defined standard polymers

[79] M.E. van Kreveld, N.J. van den Hoed, J. Chromatogr. 83 (1973) 111-124
[80] W.W. Yau, J.J. Kirkland, D.D. Bly, Modern Size-exclusion Liquid Chromatography, Wiley, New York (1979)
[81] T. Provder, Detection and Data Analysis in Size-Exclusion Chromatography, Am.Chem.Soc., Washington, DC (1986)
[82] L.G. Aggerbrandt, O. Samuelson, J.Appl.Polym.Sci. 8 (1964) 2801-2812
[83] I. Halasz, K. Martin, Angew.Chem.Int.Ed.Engl. 17 (1978) 901-908
[84] J.H. Knox, H.P. Scott, J.Chromatogr. 316 (1984) 311-332
[85] A.A. Gorbunov, L.Y. Solovyova, V.A. Pasechnik, J.Chromatogr. 448 (1988) 307-332
[86] L. Hagel, M. Österberg, T. Andersson, J.Chromatogr.A 743 (1996) 33-42

(e.g. polystyrenes) as probe molecules with a narrow particle size distribution from oligomers up to particle sizes in the million Dalton range. The procedure was further developed by Grimes et al.[87] allowing to generate valuable pore structural parameters of porous silicas from ISEC measurements and to correlate these data with mass transfer parameters of silica based columns in HPLC.

Many authors discuss the advantages of values generated via solute exclusion methods over data based on static methods[88,89], emphasizing the usability for generating valid pore size information of porous polymeric sorbens.

Small probe molecules, like monomers or dead time markers, have full access to the pore system. This results in the elution volume $V_{E,0}$, which consists of the intra-particle space V_i of the packing bed respectively the void volume of the column, the pore volume V_p of the particles itself and the dead volume of the chromatographic equipment V_d. The largest probe molecules should be fully excluded from the pore system and elute with the volume $V_{E,N}$, which is also the void volume, being the sum of V_i and V_d. The elution volume $V_{E,i}$ of any kind of probe molecules therefore is in the range between $V_{E,N} \leq V_{E,i} \leq V_{E,0}$ as long as interactions with the stationary phase are negligible (illustrated in Figure 11).

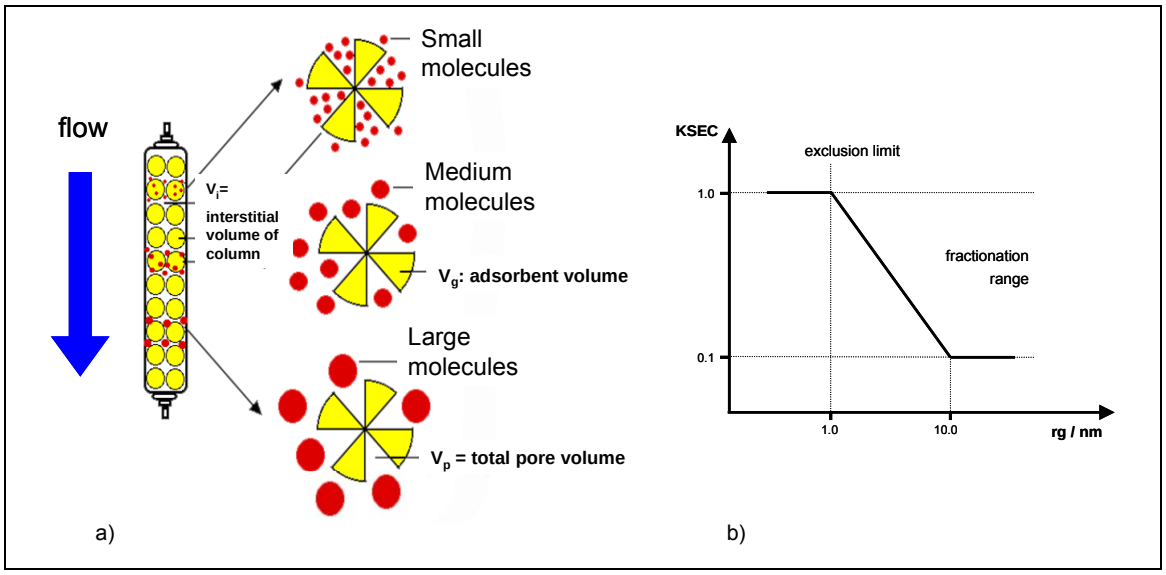

Figure 11: a) Principle of size-exclusion chromatography (SEC) and b) schematic calibration curve.

In size-exclusion chromatography, the exclusion coefficient K_{ISEC} of a given analyte is usually assigned with its experimentally determined peak maximum. It represents the permeation of the analyte into the pore system of the sorbens:

[87] B. Grimes, R. Skudas, K. Unger, D. Lubda, J.Chromatogr.A 1144 (2007) 14-29
[88] J. Hardil, D. Horák, Z. Pelzbauer, E. Votavová, F. Švec, V. Kálal, J.Chromatogr. 259 (1983) 269-282
[89] S. Koga in: P.L. Dubin, Aqueous Size-Exclusion Chromatography, Vol 40 (1988) 157

$$K_{ISEC} = \frac{V_{E,i} - V_{E,N}}{V_{E,0} - V_{E,N}}, \textit{ for i= 0,1,2,...,N} \quad [16]$$

respectively

$$V_{E,i} = V_{E,N} + K \cdot V_P \quad [17]$$

K depends on the size and geometry of the pore system as well as of the probe molecules. As for all experimental techniques the determination of the pore size distribution depends on both the accuracy of the measurement and for the validity of the applied theoretical model.

Instead of using the retention time of the peak maximum for the determination of the elution volume of the analyte, van Krefeld[90] exhibited, that the first moment of the column response has to be used to determine the elution volume $V_{E,i}$ of the analyte i. Van Krefeld determined the elution volume at different flow rates and showed that the elution volume determined is independent of the flow rate, while the determination by the peak maximum method exhibited a strong dependency of the flow rate. However, at very small flow rates, both values are in good agreement.

3.2.5 Assessment of Characteristic Pore Properties based on Pore Network Model (PNM) and Parallel Pore Model (PPM)

Parallel pore model

The most often applied theoretical model for the determination of pore size distributions is the so-called parallel pore model. This model is based on the idea of a pore system consisting of cylindrical pores with different sizes, which are not interconnected. This model is also the base for the determination of the pore size distribution via nitrogen sorption measurements (BJH-method) and the interpretation of mercury intrusion porosimetry data.

[90] M.E. van Kreveld and N. van den Hoed, Journal of Chromatography 149 (1978) 71-91

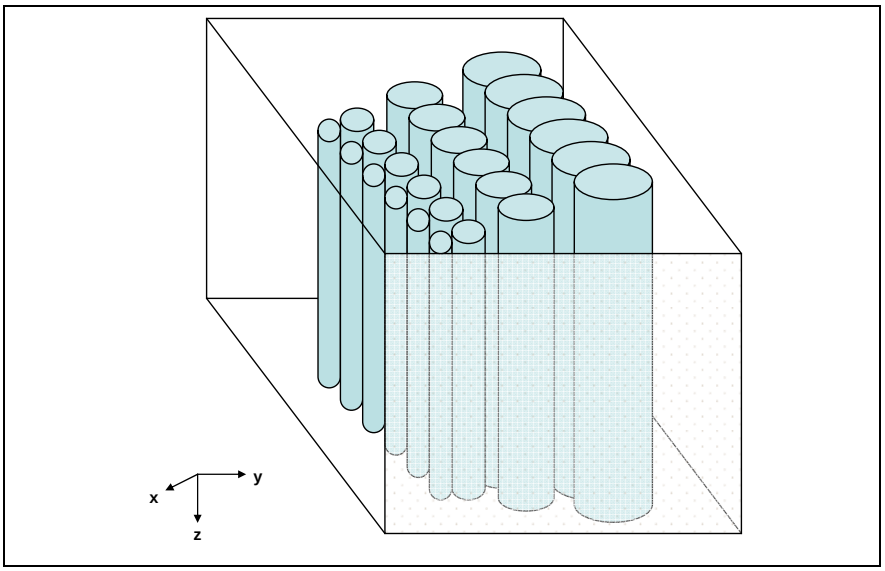

Figure 12: Schematic representation of the non connected cylindrical pores – where the parallel pore model (PPM) is based upon.

By applying cylindrical pore geometry (parallel pore network model) with the radius *R* and spherical probe molecules as hard spheres with the radius *r*, Knox[84] proposed for their interdependence:

$$K = \left(1 - \frac{r}{R}\right)^2 \text{ if } \left(\frac{r}{R}\right) < 1 \qquad [18]$$

and

$$K = 0 \text{ if } \left(\frac{r}{R}\right) > 1 \qquad [19]$$

The knowledge of the molecular dimensions of the probe molecules plays the key role for the application and validity of the equations. The relationship between the effective molecular radius r and the radius of gyration r_g is:

$$r = 0.886\ r_g \qquad [20]$$

For the typically employed linear polymers the radius of gyration can be derived from its relative molecular weight M via:

$$r_g = a\ M^b \qquad [21]$$

where a and b are constants which depend of the type of polymer and the solute. For the most common polymer/solute-pairs published data is available[80].

In the case of a continuous distribution function f(R) for the pore size distribution of the sample material the representation of *K* is given by the following expression:

$$K = \int_{R=r}^{R=\infty} f'(R)\left(1-\frac{r}{R}\right)^2 dR \qquad [22]$$

where f´(R) dR represents the pore volume fraction from R to R + dR. It is represented by the following relation:

$$f'(R) = -\frac{r^2}{2}\left(\frac{d^3K}{dr^3}\right)_{r=R} \qquad [23]$$

As r is the radius of the probe molecules and *K* is the experimental exclusion coefficient, the pore size distribution curve g(R) can be derived via inversion of this equation:

$$g(R) = 1 - \int_0^R f'(r)dr \qquad [24]$$

By integration one can obtain the following expression for g(R):

$$g(R) = K - \frac{3}{2}\left(\frac{dK}{d\ \ln r}\right)_{r=R} + \left(\frac{1}{2}\frac{d^2K}{d(\ln r)^2}\right)_{r=R} \qquad [25]$$

This expression allows the direct determination of the pore size distribution of a sample material – as long as there are enough data points for r and *K* to assume a continuous pore size distribution function. The evaluation of the data can easily be done by commercially available software.

Pore network model

The pore network model is based on the assumption of cylindrical pores which are interconnected to a certain extend. This is done by topologically mapping a set of random sized pores into a cubic lattice, which has a regular array of nodes. These nodes are connected to each other, representing the interconnecting pores. The coordination number represents the pore connectivity value n_T and therefore can reach a value of up to 18, although the maximum physically reasonable value for n_T is up to 10.

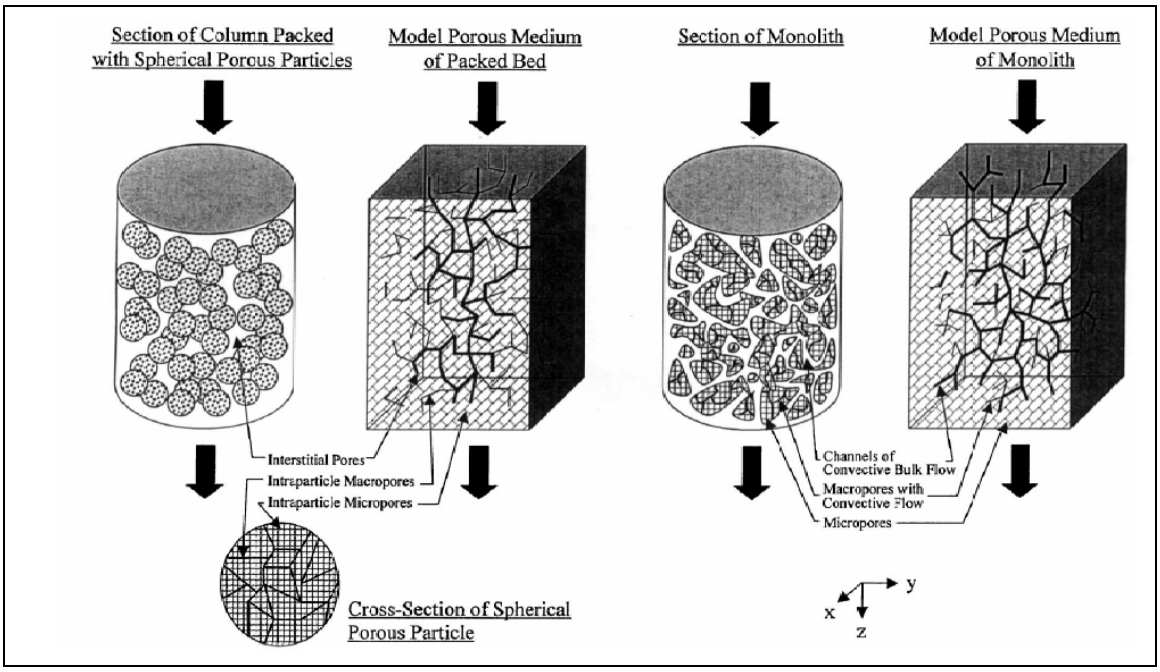

Figure 13: Schematic representation through the pore network model (PNM) of a finite small section of a packed bed with particulate silica and of a continuous bed representing monolithic silica.[91]

The first step in the evaluation of the data is to generate a set of random sized cylindrical pores into a computer model. This is e.g. done by applying the pore size distribution, which is obtained via the data treatment by parallel pore model. Then the theoretical SEC-curves are computed subsequently with variation of the n_T-values. The best fit is considered as the pore connectivity value. Once the n_T-value is set, another optimization step is processed via the variation of the pore size distribution to enhance the fit between the measured *K*-values and the computed SEC-curve.

The applied algorithm for the data treatment was developed by B.A. Grimes[87] and allowed to obtain a Gaussian pore size distribution with one centre of gravity. The pore connectivity value is a very important factor for a chromatographic sorbent, as it represents the accessibility of the pore system during a chromatographic run.

The higher the pore connectivity, the better the chromatographic performance can be expected. The minimum value for a usable stationary phase is about 6. Good chromatographic media possess a n_T-value between 7 and 9. If the n_T-value is large or equal to 10, no further improvement can be observed. Greater values are usually noted as +10 or ∞, indicating that the physical maximum for the pore accessibility is reached.

[91] J.J. Meyers, A.I. Liapis, J. Chromatogr. A 852 (1999) 3-23

3.3 Evaluation of the Chromatographic Properties of Columns in HPLC

HPLC is commonly applied for the separation of substances in both analytical and preparative chemistry. As the separation takes place via the interaction between the analyte and the stationary phase, the design and optimization of the stationary phase plays a major role for enhancing separations. In liquid chromatography all parts of the equipment have a strong influence upon the quality and speed of the separation. Although the influence of the chromatographic equipment upon the separation can easily be monitored, the evaluation of the effect of the modification of chromatographic bulk media is much more demanding.

The quality of chromatographic media is featured by the efficiency (theoretical plate height), their retentivity and selectivity towards selected target analytes and their capacity – which is one of the most important criteria for the use in preparative chromatography. These parameters are mainly influenced by the pore structural properties of the packing material, its surface chemistry, the morphology and uniformity of the particles – and to a wide extend by the density and uniformity of the packing in the chromatographic column. Furthermore, the interaction between the analytes and the stationary phase competes with the solvation strength of the chosen mobile phase and the temperature.

This makes it difficult to track changes in the chromatographic performance down to the impact of the surface modification, as each of these properties may influence the chromatographic behavior heavily.

3.3.1 Assessment of Chromatographic Performance: theoretical plate height vs. linear flow velocity

Column efficiency is the most commonly used feature for the description of the quality of chromatographic columns. The determination is easily done by the evaluation of the last peak in a test-chromatogram under analytical conditions (Gaussian peak shape). Therefore the retention time of the peak maximum t_R [min] and the peak width at one half of the peak height $w_{0.5}$ is needed. It is defined via the following expression:

$$N = 5.54\left(\frac{t_R}{w_{0.5}}\right)^2 \qquad [26]$$

The column efficiency is also called theoretical plate numbers per column. More convenient is the use of the height equivalent of a theoretical plate H (HETP), which can be derived from the column length L by the following equation:

$$H = \frac{L}{N} \qquad [27]$$

While H is independent of the column length, it is in principle usable for the comparison of different columns, the smaller the HETP-value, the more efficient the column. It is dependent on the porosity of the packing bed and of the particles and also on flow rate, particle size, pore size – and on the equilibrium adsorption coefficient[92,93,94] of the analyte, which is proportional to the analytes retention coefficient.

The retention coefficient (capacity factor) of an analyte k_i can be derived by its retention time $t_{R,i}$ and the retention time t_m of a dead time marker (unretained component) via:

$$k_i = \frac{t_{R,i} - t_m}{t_m} \qquad [28]$$

For the direct comparison of different columns one should use HETP-values of analytes, which exhibit the same k'-values. The k'-value of an analyte is dependent of the strength of its interaction with the stationary phase in concurrency with the solubility in the mobile phase. This allows adaptation of the k' value of an given analyte by adjusting the solvation strength of the solute.

The separation quality between a pair of analytes with the retention coefficients k_1 and k_2 finds its expression in the selectivity coefficient α_{21}

$$\alpha_{21} = \frac{k_2}{k_1} \qquad [29]$$

To achieve a separation between the two compounds, α_{21} must be bigger than 1. Ideally, it should be in the range between 2 and 10.

Another quality criteria for the rating of separations is the chromatographic resolution R_S. It can be derived by the already introduced values by the following expression[95]:

$$R_S = (\alpha_{21} - 1)\left(\frac{k_1}{1 + k_1}\right)\sqrt{N_1} \qquad [30]$$

R_S gives a direct hint for the separation quality and if the analytes are fully separated from each other. For example, if R_S is greater than 6 times the standard deviation of peak 1 (peak width at 0.61 peak height), then baseline separation between the two peaks is achieved.

The HETP-value depends mostly on the quality of the packing bed of the column, the medium particle size d_P of the packing media, and on the flow rate of the mobile phase. The H-value for well-packed chromatographic columns in analytical mode at the optimum flow

[92] D.D. Frey, E. Schweinheim, C. Horvath, Biotechnol.Prog. 9 (1993) 273-284
[93] B.A. Grimes, S. Lüdtke, K.K. Unger, A.I. Liapis, J.Chromatogr.A 979 (2002) 447-466
[94] K. Miyabe, G. Guiochon, J.Phys.Chem.B106 (2002) 8898-8909
[95] K.K. Unger, E. Weber, Handbuch der HPLC, Teil 1, GIT-Verlag, Darmstadt, 2. Auflage (1995) 17

rate should exhibit a value between 2 to 5 times of the particle diameter[95]: $H \approx 2\text{-}5 \cdot d_P$. The dependency of the HETP-value of the flow rate is very important for the usability of chromatographic columns. If the curve is less steep, then there is only a small loss in column efficiency by increasing the flow rate, allowing to shorten analysis time.

The theoretical plate height value at a given linear flow velocity can be separated in three processes, which contribute to the actual value. In 1972 Knox[96,97] derived from the van Deemter equation[98], the following expression for the dependency of H from the linear flow velocity u:

$$H(u) = Au^{1/3} + \frac{B}{u} + Cu \qquad [31]$$

The measurement of the H vs. u curve at different flow rates allows thus to determine the values of A, B and C via nonlinear regression. The H-value is the result of band dispersion processes, which contribute to the separation in the following manner:

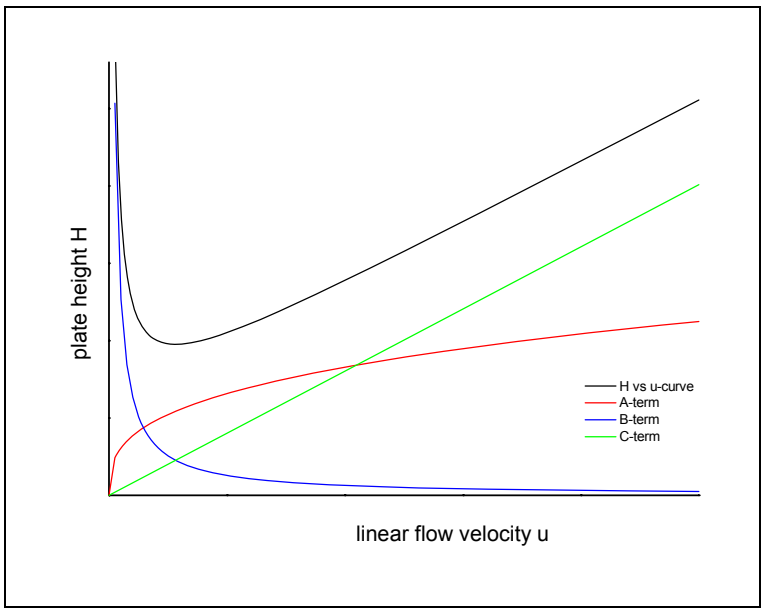

Figure 14: H-vs.-u-curve and the contributions from the A, B and C term of the Knox-equation.

A A-term, also known as Eddy diffusion, is the band broadening, which arises from different possible pathways an analyte can access through the interstitial volume between the particles of the packing bed. With increasing inhomogeneity of the packing bed – resulting from broad particle size distributions or not optimized packing procedures – the flow velocity between these pathways differs more, leading to even

[96] G.J. Kennedy, J.H. Knox, J.Chromatogr.Sci. 10 (1972) 549-556
[97] J.H. Knox, High Performance Liquid Chromatography, Edinburgh (1978)
[98] J.J. van Deemter, F.J. Zuiderweg, A. Klinkenber, Chemical Engineering Science 5 (1956) 271-289

more band broadening. As the A-term is proportional to $u^{1/3}$ it contributes more at higher flow velocities to the HETP-value

B B-term is called the molecular diffusion term. It describes the band broadening of injected analytes due to longitudinal diffusion along the flow path through the column – and in the dead volume of the chromatographic equipment. It is a function of the diffusion coefficient of the analyte in the mobile phase. The more time the analyte spend in the column, the more impact it has on band broadening. As the B-term is proportional with 1/x it contributes particularly at low and very low linear flow velocity.

C C-term is the so-called mass transfer term. It introduces the mass transfer resistance in the stationary phase as the analyte moving between the mobile and the stationary phase[99]. As the linear flow velocity increases, the more unlikely it is for the analyte to use pathways through the particles. The C-term is proportional to u. At least for well-packed columns it can be determined as a first approximation from the slope of the h vs. u curve at high linear flow rates. The mass transfer resistance is directly depending on the pore structural properties of the stationary phase and therefore is the most important parameter for the evaluation of a stationary phase. The mass transfer resistance decreases with increasing pore connectivity, pore volume and pore size of the stationary phase.

3.3.2 Assessment of Association Constants and Mass Loadability

In preparative chromatography, the loadability or the capacity of the stationary phase is one of the key features for their application. This information can be obtained from the adsorption isotherm for the desired solvent/sorbent system. The determination of the isotherm may be performed by either static or dynamic (chromatographic) methods. As the determination of adsorption isotherms by static methods requires large quantities of bulk media and analytes, the chromatographic methods are more favorable – the more as the static methods are time consuming and exhibit larger errors due to the experimental design. The most often applied dynamic methods are frontal analysis, perturbation method and elution by a characteristic point (ECP).

While the adsorption isotherms[100] of gas/solid systems are mostly of Langmuir-type, one may observe different types of isotherms in fluid/solid systems.

[99] K.M. Usher, PhD Thesis, The Florida State University (2005)
[100] F. Rouquerol, J. Rouquerol, K. Sing, Adsorption by Powders & Porous Solids, Academic Press, London (1999)

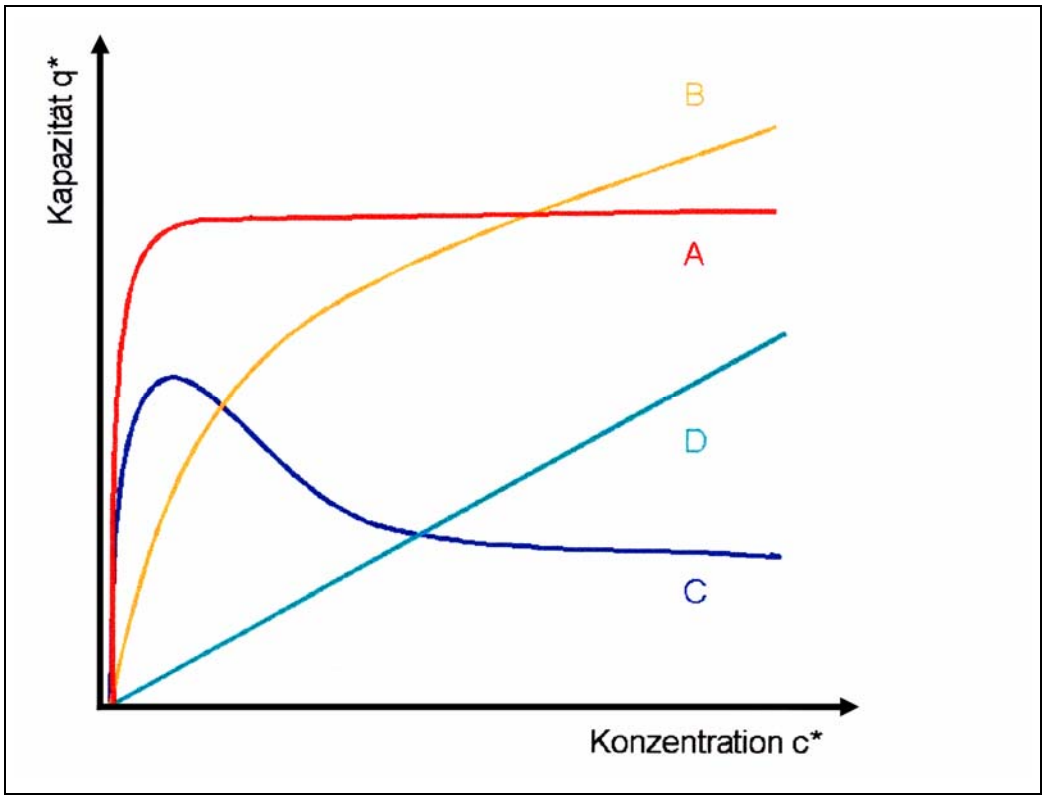

Figure 15: Different type of adsorption isotherms in fluid/solid systems with A: Langmuir isotherm; B: Bilangmuir isotherm; C: isotherm for competing substances; D: linear isotherm[101,102]

The adsorption isotherm reflects the dependency of the equilibrium of a given analyte between the mobile and the stationary phase with and the concentration of the analyte at a constant temperature. The balance is influenced by the adsorption of the substance onto the surface and desorption (solvation) of already adsorbed molecules. The most simple model is based on the assumption, that: i) the surface has a limited number of equal probable adsorption places; ii) the probability of an adsorption place is independent whether molecules are already adsorbed in the neighborhood; iii) no multilayer are allowed; iv) there are no interactions between adsorbed molecules between each other[103]. By the application of this model, one should expect the classical Langmuir-isotherm for single components. It gives for the amount of adsorbed material q at the concentration c in the mobile phase by the knowledge of the saturation capacity q_S and the temperature-depending constant b the following relation:

$$q = q_S \frac{bc}{1+bc} \qquad [32]$$

[101] M. Huber, PhD Thesis, Johannes Gutenberg University Mainz (2002)
[102] A. Seidel-Morgenstern, Mathematische Modellierung der präparativen Flüssigchromatographie, Wiesbaden (1995)
[103] A. Seidel-Morgenstern, Mathematische Modellierung der präparativen Flüssigchromatographie, Wiesbaden (1995) p. 87

In real-life materials like in silica based stationary phases, the validity of the model is not given as i) the surface is not homogeneous ii) the analyte/analyte interaction cannot be neglected and therefore iii) there is a probability for the appearance of multilayers.

The equation can easily be extended by the addition of a second binding centre (1,2). The so-called Bi-Langmuir-isotherm allows more flexibility and describes already well the adsorption isotherm of many stationary phases sufficiently:

$$q = q_{1,S}\frac{b_1 c}{1+b_1 c} + q_{2,S}\frac{b_2 c}{1+b_{2C}} \qquad [33]$$

In this equation $q_{1,S}$ and $q_{2,S}$ is the saturation capacity of both binding centers with their temperature-depending constants b_1 and b_2.

Preparative chromatography is usually applied for the separation of mixtures of different components. Therefore, the evaluation of the adsorption-isotherms of multi-component systems has to be performed. This task is much more demanding than the one for single-component systems. The concurrency between the different compounds complicates the evaluation of the isotherms. Another problem is the occurrence of local differences in the concentration of the substances during a chromatographic run. Although thermodynamically inconsistent[104], multi-component systems can be described sufficiently by the following equation for N components, where only the classical Langmuir-isotherm is applied for each component:

$$q_i = q_{i,S}\frac{b_i c_i}{1+\sum_{i=1}^{N} b_i c_i} \qquad [34]$$

In this work the adsorption isotherm is determined via frontal analysis[102]. The method is based on the measurement of breakthrough-curves at different concentrations. Via the integration of the breakthrough-curves one can obtain the adsorption capacity at a given concentration. First, the chromatographic column is conditioned with the pure mobile phase, which is pumped through the column at a constant flow rate. At $t=t_0$ the desired concentration c of the analyte is pumped through the column with the same flow rate until the concentration at the end of the column is the same as at the beginning, As this is usually observed as a steep and sudden change in the baseline of the chromatogram it is called "breakthrough-curve". The application and measurement of breakthrough-curves can be performed either in a row of subsequent injections of large volumes with the desired concentrations (adsorption followed by desorption), or – as done in this work – by a stepwise increase of the

[104] D.B. Broughton, Ind. Eng. Chem. 40 (1948) 1506-1508

concentration until the highest concentration is reached. This can be done by using an HPLC instrument with two metering pumps. The reservoir of one pump is filled with the pure mobile phase and the reservoir of the other pump contains a mixture containing the highest desired concentration of the analyte. The application of a step gradient provides the desired changes of the concentration. The so-called staircase method[105,106] is named because the resulting chromatogram reminds of a staircase, since the stepwise increase of the concentration until equilibrium is reached is reflected in its form. In this method only the adsorption steps are recorded, the desorption takes place in one single step at the end of the measurement, after the application of the highest concentration.

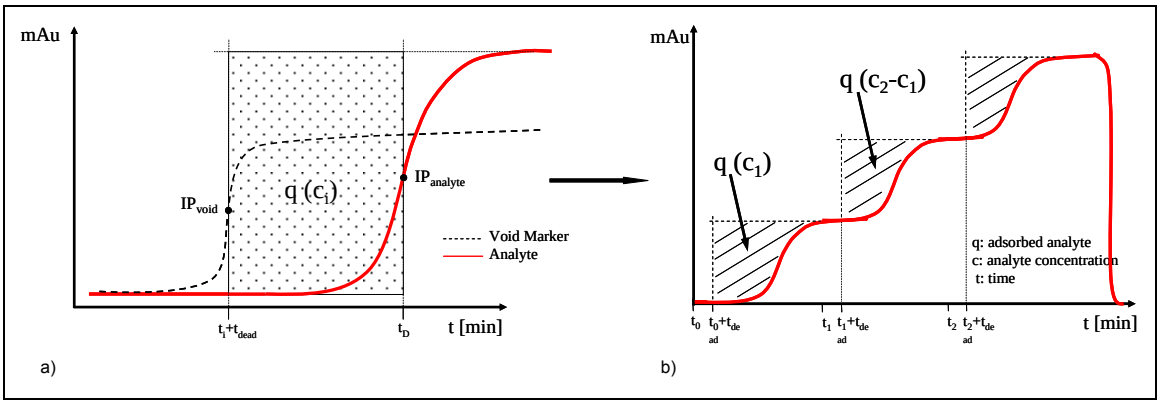

Figure 16: a) Determination of adsorbed analyte and b) Principle of staircase method.

The determination of the adsorbed amount is done by the determination of the retention time at half height respectively of the inflection points of the breakthrough-curve[107], which is reflected in the following expression in which V_S is the volume of the stationary phase, V_F is the volume till breakthrough and V_0 the volume till the starting point:

$$q = \frac{1}{V_S}\int_0^c (V_F - V_0)dc \qquad [35]$$

Integration results in the following expression:

$$q = \frac{c(V_F - V_0)}{V_S} \qquad [36]$$

This allows the direct determination of the adsorbed amount of the analyte.

[105] Y.A. Eltekov, Y.V. Kazakevich, A.V. Kiselev, A.A. Zhuchkov, Chromatographia 20 (1985) 525
[106] Y.A. Eltekov, Y.V. Kazakevich, J.Chromatogr. 365 (1986) 213
[107] G. Guiochon, S.G. Shirazi, A.M. Katti, Fundamentals of Preparative and Nonlinear Chromatography, Academic Press: Boston, MA, (1994)

Scatchard[108] developed in 1949 independent of Langmuir an alternative expression for the adsorption behaviour of an adsorbate onto a surface:

$$\frac{q^*}{c^*} = K_d(q_m - q^*) \qquad [37]$$

where q* is the concentration of the adsorbed amount, c* is the concentration of the adsorbate in the mobile phase, K_D is the dissociation constant and finally q_m reflects the maximum capacity of the sorbens [mg/mg of sorbens]. This is just another form of the classical Langmuir-isotherm. The Scatchard-plot allows via the plot of q*/c* vs. q* the direct determination of the dissociation constant via the slope of the straight line without the knowledge of q_m. The plot is more sensitive upon multiple interactions. In the case of Bi-Langmuir behavior the plot shows a positive bending of the curve. A negative bending indicates cooperative interactions, which often can be observed in the case of protein-adsorption, when the agglomeration between proteins is more favorable than the adsorption on the surface of the sorbens.

The adsorption of proteins consists of multiple steps – each with a different mechanism and association constant. As the steps cannot be separated from each other, K_d can only be determined as the sum of all adsorption steps

3.3.3 Assessment of Denaturation Potential

Common stationary phases for HPLC are frequently employed for the separation of biopolymers in analytical mode. The state-of-the-art combination with mass-spectrometers as detectors requires sharp peaks with conservation of the original mass of the proteins. Therefore, maximum interactions between the stationary phase and the proteins are favourable: very hydrophobic phases in reversed-phase mode or very hydrophilic phases in normal-phase mode generate the best separations. For the utilization in semi-preparative or preparative chemistry, a method has to deliver sufficiently pure proteins, which are still in a biological active state. The interaction with fully hydrophilic or hydrophobic surfaces may change the tertiary structure of proteins and damage their biological activity. For the use of HPLC for the separation of biopolymers in preparative mode, it is not enough to optimize the separation, but to test the biological activity of the separated proteins afterwards. The focus of this work was to optimize the surface of the stationary phase to achieve good separations by prevailing as much biological activity of the separated proteins as possible.

[108] G. Scatchard, Ann. N.Y. Acad. Sci. 51 (1949) 660-672

3.3.3.1 LCM-Test-Mixture – lysozyme, cytochrome C, myoglobin

As standard test for the separation of proteins, the lysozyme / cytochrome C / myoglobin (LCM)-test mixture was employed. The LCM-test-mixture[33,34,109] allows to evaluate the influence of stationary phases upon the tertiary structure of the proteins. As the LCM-test-mixture was used in former investigations, the comparison with the results of these investigations allows the better evaluation of selectivity, efficiency and chromatographic performance in general for the produced stationary phases. The choice of the three proteins in brief: myoglobin has a weakly bond hem-group, which can easily be split off during the chromatographic run, cytochrome C is a very stable medium-hydrophobic protein and acts as a marker for lysozyme, which is in its native form more hydrophilic and in the denatured form more hydrophobic than cytochrome C.

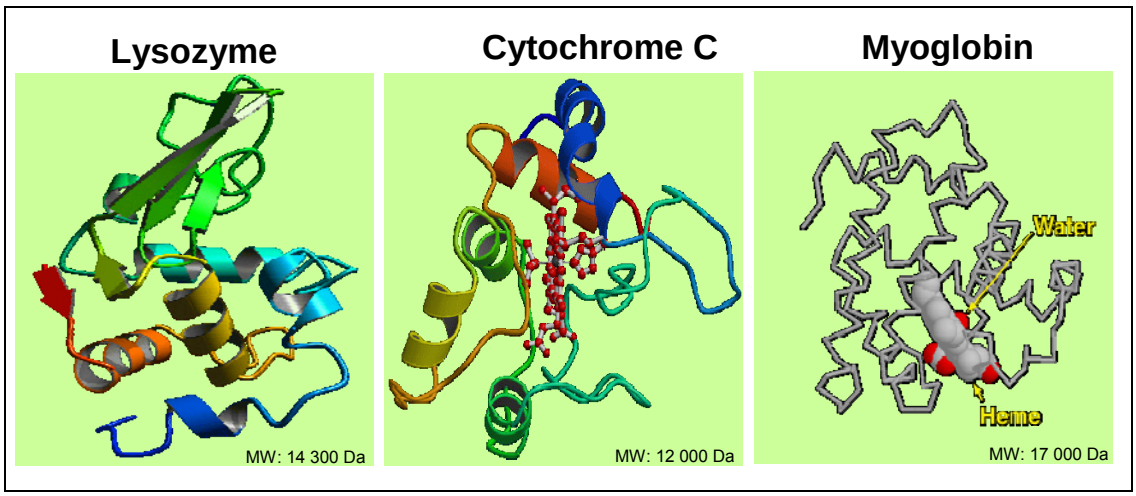

Figure 17: Molecule models of lysozyme, cytochrome C and myoglobin.

Myoglobin features a hem-group, detectable at a wavelength of 400 nm, which is not covalently bound. The rest of the molecule is detectable at 215 nm. If the hem-group is split-off during the chromatographic run, the injection of myoglobin would exhibit different retention times for the hem-peak and the one for the rest of the molecule, showing clearly the destruction of the tertiary structure of the protein. Cytochrome C holds a 400 nm detectable hem-group, too, which is covalently bound to the rest of the molecule, which is detectable at 215 nm. The tertiary structure of cytochrome C is very stable. It exhibits a medium hydrophobicity, which is not changed under the used chromatographic conditions. Lysozyme can be detected at 215 nm and is in its native form more hydrophilic than cytochrome C, resulting in a shorter retention time in RP-mode than cytochrome C. In the denatured form, it is more hydrophobic than cytochrome C and therefore it elutes later. The denaturation of

[109] C.T. Mant, R.S. Hodges, HPLC of Peptides and Proteins: Separation, Analysis and Conformation, C.T. Mant, R.S. Hodges (Eds.), CRC Press, FL (1991) 437

lysozyme is due to interactions with the stationary phase and depends on the hydrophobicity of the surface of the stationary phase.

A stationary phase with low denaturation potential should therefore exhibit the following chromatographic behavior upon the LCM-test-mixture: lysozyme elutes as a single peak before cytochrome C, and then myoglobin appears with the same retention times for the hem-group at 400 nm and the rest of the molecule at 215 nm.

3.3.3.2 Relative Enzymatic Activity Test – Alcohol Dehydrogenase (ADH)

To monitor the biological activity of a protein, it is necessary to know the biological function of the molecule. Alcohol dehydrogenase (ADH) is a well-characterized enzyme, which is catalyzing the decomposition of ethanol in the organism:

$$NAD^+ + CH_3CH_2OH \xrightarrow{ADH} NADH + CH_3CHO$$

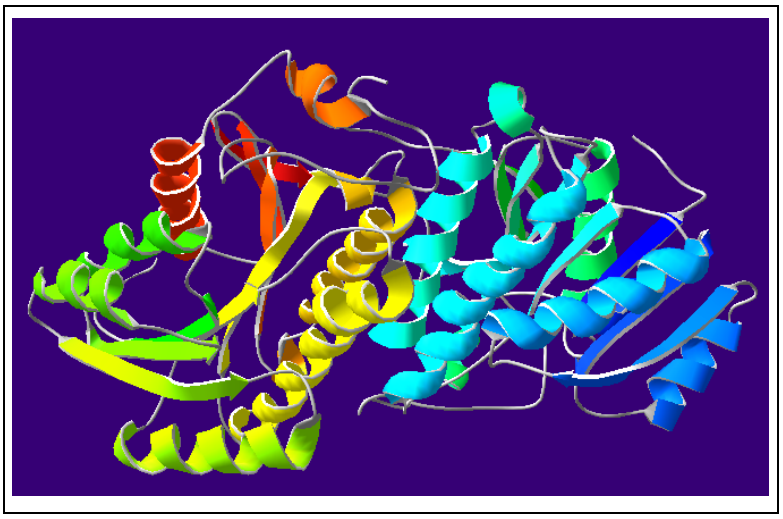

Figure 18: Molecular model of alcohol dehydrogenase (ADH).

The more active the enzyme, the faster is the decomposition of ethanol. The reaction can be followed in a photometer via the formation of NADH, which exhibits a strong absorption at 366 nm, which evolves in a linear range by choosing an appropriate composition. The focus of this work was to monitor the influence of the stationary phase upon the bioactivity of biopolymers. The testing procedure was originally[110] used to evaluate the impact of a stationary phase upon the biological activity of the enzyme in bulk phase, which requires large amounts of sample material. In this work, all stationary phases had to be packed in chromatographic columns. Therefore the testing procedure was modified to evaluate the stationary phase in packed columns. Therefore one has to discriminate between the impact of the stationary phase and the impact of the rest of the chromatographic equipment upon the reduction of the biological activity during the chromatographic run. This can be achieved

[110] L. Britsch, private communication (2002)

by using the relative enzymatic activity value of an ADH-solution. Therefore the value for an ADH-solution, which was exposed to just the pure HPLC-equipment, is set to 100 %. It can be derived from the slope of the absorption curve. By testing an ADH-solution, which is collected after a chromatographic run with built-in stationary phase, one can get the relative enzymatic activity via the comparison with the 100 %-value of the pure chromatographic equipment. This value is a direct indication of the biocompatibility of a stationary phase, the higher the value, the less denaturation of the enzyme is due to the stationary phase.

4 CASE STUDY A: IMPACT OF THE PORE STRUCTURAL PARAMETERS OF SILICAS ON THE CHROMATOGRAPHIC PERFORMANCE

4.1 Preface

The relationship between pore structural data and the chromatographic performance is rather complex. Material improvements are mostly based on the experience and skills of researchers instead of being transformation of theoretical predictions into real materials. The reasons for this are manifold but obvious: first of all, the chromatographic process is very complex and the influence of pore structural characteristics can hardly be separated from other effects, especially as single pore structural parameters cannot be changed without altering other important values at the same time. Secondly, the pore system of chromatographic adsorbent is probed by nitrogen sorption or mercury intrusion porosimetry, which are indirect measurements allowing to generate values based on certain assumptions about the pore geometry and which probe the pore system of materials in their evaporated state. Then, all stationary phase materials are based upon amorphous porous materials, where neither the pore size, nor the interconnection between the pores is exactly defined. In the case of particulate materials, which represent the vast majority of stationary phases, the mean particle size and the particle size distribution in combination with the packing procedure heavily influence the chromatographic performance and make the determination of effects from pore structural changes upon the chromatographic performance even more difficult. Approaches to overcome these limitations must therefore be based on improvements of the pore characterization methods and on investigations of well-defined stationary phase materials.

In this chapter, size-exclusion chromatography was implemented and used as "real-life"-pore characterization method, based on recently developed pore network modeling by Liapis et al.[118] and further improved by Grimes[87,119]. This method allows to gather pore structural data of stationary phases in contact with the mobile phase and generates values for the pore connectivity. This method allows furthermore the ability to detect swelling effects of polymer-coated stationary phases by changing the eluent, which was used to probe polymer-coated stationary phases.

Porous silica materials such as traditional stationary phases can be converted into micelle-templated silica materials with a sharp pore size distribution by preservation of the original particle shape as presented by Fajula et al.[19] These materials were characterized for their pore structural properties and investigated by chromatographic methods. Furthermore a series of C18-coated reversed phase materials was available, which only differed in pore structural parameters and which were well-packed in chromatographic columns from the manufacturer.

All these materials were characterized by nitrogen sorption measurements as reference method and additionally by size-exclusion chromatography in the inverse mode to gather valid pore structural data. H-vs.-u-curves where measured with special respect to the mass transfer and set in relation with the results of the pore structural data.

4.2 Comparison between Amorphous Silicas and their Micelle-Templated Silica (MTS) Derivatives

4.2.1 Introduction

Highly ordered silicas with a pore system in the mesoporous range, like MCM-41 or MCM-48 are expected to exhibit advantages in liquid separations compared to traditional stationary phases with a broad pore size distribution[11,111,112]. As those materials also show extremely high surface areas, the mass loadability, as well as the discrimination capabilities should be enhanced. Materials in the lower mesoporous and microporous range with pores smaller than 2 nm are only suited for gas phase separations, but materials with larger mesopores may be applied as stationary phases for HPLC. Materials for the application in liquid chromatography processes typically feature morphologies as particulate spheres with a particle size in the range of a few micrometers up to several hundred micrometers in packed bed, or as continuous monolithic types of beds[113], which all together possess certain pressure stability under the conditions of chromatographic applications.

Classical synthesis procedures for MCM-type of silicas result in amorphous agglomerates in the lower micrometer or upper nanometer range with low mechanical stability, which cannot be used in liquid separation processes. Several attempts were made to obtain MCM-type of particles, which meet the requirements for liquid separation processes. The synthesis of micron-size spherical particles was reported by Grün et al.[114,115,116]. These particles can be agglomerated via a spray drying process to larger spherical beads, which exhibit a secondary pore system, formed by the macroporous interstitial voids[20]. Up to now, none of these attempts resulted in sufficiently pressure stable, packable beads for liquid separation processes.

---

[111] T. Yanagisawa, T. Shumizu, K. Kuroda, C. Kato, Bull.Chem. Soc. Jpn. 63 (1990) 988

[112] F. Schüth in Zeolites and Mesoporous Materials at the Dawn of the 21st Century (A. Galarneau, F. Di Renzo, F. Fajula, J. Vedrine; Editors) Elsevier Science B.V., Amsterdam (2001) 1-12

[113] K.K. Unger, C. du Fresne von Hohenesche, M. Schulte in Preparative and Process Chromatography of Pharmaceuticals (H. Schmidt-Traub, Editor) VCH, Weinhein (2005)

[114] M. Gruen, K.K. Unger, A. Matsumoto, K. Tsutsumi, Microporous and Mesoporous Materials 27 (1999) 207-216

[115] M. Gruen, K. Schumacher, K.K. Unger, Fundamentals of Adsorption 6 (1999) 569-574

[116] M. Grün, G. Büchel, D. Kumar, K. Schumacher, B. Bidlingmaier, K.K. Unger in Studies in Surface Science and Catalysis 128 (K.K. Unger et al. Editors), Elsevier Science Publishers, Amsterdam, (2000) 155 – 165

Another approach to produce mesostructured materials is the so-called pseudomorphical transformation process[19], where an amorphous porous silica source is transformed into an MCM-41 or MCM-48 type of structure under full retention of the original morphology. The silica beads are subjected to a micelle-templated reaction procedure in an alkaline medium via dissolving and reprecipitation of the silica source material generating the final MCM-41 or MCM-48-structured material. The treatment of typical mesoporous chromatographic materials with spherical morphology and a narrow particle size distribution via the pseudomorphical transformation process should therefore generate mesostructured materials with optimum properties in terms of particle shape and -size, which can be used as packing materials for the preparation of chromatographic columns. Via this approach, a direct comparison between the chromatographic performance of the originally low-ordered material and the highly-ordered MCM-type derivatives should be possible.

Two different mesoporous packing materials were transformed via pseudomorphical transformation into their MCM-41-type derivatives[117] (Micelle-Templated Silicas, MTS) and packed into HPLC-columns (see Appendix 7.3.2). The pore system generated by pseudomorphical transformation are expected to exhibit a typical pore diameter of around 6 nm, therefore starting materials with both smaller and larger pore diameters were chosen. As material with a smaller medium pore diameter, the commercially available LiChrospher™ Si60 (Merck KGaA, Darmstadt, Germany) material with a typical pore diameter of 4.6 nm was employed. As material with bigger nominal pore size, a highly porous silica, HP Silica 30nm (produced in the working group of Prof. K.K. Unger, Johannes Gutenberg University Mainz, Germany) with a medium pore diameter of 25 nm was used.

The comparison of the particle size distribution in bulk before and after the transformation as well as the assessment of the particle shape via scanning electron microscopy exhibited a nearly complete prevention of the spherical morphology of the original material. As only minor changes in the morphology between the original material and the MTS-materials can be observed, all changes in the chromatographic performance may therefore be traced back to pore structural changes due to the pseudomorphic transformation with the evolution of the MCM-41-structure.

Changes in the pore structure were investigated in bulk via nitrogen sorption measurements at 77 K and in the packed column by size-exclusion experiments employing polystyrenes in THF. The application of the pore network model proposed by Meyers et al.[118]

[117] Julien Iapichella, Benoit Lefevre, Anne Galarneau, François Fajula CNRS, Institut Gerhardt, 8 rue de l´École Normale, F-34296 Montpellier Cédex 5

[118] J.J. Meyers, S. Nahar, D.K. Ludlow, A.I. Liapis, J. Chromatogr. A 907 (2001) 57-71

and improved by Grimes et al.[87,119] allowed to calculate the pore connectivity value n_T of the materials. The column performance was assessed via the plate height to linear flow-rate dependencies in High Performance Liquid Chromatography (HPLC) employing phthalates as probe molecules.

4.2.2 Influence of Pseudomorphical Transformation upon the Morphology

Structural changes due to the pseudomorphical transformation process can be monitored by the combination of imaging and bulk methods. While for the evaluation of the particle shape, scanning electron microscopy was employed, the particle size distribution of the materials was investigated in bulk by SILAS Naß (see Appendix 7.3.1).

Figure 19 shows the SEM-image of LiChrospher™ Si 60 and its pseudomorphic transformation MTS1. The particle size distribution values are listed in Table 2.

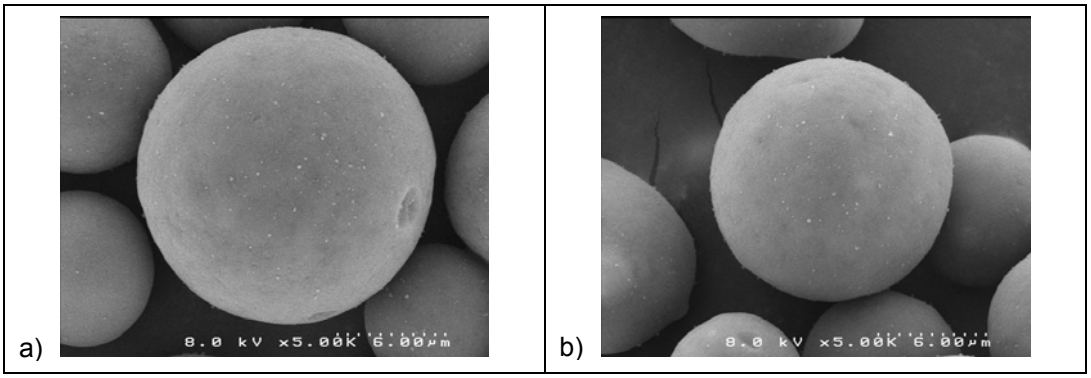

Figure 19: SEM images – a) SEM image of silica precursor LiChrospher™ Si 60 and b) SEM image of MCM-41 type derivative MTS1.[123]

[119] B.A. Grimes, C. du Fresne von Hohenesche, M. Quaglia, D. Lubda, K.K. Unger, "Theoretical Definition of the Partition Coefficient for the Description of Experimental Inverse Size-Exclusion Chromatography: Applications with Parallel Pore and Pore Network Models", Tenth International Symposium on Preparative and Industrial Chromatography and Allied Techniques (SPICA 2004), Lecture Session 1, October 17-20, (2004), Aachen, Germany

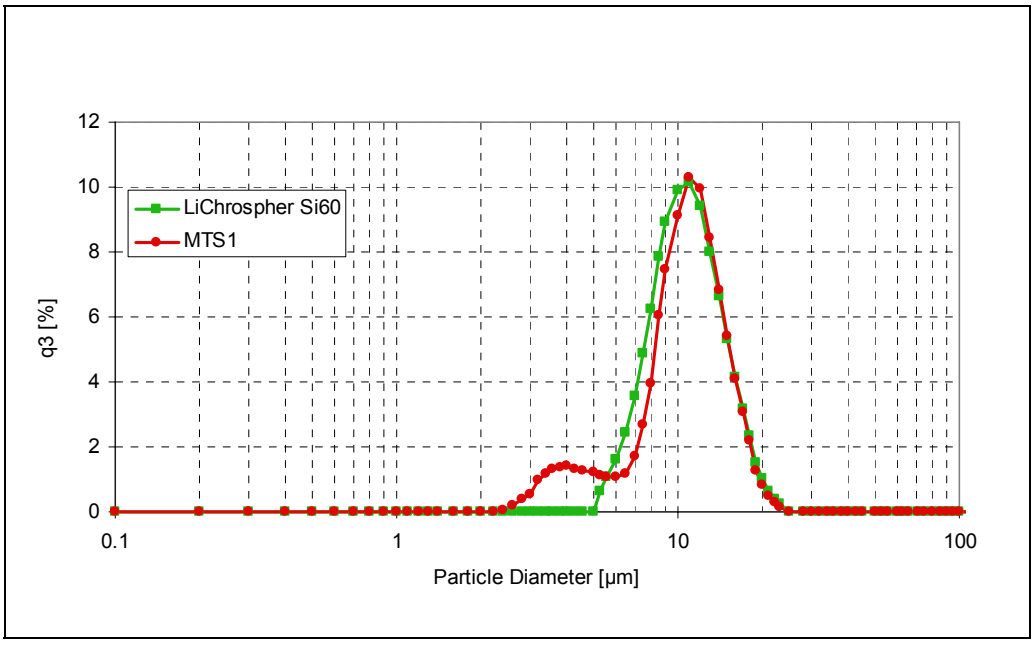

Figure 20: Particle size distribution (PSD) of silica precursor LiChrospher™ Si 60 and of MCM-41 type derivative MTS1.

Table 2: Particle size distribution (PSD) of silica precursor LiChrospher™ Si 60 and of MCM-41 type derivative MTS1.

sample	type of structure	d_{p10} [µm]	d_{p50} [µm]	d_{p90} [µm]	Ø d_p [µm]
LiChrospher™ Si 60	amorphous	7.13	10.32	15.14	10.79
MTS1	pseudomorphically transformed	5.08	10.39	14.96	10.41

Figure 21 shows the SEM-image of HP Silica 30nm and its pseudomorphic transformation MTS2. The particle size distribution values are listed in Table 3.

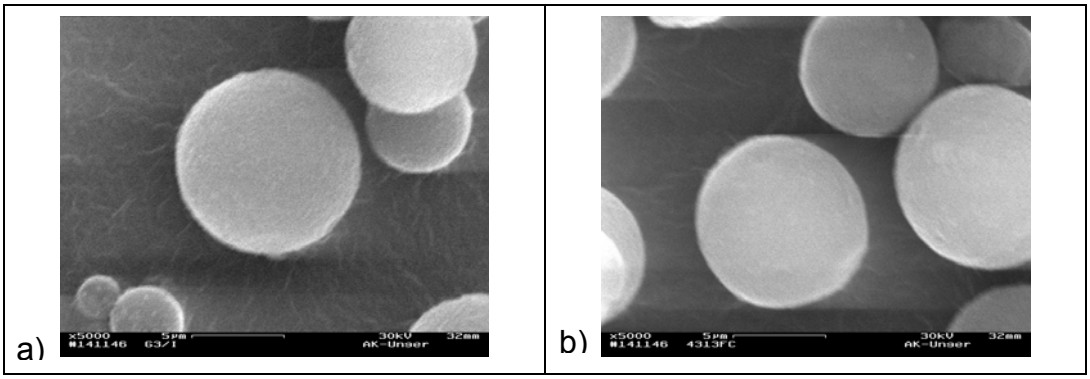

Figure 21: SEM images – a) SEM image of silica precursor HP Silica 30nm and b) SEM image of MCM-41 type derivative MTS2.

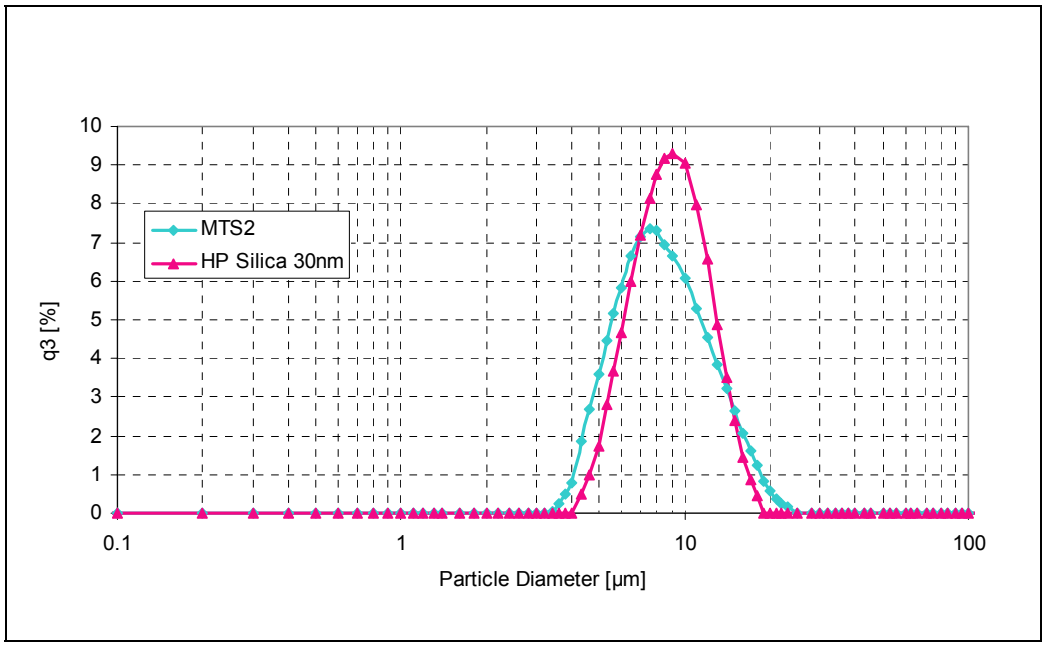

Figure 22: Particle size distribution (PSD) of silica precursor HP Silica 30nm and of MCM-41 type derivative MTS2.

Table 3: Particle size distribution (PSD) of silica precursor HP Silica 30nm and of MCM-41 type derivative MTS2.

sample	type of structure	d_{p10} [µm]	d_{p50} [µm]	d_{p90} [µm]	Ø d_p [µm]
HP Silica 30nm	amorphous	5.76	8.58	12.61	8.93
MTS2	pseudomorphically transformed	5.02	7.89	13.48	8.66

The results clearly indicate that the original morphology is widely maintained during the pseudomorphical transformation, although the transformed materials exhibit a slightly broader particle size distribution. All of the tested materials show a spherical particle shape and exhibit narrow particle size distribution; therefore these materials maybe employed as packing materials in HPLC-columns. The slight broadening of the particle size distribution between the original materials and the MTS-materials should only cause minor loss of chromatographic performance.

4.2.3 Pore Structural Data by Nitrogen Sorption at 77K

Nitrogen sorption measurement at 77 K in bulk phase is the commonly applied method for the assessment of pore structural parameters of mesoporous materials. The pore structural properties were calculated according to NLDFT (cylindrical pores, equilibrium model, p_{dNLDFT} average pore diameter)[120,121,122], BET[67] (a_s specific surface area), Gurvitsch[68] (v_p specific pore volume) and BJH[69] (p_d average pore diameter) from the adsorption-desorption isotherm.

[120] A.V. Neimark, P.I. Ravikovitch, Microporous Mesoporous Mater. 44 (2001) 697-707

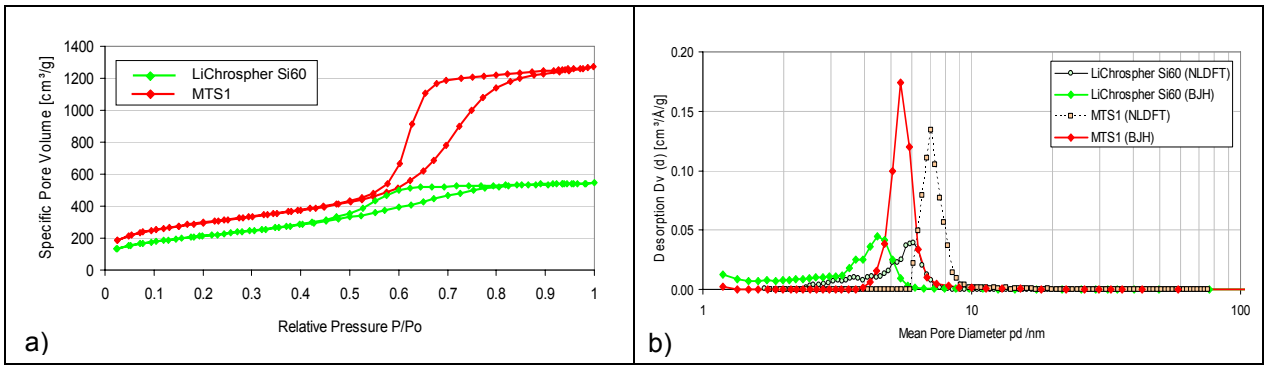

Figure 23: Nitrogen sorption measurements of silica precursor LiChrospher™ Si 60 and of MCM-41 type derivative MTS1 – a) isotherms and b) pore size distributions.

Table 4: Pore structural data of silica precursor LiChrospher™ Si 60 and of MCM-41 type derivative MTS1 by nitrogen sorption at 77 K.

sample	type of structure	a_S (BET) [m^2g^{-1}]	v_p (G) [ml g^{-1}]	p_d (BJH) [nm]	p_d (NLDFT) [nm]
LiChrospher™ Si 60	amorphous	769	0.896	4.5	6.1
MTS1	pseudomorphically transformed	1,042	2.170	5.4	7.0

Figure 23a) shows the nitrogen adsorption-desorption isotherms of both the initial silica source LiChrospher™ Si60 and its pseudomorphical transformation MTS1, both exhibiting a course of type IV according to the IUPAC classification[61]. Figure 23b) exhibits the pore size distributions of the materials derived from the isotherms according to BJH and NLDFT. The derived values for a_S / v_P / p_d are listed in Table 4. The average pore diameter is slightly increased due to pseudomorphical transformation, as MTS1 shows an average pore diameter of 5.4 nm (BJH) / 7.0 nm (NLDFT), whereas the initial silica LiChrospher™ Si60 has an average pore diameter of 4.5 nm (BJH) / 6.1 nm (NLDFT). The specific surface area significantly increases from 769 m^2g^{-1} to 1,042 m^2g^{-1}, and the most drastic change can be found for the specific pore volume value which is more than doubling from 0.896 mlg^{-1} to 2.170 mlg^{-1} due to the pseudomorphical transformation.

[121] P.I. Ravikovitch, A.V. Neimark, Colloids Surf. A 187 (2001) 11-21
[122] P.I. Ravikovitch, A.V. Neimark, Langmuir 18 (2002) 1550-1560

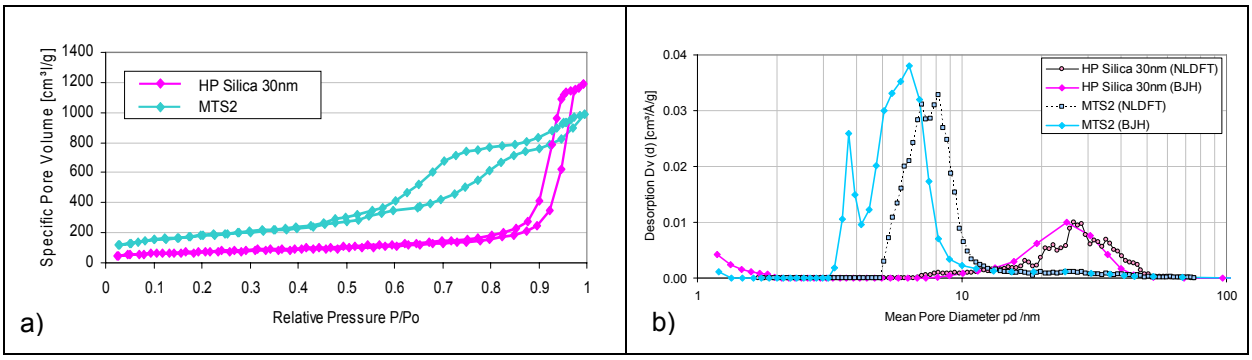

Figure 24: Nitrogen sorption measurements of silica precursor HP Silica 30nm and of MCM-41 type derivative MTS2 – a) isotherms and b) pore size distributions.

Table 5: Pore structural data of silica precursor HP Silica 30nm and of MCM-41 type derivative MTS2 by nitrogen sorption at 77 K.

sample	type of structure	a_S (BET) [m^2g^{-1}]	v_p (G) [ml g^{-1}]	p_d (BJH) [nm]	p_d (NLDFT) [nm]
HP Silica 30nm	amorphous	244	1.871	25	26
MTS2	pseudomorphically transformed	639	1.630	6.3	8.1

The nitrogen adsorption-desorption isotherms of HP Silica 30 nm, IUPAC-type V and its pseudomorphical transformation MTS2, IUPAC-type IV are shown in Figure 24a). In the course of the latter are discrete steps visible as an indication for a multi modal pore system, which finds its expression in the pore size distribution according to BJH and NLDFT (see Figure 24b)), based on the isotherms. While the initial silica shows only one maximum in the range of 25 nm (BJH) / 26 nm (NLDFT), the pseudomorphical transformed MTS2 exhibits three maxima reflecting pore diameters of 3.7 nm (BJH), 6.3 nm (BJH) and finally 25 nm (BJH), whereas the largest pores seem to be leftovers from the original material. The NLDFT based pore size distribution shows the formation of mesopores with two maxima at 7.0 nm and 8.1 nm. From this data one can deduce, that the pseudomorphical treatment is in this case not as intense or complete than in the previously described material. The formation of smaller mesopores explains well the increase of the specific surface area by a factor of more than two, from 244 m^2g^{-1} to 639 m^2g^{-1}. The slight decrease in the specific pore volume, from 1.871 mlg^{-1} for the initial silica source HP Silica 30nm to 1.630 mlg^{-1} for the MTS2 material may be explained by an incomplete transformation and the already high value of the starting material.

The measurements show, that the pseudomorphical transformation increases the specific surface area for all the investigated materials. Furthermore the evolution of a pore system with a pore diameter in the range of 6 nm is clearly exposed in the results as listed in Table 5 and reflected in the pore size distribution curves.

4.2.4 Pore Structural Data of Original Treated Silicas by SEC using Polystyrenes Standards employing PPM and PNM

The application of size-exclusion chromatography in the inverse size mode (ISEC) allows the characterization of the pore structure of chromatographic materials in the packed column as a “real life method”. In addition to the nitrogen sorption method, the data treatment allows the application of pore network model to gather values for the pore connectivity n_T, which is an important criteria for the evaluation of chromatographic media.

For the investigation of the samples via ISEC, both the initial silicas and the MTS-materials were packed into HPLC-columns and the SEC properties were gathered by applying a range of well-defined poly(styrene) standards (see Table 88, Appendix 7.3.4) as target analytes in tetrahydrofuran (THF) as eluent. As the radii of gyration for the applied standards in THF are well known[79,123,124] , these molecules can be used to probe the pore system of the sample materials. Up to 22 different samples from small oligomers to large polymers were employed and the experiments were repeated three times to ensure adequate precision for the experimental size-exclusion data, from which the pore size distribution was deduced.

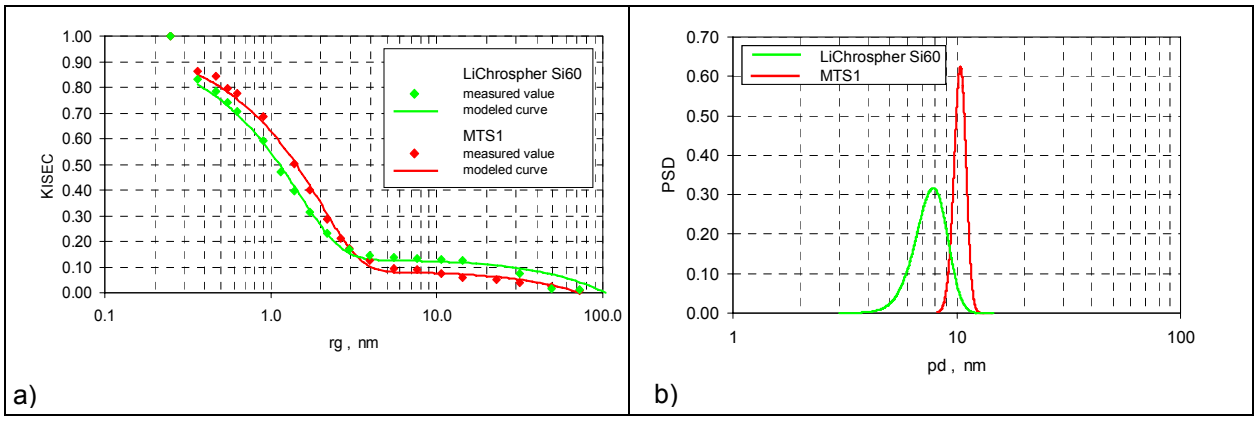

Figure 25: ISEC measurements for LiChrospher™ Si60 and its pseudomorphically transformed intermediate MTS1 using polystyrene standards – a) calibration plots and b) volume based pore size distribution.

Table 6: Pore structural data of silica precursor LiChrospher™ Si 60 and its pseudomorphically transformed intermediate MTS1 applied by PPM and PNM.

sample	p_d (BJH) [nm]	p_d (NLDFT) [nm]	$p_{d,ave}$ (PPM) by volume [nm]	σ_{pd} by volume [nm]	n_T (PNM)
LiChrospher™ Si 60	4.5	6.1	7.8	1.25	> 10
MTS1	5.4	7.0	10.4	0.56	> 10

[123] M. Ousalem, X.X. Zhu, J. Hradil, J. Chromatogr. A 903 (2000) 13-19
[124] Y. Yao, A.M. Lenhoff, J. Chromatogr. A 1037 (2004) 273-282

In Figure 25a) the experimental data for the initial silica LiChrospher™ Si60 and its pseudomorphical transformation MTS1 is displayed in the calibration curves, plotting the exclusion coefficient K_{ISEC}[114,115] against the radii of gyration r_g of the polystyrene standards in THF in nm[11,112,113], together with the fitted calibration curves based on the pore network model, reflecting the differences between theory and experiment. While the exclusion limit for LiChrospher™ Si60 is in the range of 3.9 nm (MW: 17,900 $gmol^{-1}$, see Table 88), its pseudomorphical transformation MTS1 features an exclusion limit at a higher molecular weight fractionation range of 5.5 nm (MW: 34,000 $gmol^{-1}$, see Table 88) reflecting the increase of the nominal pore size. The course of the experimental data of both columns features nearly identical trends. In detail, for small solutes the initial silica represents smaller values than its pseudomorphic transformation MTS1. In combination with less steep decline, this indicates smaller pores and a wider pore size distribution for LiChrospher™ Si60 than for MTS1.

Figure 25b) displays the computed volume based on pore size distribution curves, derived from the experimental data via the application of pore network modelling, featuring bigger pores and a narrower pore size distribution for the pseudomorphical transformed material. The values are summarised in Table 6 and compared with the data obtained via nitrogen sorption measurements. The increase of the pore volume by pseudomorphic transition is reflected in the increase of the particle porosity in the SEC measurements (see Table 6). The pore connectivity n_T does not change at all by pseudomorphic transformation and exhibits the highest possible value of >10.

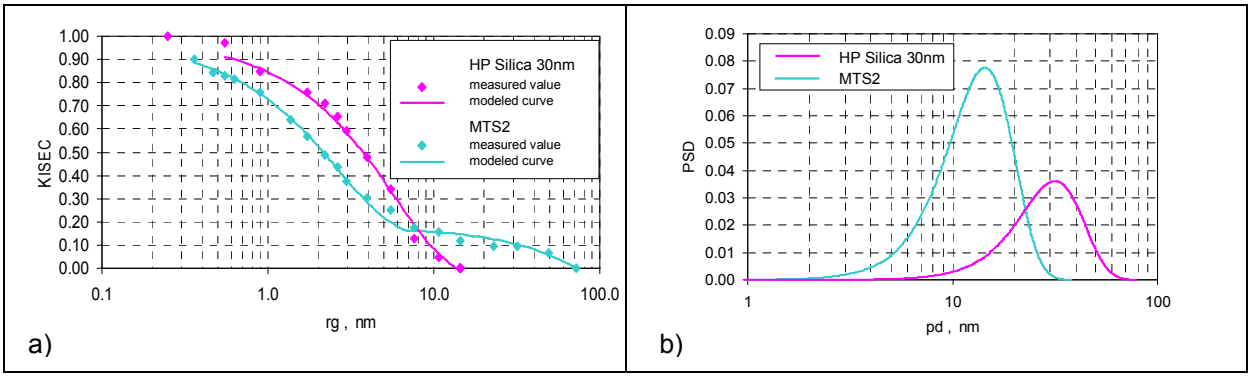

Figure 26: ISEC measurements for HP Silica 30nm and its pseudomorphically transformed intermediate MTS2 using polystyrene standards – a) calibration plots and b) volume based pore size distribution.

Table 7: Pore structural data of silica precursor HP Silica 30nm and its pseudomorphically transformed intermediate MTS2 applied by PNM.

sample	p_d (BJH) [nm]	p_d (NLDFT) [nm]	$p_{d,ave}$ (PPM) by volume [nm]	σ_{pd} by volume [nm]	n_T (PNM)
HP Silica 30nm	25	26	33	10.90	9
MTS2	6.3	8.1	15.2	5.07	> 10

Figure 26a) shows the theoretical ISEC calibration curves, which are plotted together with the experimental data for HP Silica 30nm and its pseudomorphical transformation MTS2. In contrast to the first silica source the pseudomorphic transition changes the SEC curve more drastically. The theoretical SEC curve features an exclusion limit for the initial silica HP Silica 30nm at a molecular weight fractionation range of 10.6 nm (MW: 125,000 g mol^{-1}, see Table 88), which can also be found for its pseudomorphical transformation MTS2, reflecting an incomplete transformation process with residual large pores of the initial silica. Additionally, there appears a distinct second fractionation range at a low molecular weight range of 3.9 nm (MW: 17,900 $gmol^{-1}$, see Table 88) due to the formation of smaller mesopores by pseudomorphic transition (see Table 7). In the lower molecular weight range the MTS2 packed column shows smaller K_{ISEC} values than the column packed with HP Silica 30nm. As the theoretical fit of the MTS2 calibration curve is based on a monomodal pore size distribution, more deviation with the experimental data can be observed due to the second fractionation range. The modelled pore size distributions are displayed in Figure 26b), illustrating the narrowing of the pore system by pseudomorphic transition. The values obtained by ISEC are listed together with those generated by nitrogen sorption measurements in Table 7. The decrease of the pore volume of MTS2 compared to HP Silica 30nm is also reflected in the SEC measurements as a slight decrease of the particle porosity. Finally, the pore connectivity n_T value is increasing due to pseudomorphical transformation from 9 for the HP Silica 30nm up to the highest possible value of >10 for MTS2.

4.2.5 Chromatographic Performance: theoretical plate height vs. linear flow velocity

The plate height vs. linear flow velocity dependencies (HETP-curves) is one of the most relevant information on the performance of chromatographic adsorbents. The mass transfer kinetics for small solutes can be deduced by the usage of dibutyl phthalate as solute. In contrast with ISEC-measurements, very well-packed columns are inevitable for the correct and meaningful interpretation of the HETP-curves. Figures 27 and 28 display the HETP-curves for columns packed with the initial silica and the MTS-materials. All HETP curves

exhibit the typical progression for well packed columns with a minimum of H [μm] in the range of 3-5 times of the particle diameter d_p, as an indication for well-packed columns and the validity of the data. There is no indication for breakdown of the packing material at higher flow rates.

Table 8: Chromatographic conditions for testing the theoretical plate height vs. linear flow velocity dependency.

column dimension: 125 x 4 mm ID; injection volume: 1 µl;
detection: 254 nm; @ room temperature;
flow rate: 0.25 – 5.0 ml/min; k'= 3
analytes: uracil, diethyl phthalate, dibutyl phthalate
mobile phase: n-heptane / dioxane

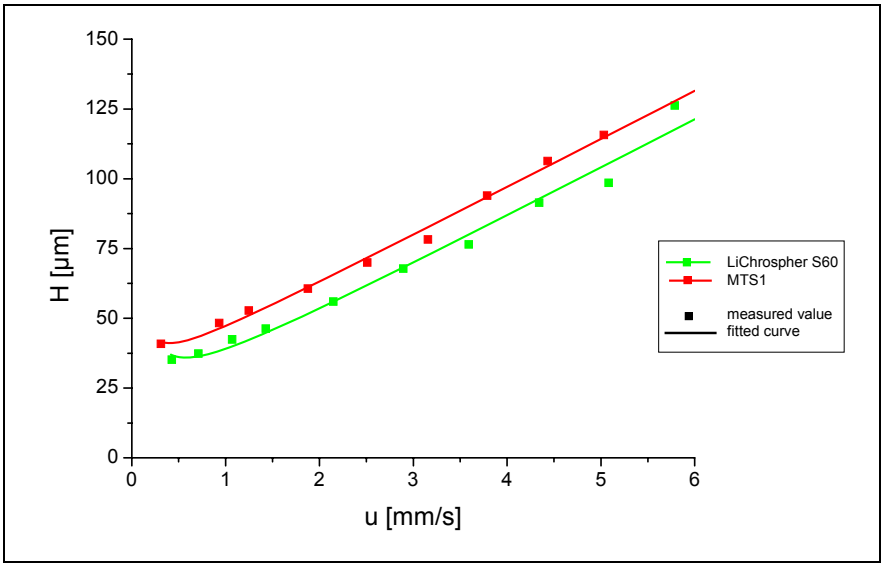

Figure 27: H-vs.-u-plots of LiChrospher™ Si60 and its pseudomorphically transformed intermediate MTS1.

Table 9: H-values and C-values of silica precursor LiChrospher™ Si60 and its pseudomorphically transformed intermediate MTS1.

sample	**Plate Height H** [µm] at 1.0 mms^{-1}	**C-term** [ms] according to Knox	**A-term** [$10^{-5}m^{2/3}s^{1/3}$] according to Knox
LiChrospher™ Si60	46 ± 1	17.39 ± 1.34	15.92 ± 6.12
MTS1	53 ± 1	17.29 ± 0.77	27.18 ± 2.94

The H-vs.-u-plots of LiChrospher™ Si60 and its pseudomorphical transformation MTS1 are displayed in Figure 27. Both columns show nearly identical efficiencies. The highest efficiency of the columns is expressed in the minimum of the plate height H [µm]. The

minimum of the curves scatter around the linear flow velocity of 0.5 to 1 mms^{-1} and gives a theoretical plate height for LiChrospher™ Si60 of around 46 μm and for MTS1 of 53 μm (see Table 9). Non-linear regression gives for the important mass transfer resistance C´ = 17.39 ms for the initial silica LiChrospher™ Si60, and C' = 17.29 ms for the MTS1 material. This means, that the internal mass transfer resistance of the material was lowered 14.6 % with the pseudomorphic transformation. The benefit to the overall efficiency of the column is offset by the larger interstitial porosity, ε_b, which manifests itself in the increased value of the A' term of 27.18 in the MTS1 column, relative to the initial silica LiChrospher™ Si60 with 15.92. As the pore connectivity is unchanged from an ideal value through the pseudomorphic transformation, one can conclude that the pseudomorphic transformation of the initial silica LiChrospher™ Si60 does improve the mass transfer resistance of the particle by (a) increasing the pore volume, (b) increasing the pore size, and (c) decreasing the width of the pore volume distribution. However, in order to take advantage of these benefits, the particle size distribution of the particles should be more narrow and the packing procedure of the columns should be optimized to obtain a lower value for the interstitial porosity.

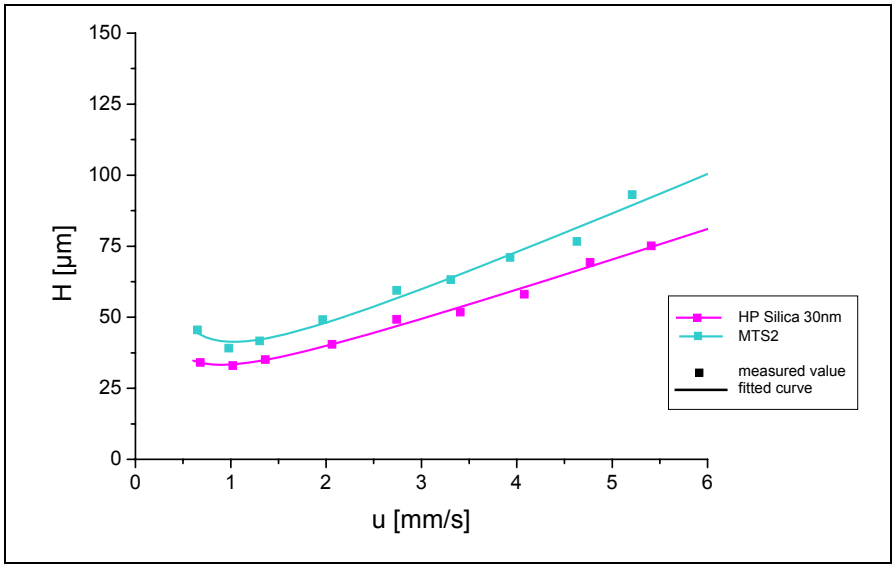

Figure 28: H-vs.-u-plots of HP Silica 30nm and its pseudomorphically transformed intermediate MTS2.

Table 10: H-values and C-values of silica precursor HP Silica 30nm and its pseudomorphically transformed intermediate MTS2.

sample	**Plate Height H** [µm] at 1.0 mms^{-1}	**C-term** [ms] according to Knox	**A-term** [$10^{-5}m^{2/3}s^{1/3}$] according to Knox
HP Silica 30nm	35 ± 1	11.02 ± 0.70	13.40 ± 3.42
MTS2	42 ± 1	14.33 ± 1.29	11.83 ± 6.12

The HETP-curves for HP Silica 30nm and its pseudomorphic transformation MTS2 are displayed in Figure 28, exhibiting a slight reduction in the overall efficiency of the column packed with MTS2 compared to the column with the initial HP Silica 30nm. At a linear flow velocity of 1 mm/s, a theoretical plate height for the initial silica of about 35 μm was obtained, while for MTS2 a value of 42 μm can be observed (see Table 10). Non-linear regression yields for the mass transfer resistance value C´ = 11.02 ms for the initial silica HP Silica 30nm and C' = 14.33 ms for the pseudomorphically transformed MTS2 material, representing a worsening of the mass transfer by 23 %. It is clear from these figures, that the pseudomorphic transformation of the highly porous, large pore support HP Silica 30nm significantly increases the internal mass transfer resistance of the particle due to the fact that the pore volume and nominal pore diameter are significantly lower in the MTS2 material. Despite a small reduction of the external porosity of the columns packed with the MTS2 material (A´ = 11.83) compared with the initial silica HP Silica 30nm (A´ = 13.40), indicating a better packing of the columns, the HETP-curve of the pseudomorphically transformed MTS2 still lies above the curve of the initial silica and no benefit at all was realized through the pseudomorphic transformation.

4.2.6 Summary

Two different particulate porous amorphous silica materials, LiChrospher™ Si60 and HP Silica 30nm, were converted by a pseudomorphical transformation process[19,117] to ordered mesoporous silica materials (micelle-templated silica, MTS), under nearly full retention of their original spherical morphology. The starting amorphous beads were subjected to a micelle templated reaction in an alkaline medium where they dissolve and reprecipitate generating a MCM-41 type of structure maintaining their original morphology, which was verified by scanning electron microscopy and the determination of the particle size distribution before and afterwards. The starting materials, which are typical chromatographic packing media and their pseudomorphically transformed MTS materials could be packed into chromatographic columns, allowing the investigation of their chromatographic properties as well as the gathering of pore structural data in size-exclusion experiments. The changes to the pore structure of the materials resulting from the pseudomorphic transformation have been quantified through network model simulations of experimental data obtained with nitrogen sorption and ISEC. Furthermore, column performance via the plate height to linear flow-rate dependencies in HPLC was evaluated experimentally.

The agreement between the results obtained from the network modeling simulations of the nitrogen sorption experiments and the ISEC experiments was fair. The nitrogen sorption measurements indicated that the pseudomorphic transformation results in a significant increase in the specific surface area for both silicas. However, both the nitrogen sorption

experiments and ISEC experiments indicated that the pseudomorphic transformation of the LiChrospher™ Si60 results in a material with a higher specific pore volume, pore volume fraction and increased nominal pore diameter with a narrower pore volume distribution, but the pseudomorphic transformation of the HP Silica 30nm results in a material with a lower specific pore volume, pore volume fraction, and nominal pore diameter with a broader pore volume distribution. The results of the plate height vs. linear velocity experiments indicated that for both particle pairs (original and transformed silicas) studied, the separation efficiency of columns packed with the pseudomorphically transformed silicas decreases slightly.

By comparing the results presented above, one can conclude that pseudomorphic transformations would only be advantageous when the transformation would result in (a) an increase in the overall pore volume fraction, ε_p, of the particle, (b) an increase in the nominal pore diameter, p_d, of the pore volume distribution, and (c) a decrease in the width of the pore volume distribution.

Due to the fact that all materials studied in this work had a pore connectivity value indicating an almost ideal pore connectivity, it is not clear how the pore connectivity is affected by the pseudomorphic transformation. However, the results indicate that there is no evidence of a worsening of the pore connectivity due to a detrimental effect by the pseudomorphic transformation process – conversely the slight increase in pore connectivity for the HP Silica 30nm might even indicate that there could be a positive effect. In conclusion there does not seem to be any noticeable advantage, with respect to the pore connectivity, in transforming the amorphous silicas into an ordered structure.

4.3 Comparison of C-18 Bonded Mesoporous Silicas with Varying Pore Structural Data

4.3.1 Introduction

The optimization of chromatographic packing media is still a more or less trial-and error-process, in which the influence of the single parameters on the overall performance of the individual chromatographic column can only hardly be fully evaluated. Recent works on wide-pore silica materials[125] indicate that the chromatographic performance by means of mass transfer resistance is strongly depending upon the specific pore volume of the chromatographic medium. For further investigation of this phenomenon a series of five chromatographic media with different specific pore volumes was produced and, after tight size classification and modification with octadecyl-siloxane groups packed into HPLC-columns by an optimized procedure from the manufacturer EKA Chemicals AB, Bohus, Sweden. The pore system of the spherical materials with a medium particle size of 13 µm and a nominal pore diameter of about 10 nm was characterized in bulk by N_2-sorption measurements at 77 K and by ISEC-measurements in the packed column. The data treatment was performed employing the pore network model developed by Meyers et al.[118] and improved by Grimes et al.[87,119] allowing to calculate the pore connectivity value n_T of the materials. Finally, the chromatographic performance by means of mass transfer resistance was gathered via the recording of the HETP-curves employing phthalates.

4.3.2 Pore Structural Data by Nitrogen Sorption at 77K

The pore system of the packing material was investigated after the surface modification with C18-groups in the bulk phase via nitrogen sorption measurements. Characteristical data like specific surface area a_S after BET[67], specific pore volume v_P according to Gurvitsch[68], pore size distribution and the average pore diameter p_d according to BJH[69] were determined from the following isotherms for all investigated materials.

[125] K.K. Unger, B. Bidlingmaier, C. du Fresne von Hohenesche, D. Lubda; Studies on Surface Science and Catalysis 144, Editors: F. Rodriguez-Reinoso, J. Rouquerol and K. Unger, (2002) Elsevier Science B.V.

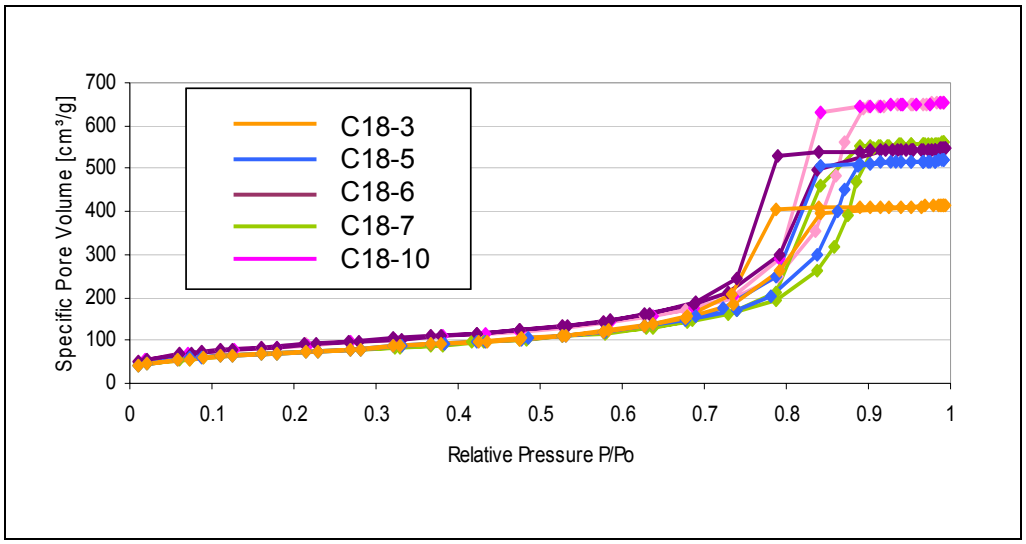

Figure 29: Nitrogen sorption isotherms (measured by manufacturer) at 77 K for C18-3, C18-5, C18-6, C18-7 and C18-10.

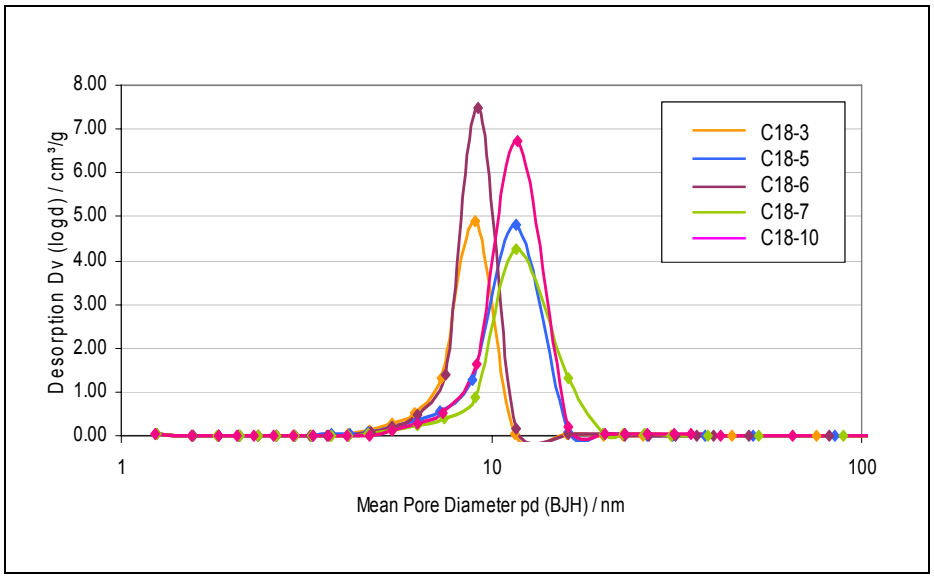

Figure 30: Pore volume distribution of C18-3, C18-5, C18-6, C18-7 and C18-10 obtained from nitrogen sorption measurements.

Figure 29 shows the nitrogen adsorption-desorption isotherms of all five sample being of type IV according to IUPAC classification[61] indicating mesopores. From the desorption branch of the isotherms, the pore size distributions are derived according to BJH and displayed in Figure 30.

The values for a_S / v_P and p_d are listed in Table 11.

Table 11: Pore structural data of C18-3, C18-5, C18-6, C18-7 and C18-10 by nitrogen sorption at 77 K.

sample	a_S (BET) [m^2g^{-1}]	v_p (G) [ml g^{-1}]	p_d (BJH) [nm]
C18-3	262.86	0.6399	7.96
C18-5	263.20	0.8033	9.88
C18-6	319.61	0.8459	8.30
C18-7	259.87	0.8671	10.95
C18-10	318.69	1.0143	10.33

The materials exhibit increasing values for the specific pore volume ranging from 0.64 mlg^{-1} up to 1.01 mlg^{-1}, The materials display nominal pore sizes from 8 nm to 11 nm, giving nearly identical values for materials C18-3 and C18-6 of about 8 nm and for the materials C18-5, C18-7 and C18-10 with 10-11 nm. The BET surface area range is from 260 m^2g^{-1} to 320 m^2g^{-1}, showing similarities between the samples C18-3, C18-5 and C18-7 with about 260 m^2g^{-1} and finally between the samples C18-6 and C18-10 with about 320 m^2g^{-1}.

4.3.3 Pore Structural Data by SEC using polystyrenes Standards employing PPM and PNM

The pore system of the materials was also investigated in the packed column via size-exclusion chromatography in the inverse size mode (ISEC) by applying a series of up to 22 well defined poly(styrene) samples (see Table 88, Appendix 7.3.4) as target analytes in THF as eluent. The data treatment employing the pore network model allows to gather information for the pore size distribution and for the pore connectivity value n_T, as an important criteria for the quality of chromatographic media. All experiments were repeated three times to ensure adequate precision for the experimental size-exclusion data.

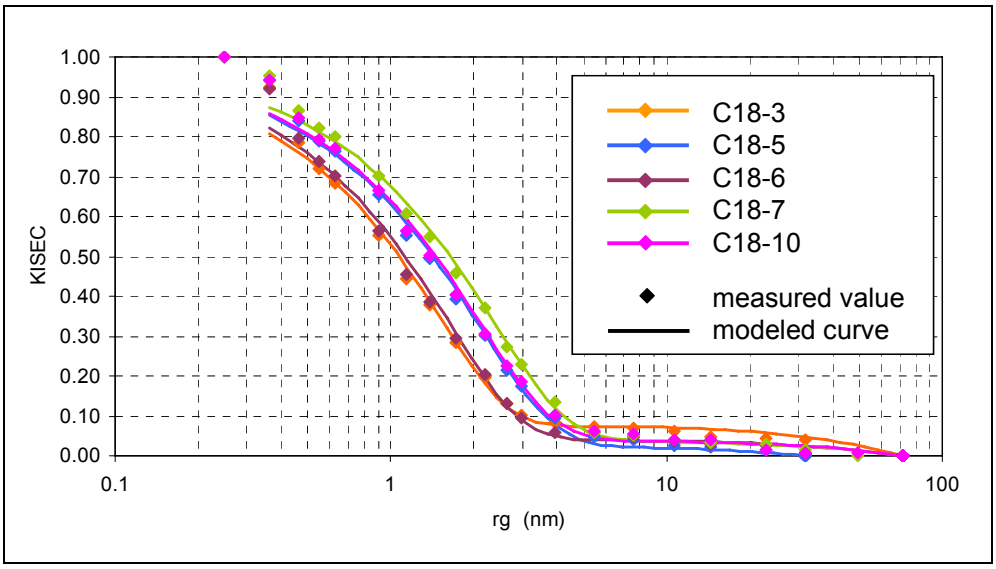

Figure 31: ISEC calibration plots of C18-3, C18-5, C18-6, C18-7 and C18-10.

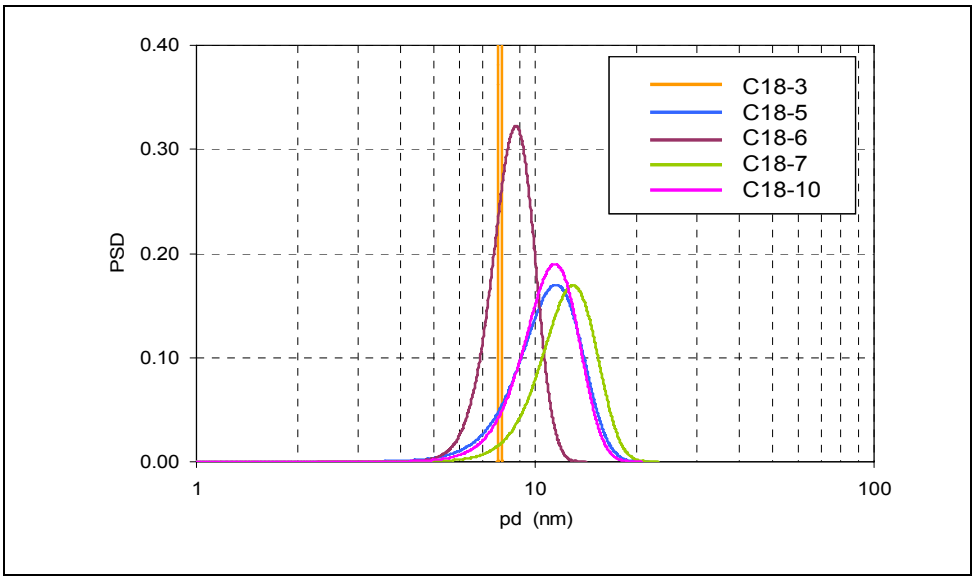

Figure 32: Volume based pore size distribution of C18-3, C18-5, C18-6, C18-7 and C18-10 obtained from PNM of ISEC calibration curves.

Figure 31 shows the experimental data for all five materials in the size-exclusion curves, where the exclusion coefficient K_{ISEC} is plotted against the radii of gyration r_g of the polystyrene standards in THF in nm. All curves show a course with a single distinct exclusion limit, which is typical for materials with monomodal pore size distributions. Also displayed in the figure are the fitted calibration curves based on the pore network model, visualizing the good correlation between theory and experiment. The exclusion limit for all the materials is in the range of 4 nm (MW: 17,900 $gmol^{-1}$, see Table 88). The figures feature two sorts of curves with nearly identical course, pairing the columns packed with the materials C18-3 and C18-6 at a lower exclusion range and the curves for the samples C18-4, C18-7 and C18-10, which are shifted to slightly higher exclusion volumes. This results in the computed volume based pore size distribution curves as derived by the application of pore network modelling upon the size-exclusion data, shown in Figure 32.

Table 12: Pore structural data of C18-3, C18-5, C18-6, C18-7 and C18-10 applied by PNM.

sample	p_d (BJH) [nm]	$p_{d,ave}$ (PPM) by volume [nm]	σ_{pd} by volume [nm]	n_T (PNM)
C18-3	7.96	7.86	0.03	> 10
C18-5	9.88	11.51	2.34	> 10
C18-6	8.30	8.76	1.23	> 10
C18-7	10.95	12.92	2.35	> 10
C18-10	10.33	11.43	2.10	> 10

The values are summarised in Table 12 together with the data from nitrogen sorption measurements showing an excellent agreement between the PSD values obtained from both methods. There is no correlation between the particle porosity data by ISEC and the pore

volume derived by nitrogen sorption experiments. All materials feature the highest possible value for n_T of >10, reflecting an ideal highly interconnected pore system

4.3.4 Chromatographic Performance: theoretical plate height vs. linear flow velocity

The theoretical plate height vs. linear flow dependencies (HETP-curves) for the sample materials were gathered employing dibutyl phthalate as analyte in water/acetonitrile as solvent and repeated three times. The mass transfer kinetics can be derived from the HETP-curves, which are displayed in Figure 33. All HETP curves exhibit the typical progression for well packed columns with a minimum of H [µm] in the range of 3-5 times of the particle diameter d_p (see Table 14), as an indication for well-packed columns and the validity of the data. There is no indication for breakdown of the packing material at higher flow rates.

Table 13: Chromatographic conditions for testing the theoretical plate height vs. linear flow velocity dependency.

column dimension: 150 x 4.6 mm ID; injection volume: 5 µl;
detection: 254 nm; @ room temperature;
flow rate: 0.25 – 5.0 ml/min; k'= 3
analytes: uracil, diethyl phthalate, dibutyl phthalate
mobile phase: water/ACN

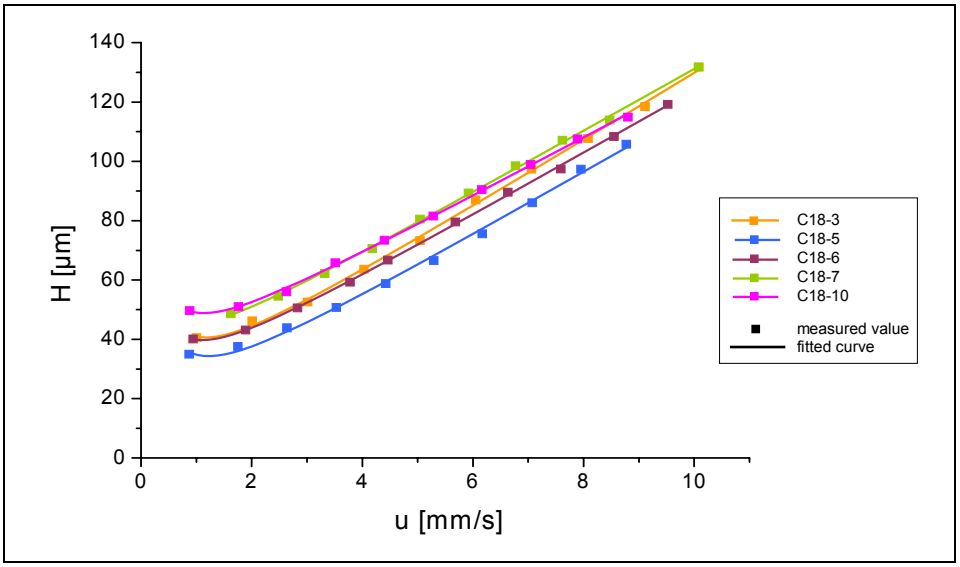

Figure 33: H-vs.-u-plot of C18-3, C18-5, C18-6, C18-7 and C18-10.

Table 14: H-values and C-values of C18-3, C18-5, C18-6, C18-7 and C18-10.

sample	**Plate Height H** [µm] at 1.0 ms^{-1}	**C-term** [ms] according to Knox	**B-term** [$10^{-9}m^2s^{-1}$] according to Knox	**A-term** [$10^{-5}m^{2/3}s^{1/3}$] according to Knox
C18-3	40.94 ± 1	11.4 ± 0.2	15.6 ± 2.5	13.9 ± 1.9
C18-5	35.78 ± 1	10.8 ± 0.3	15.5 ± 2.5	8.0 ± 2.3
C18-6	40.12 ± 1	10.7 ± 0.1	13.3 ± 1.3	16.0 ± 1.1
C18-7	49.49 ± 1	10.5 ± 0.2	10.4 ± 3.6	24.7 ± 2.0
C18-10	49.71 ± 1	10.0 ± 0.2	12.8 ± 1.4	26.1 ± 1.3

The H-vs.-u-plots of the series of columns are displayed in Figure 33. All curves show similar course with only slight differences. Except for column C18-7, the value for the column efficiency is used at the lowest linear flow rate because the minimum in the HETP-curve is not reached. All columns exhibit similar efficiencies of about 40-50 µm at a linear flow velocity of about 1.0 mms^{-1}, indicating very well packed columns, as this is even less than the required factor of 3 from the particle size of 13 µm. Non-linear regression gives for the important mass transfer resistance value C´ in the Knox-equation C´ = 11.4 ms for the C18-3 column, which is in fact the material with the lowest porosity. The column packed with the material of the highest porosity exhibits the lowest mass transfer resistance with C´ = 10.0 ms for column C18-10.

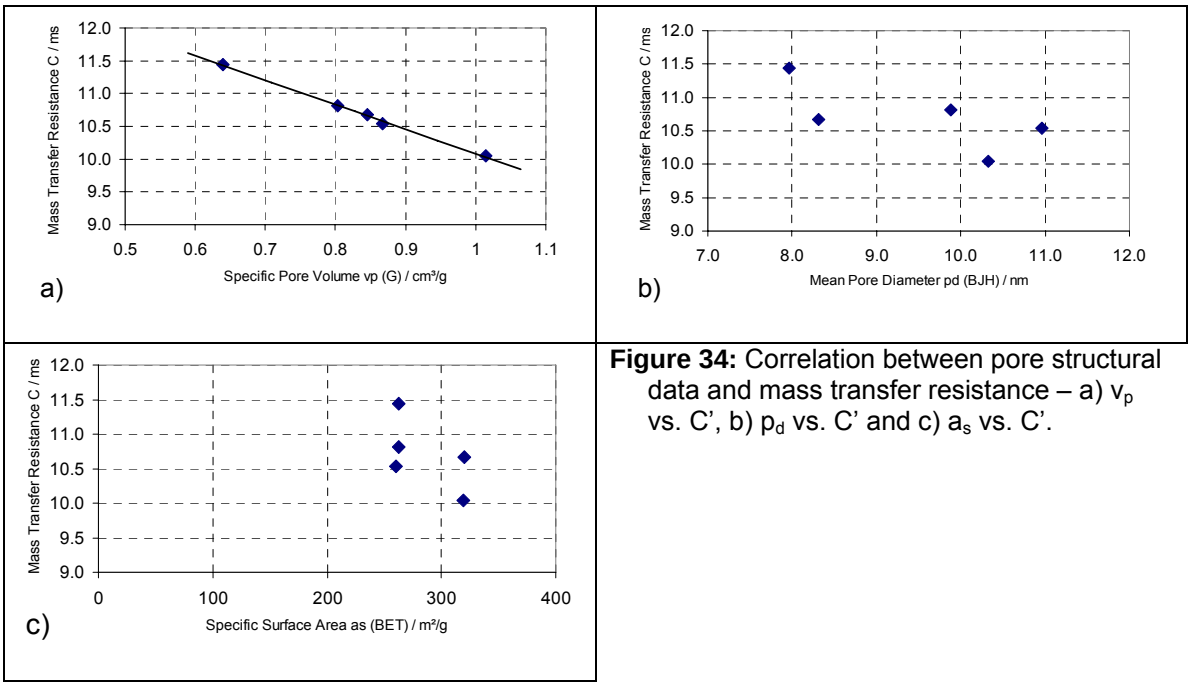

Figure 34: Correlation between pore structural data and mass transfer resistance – a) v_p vs. C', b) p_d vs. C' and c) a_s vs. C'.

In Figure 34a) the specific pore volume is plotted against the mass transfer resistance, showing clearly, that the mass transfer resistance decreases with increasing pore volume. The A´-values derived by non-linear regression should not be used for interpretation, because the minimum of the HETP-curves is not reached and therefore the error in these values is much too high for interpretation of the data.

The pore diameter is plotted vs. the mass transfer resistance value in Figure 34b) indicating that there is no correlation between these values, as the radius of the employed probe molecules is much smaller than the pore radius.

Also there is no correlation between the C´ value and the BET-surface area, which is shown in Figure 34c).

4.3.5 Summary

The pore system of a series of reversed phase materials with increasing pore volume was investigated in bulk phase and in the packed column via nitrogen sorption measurements and inverse size-exclusion experiments and compared with the chromatographic performance of the columns by means of HETP-curves of dibutyl phthalate. The investigations showed a direct relationship between the mass transfer resistance and the porosity of the material. By increasing the pore volume from 0.64 ml/g to 1.01 ml/g the mass transfer resistance is lowered from 11.4 ms to 10.0 ms, which can also be seen in a less steep slope of the HETP-curve, lowering from 11.2 ms to 9.5 ms.

Further relationships between other parameters like the BET-surface area or the pore diameter could not be observed. This is also true for the pore connectivity value, which is for all of the investigated materials the same with n_T >10, representing the highest possible value.

The agreement between the values for the specific pore size value derived by nitrogen sorption measurements and by ISEC was very good, although all materials were C18-modfied, which obviously doesn't affect the validity of the data in this case.

4.4 Investigation of the Swelling-Effect of Poly(methacrylate)-Coated Silicas

4.4.1 Introduction

Conventional methods for the investigation of the pore system of porous solids are usually applied upon evaporated samples. Although this works sufficiently well in the case of rigid structures like porous silica gels, elastic porous structures like polymers or polymer-coated silica gels cannot be characterized adequately via this pathway as the pore system may be collapsed in the vacuum. In the case of nitrogen sorption measurements even the building of the mufti-layers may be hindered, leading to faulty results for the characteristical data.

Another problem, which cannot be addressed by conventional methods is the change of the pore system due to swelling of polymer resins, respectively, polymer coating of chromatographic materials, which may result in different pore size, when the polarity of the eluent changes. By probing the pore system of a porous material via ISEC in solvents with different polarities, the relevance of this undesirable effect for chromatographic applications may be evaluated.

For the evaluation of this effect, a series of polymer-coated silica materials with increasing polymer load was produced (see 5.3.4). The polymer load was characterized by thermogravimetric analysis and elemental analysis. The initial wide-porous silica material LiChrospher™ WP 300 (Batch No. ATP107g, Merck KGaA, Darmstadt, Germany) was coated with a polymer layer based on 50/50 % (n/n) monomer composition of 2-HEMA/EMA and 10 % (n/n) EDMA as cross-linker. All materials including the initial silica source were investigated in bulk by nitrogen sorption measurements at 77 K and in the packed column via ISEC with poly(styrenes) in tetrahydrofuran, dioxane and dimethylformamide employing solvents with different polarities (see Table 16).

4.4.2 Pore Structural Data by Nitrogen Sorption at 77K

Nitrogen sorption measurements were employed to gain pore structural data of the materials in the dry state. Characteristical data like specific surface area a_S corresponding to BET[67], specific pore volume v_P according to Gurvitsch[68], pore size distribution and the average pore diameter p_d according to BJH[69] were determined from the isotherms for the basic silica and the series of polymer-coated materials:

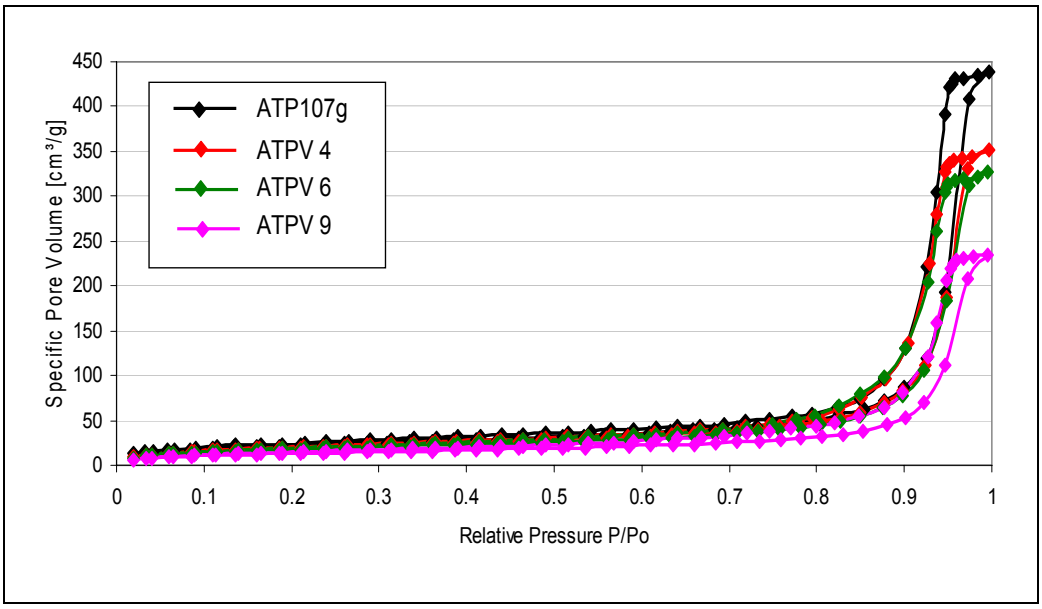

Figure 35: Nitrogen sorption isotherms at 77 K of unmodified silica ATP107g and modified silicas ATPV 4, ATPV 6 and ATPV 9.

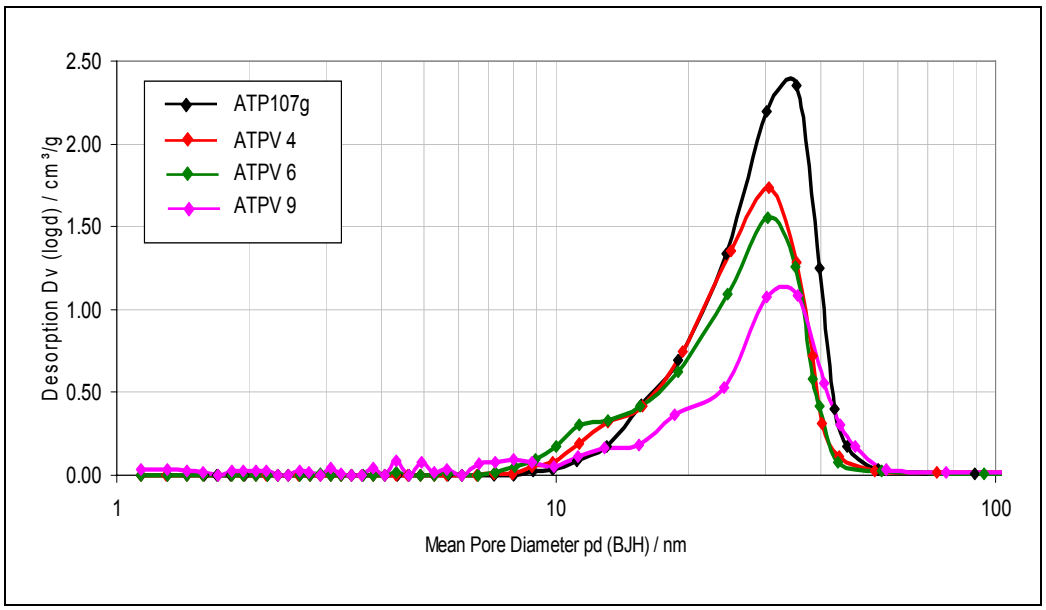

Figure 36: Pore volume distribution of unmodified silica ATP107g and modified silicas ATPV 4, ATPV 6 and ATPV 9.

Table 15: Pore structural data of unmodified silica ATP107g and modified silicas ATPV 4, ATPV 6 and ATPV 9.

sample	a_S (BET) [m^2g^{-1}]	v_p (G) [ml g^{-1}]	p_d (BJH) [nm]
ATP107g	79	0.701	30.2
ATPV 4	70	0.565	30.5
ATPV 6	63	0.524	30.3
ATPV 9	46	0.378	30.1

Figure 35 shows that the nitrogen adsorption-desorption isotherms of all four sample materials are of type IV according to the IUPAC classification[61] indicating mesopores. The desorption branch of the isotherms is the base for the pore size distributions according to BJH, which are displayed in Figure 36. Table 15 summarises all the characteristic data gained from the nitrogen sorption measurements like a_S, v_P and p_d. While the nominal pore size p_d is not changed significantly by the polymer coating with a value of approx. 30 nm for all samples, the other parameters significantly decrease with increasing polymer load. The unmodified silica material (ATP107g) displays the highest values with a specific pore volume v_P = 0.701 mlg^{-1} and a specific surface area a_S = 79 m^2g^{-1}. Polymer-coated materials with 4.55% (ATPV 4), 5.82% (ATPV 6) and 9.15 % (ATPV 9) carbon content feature a surface area of 70, 63 and 46 m^2g^{-1}. The specific pore volume decreases in the same direction with values of 0.565, 0.524 and 0.378 mlg^{-1}.

4.4.3 Pore Structural Data by SEC using Polystyrene Standards employing PPM and PNM

To probe the pore system of the materials in the swollen state, the materials were packed into chromatographic columns (see Appendix 7.3.2) and investigated via size-exclusion chromatography in the inverse size mode (ISEC) by applying a series of up to 22 well defined polystyrene samples (see Table 88, Appendix 7.3.4) as target analytes. Additionally to the usually employed eluent THF, DMF and dioxane were used to check if there is a noticeable swelling effect of the polymer coating upon the effective pore size of the packing material by changing the polarity of the eluent. The data treatment employing the parallel pore model to gather information for the pore size distribution and the pore network model allows for the pore connectivity value n_T, as an important criteria for the quality of chromatographic media. All experiments were repeated three times to ensure adequate precision for the experimental size-exclusion data.

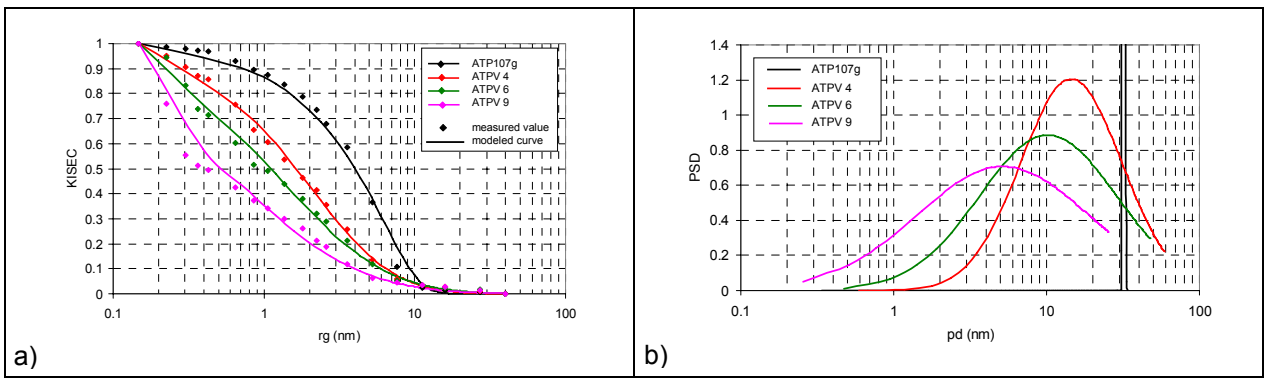

Figure 37: ISEC measurements with dioxane of unmodified silica ATP107g and modified silicas ATPV 4, ATPV 6 and ATPV 9 – a) calibration plots and b) volume based pore size distribution obtained by PPM.

Figure 37a) shows the experimental data of the initial silica material and the polymer-coated silicas in dioxane as the most unpolar eluent, where the exclusion coefficient K_{ISEC}, is plotted against the radii of gyration r_g of the polystyrene standards in dioxane in nm. All curves show a course with a single distinct exclusion limit, which is typical for materials with monomodal pore size distributions. Also displayed in the figure are the fitted calibration curves based on the parallel pore model, visualizing the good correlation between theory and experiment. The initial silica exhibits the highest exclusion curve, which is stepwise degrading with increasing polymer load. This is visualized in Figure 37b) where the computed pore size distributions are displayed, showing a steep decrease of the pore size of the materials by increasing the polymer load. The exact values of the characteristic data are summarized in Table 16.

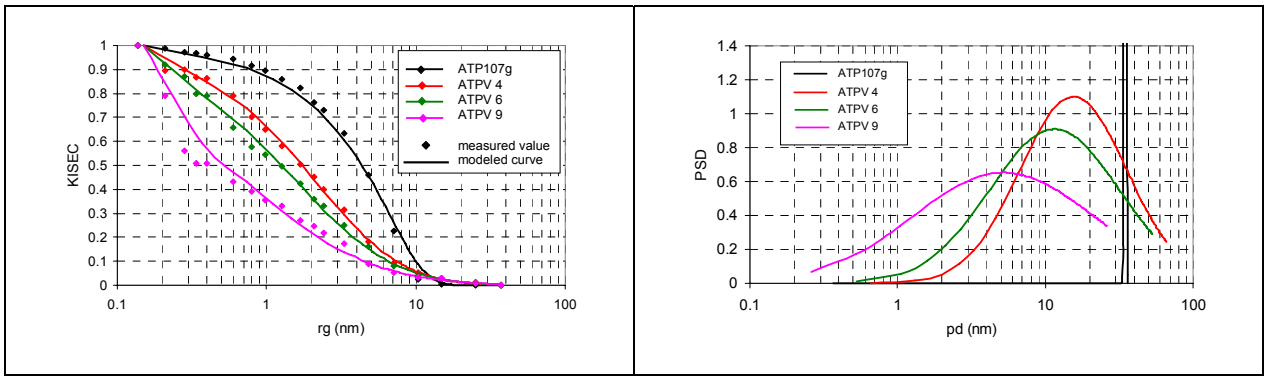

Figure 38: ISEC measurements with THF of unmodified silica ATP107g and modified silicas ATPV 4, ATPV 6 and ATPV 9. – a) calibration plots and b) volume based pore size distribution obtained by PPM.

Figure 38 show the analogous data for the medium polar solvent THF, with a similar course of the SEC-curves and comparable pore size distributions. All values are summarized in Table 16.

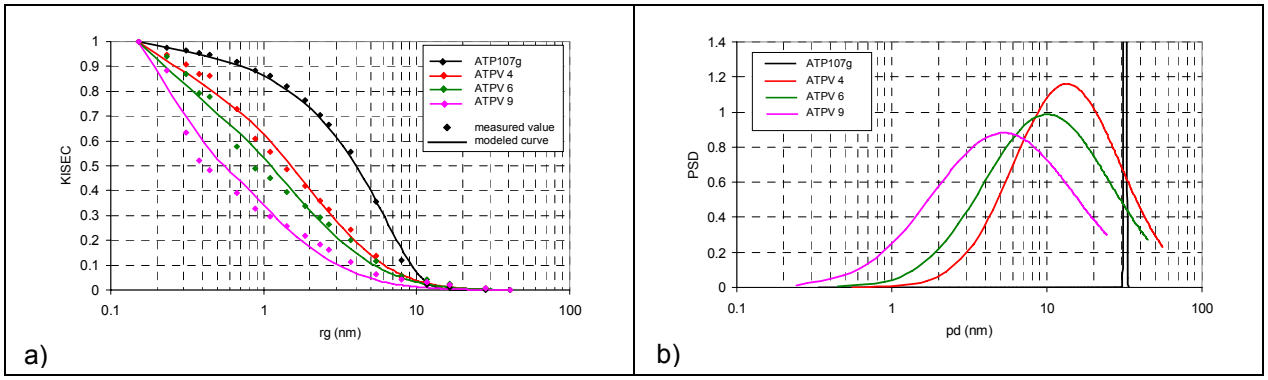

Figure 39: ISEC measurements with DMF of unmodified silica ATP107g and modified silicas ATPV 4, ATPV 6 and ATPV 9. – a) calibration plots and b) volume based pore size distribution obtained by PPM.

The data of the ISEC measurements in DMF as the most polar solvent of this series is displayed in Figures 39 exhibiting very similar courses of the SEC-curves and of the computed pore size distributions as the values gained in less polar solvents. The exact figures are given in Table 16.

Table 16: Pore structural data of unmodified silica ATP107g and modified silicas ATPV 4, ATPV 6 and ATPV 9 applied by PPM.

sample	p_d (BJH) [nm]	$p_{d,v,ave}$ (PPM) [nm] using dioxane rel. polarity[126] 0.164	$p_{d,v,ave}$ (PPM) [nm] using THF rel. polarity[126] 0.207	$p_{d,v,ave}$ (PPM) [nm] using DMF rel. polarity[126] 0.404	n_T (PNM)
ATP107g	30.2	32.0 ± 1.0	34.6 ± 1.0	32.0 ± 0.6	> 10
ATPV 4	30.5	10.8 ± 0.6	11.0 ± 0.6	9.8 ± 0.8	> 10
ATPV 6	30.3	6.0 ± 0.8	7.0 ± 0.6	6.6 ± 0.8	8.2
ATPV 9	30.1	2.2 ± 0.6	2.0 ± 0.6	3.0 ± 0.8	3.6

Table 16 summarizes all the values gained by ISEC measurements revealing a strong decrease in the nominal pore size value of the chromatographic material with increasing polymer load. The 30 nm pores constrict to 11 nm even by applying a polymer coating with a resulting 4.55 % (ATPV 4) carbon content. A polymer load with 5.82% (ATPV 6) and 9.15 % (ATPV 9) carbon content constricts the pore size to ~7 and ~2 nm, find the carbon content in Table 44. Furthermore the pore connectivity value n_T is decreasing from an ideal value of n_T = >10 for the initial silica ATP107g and the material with 4.55 % carbon content to - a still acceptable value - n_T = 8.2 for the sample with 5.82 % carbon content down to 3.6 for the material with the highest polymer load 9.15%.

With the exception of the values for the unmodified silica, there is a large discrepancy for the values of the nominal pore size derived by nitrogen sorption measurements and those derived from ISEC measurements, indicating pore systems with much smaller pore diameters in the wetted state due to the swelling of the polymer coating in the presence of solvents.

On the other hand, the pore size distributions of the polymer-coated sample materials derived by ISEC-measurements do not differ significantly between the used solvents, indicating that the thickness of the polymer coating is not affected by the change of the solvent polarity in the investigated range.

4.4.4 Summary

The investigation of the pore system of poly(methacrylate) coated silica samples reveals a large discrepancy between the data obtained by nitrogen sorption measurements and those obtained by inverse size-exclusion experiments, although both methods give similar results in the case of the unmodified silica material.

[126] Christian Reichert, Solvents and Solvent Effects in Organic Chemistry, VCH Publishers, 2nd ed. (1988)

Nitrogen sorption measurements indicate that the pore size of the initial silica material is not affected by the polymer coating, while the specific surface area as well as the pore volume is decreasing with increasing polymer load.

Inverse size-exclusion experiments reveal a strong decrease of the nominal pore size with increasing polymer load. Furthermore the application of the pore network model shows the worsening of the pore connectivity value with increasing polymer load.

The poor chromatographic performance of the polymer-coated materials (see 5.3.4.4) with high polymer content can be very well explained with the values obtained via inverse size-exclusion experiments: all of the important values like the nominal pore size and the pore connectivity are strongly decreasing with increasing polymer load. On the other hand, the data obtained via nitrogen sorption experiments does not give sufficient arguments for the poor chromatographic performance of the polymer-coated materials, as this method only exhibits a decrease of the specific pore volume with increasing polymer load, while the nominal pore size data does not change with increasing polymer load.

Furthermore, the application of size-exclusion chromatography in solvents with different polarities shows that the swelling of the investigated polymer coating is negligible in the investigated polarity range. This allows deducing, that the percentage of the cross-linker in the polymer layer is high enough to produce a rigid structure as important information for the optimization of the polymer coating.

4.5 Conclusion

Micelle-templated silica (MTS) are expected to be highly ordered MCM-type of materials with a very narrow pore size distribution, made out of porous silica under full prevention of the original particle shape. This is expected to lead to an improved chromatographic performance with the increase of the order of the pore size values. One commercial silica and one highly porous stationary phase material was transformed into MTS and packed into chromatographic columns. The morphological investigations show that this process does not fully conserve the original particle shape, as the particle size distribution is significantly broader than the one of the initial silica. While MTS1 based on small-porous silica showed a narrow pore size distribution with larger pores and pore volume than the original material, the transformation of wide-porous silica into MTS2 was not complete, leading to a material with a tri-modal pore size distribution, smaller pores and a smaller pore volume. All pore structural data of MTS1 are higher than those of the initial silica, which is also true for the sharpness of the pore size distribution, which is increased by the transformation procedure. The opposite is detected in the case of MTS2, where the mean pore size and specific pore volume are lowered plus a decrease in order is detected with a tri-modal pore size distribution although

the pore connectivity value is slightly increased. Only specific surface values are increased in both cases. Although the transformation process improves all chromatography-related pore structural values of MTS1, no significant change of the chromatographic performance by means of mass transfer can be observed. The small worsening of the theoretical plate height values is related with the broader particle size distribution of MTS1. In the case of MTS2 the chromatographic performance is inferior to the one of the initial silica, which is highly expected as all chromatography-related pore structural values are worsened plus a broadening of the particle size distribution occurs during the transformation process.

In conclusion, no positive effect of the higher order upon the chromatographic performance by the transformation process was detected and there might even be a negative effect from the higher pore structural order, as MTS1 shows no improvement in the chromatographic performance at all compared with the initial silica. Further investigations on a larger variety of materials have to be performed to clarify this issue, as the MTS-materials presented here are not representative enough.

A set of C18 coated chromatographic materials, tightly classed and packed in chromatographic columns by the manufacturer EKA Chemicals AB, Bohus, Sweden was used for the investigation of the relation between pore structural parameters and chromatographic performance. The materials exhibited distinct but small variations in the values of mean pore size, pore volume and surface area, while the morphological properties were kept constant. While no impact of the specific surface area or the pore diameter upon the chromatographic performance of small molecules was detected, the mass transfer values benefit much from an increase of the specific pore volume. ISEC-measurements agree very well with the results obtained from the nitrogen sorption method and show an ideal pore connectivity value $n_T > 10$ for all materials.

In conclusion, a direct impact of the pore volume upon the chromatographic performance could be shown, where the mass transfer value benefits much from an increasing pore volume, while no influence from the pore size values or the specific surface area can be deduced from the experimental values.

The investigations on polymer-coated stationary phases reveal that the pore structural values obtained by ISEC give a much more realistic impression of the pore system, than those obtained by nitrogen sorption measurements, which do not show any impact of the polymer load upon the mean pore diameter or surface area. Only the specific pore volume values derived by nitrogen sorption measurements are affected by the polymer load.

In principle, ISEC is furthermore able to detect swelling effects of polymers by changing the polarity of the eluent. The investigated polymer-coated stationary phases show no swelling effect in the investigated polarity range of eluents, which may be due to a high

cross-linker content of the polymer layer. The data obtained by ISEC reveal furthermore a strong decrease of the mean pore diameter and of the pore connectivity value with increasing polymer load, which will negatively influence the chromatographic performance. The initial pore size value of the materials is reduced to one third of the original value by applying a polymer generating 4.55 % of carbon content, which might be an issue for the separation of large molecules.

The investigations reveal an excellent agreement of pore structural data derived from nitrogen sorption experiments as reference method with those obtained by size-exclusion chromatography in the inverse mode (ISEC) for native and C18-coated silica-based stationary phases. Only in the case of multimodal pore size distributions like for the MTS2-material, the values differ significantly. The data treatment used for ISEC was in the state of development and limited to fit only monomodal pore size distributions, although the derived average gives a "real-life-value" for chromatographic applications. ISEC probes the pore system in contact with a mobile phase in a working chromatographic environment, while nitrogen sorption or other measurements probe the pore system in evaporated bulk phase. Additionally, and in some cases even more important, ISEC allows determining the pore connectivity value, which may be a useful criterion for the evaluation of stationary phase materials.

5 CASE STUDY B: SURFACE FUNCTIONALIZATION OF MESO POROUS AND MACRO POROUS SILICAS WITH BONDED POLY(METHACRYLATES)

5.1 Preface

Commonly used stationary phases for reversed phase HPLC are based on hydrophobic coated porous silica materials. These materials offer excellent chromatographic properties with high efficiency for typical analytical applications. They generate very well separations for biopolymers, too, because of strong interactions between the alkyl-chains of the coating and hydrophobic parts of proteins and peptides. But this strong hydrophobicity also induces a high tendency for denaturation of biopolymers - so proteins may be well separated, but leave the chromatographic column in a biologically inactive state.

In previous works it could be shown that medium hydrophobic phases exhibit promising properties for the separation of proteins by means of lower denaturation potential. Porous particulate materials based on porous and highly cross-linked poly(hydroxyl-ethylene-methacrylate) (HEMA) are widely used as stationary phase for gel permeation chromatography of biopolymers in hydrophilic or aqueous media, but these materials cannot be used in HPLC because of their very low efficiency and sensitivity about changes of the mobile phase due to their lack of stability. Approaches to overcome this problem are based on the coating of pre-polymerized methacrylates onto the rigid skeleton of chromatographic silica employing physisorption methods[33,34,38]. The main advantage of using poly(methacrylates) is their tunable hydrophobicity by adjusting the co-monomer composition, as methacrylates are available in a wide range of hydrophobicitys[127,128]. The final coated materials offered very promising chromatographic properties for the separation of biopolymers but lacked of thermal and chemical stability due to the physisorption procedure.

Further development of these phases had therefore to be based on a coating procedure that enables one to produce a covalently bonded polymer layer onto the surface of the silica support, which was one important part of this work. Special attention had to be paid towards issues like reproducibility of the whole synthesis route and the tuneability of the coating by means of polymer load and polymer composition for tuning of the hydrophobicity. All properties of the polymer-coated material should then be optimized for the use in chromatographic applications by means of adsorption capacity, mass transfer resistance, efficiency and the biocompatibility of the stationary phase.

Especially for the last feature no established method is given in the literature, demanding the development of a test for the biocompatibility of stationary phases as another task for this

[127] M. Hanson, K.K. Unger, C.T. Mant, R.S. Hoges, J.Chromatogr. 599 (1992) 65-75
[128] M. Hanson, K.K. Unger, C.T. Mant, R.S. Hoges, J.Chromatogr. 599 (1992) 77-85

work. The first indications towards a lower denaturation potential of medium hydrophobic stationary phases are based on a chromatographic test procedure with lysozyme, myoglobine and cytochrome C. The LCM-test-procedure gives only indirect information, where the denaturation of the proteins is deduced from changes in the retention time, but no structural investigations of the proteins after passing the chromatographic run were performed. As alternative to a complex structural characterization of a protein, its biological activity can also be used as a 'real-life-method' for the determination of the denaturation potential of a stationary phase. The implementation of this approach was followed by the application of an enzyme as biopolymer in a chromatographic run and determination of its enzymatic activity afterwards. This allows the generation of an enumerable criterion for the denaturation potential of a stationary phase, enabling the quantitative comparison and optimization of packing media.

5.2 Synthesis

5.2.1 Introduction

A reproducible and dense coating of porous support materials with a polymer layer can best be performed by a grafting-from approach, where the polymerization is started from a surface-bound initiator-group. Small monomer molecules possess negligible diffusion barriers and can easier reach the intraparticle space than the large macromolecules required for grafting-to approaches[129]. Furthermore an excellent binding of the polymer coating onto the substrate is obtained as the surface-bound initiator-groups start the polymer chain, which is then also covalently bound to the support-material. The crafting density of this method can typically be controlled by the amount and concentration of monomer in the solution. The synthesis must be performed in dry nitrogen atmosphere as oxygen terminates the radical polymerization. As the polymerization procedure should be performed on both particulate and monolithic silica, only initiator groups like azo-initiators, which can be started under mild thermally conditions, should be used.

The main disadvantage of this method is mainly due to the usually difficult way for the synthesis of the surface-bound initiator group. The covalent binding of the initiator group onto the substrate involves multiple step reactions, which sometimes have a poor reproducibility, resulting in a low grafting density of the initiator. Another problem is due to the splitting of the initiator resulting in two active radicals, of which only one is surface-bound. The other consists of a small volatile molecule that may start a polymer chain reaction in solution. Strategies to overcome this problem involve a one-step-coupling reaction of the azo-initiator or using a mono-functional initiator-group. A monomer-solution with cross-linker molecules

[129] I. Luzinov, I. Evchuk, S. Minko, S. Voronov, J.Appl.Polym.Sci. 67 (1998) 299

can also prevent the production of unbound polymer chains as they hardly can leave the pore system of the substrate and will be inter-grown with the surface-bound polymer layer.

5.2.2 Synthesis Route

5.2.2.1 Survey on the Work Flow of Experiments

For a better understanding of the meaning and sequence of the extended number of experiments it appears to be advisable to introduce the following scheme of the work flow including the aims of the particulate studies. In chapter 6, Discussion and Outlook, a similar scheme will be presented for a brief summerize of the results.

Chapter	Action	Aim	Page
5.2.	**Assessment of the basics of the synthesis**		71
5.2.2.2	Selecting the way of binding the initiator group to the silica surface	Finding the optimum way to bind the polymer layer to the support	73
5.2.2.3	Polymer bonding aspects and kinetics of the polymerization procedure	Controlling the polymerization step as key parameter for best reproducibly of the coating procedure	81
5.2.2.4	Reproducibility of the synthesis procedure	Manifesting the most important parameter at a surface reaction	89
5.2.2.5	Up scaling the synthesis procedure	Extending the batch size while maintaining the product properties	90
5.2.2.6	Transfer of the recipe to other brands of silicas	Is the coating procedure transferable to other silica sources and are there notable differences in the product properties when changing the support material?	92
5.3	**Optimization of the reaction composition, reaction route and reaction conditions with respect to enhanced column performance, maintenance of bioactivity and biorecovery**		93
5.3.3	Adjustment of the hydrophobicity of the polymer layer	Choosing the right surface composition with regard to high biorecovery and low denaturation potential towards selected proteins	98
5.3.4.	Variation of the polymer load	Avoiding pore blocking effects and drastic reduction of mass transfer kinetics	118
5.3.5.	Adjustment of the linker density	Can the linker density affect the results of the chromatographic performance at otherwise constant conditions?	127

5.2.2.2 Binding of the Initiator Group onto the Silica Surface

5.2.2.2.1 State of the Art

The initiator group plays an important role in each polymerization reaction, as it delivers the radicals to start the polymer chain reaction, affecting both the reaction rate and the molecular weight of the polymer. Depending on the nature of the initiator-group, the radical production can either be initiated thermally or by UV-radiation, where the number of generated radicals is depending on the intensity of the radiation respectively the temperature, the concentration of the initiator and the number of radicals produced by the decomposition of each initiator molecule. All these parameters can easily be adjusted as long as the reaction takes place in liquid phase and a large variety of initiators can be used. A polymerization via the grafting-from-approach is more difficult to adjust, as it requires a surface bound initiator-group, which is in first place quite difficult to synthesize. Another experimental issue is the control and adjustment of the initiator concentration on the surface of the substrate, which affects the reaction rate, the connection of the polymer layer onto the surface and the homogeneity of the polymer layer.

Different principles are employed for the initiation of a radical polymerization from the surface of a substrate ranging from physically attached initiator-groups to covalently bound initiator-groups, which even can be “immobilized” by means of multiple bonds per initiator molecule, which prevents the formation of unbound radicals, which may initiate a polymer chain reaction in solution[130]. As only covalently bound initiator groups offer the ability of generating chemically attached polymer layers onto the surface of a substrate, the further work is based on the implementation of this principle.

[130] A. Guyot, P. Hodge, D.C. Sherrington, H. Widdecke, React. Polym. 16 (1991/1992) 233-259

The synthesis of a covalently bound initiator group upon the surface of a silica-based substrate can either be performed in a two or multiple step-reaction by first attaching an anchor-molecule onto the surface and then coupling the initiator group, or by synthesizing an initiator-group, which is able to be coupled directly onto the silica surface. The most often applied method is based on a multiple step mechanism, which was introduced by Challa et al.[131]. Some authors depicted issues with side reactions, leading to poor initiator concentration and bad reproducibility[136]. Especially the use of aminoalkylsilanes in the coupling reaction may lead to multiple layers[132].

Guyot[133] and Boven[134] reported the grafting of 4,4'-Azobis-(4-cyano-pentanoic-acid) (ACPA) onto a silica-substrate with covalent bonds in a two-step reaction (see Figure 40). The method generates reproducible layers with high grafting yields, enabling the initiation of polymer chains with high molecular weight:

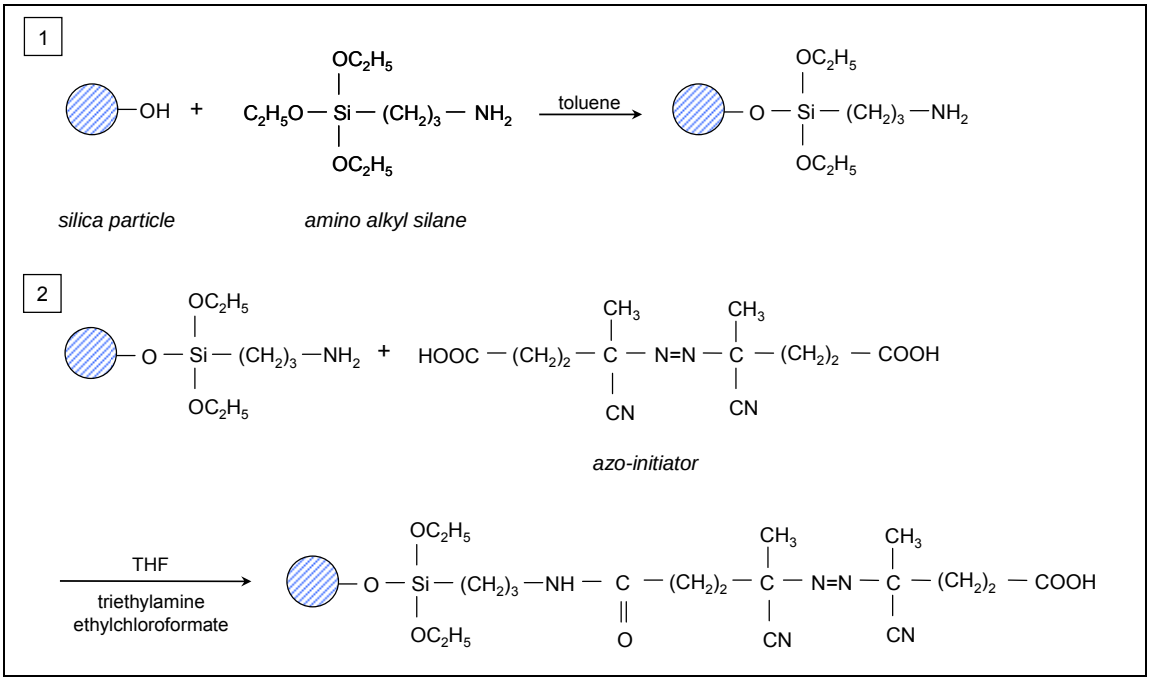

Figure 40: Covalent binding of 4,4'-Azobis-(4-cyano-pentanoic-acid) (ACPA) onto amino alkyl silane modified silica-substrate.

Another successful grafting of silica-based substrates with azo-initiator groups was done by Tsubokawa[135] and repeated by Sulitzky[136] (see Figure 41). The first step is the immobilization of the anchor-group glycidoxypropyltrimethoxysilane (GPS) onto a rehydroxylated silica substrate, which requires the heating in toluene up to reflux for 8 hours.

[131] J.P.J. Verlaan, J.P.C. Bootsman, G. Challa, J.Mol.Catal. 14 (1982) 211
[132] O. Prucker, J. Rühe, Macromolecules 31 (1998) 602
[133] E. Carlier, A. Guyot, A. Revillon, M.-F. Llauro-Darricades, R. Retiaud, React.Polym. 16 (1991/1992) 41
[134] G. Boven, M.L.C.M. Oosterling, G. Challa, A.J. Schouten, Polymer 31 (1990) 2377
[135] N. Tsubokawa, A. Kogure, K. Maruyama, Y. Sone, M. Shimomura, Polym. J. 22 (1990) 827-833
[136] C. Sulitzky, PhD Thesis, Johannes Gutenberg University Mainz (2002)

Afterwards, the silica gel is extracted with methanol in a Soxhlet-apparatus for 24 hours and then dried under vacuum at room temperature.

In the second reaction step, the azo-component is inserted by the addition of ACPA. The reaction is performed in DMF at 50 °C for 5 hours. The final product is obtained after washing with methanol and drying in vacuum at room temperature:

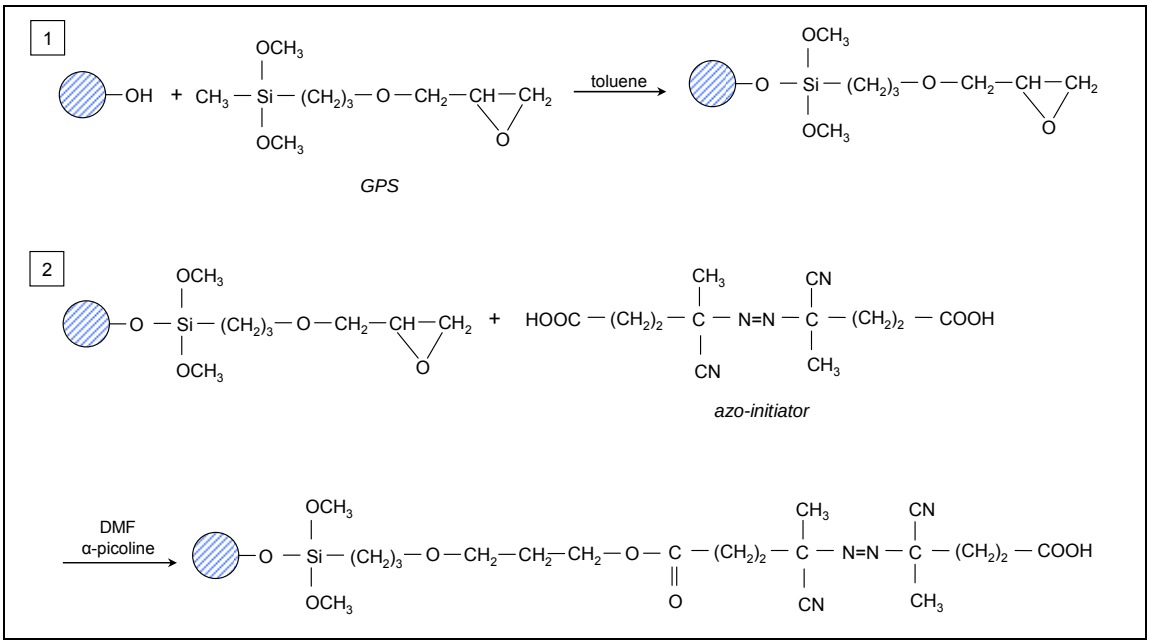

Figure 41: Covalent binding of 4,4'-Azobis-(4-cyano-pentanoic-acid) (ACPA) onto GPS modified silica-substrate.

Rückert[56] was using p-(chloromethyl)phenyltrimethoxysilane as anchor-group. The reaction is performed in THF for 50 hours at 60 °C on a freshly rehydroxylated silica support. The product is then washed with THF and dried in vacuum at 40 °C. By this procedure a complete occupancy of the silica substrate could be achieved.

The coupling of the azo-initiator was performed employing ACPA in THF 50 °C for 5 hours, where α-picolin was employed as catalyst and to remove the formed hydrochloric acid:

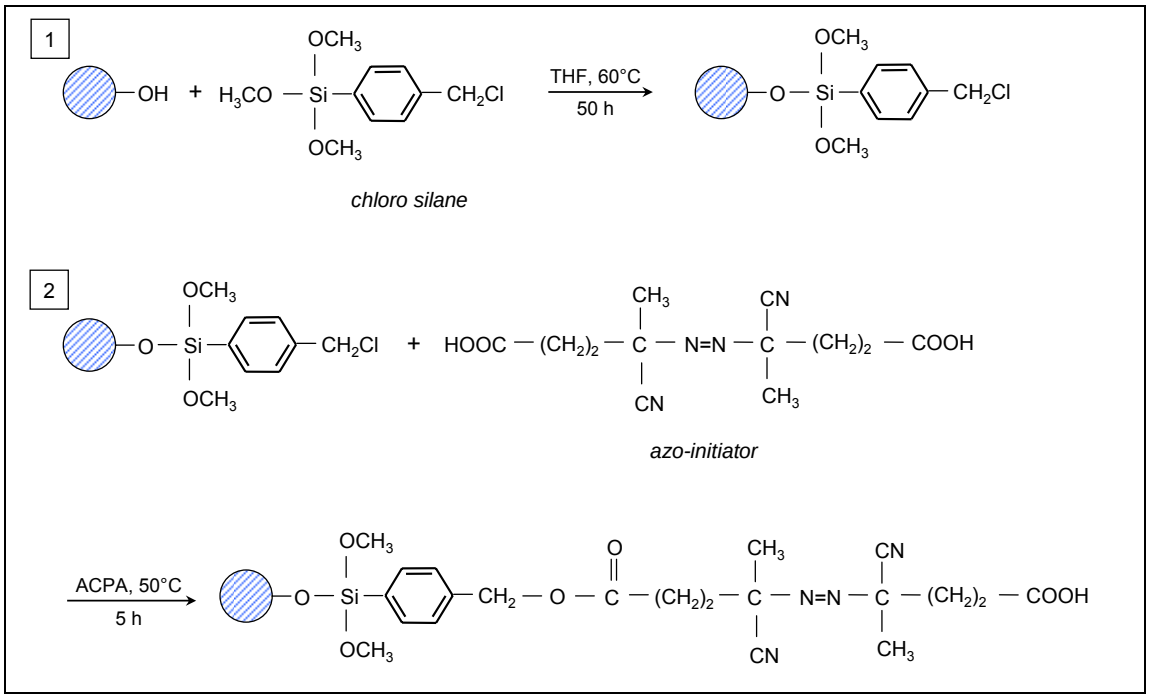

Figure 42: Covalent binding of 4,4'-Azobis-(4-cyano-pentanoic-acid) (ACPA) onto chloro-silane modified silica-substrate.

Rühe et al.[55] reported on the successful coupling of an initiator group as self-assembled monolayer onto a high surface area silica as well as on planar silica substrates in a one-step-reaction (see Figure 43). Therefore it was possible to achieve brush-type, well-defined polymer coatings and to further investigate both the self-assembly process[137] and the polymerization via the grafting-from approach[132]. The synthesis of this initiator involves a multiple-step reaction with a poor overall yield of the final chlorosilane, which contains the azo group. The coupling of the final initiator is then carried out under mild conditions in dry toluene at room temperature for 12 hours in the presence of pyridine. After a thorough washing procedure and drying in vacuum, the final product is obtained:

[137] O. Prucker, J. Rühe, Langmuir, 14 (1998) 6893-6898

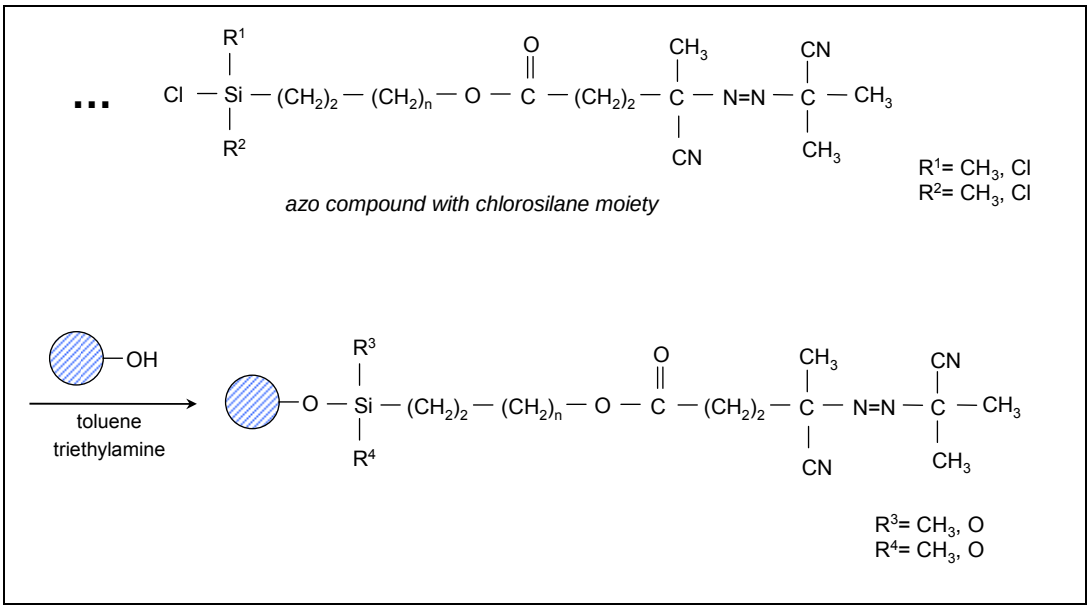

Figure 43: Coupling of azo compound with the chlorosilane moiety onto the silica surface.

5.2.2.2.2 Synthesis Procedure

In this part of work, the aim was the reproducible and uniform coating of chromatographic support materials with an initiator group. As not only particulate silica had to be modified, but also monolithic support materials should be evaluated, a method had to be chosen, that allows also the modification in the packed bed. Furthermore, the costs should be kept in mind, as the resulting material may be interesting for commercial use. By applying these criteria, the method used by Rückert[56] was chosen for further development, which offers a good reproducibility and high grafting density under mild conditions. The original method was optimized for the coating of a large pore material with a small surface area to give a maximum grafting density. In the case of medium-pore materials, this leads to a distinct reduction of the pore volume, therefore the method was optimized to generate ca. 20 % of the theoretical grafting density. This could be achieved mainly by lowering the temperature down to room temperature and limit the amount of anchor-groups.

The grafting of the azo-initiator is done by the following procedures (see Figure 42):

First the rehydroxylation of the initial silica is done (see Appendix 7.1.3.1). After the rehydroxylation step, the amount of silanol groups was determined by thermo gravimetric analysis (TG). Based on this measurement, the amount of p-(chloromethyl) phenyltrimethoxysilane is determined for the grafting of the silica with the anchor-group. The reaction is done at room temperature (see Appendix 7.1.3.2). Afterwards the binding of the azo-initiator-group 4,4'-azobis-(4-cyano-pentanoic-acid) (ACPA) is done via base-catalyzed estherification (see Appendix 7.1.3.3).

All intermediate products were characterized by elemental analysis, thermogravimetric measurements and nitrogen sorption measurements.

Table 17: Elemental analysis of the initial silica ATP107g, silane modified ATPSV 0 and azo modified ATPAV 0.

sample	modification	%C (w/w)	%H (w/w)	%N (w/w)
ATP107g	-	0.13	0.46	< 0.01
ATPSV 0	silane	1.44	0.77	< 0.01
ATPAV 0	azo	2.76	0.43	0.73

Table 17 shows the results of the elemental analysis for some exemplary samples. The figures exhibit a good agreement between the calculated values and the experimental data, indicating a complete reaction of ACPA with the anchor groups. Nearly identical values between different samples show the good reproducibility of the synthesis procedure.

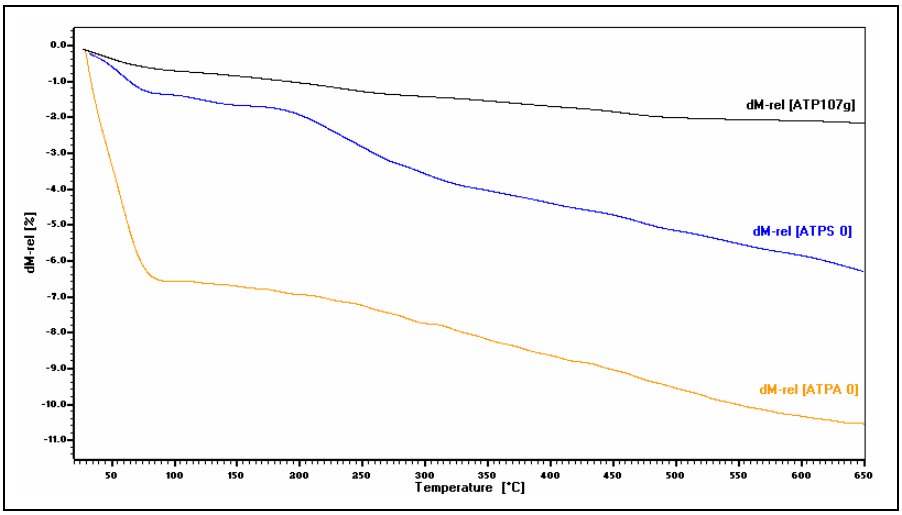

Figure 44: TG/DTA curves of the initial silica ATP107g, silane modified ATPS 0 and azo modified ATPA 0.

Figure 44 shows the TG/DTA curves of the different stages of the coupling reaction. The decomposition of the silanol groups can be detected as loss of weight in the range between 200 and 1000 °C, while the decomposition of the azo-initiator can be observed as step in the TG curve in the range of 60 °C. The amount of silanol groups in mol can directly be determined from the loss of mass.

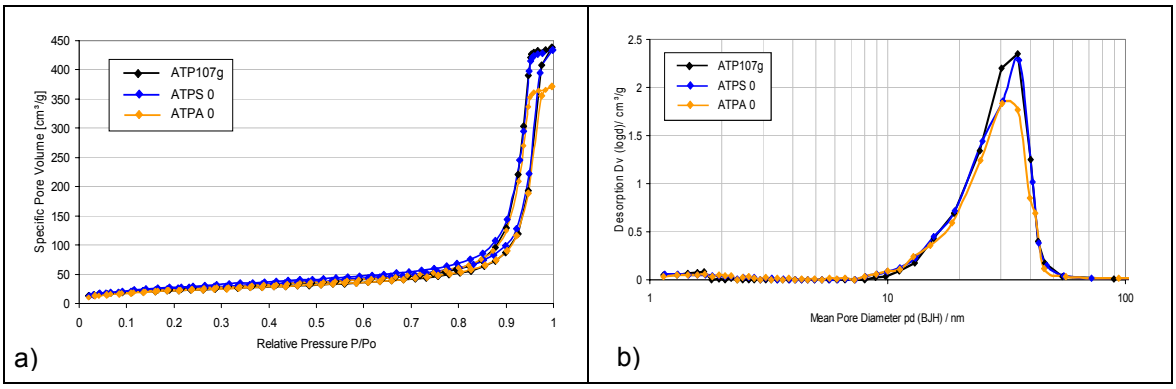

Figure 45: Nitrogen sorption measurements of the initial silica ATP107g, silane modified ATPS 0 and azo modified ATPA 0 – a) isotherms and b) pore size distributions.

Table 18: Pore structural data of the initial silica ATP107g, silane modified ATPSV 0 and azo modified ATPAV 0.

sample	**a_S** (BET) [m^2g^{-1}]	**v_p** (G) [$ml\ g^{-1}$]	**p_d** (BJH) [nm]
ATP107g	79	0.701	30.2
ATPSV 0	91	0.680	30.5
ATPAV 0	98	0.670	30.0

Figure 45 and Table 18 shows the results of the nitrogen sorption measurements, exhibiting the decrease of pore volume due to the volume that is occupied by the coating. The BET-surface area value slightly increases with each step of the coating procedure, while the pore diameter according to BJH is not changed significantly.

The grafting density was determined using the BET surface area and the carbon contents (%C w/w) respectively the nitrogen contents (%N w/w) obtained by elemental analysis. A value of 8 µmol/m^2 was used as maximum concentration of surface silanol groups[138], representing a theoretical grafting density of 100 % for a fully covered surface. The grafting density of the anchor groups and the initiator was calculated by using the following equations:

$$D = \frac{m_C}{M_C \cdot a_S} \qquad [38]$$

$$D = \frac{m_N}{M_N \cdot a_S} \qquad [39]$$

[138] K.K. Unger, Adsorbents in column liquid chromatography, K.K. Unger Ed., Marcel Dekker Inc., New York, 47 (1990) 331

where

$$m_N = \frac{\%N}{100 - \left(\%N \cdot M_w / M_N\right)} \quad [40]$$

$$m_C = \frac{\%C}{100 - \left(\%C \cdot M_w / M_C\right)} \quad [41]$$

M_w = molecular weight of anchor-group respectively of azo-initiator-group

M_C = molecular weight of all carbon atoms in the anchor-group respectively in the azo-initiator-group

M_N = molecular weight of all nitrogen atoms in the anchor-group respectively in the azo-initiator-group

a_s = specific surface area by nitrogen sorption measurements according to BJH

Table 19: Grafting density and surface coverage.

sample	[µmol/g_{silica}]	[µmol/m^2]	**Grafting density** in per cent %
ATPSV 0	124.8	1.56	19.52
ATPAV 0	109.6	1.37	17.15

In Table 19 calculated values for the grafting density and the surface coverage of a variety of samples are shown. The small variations between the values of different samples exhibit the good reproducibility of the synthesis procedure. The good match between the surface coverage of the anchor-group grafted silica and the final azo-initiator grafted silica shows a nearly quantitative coupling of the anchor groups with the azo-initiator.

5.2.2.2.3 Summary

The employed synthesis procedure allows the controlled grafting of porous silica substrates with an azo-initiator under mild conditions. The coupling reaction is nearly quantitative and generates reproducible controlled grafting density with azo-initiator of nearly 20 % of the active surface-silanol groups. The grafting procedure could be performed on both particulate and monolithic silica sources (see 5.4.2).

5.2.2.3 Polymer Modification by Chemisorption

5.2.2.3.1 Reaction Scheme

The azo-initiator-grafted silica was modified with poly(methacrylates) by a radical polymerization procedure. The following graphics represents the reaction scheme for the polymerization reaction:

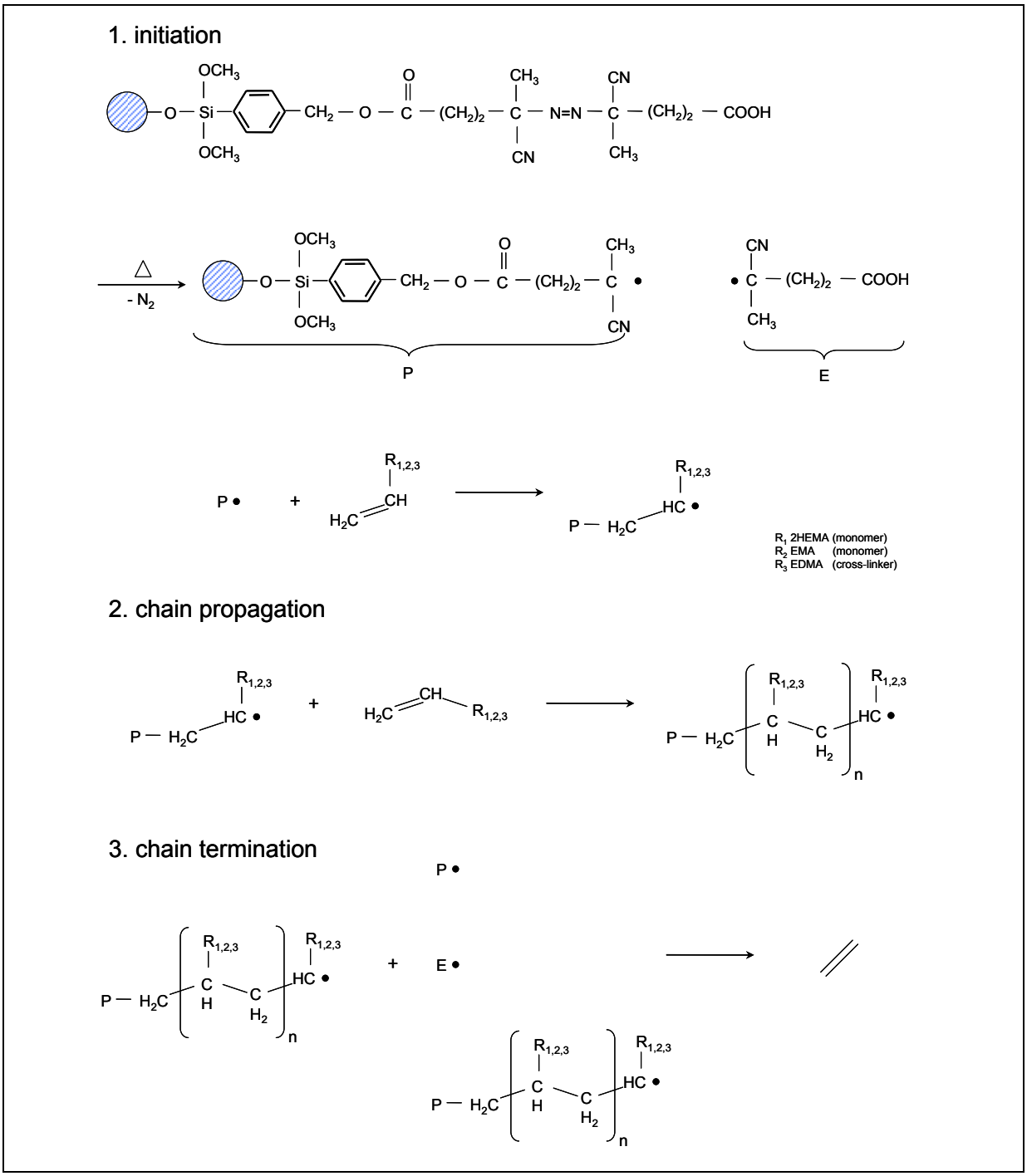

Figure 46: Reaction scheme of the polymer modification step.

Different methacrylate-based co-monomer mixtures were successfully applied with the polymerization procedure. Typically, a polymerization mixture contains 10 % (n/n) of EDMA as cross-linker to generate a stable polymer coating.

5.2.2.3.2 Kinetics of the Polymerization Step

The aim of this work was to develop a reproducible and variable polymer coating procedure onto chromatographic silica. Therefore optimum polymerization conditions had to be defined, that enables both best reproducibility and adjustability of the polymer layer. As the base material contains pure silica, the carbon content of the final product is a sufficient approximation to be used as criterion for the amount of applied polymer.

The first step in finding suitable conditions for the polymerization procedure is to look for the time dependency of the polymerization step in a batch-wise experimental set-up, keeping all experimental parameters constant except the reaction time, which was varied in a range between 15 and 240 minutes. The experiment at a duration of 120 minutes was repeated twice and the reaction with a duration of 240 minutes was repeated three times. The results of time-dependent kinetics are shown in Figure 47.

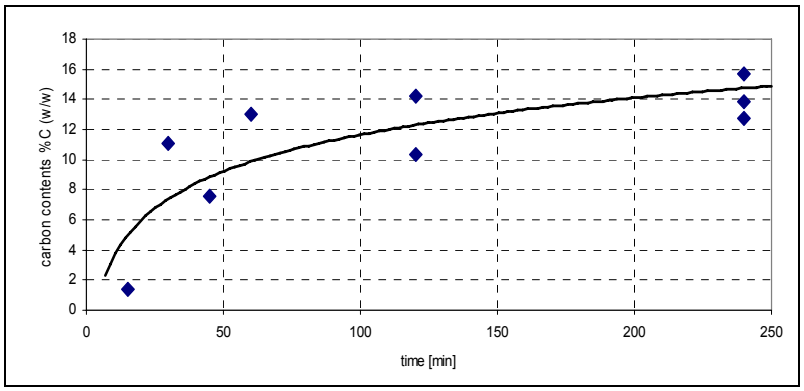

Figure 47: Time-dependent kinetics of the polymerization step with 6 mmol/cl of a co-monomer of 2-hydroxy-ethylmethacrylate and ethyl- methacrylate 1:1 (n/n).

The experiment reveals the typical course of a temperature-induced radical polymerization reaction. After a short induction period, the reaction starts very fast as the initiator decomposes and the concentration of unreacted monomer is at its maximum. The reaction rate decreases with the reduction of monomer in the solution until finally chain termination by combination of free radicals ends the reaction. The carbon load of the isolated products show especially at short reaction times a poor reproducibility, what is also typical for temperature-induced radical polymerization reactions, as even small variations in the experimental parameters have a large effect on the product.

By means of reproducibility, a reaction time of 240 minutes is the best choice for a monomer concentration of 6 mmol/cl to produce an acceptable conformity of the final product, with a carbon content of 14.5 +/- 1.5 %.

Controlling the polymer load of the final product was therefore tried in the next step by a set of experiments with variation of the monomer concentration in the range between 1 mmol/cl and 6 mmol/cl at a reaction time of 240 minutes. Figure 48 shows the result of these experiments.

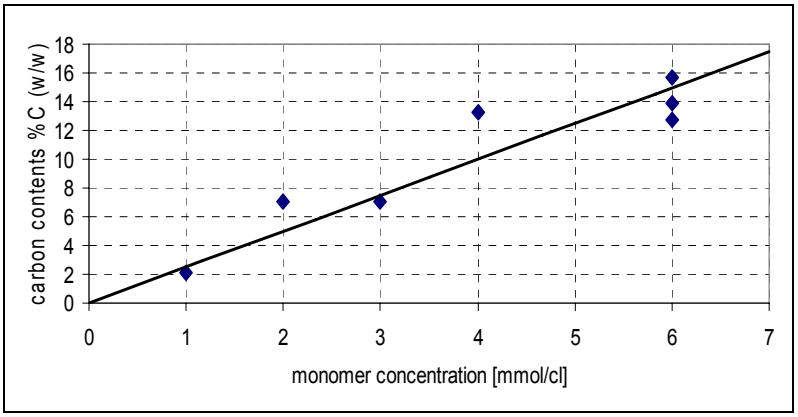

Figure 48: Concentration-dependent kinetics of the polymerization step at a constant reaction time of 240 min with a co-monomer of 2-hydroxy-ethylmethacrylate and ethyl-methacrylate 1:1 (n/n).

The graphic shows that there is an almost linear relation between the monomer concentration and the carbon contents. But the reproducibility at lower monomer concentrations is poor and therefore especially to adjust small polymer loads is very difficult to achieve.

Therefore the next set of experiments was performed at a shorter reaction time of 120 minutes, accepting a poor reproducibility at high monomer concentrations, which may be due to local overheating because of the higher reaction rates. Again, the monomer concentration was varied in a range between 1 mmol/cl and 6 mmol/cl. The resulting carbon contents of this series of experiments are shown in Figure 49.

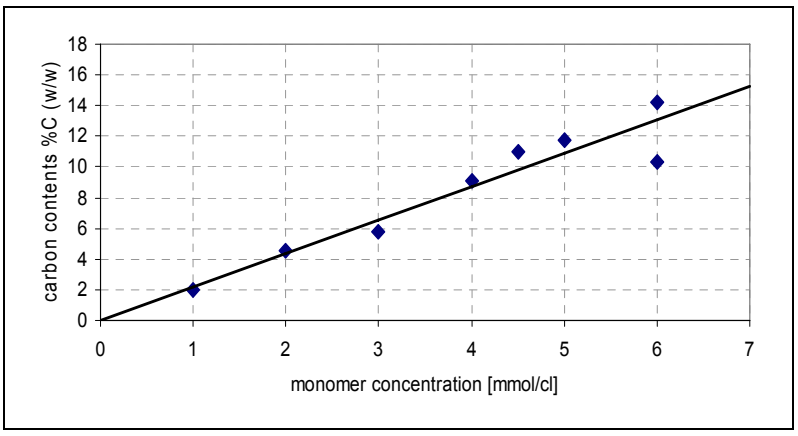

Figure 49: Concentration-dependent kinetics of the polymerization step at a constant reaction time of 120 min with a co-monomer of 2-hydroxy-ethylmethacrylate and ethyl-

methacrylate 1:1 (n/n).

This figure exhibits also an almost linear relation between the monomer concentration and the carbon contents. But unlike the results obtained before at longer reaction times, a much better correlation of the monomer concentration with the resulting polymer load is achieved at a reaction time of 120 minutes. The linearity of the curve is especially at lower monomer concentrations very good and allows the synthesis of polymer-coated silica with small and well-defined carbon contents.

5.2.2.3.3 Assessment of Thermal Stability by Thermogravimetric Analysis

The temperature dependant weight loss of the polymer-coated silica as investigated by thermo-gravimetric analysis is directly related to its thermal stability as an important indication for the overall ruggedness of the coating. Especially for the use in analytical applications in protein research, rugged coatings are necessary as a mass spectrometer is employed as detector, which requires a stationary phase with as low bleeding as possible. As reference, a commercially available C18-coated silica material was also investigated. Figure 50 shows the resulting thermo-gravimetric measurements of three polymer-coated samples in comparison with unmodified silica (ATP107g) and commercially available C18-modified silica from room-temperature up to 600 °C in air atmosphere.

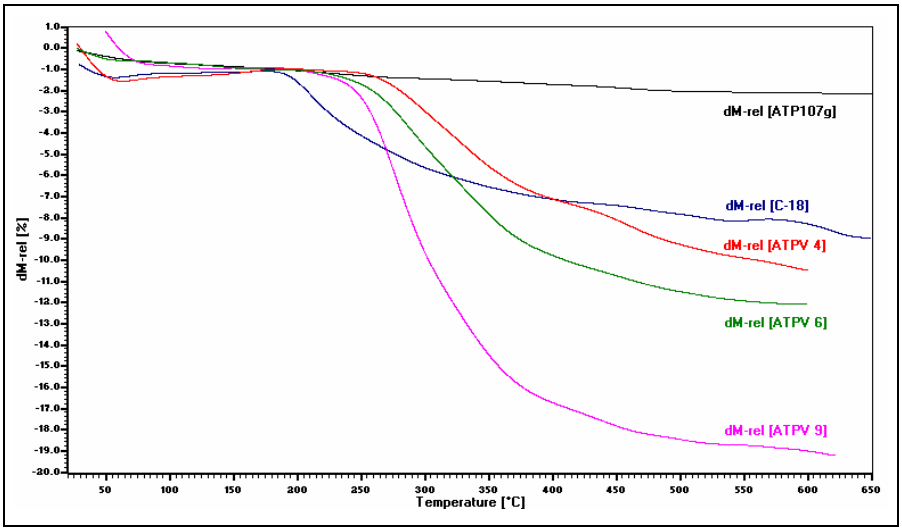

Figure 50: TG/DTA curves of the initial silica ATP107g, C18 and polymer modified silicas.

As expected, the uncoated silica sample ATP107g shows the small mass loss in the observed range, which is related to adsorbed water and surface-silanol groups. The decomposition of the coating starts in case of the commercial C18-modified silica sample at 190 °C with the maximum mass loss rate at 209.5 °C. The polymer-coated materials are significantly more stable, exhibiting 40 °C higher temperature stability with a start of the

decomposition at ca. 230 °C, while the maximum decomposition rate is shifted to values between 275.7 – 298.5 °C. Besides this, the overall mass loss of all polymer-coated silica samples as detected at 500 °C is higher than the value of the C18-coated silica sample. All values from the thermo-gravimetric analysis are listed in Table 20.

Table 20: Thermogravimetric values of the initial silica ATP107g, C18 and polymer modified silicas.

sample	**%C** (w/w)	**mass loss** between 200-500 °C in %	**temperature of max. mass loss rate** [°C]
ATP107g	0.13	1.17	-
C18	4.52	6.70	209.5
ATPV 4	4.55	8.30	298.5
ATPV 6	5.82	10.49	288.9
ATPV 9	9.15	17.21	275.7

5.2.2.3.4 Morphological Investigation by Scanning Electron Microscopy

By employing scanning electron microscopy (SEM) the morphology of the particles was investigated. As the base material is chemically and mechanically very stable and the polymer coating was performed under mild conditions, no structural change of the particles was expected. Therefore the focus of these investigations was to check the samples for potentially existing agglomerates respectively polymer-'bulk'-phases.

None of the investigated polymer modified materials showed agglomerates due to polymer bulk phases. Figure 51 exhibits exemplary SEM-images by a 500 times and 2000 times enlargement of native and polymer coated samples.

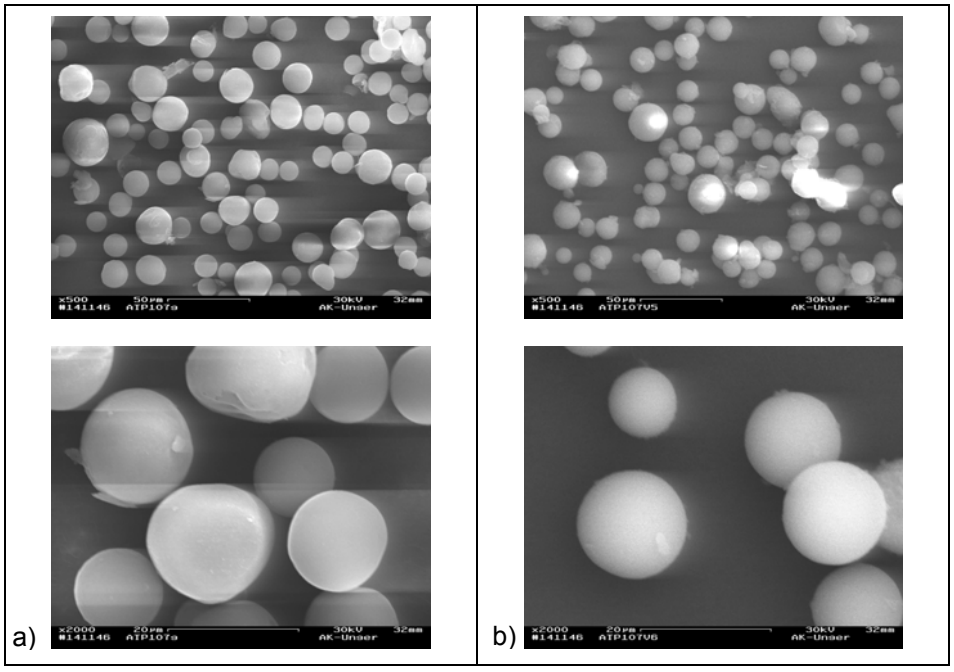

Figure 51: SEM images – a) SEM image of silica precursor ATP107g and b) SEM image of polymer modified silica.

5.2.2.3.5 Transmission Electron Microscopy and Energy Dispersive X-ray Spectroscopy (EDX)

Introduction

Transmission electron microscopy (TEM) in the scanning mode (STEM) may be employed for the visualization of the pore system of a material by scanning thin slices in the range of less than 100 nm of a sample. The combination with energy dispersive x-ray spectroscopy (EDX) during the scan allows the allocation of chemical elements in the sample.

For the slicing process a microtome is employed, which cuts the sample by using a diamond knife with a very small cutting angle. Therefore, the sample is embedded in an epoxy resin, which fills completely the cavities of the pore system and the space between individual particles, enabling the handling of the sample and preventing the breakdown of the silica skeleton during the slicing process.

As both the polymer coating of the sample and the epoxy-resin from the sample preparation have similar elemental compositions, they cannot be directly distinguished from each other in the EDX scan. Rückert and Kolb[139] showed that this could be achieved by a staining process of the sample prior to the embedding in epoxy resin with Ruthenium. RuO_4 oxidizes unreacted C-C double bonds of the polymer layer and also the C-C-double bonds of the phenyl rest from the anchor group by precipitation of RuO_2. The silica surface is not touched at all by the staining process, which can be experimentally proven via the investigation of bare silica, which was also treated with the same sample preparation process.

The staining procedure is represented by the following reaction scheme:

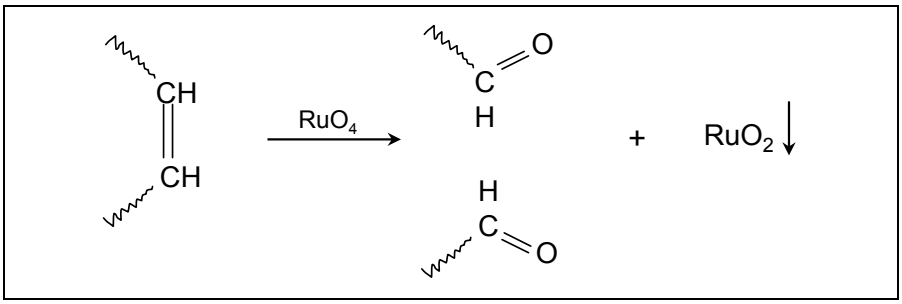

Figure 52: Reaction scheme of RuO_4 with C-C-double bonds.

Experimental

For the staining procedure a few milligrams of the sample material are put into a small watchglass, which is placed into a beaker. Putting a few crystals of $RuCl_3$ into the beaker and

[139] B. Rückert, U. Kolb, Micron 36(3) (2005) 247-260

then adding a few drops of sodium-hypochloride-solution produce gaseous RuO_4. The sample was kept in the RuO_4-atmosphere for at least 30 min.

Afterwards the samples were embedded in an epoxy resin and after 24 hours of hardening cut into 40 nm thick slices by using a microtome equipped with a 2.5 – 2.9° mm diamond knife. Then the slices were transferred onto copper grids coated with Quantifoil. The TEM measurements were carried out with a FEI Tecnai F3 ST at 300 kV, equipped with a field emission gun, a scanning unit with a high angular annular dark field detector and an energy dispersive x-ray spectroscope. The beam size can be adjusted down to 1 nm and a dispersion of 5 eV. The image processing was performed with the software AnalySIS.

Two samples were investigated, a freshly rehydroxylated base silica ATP107g as well as a polymer-coated sample ATPV 9 with 9.15 % carbon load. All measurements showed that there are no polymer-bulk phases, although the polymer coating could not be directly visualized.

The following pictures show TEM-images of the border of individual particles of bare silica and polymer-coated silica without embedding in resin.

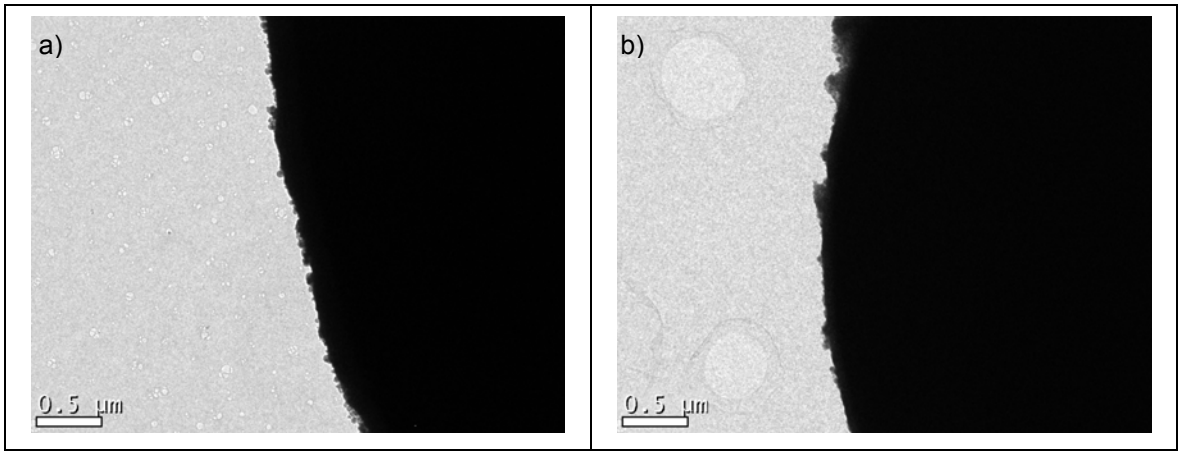

Figure 53: TEM images – a) TEM image of silica precursor ATP107g and b) TEM image of polymer modified silica ATPV 9.

Figures 53b) show, that there are no polymer-bulk-phases on the outer surface of the polymer modified material. Furthermore, the morphology of the silica particles is not changed at all by the coating procedure.

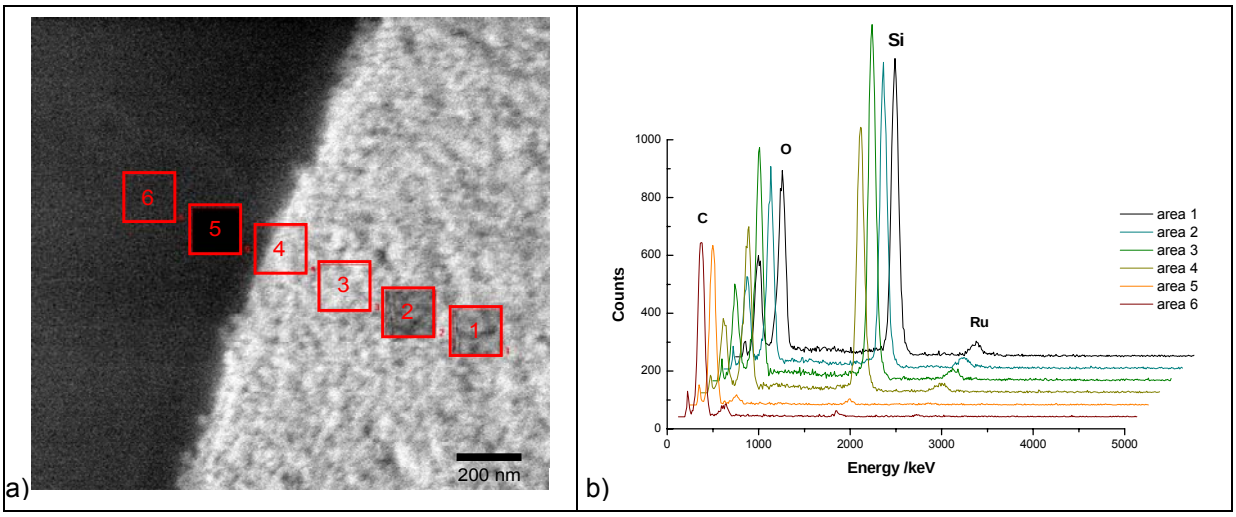

Figure 54: a) STEM image with areas 1 to 6 for EDX area scans and b) EDX-spectra of areas 1 to 6 of polymer modified silica.

Figure 54 displays ca. 1 µm at the boundary of a 40 nm thick slice in the centre from a spherical particle. The polymer-coated sample was stained with Ruthenium prior to embedding in epoxy resin. The red squares indicate the points investigated with the EDX-measurement starting from ca. 1 µm inside the particle with point 4 already scanning the embedding resin. The last points are only touching the polymer resin from the sample preparation. The related EDX-spectra are shown in Figure 54b).

Table 21: EDX counts of areas 1 to 6 in the Ruthenium range.

Areas	6	5	4	3	2	1
Ruthenium-counts*	82	88	493	624	611	718

*addition of counts from 2,500 to 2,750 keV

Table 21 represents the course of the Ruthenium-distribution of the sample. The EDX-counts in the area from 2,500 to 2,750 keV show, that there is a large difference between the Ruthenium contents in the particle of ca. 650 counts and in the embedding resin with ca. 85 counts. This tendency was well expected, as the resin was not exposed directly to the staining process. The value reflects the normal baseline scattering of the method and can therefore be useful as experimental error. The measurements show, that the particle exhibits a uniform staining with Ruthenium of ca. 650 +/- 85 counts. The Ruthenium-staining is also in the same range at the border of the particle: point no. 4 only touches 75 % of the particle, giving an expected value of 629 counts =(493-85)/0.75 + 85) for full coverage.

As only C=C double bonds from the polymer coating and the anchor group are affected by the staining process, these values can be used as an indicator for a uniform polymer-distribution inside and at the border of the silica particles.

The staining is not as intense as reported in the examples in the literature, which is well explained in first place by only a fifth of the carbon-load and a fifth of cross-linker compared to the reported examples. Mainly partially unreacted cross-linker delivers most of the C=C-double bonds in the polymer coating for the staining process.

5.2.2.4 Reproducibility of the Synthesis Procedure

The reproducibility of the synthesis procedures was checked by repetition of each synthesis for at least three times. The results of the carbon content (%C (w/w)) of elemental analysis of the dried product are employed as main criterion for the reproducibility of the synthesis procedure. Table 22 lists experimental parameters of three batches for the silane-modification step of the initial silica.

Table 22: Reproducibility of silane modification onto initial silica.

sample	**Net weight of initial silica** [g]	**Net weight of silane** [g]	**%C** (w/w)	**%H** (w/w)	**%N** (w/w)
ATPSH 0	13	0.89	0.94	0.38	0.01
ATPSH 1	10	0.61	0.83	0.16	0.02
ATPSH 2	14	0.93	0.92	0.32	0.02
average value			0.90	0.29	0.02
standard deviation δ			± 0.048	± 0.093	± 0.005

The overall reproducibility of this synthesis step is very good for a lab-scale synthesis procedure, as a standard variation of about $\pm$ 5 % based on the carbon content is reached.

The second step of the coating procedure is the coupling of the azo-initiator. The following Table 23 lists the synthesis parameters of three synthesis batches and the results of elemental analysis of carefully dried products.

Table 23: Reproducibility of azo modification onto silane-coated silica.

sample	**Net weight of silane silica** [g]	**Net weight of azo** [g]	**%C** (w/w)	**%H** (w/w)	**%N** (w/w)
ATPAH 0	13	11.03	1.40	0.31	0.17
ATPAH 1	10	8.15	1.03	0.13	0.10
ATPAH 2	14	11.84	1.27	0.23	0.13
average value			1.23	0.22	0.13
standard deviation δ			± 0.153	± 0.074	± 0.017

Again, the overall reproducibility of this synthesis step is in a quite acceptable range for the second step of a lab-scale synthesis procedure. The standard deviation of the carbon content is about $\pm$ 12 % and for the nitrogen content is about 20 %.

The final step of the coating procedure is the polymerization step, giving the final polymer-coated product. The following Table 24 lists the synthesis parameters of three batches as

synthesized according to the procedure given in Appendix 7.1.3.4 and the results of the elemental analysis of dried products.

Table 24: Reproducibility of polymer modification.

sample	**Net weight of azo silica** [g]	**Net weight of co-monomer** [g] 2HEMA	EMA	**%C** (w/w)	**%H** (w/w)	**%N** (w/w)
ATPH 4	2.5	0.13	0.11	4.52	0.62	0.05
ATPH 4.1	2.5	0.12	0.10	4.57	0.70	0.03
ATPH 4.2	2.0	0.10	0.09	4.40	0.50	0.04
average value				4.50	0.61	0.04
standard deviation δ				± 0.071	± 0.082	± 0.008

The overall reproducibility of the whole polymer coating procedure is very good, especially as this synthesis is in lab-scale based on temperature-initiated radical polymerization. The standard deviation of the carbon content is only 2 % of the average value, highlighting the excellent reproducibility of the chosen reaction conditions.

5.2.2.5 Upscaling of the Synthesis Procedure

An important issue for the usability of a polymer modification procedure is the possibility for the upscaling of the whole process. This enables both easy production of larger quantities of modified material if needed and also small-scale optimization of the material with small quantities. The upscaling possibilities of the synthesis steps is evaluated by comparing batches, which differ by at least tenfold in the amount of educts.

Table 25: Upscaling of silane modification procedure.

sample	**Net weight of initial silica** [g]	**Net weight of silane** [g]	**%C** (w/w)	**%H** (w/w)	**%N** (w/w)
ATPSV 0	10	1.23	1.44	0.77	< 0.01
ATPSV 1*	130	15.23	1.37	0.41	< 0.01

* Batch size was 13 times of the original batch size.

Comparing a synthesis based on 10 g silica and a synthesis based on 130 g silica allows checking for the upscaling behavior of the silane modification step as given in Appendix 7.1.3.2. Table 25 lists the synthesis parameters of both batches and the results of elemental analysis of the final dried products.

Table 26: Upscaling of azo modification procedure.

sample	**Net weight of silane silica** [g]	**Net weight of azo** [g]	**%C** (w/w)	**%H** (w/w)	**%N** (w/w)
ATPAV 0	10	8.43	2.76	0.43	0.73
ATPAV 1*	130	78.08	2.70	0.72	0.54

* Batch size was 13 times of the original batch size.

The carbon content value by elemental analysis shows a very good agreement between both batches, indicating an excellent upscaling behavior of the procedure.

Comparing a synthesis based on 10 g silane-modified silica and a synthesis based on 130 g of the same material allows checking for the upscaling behavior of the azo modification procedure. Table 26 lists the synthesis parameters of both batches and the results of elemental analysis of the final dried products.

The carbon content value by elemental analysis shows a very good agreement between both batches, while the nitrogen content differs significantly but not to such an extend, that it influences the usability of the product. Anyway, a lot of care must be taken in this synthesis step especially during the washing and drying of the product as the azo-initiator starts decomposing at relatively low temperatures.

Table 27: Upscaling of polymer modification procedure.

sample	**Net weight of azo silica** [g]	**Net weight of co-monomer** [g] 2HEMA	EMA	**%C** (w/w)	**%H** (w/w)	**%N** (w/w)
ATPV 10	0.2	0.04	0.03	10.73	1.42	0.08
ATPV 10.1*	8.0	1.31	1.12	11.76	1.70	0.10

* Batch size was 40 times of the original batch size.

The check for the upscaling of the final polymerization step is based on the synthesis procedure described in Appendix 7.1.3.4. Table 27 lists the experimental parameters of the original procedure for the modification of 0.2 g silica with azo-initiator and a 40 times upscaled batch.

5.2.2.6 Application of the Synthesis Procedure on Different Base Materials

The applicability of a coating procedure onto different chromatographic base materials is another important issue as the base material plays an important role for the overall chromatographic performance. Three different commercially available so-called "wide-porous" particulate materials were modified by the coating procedure as given in Appendix 7.1.3. The materials are commonly used for the chromatographic separation of large molecules like biopolymers. Sample ATPV 4 is based on LiChrospher™ WP 300, 15µm (Batch No. ATP107g, Merck KGaA, Darmstadt, Germany), KROV 4 uses Kromasil 300Å, 16µm (EKA Chemicals AB, Bohus, Sweden) and NUCV 4 uses Nucleosil 300-10, 10µm (Macherey-Nagel, Düren, Germany) as base silica. Furthermore a wide-porous monolithic silica material Chromolith™ (Merck KGaA, Darmstadt, Germany) was polymer-coated CM P2HE.-E by a slightly modified synthesis procedure, as the coating procedure has to be performed in-column (see 5.4.2).

All synthesis steps like hydroxylation, silane-modification and azo-modification could be successfully applied upon the different base materials (see 5.4.1), which is also true for the last polymerization step. Table 28 lists the experimental parameters and the results of elemental analysis of the product of some example batches of the final polymerization step.

Table 28: Application of polymer modification procedure on different base materials.

sample	**Net weight of azo silica** [g]	**Net weight of co-monomer** [g] 2HEMA	EMA	**%C** (w/w)	**%H** (w/w)	**%N** (w/w)
ATPV 4	2.5	0.167	0.142	4.55	1.02	0.05
KRV 300	2.5	0.173	0.144	4.52	0.62	0.05
NUV 300	2.5	0.137	0.110	4.99	0.52	0.04
CM P2HE.-E	-	0.226	0.203	11.10	2.01	0.05

The carbon content value by elemental analysis shows also in this test a very good agreement between the different batches, indicating an easy applicability of the complete polymer coating procedure upon different base materials. This is also remarkable, as the application of coating procedures upon different base materials is sometimes not easy to achieve, especially as several synthesis steps are involved.

Furthermore the successful application of the coating procedure upon monolithic silica in-column with very comparable results highlights the good choice of the synthesis parameters, allowing a good control of the synthesis.

5.2.3 Conclusion

The grafting of porous silica sources with a poly(methacrylate) based polymer layer was performed by a grafting from-approach initiated by a surface-bound Azo-initiator group, which thermally initiated a radical polymerization. All synthesis steps were optimized to work under mild reaction conditions, giving an excellent reproducibility of each step. Kinetic studies provided suitable reaction conditions for adjusting the amount of polymer layer of the final product in a range of 2 to 15 % carbon content.

The mild synthesis conditions are ideal preconditions for a successful upscaling of each synthesis step, which results in very small differences of the physical properties of products from syntheses with different batch-sizes. Furthermore, different porous silica materials including monolithic silica could be coated with poly(methacrylate) with very comparable results.

Imaging methods showed no morphological change of the support material by the modification procedure and the absence of bulk-phases. STEM with energy dispersive x-ray-measurements on Ruthenium-stained samples exhibits a uniform coating inside the porous particles. The very small staining intensity is the result of a low concentration of C=C-double bounds in the polymer layer indicating a nearly complete insertion of the cross-linker into the

polymer chain. This is also reflected in the thermal stability of the final product, which is found by thermogravimetric measurements to be significantly higher than the one of a commercial C18-coated material, which was used as reference.

5.3 Optimization of the Polymer Coating for HPLC of Biopolymers

5.3.1 Introduction

The optimization of the polymer layer is done in a several stage process, now that a reproducible and tunable synthesis procedure for the polymer coating is established. As the polymer layer is based on methacrylates, a large variety of properties can be adjusted. The hydrophobic properties can be varied via the co-monomer composition, the amount of polymer of the final product can be regulated by the monomer concentration in the synthesis mixture. Further properties of interest are the linker density and the rigidity of the polymer layer. In this paragraph, the influence and optimization of these properties for the chromatographic evaluation of biopolymers is subject of the investigation. For best comparability of the results, the investigations are based on a single batch of chromatographic silica.

The optimization process is partially based on the design of experiments (DOE) concept, which can be employed for the optimization of any process or material feature based on the use of statistical theory. In the first stage of material development, DOE is used for the screening of the relevance of experimental parameters upon the target features and their interdependency with reduced experimental effort and better results compared to traditional methods like “shotgun”-methods or by the optimization of single parameters[140,141].

In this work, DOE approaches were applied to check for the relevance of different factors like polymer load or the polymer composition upon the chromatographic performance or for the optimization of the chromatographic test method.

In the first stage, the hydrophobic properties of the polymer layer are investigated and optimized, followed by the amount of polymer, then the influence of the linker density is investigated until the rigidity of the polymer layer is varied to investigate its influence upon the chromatographic performance.

5.3.2 Design of Experiments (DOE)

The DOE approach is a problem depending process which involves the design of a set of representative experiments with regards to a given question. This is usually done by defining

[140] A. Orth, D. Wenzel, Leitfaden Modellgestützte Versuchsplanung und Optimierung, Hessisches Zentrum für Qualitätssicherung und Qualitätsmanagement, Frankfurt am Main (2003)
[141] J. Trygg, S. Wold, Introduction to Statistical Experimental Design, http://www.chemometrics.se/editorial/aug2002.pdf as of January 10, 2006

a reasonable standard experiment and then defining additional experiments by varying the values of those parameters, which might influence the result, symmetrically around the standard experimental layout up to still reasonable maximum or minimum values. This is illustrated in the following graphic for a experimental design for two varied parameters where the point in the center represents the experiment with the standard value:

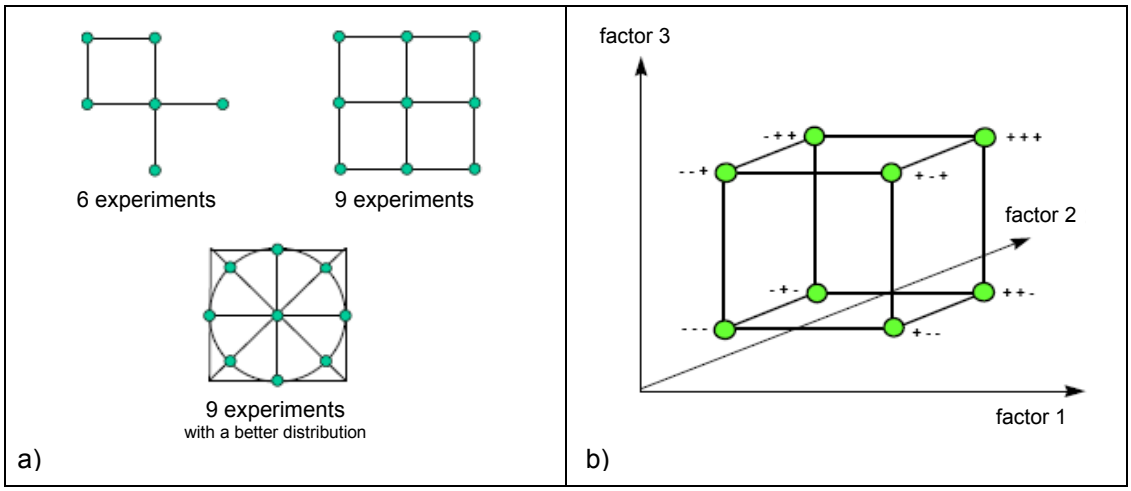

Figure 55: Standard experimental layouts with center-point and full edges - a) quadratic coherences and b) full factorial 2^3-experimental design (3 factors with 2 levels).[140]

The edges represent the minimum and maximum values for the investigated parameters and each point stands for an experiment in a so-called full factorial design, which is typical for DOE-setup for the first series of screening experiments, if the single experiments can easily be run. In most cases, e.g. if the experiments are time consuming or expensive, reduced setups are employed. Figure 56 displays examples for full factorial, fractional factorial and balanced designs typically used in DOE approaches for two (x_1, x_2) and three factors (x_1, x_2, x_3).

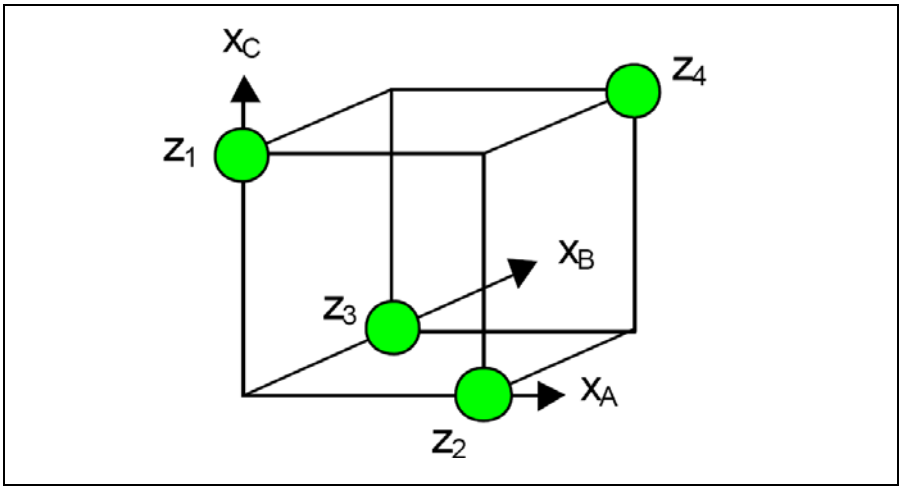

Figure 56: Example for full factorial, fractional factorial and composite design.[140]

DOE layouts for more than three factors are also available, but in most cases the dependencies are checked via multi-stage strategies with up to three factors in each stage.

Depending on the complexity of a single experiment and the number of investigated factors the first series of experiments can be performed as a full factorial design or as a design with a reduced number of experiments. All designs contain a series of experiments with the standard values to check for the validity respectively the variance of the data. Once the experiments are chosen, a plan is generated with a fixed order in which the experiments have to be performed. Via this way, the time dependency of the investigated factors upon the target values can be checked. The experimental data is then evaluated by statistical methods to check for and the kind of interdependencies of the factors and for defining additional experiments. The result or response (y) of the system which should be optimized is therefore checked for the validity of different types of models:

linear model:

$$y = \beta_0 + \beta_1 x_1 + \beta_2 x_2 + \ldots + \beta_i x_i \quad [42]$$

interaction model:

$$y = \beta_0 + \beta_1 x_1 + \beta_{12} x_1 x_2 + \beta_{13} x_1 x_3 + \ldots + \beta_{1i} x_1 x_i + \ldots + \beta_i x_i \quad [43]$$

quadratic model:

$$y = \beta_0 + \beta_1 x_1 + \beta_{12} x_1 x_2 + \ldots + \beta_{nn} x_n^2 + \ldots + \beta_i x_i + \beta_{ii} x_i^2 \quad [44]$$

Where: y is the response of the system; x_1 is the value for factor 1 in the experiment; i is the number of investigated factors and β_n the parameter which has to be determined reflecting the influence of the experimental factor upon the response of the system.

This can experimentally be checked experimentally by the use of the following model-equation:

$$y = \beta_0 + \beta_1 x_1 + \beta_{12} x_1 x_2 + \beta_{11} x_1^2 + \beta_2 x_2 + \ldots + \beta_i x_i + \beta_{ii} x_i^2 + \varepsilon \quad [45]$$

where

y is the response of the system

β_0 is a constant

$\beta_1 x_1 + \beta_2 x_2 + \ldots + \beta_i x_i$ represents the linear part

$\beta_{12}x_1x_2 + \beta_{13}x_1x_3 + ...+ \beta_{1i}x_1x_i...+ \beta_{23}x_2x_i +.....+ \beta_{i-1i}x_{i-1}x_i$ represents the interaction of the factors

$\beta_{11}x_1^2 + \beta_{22}x_2^2 + ... + \beta_{ii}x_i^2$ represents the quadratic contribution to the response

ε represents the error respectively the variance of the experimental data

In the case of a 2-factorial design the model is reduced to the following:

$$y = \beta_0 + \beta_1x_1 + \beta_{12}x_1x_2 + \beta_{11}x_1^2 + \beta_2x_2 + \beta_{22}x_2^2 + \varepsilon \quad [46]$$

In the case of a 3-factorial design the model is reduced to the following:

$$y = \beta_0 +\beta_1x_1 +\beta_{12}x_1x_2 +\beta_{13}x_1x_3 +\beta_{11}x_1^2 +\beta_2x_2 +\beta_{23}x_2x_3 +\beta_{22}x_2^2 +\beta_3x_3 +\beta_{33}x_3^2 + \varepsilon \quad [47]$$

The best model is then taken as the one, which fits the experimental data best. By plotting the response vs. the values of the factor one can get a first impression of the kind of model which may be adapted. Depending on the result or nature of the model, additional experiments can be planned. In the simple case of a linear model, all parameters may be independently optimized, while for the interaction model or the quadratic model multiple experimental compositions have to be evaluated. If the experiments indicate, that the maximum value for the system response is outside the borders of the chosen compositions, the center experiment should be redefined. Examples for the response surface representing the most common types are shown in Figure 57:

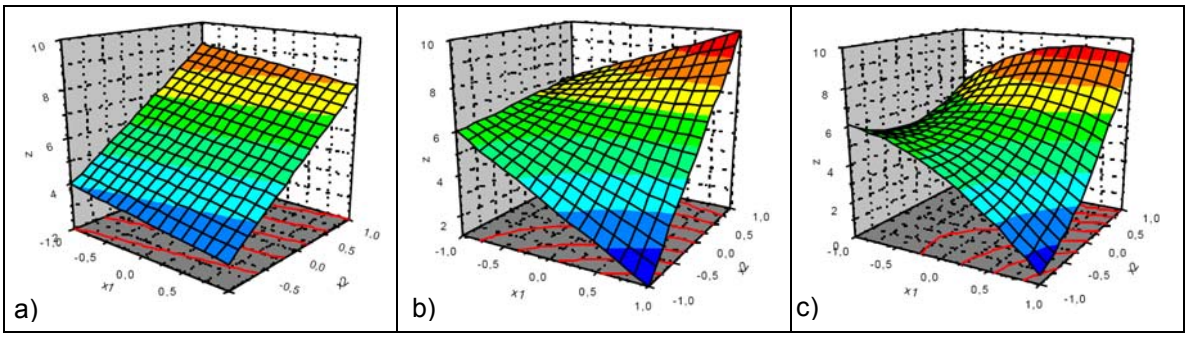

Figure 57: Response surface for a) linear model, b) interaction model and c) quadratic model types.[140]

The mathematical treatment is usually performed with dimensionless, normalized values for the factors by setting the values for the center experiment to zero and the maximum value to +1 while the minimum value is defined as -1:

$$\bar{x}_i = \frac{x_i - \left(x_{i,max} - \left(\frac{x_{i,max} - x_{i.min}}{2}\right)\right)}{\left(\frac{x_{i,max} - x_{i.min}}{2}\right)} \quad [48]$$

The fitting of the parameters is usually done by the least square fit method. If a linear model can be assigned, additional experiments are only necessary for the reduction of the experimental uncertainty, while for the verification of interaction models or quadratic models additional experiments are required.

Divergences between the guessed model and the experimental data can best be detected and displayed by plotting the differences between the experimental data points and their predicted values, called residues against the factor of interest. Plotting the residues vs. any factor or parameter can easily reveal dependencies, as for a valid model the residues should only reflect the experimental error and scatter randomly around the zero-line according to a Gaussian distribution. Time dependencies of the investigated processes can be monitored by plotting the residues vs. the run order, revealing for example worn out instruments, loss in activity of an initiator but also a bettering of the results may be observed, for example via improving experimental skills.

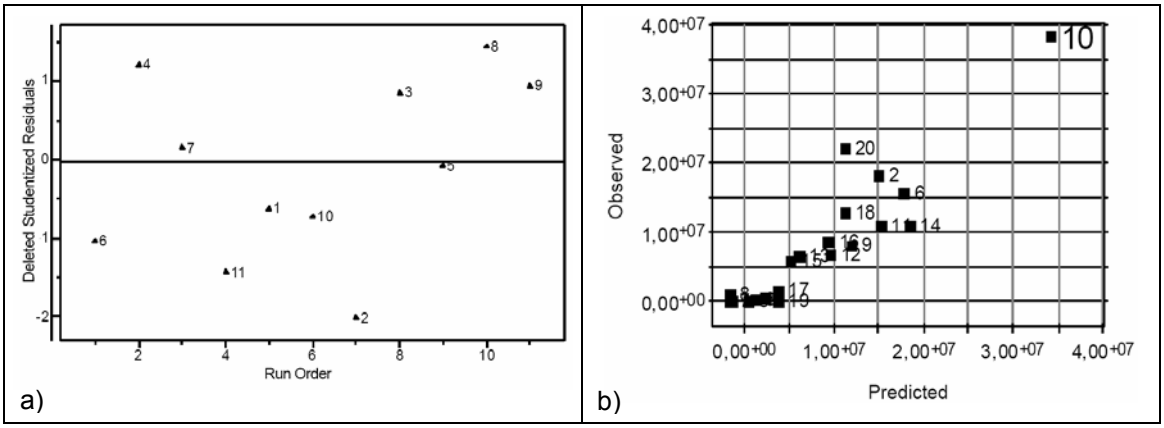

Figure 58: Examples for Residues vs. RunOrders – a) to identify time dependent trends and b) to identify outlier.[140]

5.3.3 Optimization of the Polymer composition

5.3.3.1 Introduction

Poly(methacrylates) offer the ability to produce polymer coatings with a large variety of different hydrophobicitys, depending on the type of methacrylate-monomer used in the synthesis. A fine tuning of the hydrophobicity of the final polymer-layer can be achieved via co-polymerization of different methacrylate-types.

One cause for denaturation of proteins during a chromatographic run are the hydrophilic and hydrophobic interactions between the protein and the surface of the chromatographic media. Therefore an optimized surface by means of medium hydrophobicity should exhibit less denaturation potential towards proteins, which was shown as a first hint by the application of an LCM-test-mixture[33,34] upon stationary phases with different hydrophocitys. In

this work, an enzymatic activity test as additional testing procedures was employed, as a sort of a real life-method to show, whether the protein is still in a biological active state after the chromatographic run.

The optimization of the hydrophobicity of the polymer layer was done in different stages. In the first stage, chromatographic media were investigated, which were modified via a physisorption procedure with different methacrylates representing the complete range from hydrophilic to hydrophobic surfaces. In the second stage, the best polymer compositions were investigated with chemisorbed polymer coatings to ensure reproducibility of the results. Afterwards, DoE was employed for the fine tuning of the polymer layer based on chemisorbed coatings.

5.3.3.2 From Hydrophilic to Hydrophobic Phases via Physisorbed Materials

The first screening was done by the investigation of chromatographic media, which were coated with poly(methacrylates), ranging from hydrophilic to hydrophobic by a physisorption process.[142] As base silica LiChrospher™ Si 300, 10µm (Merck KGaA, Darmstadt, Germany) was utilized. The investigated polymer coatings were based on the following monomer respectively co-monomer compositions:

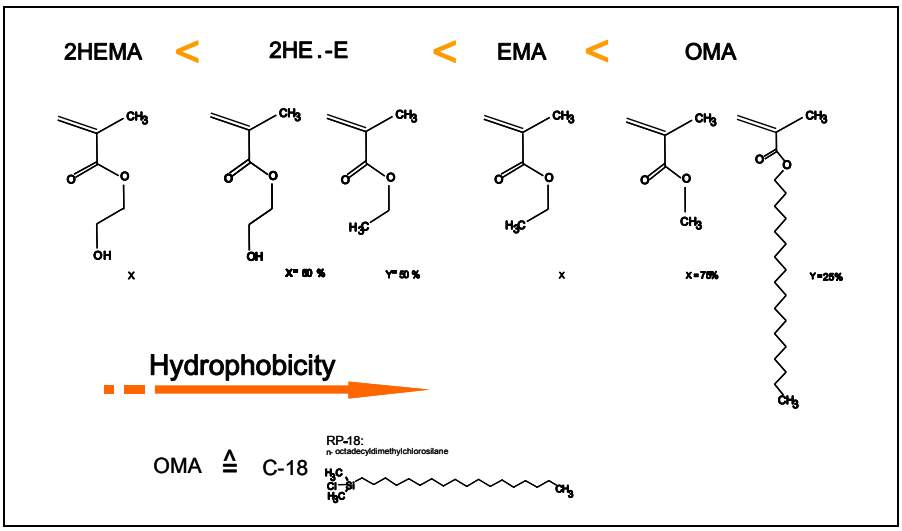

Figure 59: Chemical structure of employed methacrylate monomers by increasing hydrophobicity.

In addition to the polymer-coated silica, unmodified silica and the same silica source hydrophobically modified with C18-groups was investigated. All materials were packed into chromatographic columns (25 x 4.6 mm ID) prior to the chromatographic testing by a standardized packing procedure (see Appendix 7.3.2) with toluene/dioxane/cyclohexanol

[142] Z. Bayram-Hahn, Diploma Thesis, Johannes Gutenberg University Mainz (2002), p.18

1:1:2 (v/v) as solvent mixture. The coating procedures resulted in the following carbon contents:

Table 29: Elemental analysis pore structural data of the initial silica LiChrospher™ 300 and the polymer modified materials.

sample	average particle diameter [µm]	%C (w/w)	a_S (BET) [m^2g^{-1}]	v_p (G) [ml g^{-1}]	p_d (BJH) [nm]
LiChrospher™ 300	10	0.27	117	1.092	24.6
P2HEMA	10	4.22	102	0.968	24.9
P2HE.-E	10	2.34	107	1.023	24.8
PEMA	10	1.83	115	1.073	24.6
POMA	10	1.25	116	1.065	24.8
RP18	10	8.34	99	0.886	24.5

5.3.3.2.1 Chromatographic Evaluation – LCM-test-mixture

A test mixture consisting of lysozyme (L), cytochrome C (C) and myoglobin (M) was used for the evaluation of the chromatographic performance and as a hint for the denaturation potential of the materials towards proteins (see 3.3.3.1). The chromatographic evaluation was done in reversed-phase gradient mode from the aqueous phase to the organic phase, resulting in an increasing retention time for the proteins with increasing hydrophobicity of the stationary phase.

The results of the chromatographic evaluation are shown in detail in Figure 60. Table 30 lists the chromatographic conditions.

Table 30: Chromatographic conditions for LCM-test-mixture as shown in Figure 60.

column dimension: 25 x 4.6 mm ID
flow rate: 1 ml/min; concentration: 1 mg/ml;
injection volume: 5 µl; detection: 215 nm, 400 nm;
@ room temperature;
from 95/5 % (v/v) A/B in 5 min to 5/95 % (v/v) A/B; with
A: water + 0.1 % TFA,
B: acetonitrile + 0,09 % TFA

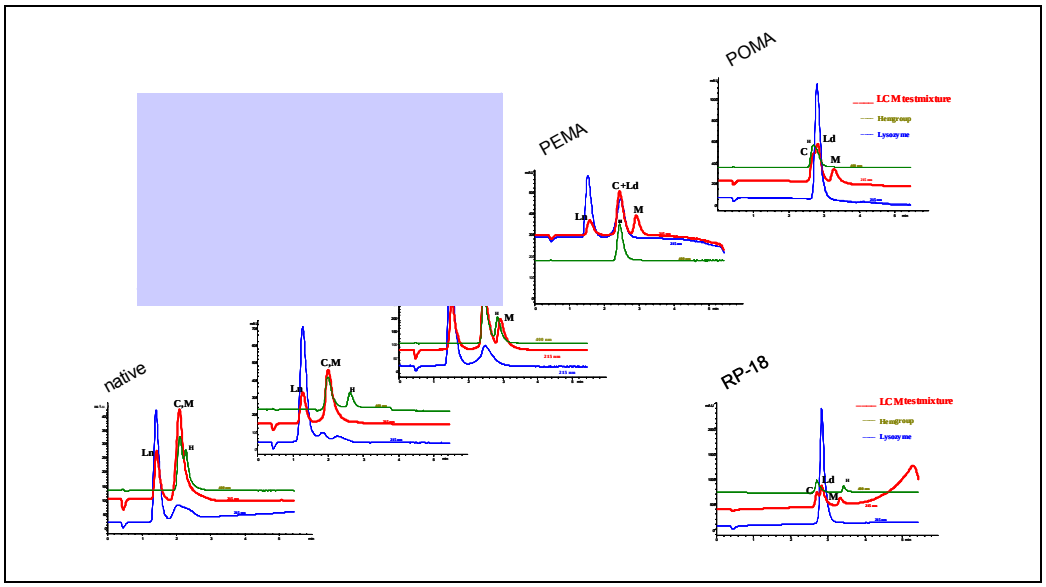

Figure 60: Elution profiles of LCM-test-mixture at different wave lengths on different stationary phases.

As expected, the chromatograms exhibit an increase in the retention times with increasing hydrophobicity of the stationary phases in the following order:

P2HEMA < P2HE.-E < PEMA < POMA

While the native silica is even more hydrophilic, than the polymer-coated silicas, the C18-modified silica exhibits the same chromatographic properties as the POMA-coated phase. As the surface of the silica is only covered with polymer by a physical adsorption process, surface silanol-groups may not be completely shielded by the coating[38], especially as only relatively small carbon loads in comparison to the C18-phase could be achieved by the physisorption process.

The unmodified LiChrospher™ Si300 exhibits the smallest retention and worst separation capabilities for the LCM-test-mixture of all of the tested stationary phases. Lysozyme (Ln) in the native form elutes first, then myoglobin (M) elutes together with cytochrome C (C) in a single peak, which is proven by experiments where only the single compounds are injected in the HPLC-instrument. Lysozyme elutes in two peaks: the first, sharp peak represents the native form, and a broad peak in the 215 nm signal after cytochrome C is generated by the denatured form.

A more hydrophobic behavior than the unmodified silica can be observed for the stationary phase coated with poly(2-hydroxy-ethylmethacrylate) (P2HEMA) as the most hydrophilic polymer. Again, lysozyme in its native form (Ln) elutes first, followed by cytochrome C and myoglobin in one single peak, which is proven by injection of the single components. In contrast to the native silica, lysozyme is not denaturing on the P2HEMA-

coated material, as only one single peak can be observed, which elutes before cytochrome C.

More hydrophobic than the P2HEMA-coated silica is the stationary phase coated with 2-hydroxyethylmethacrylate-ethylmethacrylate-copolymer (P2HE.-E). The chromatogram exhibits much better separations than those obtained with the more hydrophilic phases. Lysozyme (Ln) elutes first, followed by cytochrome C, then denatured lysozyme (Ld) and finally myoglobin, which is baseline-separated from cytochrome C. Lysozyme is partially denatured, with a much less intense peak for the denatured form, which can be checked by the injection of single components.

Poly(ethyl-methacrylate) (PEMA) coated silica is even more hydrophobic as no hydroxyl-groups are present in the polymer-chain and thus leads also to an even more denaturing of lysozyme. Native lysozyme (Ln) elutes first, followed by cytochrome C (C), then denatured lysozyme (Ld) and finally myoglobin. Although denatured lysozyme is not separated from cytochrome C as visible at the detection wavelength of 215 nm, the PEMA-coated material exhibits the best peak geometry of the investigated materials.

Poly(octadecyl-methacrylate)-(methyl-methacrylate) copolymer (POMA) exhibits a C18-group attached to the polymer chain, representing the most hydrophobic kind of polymer in this series. The strong hydrophobic interactions cause complete denaturing of lysozyme during the chromatographic run. Therefore cytochrome C (C) elutes first and then denatured lysozyme (Ld) followed by myoglobin.

The octadecyl-silane modified silica (C18) represents the standard-phase for reversed phase chromatography with a very high hydrophobicity. The chromatogram exhibits the same properties as obtained with the POMA coated phase.

Figure 61 shows the biorecoverys of all three proteins observed on polymer-coated silicas, representing a very good biorecovery of the analytes, with only small variations between the different proteins and columns (see Table 31).

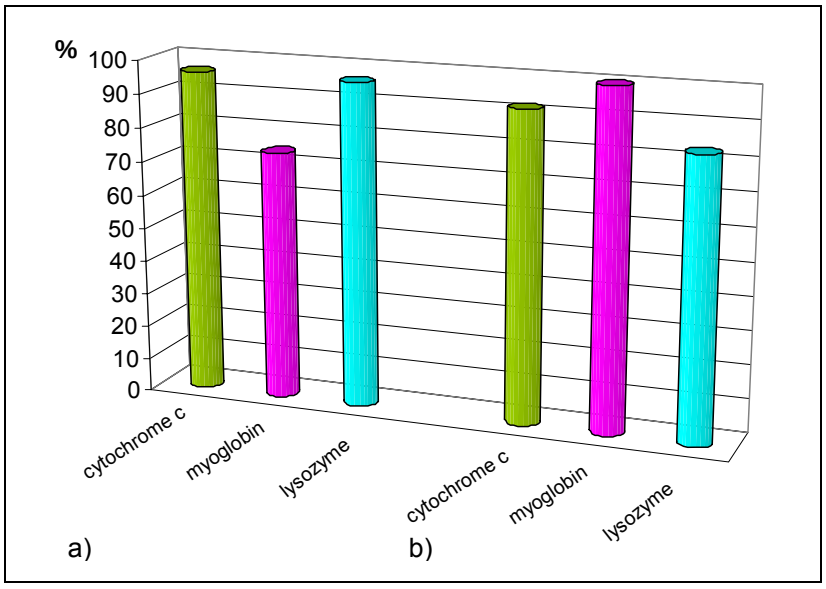

Figure 61: The overall biorecovery of three proteins by a mixture of lysozyme, cytochrome C and myoglobin a) P2HEMA and b) PEMA.

Table 31: Biorecovery data of lysozyme, cytochrome C and myoglobin in per cent.

analytes	**biorecovery** in % on P2HEMA modified column	**biorecovery** in % on PEMA modified column
cytochrome C	96.24	91.93
myoglobin	73.97	100.00
lysozyme	96.26	83.06

5.3.3.2.2 Relative Enzymatic Activity Test – Alcohol Dehydrogenase (ADH)

Alcohol dehydrogenase (ADH) was employed as indicator for the biocompatibility of the stationary phases (see 3.3.3.2) by comparing the enzymatic activity of ADH which was applied to the stationary phase with the activity of ADH, which was only exposed to the stress of the chromatographic equipment as 100 %-reference. The chromatographic conditions are shown in Table 32.

Table 32: Chromatographic conditions for the enzymatic activity test as shown in Figure 62.

HPLC conditions
analyte: ADH; mobile phase: 0.1 M Tris-HCL, pH= 8.8
concentration: 2mg/ml; injection volume: 8 µl
flow rate: 1 ml/min
Collection of Samples
empty column from 0.0-0.7 min = 700 µl
test column from 0.3-1.0 min = 700 µl

The collected ADH was used for catalysing the decomposition of ethanol with NAD^+ to acetaldehyde and NADH. The reaction (see 3.3.3.2) was followed in a photometer (see Appendix 7.3.6) via the formation of NADH, which exhibits a strong absorption at 366 nm.

Figure 62 represents the formation of NADH after applying ADH samples to the reaction mixture. The samples were collected after the exposure to different stationary phases and the HPLC equipment without a column.

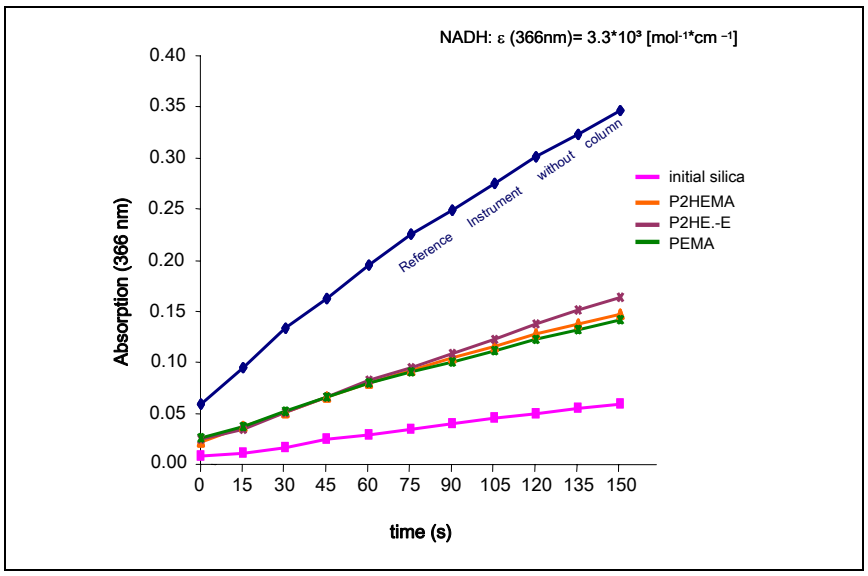

Figure 62: ADH-catalyzed formation of NADH by the application of ADH-samples after passing different stationary phases.

The enzymatic activity for the ADH samples was determined by dividing the slope of the sample-curve with the reference curve and multiplying with 100 %. The results are listed in Figure 63. ADH did not elute from the POMA- and C18-coated phases, therefore the enzymatic activity was set to 0 %.

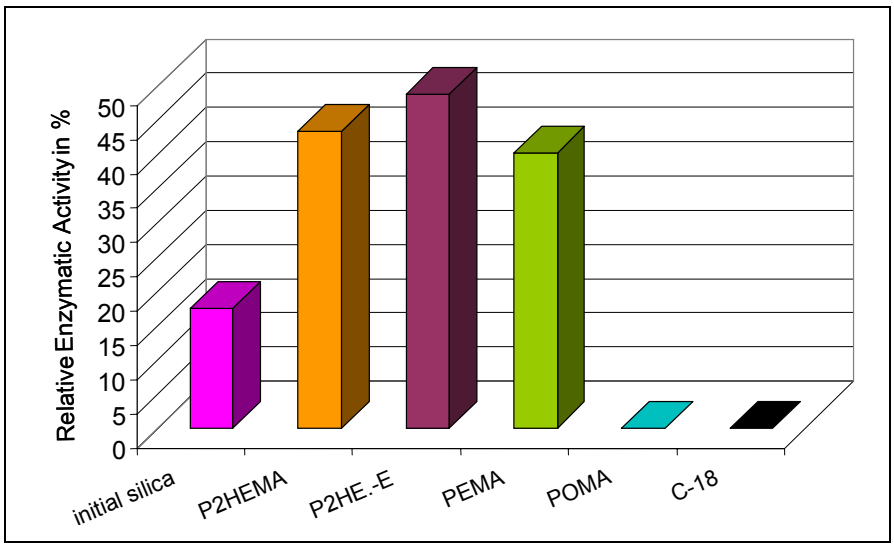

Figure 63: Relative enzymatic activity of ADH in per cent on different stationary phases by increasing hydrophobicity.

The contact of the enzyme with the stationary phase during the chromatographic run causes for all listed materials a strong decrease in the enzymatic activity of ADH. Medium hydrophobic phases exhibit the smallest denaturation potential towards ADH. Hydrophilic (initial silica) and the most hydrophobic (POMA / C18) phases have the largest denaturation potential. The P2HE.-E-coated stationary phase shows the smallest denaturation potential resulting in an enzymatic activity of ADH of nearly 50 %.

Table 33: Relative enzymatic activity data of ADH in per cent on different stationary phases by increasing hydrophobicity.

sample	initial silica	P2HEMA	P2HE.-E	PEMA	POMA	C18
relative enzymatic activity in per cent	17.51	43.40	48.76	40.24	0	0

5.3.3.2.3 Summary

Both of the testing procedures, LCM-test-mixture and enzymatic activity tests are favouring the medium hydrophobic phases as the best candidates for further optimization of the polymer coatings. P2HE.-E- and PEMA-coated stationary phases exhibited good chromatographic resolution for the LCM-test-mixture by only partial denaturing of lysozyme. Furthermore, these phases exhibited the smallest denaturation potential towards ADH, leaving the enzyme in a widely intact state after the chromatographic run.

As only partial coverage of the surface with polymer coating by the physisorption method can be assumed, denaturation may be caused by the contact of ADH with uncovered silanol-groups from the silica surface. Therefore further investigations had to be performed with a higher surface coverage with polymer. For the optimization of the polymer layer in the next stage of experiments, the intermediate hydrophobic phases P2HE.-E and PEMA were chosen.

5.3.3.3 Intermediate Hydrophilic Phases via the chemisorption route

Further investigations are performed on stationary phases with chemisorbed polymer coatings generated via a grafting-from approach (see 3.1.6.2.2.). The first set of experiments was used for comparison respectively confirmation of the results obtained with physisorbed polymer-coated stationary phases. As base silica LiChrospher™ WP 300, 15µm (Batch No. ATP107g, Merck KGaA, Darmstadt, Germany) was utilized. The investigated polymer coatings were based on the following monomer respectively co-monomer compositions: poly-(ethylmethacrylate) (PEMA) for ATPE 10 and 2-hydroxyethyl-methacrylate-ethylmethacrylate-copolymer (P2HE.-E) for ATPV 10.1.

Synthesis parameters

The materials were coated with a standardized polymerization procedure (see Appendix 7.1.3), represented by the following reaction parameters: Results of the elemental analysis for the polymer-coated materials are listed in Table 34:

Table 34: Synthesis parameters and elemental analysis of the initial silica ATP107g, P2HE.-E and PEMA modified phases.

sample	Net weight of azo silica [g]	Net weight of co-monomer [g] 2HEMA	EMA	%C (w/w)	%H (w/w)	%N (w/w)
ATP107g	-	-		0.13	0.46	< 0.01
ATPV 10.1	8.0	1.31	1.12	11.76	1.70	0.10
ATPE 10*	5.0	0	1.71	7.69	1.20	0.06

*The reaction-time was 4 hours at 90 °C.

Characterization of the pore system was performed by nitrogen sorption measurements and by ISEC-experiments.

Pore structural data by N_2-sorption at 77 K

Nitrogen sorption measurements were performed at 77 K and the results are shown in Figure 64:

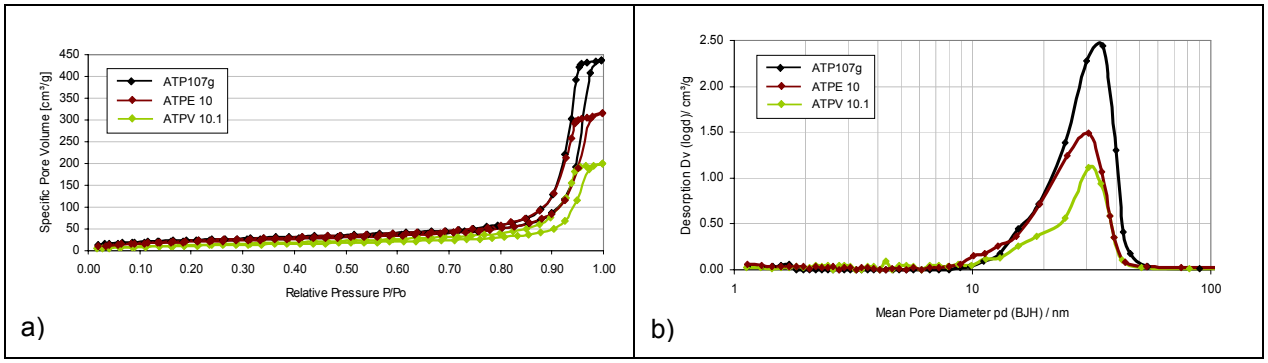

Figure 64: Nitrogen sorption measurements of P2HE.-E and PEMA modified phases in comparison with the initial silica - a) isotherms and b) pore size distributions.

Table 35: Pore structural data of the initial silica ATP107g, P2HE.-E and PEMA modified phases.

sample	a_S (BET) [m^2g^{-1}]	v_p (G) [ml g^{-1}]	p_d (BJH) [nm]
ATP107g	79	0.701	30.2
ATPV 10.1	43	0.326	30.6
ATPE 10	75	0.509	25.0

The nitrogen sorption isotherms (see Figure 64a)) show a strong decrease of adsorbed nitrogen at any given p/p_0-value in comparison with the uncoated silica ATP107g, indicating the loss of accessible pore volume due to the space occupied by the polymer coating. The steep increase of the p/p_0-value, where the pores are filled is not influenced remarkably by

the polymer coating, which can be interpreted as only small changes of the pore size distribution, which is visible in Figure 64b).

Pore structural data by ISEC employing PPM

ISEC measurements were performed with polystyrenes in THF. The results are shown in Figure 65. Details are listed in Table 36 together with the results of the nitrogen sorption measurements.

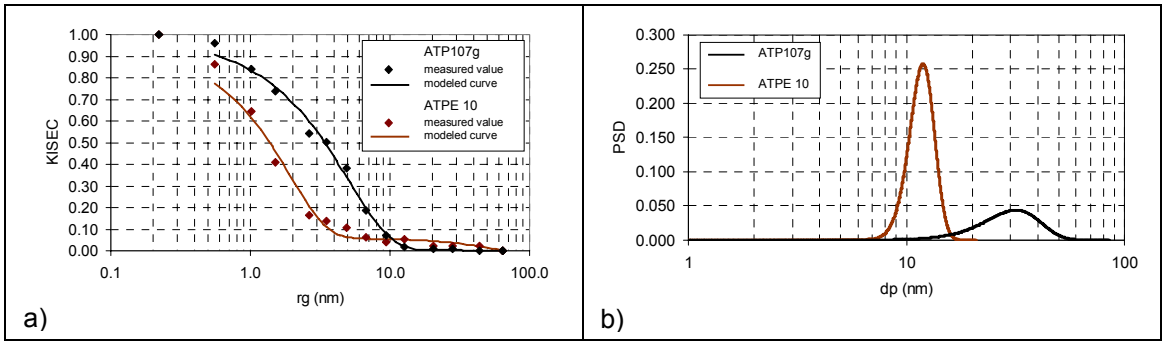

Figure 65: ISEC measurements with THF of unmodified silica ATP107g and modified silica ATPE 10 – a) calibration plots and b) volume based pore size distribution obtained by PPM.

Table 36: Pore structural data of unmodified silica ATP107g and modified silica ATPE 10 applied by PPM and PNM.

sample	p_d (BJH) [nm]	$p_{d,ave}$ (PNM) by volume [nm]	σ_{pd} by volume [nm]	n_T (PNM)
ATP107g	30.2	32.5	8.96	> 10
ATPE 10	25.0	11.9	1.55	> 10

The ISEC-measurements also indicate a decrease of the porosity of the sample material. But in contrast with the nitrogen sorption measurements, a distinct constriction of the pore system is detected down to less than its initial value. The pore connectivity value n_T is not changed at all by the polymer coating exhibiting the ideal value of >10 for all investigated materials.

5.3.3.3.1 Chromatographic Evaluation – LCM-test-mixture

A test mixture consisting of lysozyme, cytochrome C and myoglobin (LCM) was used as standard test application for gathering information about the chromatographic capabilities towards biopolymers of the stationary phases. The polymer-coated materials were packed into stainless steel columns with 25 mm length and an inner diameter of 4 mm (see Appendix 7.3.2) to allow best comparison with the results obtained with the physisorbed materials (see 5.3.3.2). Furthermore, identical chromatographic conditions (see Table 30) were chosen for the separation of the LCM-test-mixture. The chromatograms are shown in Figure 66.

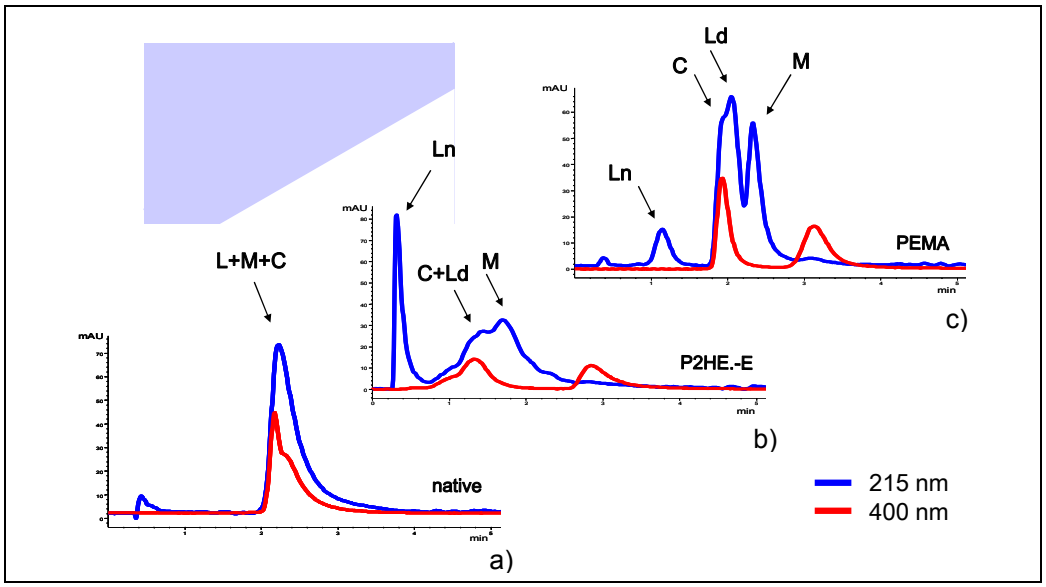

Figure 66: Elution profiles of LCM-test-mixture at different wave lengths applied on columns packed with the initial silica ATP107g (native), P2HE.-E - and PEMA – modified silica.

Figure 66a) displays the chromatogram of the unmodified silica ATP107g. The chromatogram exhibits only two peaks. The very small first peak represents lysozyme (Ln) in its native state. Lysozyme gets nearly completely denatured during the chromatographic run, which was checked by injecting the single components. Denatured lysozyme (Ld) elutes together with cytochrome C and myoglobin in one broad peak. The hem-group of myoglobin elutes shortly after the rest of the molecule, which was checked in the single component runs at a wavelength of 400 nm.

Figure 66b) displays the chromatogram of the P2HE.-E-modified silica ATP107g. The first, large and narrow peak represents lysozyme (Ln) in its native state. Lysozyme is only partially denatured during the chromatographic run, which was checked by the single component-runs. Denatured lysozyme (Ld) elutes shortly after cytochrome C and just before myoglobin, but they are only partially separated from each other. The hem-group of myoglobin is split off during the chromatographic run and elutes much later, which is detected as the second peak at 400 nm wavelength.

Figure 66c) displays the chromatogram of the PEMA-modified silica ATP107g. Lysozyme (Ln) in its native state elutes first, but most of the lysozyme is denatured during the chromatographic run and elutes not well separated shortly after cytochrome C. Myoglobin elutes in a sharp peak afterwards, which is not baseline-separated from the previous one. Again, the hem-group of myoglobin is split off and elutes later, detected as second peak at 400 nm wavelength.

The biorecovery of the analytes was determined by chromatographic runs with injection of the single components. The results are listed in Table 37.

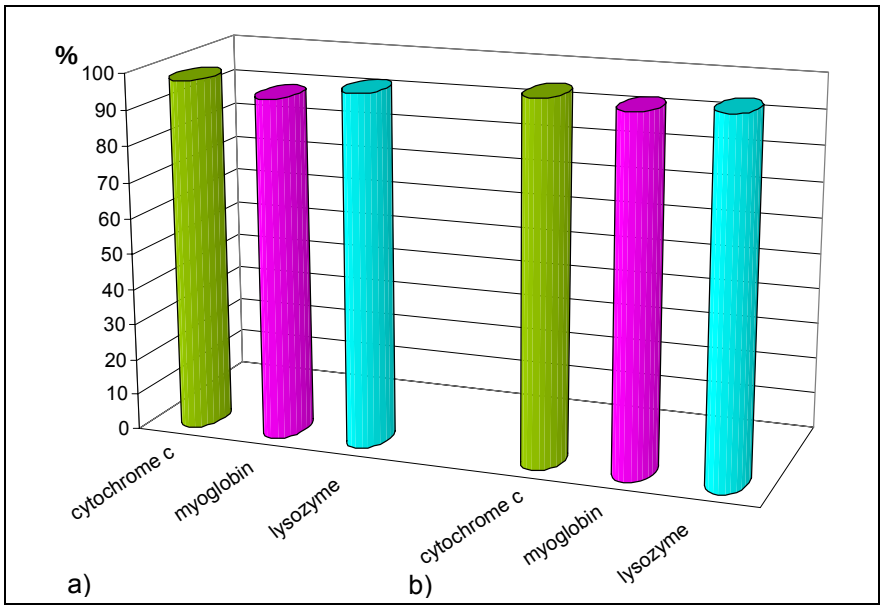

Figure 67: The overall biorecovery of three proteins by a mixture of lysozyme, cytochrome C and myoglobin a) P2HE.-E - and b) PEMA – modified silica.

Table 37: Biorecovery data of lysozyme, cytochrome C and myoglobin in per cent.

analytes	**biorecovery** in % on P2HE.-E modified column	**biorecovery** in % on PEMA modified column
cytochrome C	97.74	99.73
myoglobin	94.39	97.79
lysozyme	97.54	99.12

The best chromatographic resolution was achieved with the PEMA-coated stationary phase. The P2HE.-E coated stationary phase show much broader peaks compared to the PEMA-coated stationary phase, but offers the smallest denaturation potential towards lysozyme of all investigated stationary phases. The unmodified base silica ATP107g is nearly completely denaturing lysozyme during the chromatographic run.

5.3.3.3.2 Relative Enzymatic Activity Test – Alcohol Dehydrogenase (ADH)

As explained in 5.3.3.2.2 ADH was used as indicator for the impact of the stationary phase upon the biological activity of a biopolymer by probing the loss in its enzymatic activity. The chromatographic conditions are listed in Table 38.

Table 38: Chromatographic conditions for the enzymatic activity test as shown in Figure 68.

HPLC conditions
analyte: ADH; mobile phase: 0.1 M Tris-HCL, pH= 8.8
concentration: 2mg/ml; injection volume: 6 µl
flow rate: 1 ml/min
Collection of Samples
empty column from 0.0-0.7 min = 700 µl
test column from 0.1-0.8 min = 700 µl

After exposure to the stress of the chromatographic equipment and the stationary phase, ADH was collected for catalysing the decomposition of ethanol with NAD^+ to acetaldehyde and NADH. The reaction was followed in a photometer via the formation of NADH, which exhibits a strong absorption at 366 nm.

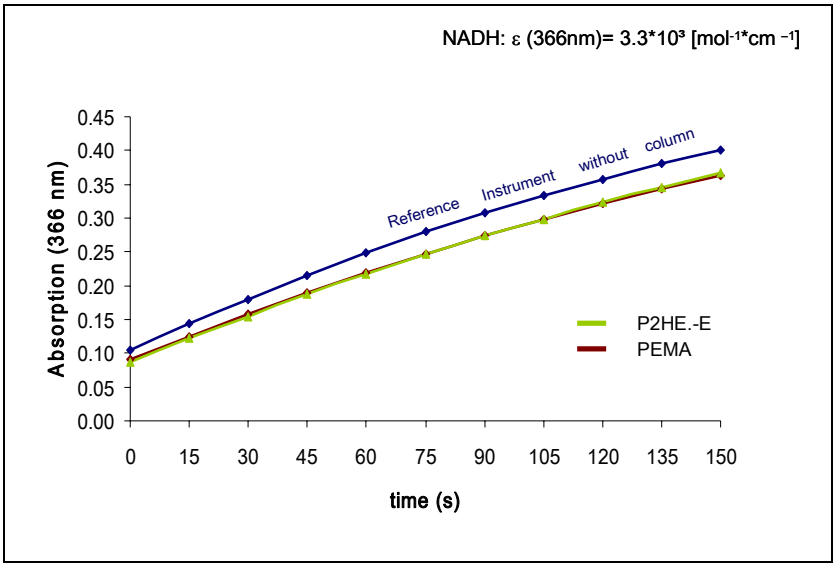

Figure 68: ADH-catalyzed formation of NADH by the application of ADH-samples after passing different stationary phases.

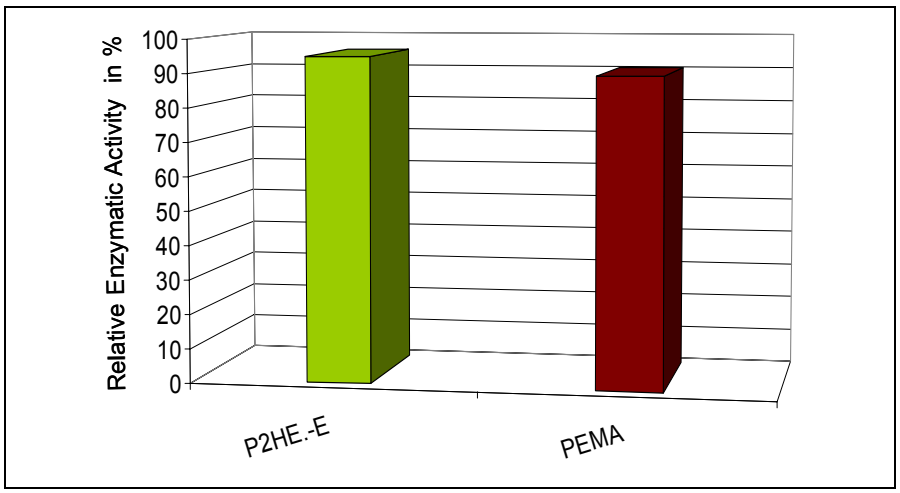

Figure 69: Relative enzymatic activity of ADH in per cent on P2HE.-E and PEMA coated stationary phases.

The enzymatic activity was determined by division of the slope of the curves and multiplication with 100 %. The results are listed in Table 39.

Table 39: Relative enzymatic activity data of ADH in per cent on P2HE.-E and PEMA coated stationary phases.

sample	P2HE.-E	PEMA
relative enzymatic activity in per cent	95	90

The contact of ADH with the polymer-coated stationary phases has only a minor impact upon its enzymatic activity, with an enzymatic activity in the range of about 90 % for both of the polymer-coated stationary phases. The highest enzymatic activity is obtained with the P2HE.-E-coated stationary phase.

5.3.3.3.3 Summary

The grafting-to-approach allows the synthesis of chemisorbed polymer-coated stationary phases with higher grafting densities than those obtained via a physisorption process. P2HE.-E respectively PEMA-coated materials obtained via a chemisorption process exhibited nearly identical chromatographic properties for the LCM-test-mixture, than those coated with the same polymer composition via a physisorption process. The polymer-coated stationary phases via the grafting-from approach caused only a minor decrease of the enzymatic activity of ADH in the enzymatic activity test, indicating a small denaturation potential.

By means of smallest denaturation potential, the P2HE.-E coated stationary phase exhibited the best qualities. It denatures lysozyme to only a small extend in the LCM-test-mixture and ADH shows the highest enzymatic activity after contact with the P2HE.-E coated stationary phase. Therefore the intermediate hydrophobic phases P2HE.-E was chosen as candidate for the further optimization of the polymer coating.

5.3.3.4 Fine Tuning of the Polymer Composition

The P2HE.-E-coating is a copolymer consisting of equal parts of 2HEMA and EMA co-monomers also referred to as 50/50 (n/n) composition. In the following experiments, composites with 75/25 (n/n) and 25/75 (n/n) 2HEMA/EMA were investigated to monitor the effect of a slightly change in hydrophobicity. The application of the DoE principles may simultaneously generate hints for the optimization of the polymer layer thickness. As base

silica LiChrospher™ WP 300, 15µm (Batch No. ATP107g, Merck KGaA, Darmstadt, Germany) was utilized.

5.3.3.4.1 Design of Experiments (DOE)

As standard experimental layout, values of 10 % carbon content and a 50/50 composition was chosen. This experiment was performed three times to gather information about reproducibility and experimental error. For the carbon content, 5 % as low value and 15 % as high value was applied for the first set of experiments. The polymer composition should be varied in the range from 25/75 to 75/25 2HEMA/EMA content. This yields the experimental layout for the target values as listed in Table 40 for the first set of experiments. Also listed in Table 40 are the experimentally obtained values.

Table 40: Target parameters according to DoE principles for the optimization of the P2HE.-E coating and experimentally obtained values.

2HEMA / EMA ratio	**% C** (w/w) (target value)	**% C** (w/w) (experiment)
75/25	~ 5	5.71
75/25	~ 15	13.25
50/50	~ 10	12.70
50/50	~ 10	11.75
50/50	~ 10	11.03
25/75	~ 5	3.09
25/75	~ 15	17.31

All polymer coatings were produced by using a standard polymerization procedure (see Appendix 7.1.3) by variation of monomer composition, monomer concentration and reaction time. As base silica ATP107g was employed. Table 41 lists the reaction parameters together with the results of the physical characterization by elemental analysis and nitrogen sorption experiments.

Table 41: Synthesis parameters and results of physical characterization for the base silica ATP107g and the polymer-coated silicas.

2HEMA / EMA ratio	sample name	amount monomer [mmol]	reaction time [h]	elemental analysis % C (w/w)	a_S (BET) [m^2g^{-1}]	v_p (G) [ml g^{-1}]	p_d (BJH) [nm]
Reference	ATP107g	-	-	0.13	79	0.701	30.2
AZO	AZO19D04	-	-	2.70	79	0.578	30.2
75/25	ZB13D04B	4	4	13.25	66	0.276	30.7
75/25	ZB13D04C	2	4	5.71	33	0.524	30.5
50/50	ZB24C04D2	6	4	12.70	28	0.234	30.5
50/50	ZB6D04D1	5	2	11.75	38	0.2976	30.7
50/50	ZB6D04D2	4.5	2	11.03	37	0.2979	35.1
25/75	ZB24C04F	3	4	3.09	80	0.604	30.0
25/75	ZB24C04E	10	4	17.31	3	0.040	25.0

The polymer load could be adjusted in most cases by the variation of the amount of monomer. The nitrogen sorption measurements indicate a strong decrease of the specific pore volume v_P and specific surface area a_s according to BET with increasing polymer load, while no significant change of the pore diameter values according to BJH were observed.

This is reflected by the DoE-data treatment. The relation of the N_2-sorption data with the carbon load is shown in the following Figure 70.

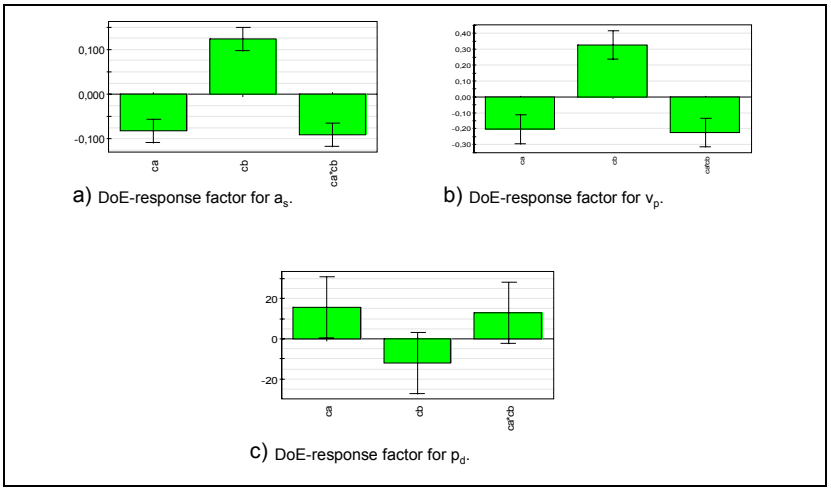

Figure 70: DoE-response factors for a) a_s, b) v_p, and c) p_d retrieved by nitrogen sorption data corresponding to the carbon load of the stationary phases.[143]

Figure 70a) and b) exhibit the typical behaviour for a linear correlation of response factors. This implicates, that there is a linear correlation between a_s, v_p and the carbon load of the stationary phase. Figure 70c) shows that there is no correlation between p_d from nitrogen

[143] A. Bamberg, internal communication, 1. Versuchsplan, Darmstadt june 2004

sorption experiments and the carbon load. The linear dependency between a_s, v_p and the carbon load is visualized in Figure 71, by plotting experimental data vs. predicted values based on standardized values.

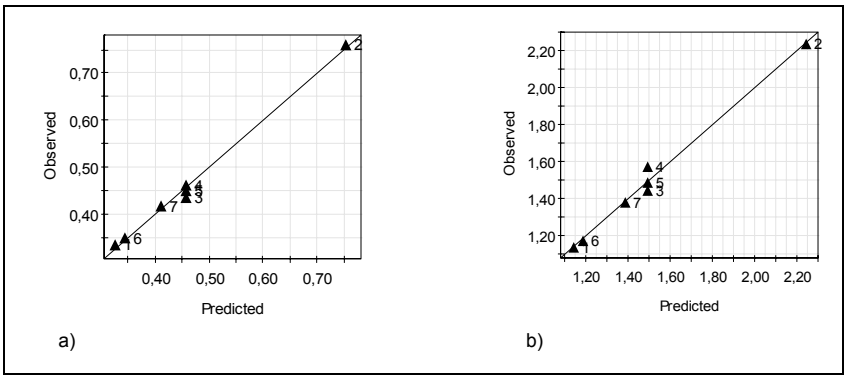

Figure 71: Observed vs. predicted values for a) a_s and b) v_p by using a linear relation based on standardized values.[143]

No dependency between the co-monomer composition and other experimental data was observed by DoE methods.

5.3.3.4.2 Chromatographic Evaluation

All materials were packed in chromatographic columns of 125 mm length and 4 mm inner diameter. A standard mixture of dioxane/toluene/cyclohexanol 25/25/50 v/v/v was used for the packing procedure (see Appendix 7.3.2).

LCM-test-mixture

The separation capabilities towards proteins were checked with a test mixture consisting of lysozyme, cytochrome C and myoglobin in gradient mode by reversed phase chromatography. The chromatographic conditions are listed in Table 30. Figure 72 shows the chromatograms of all tested columns.

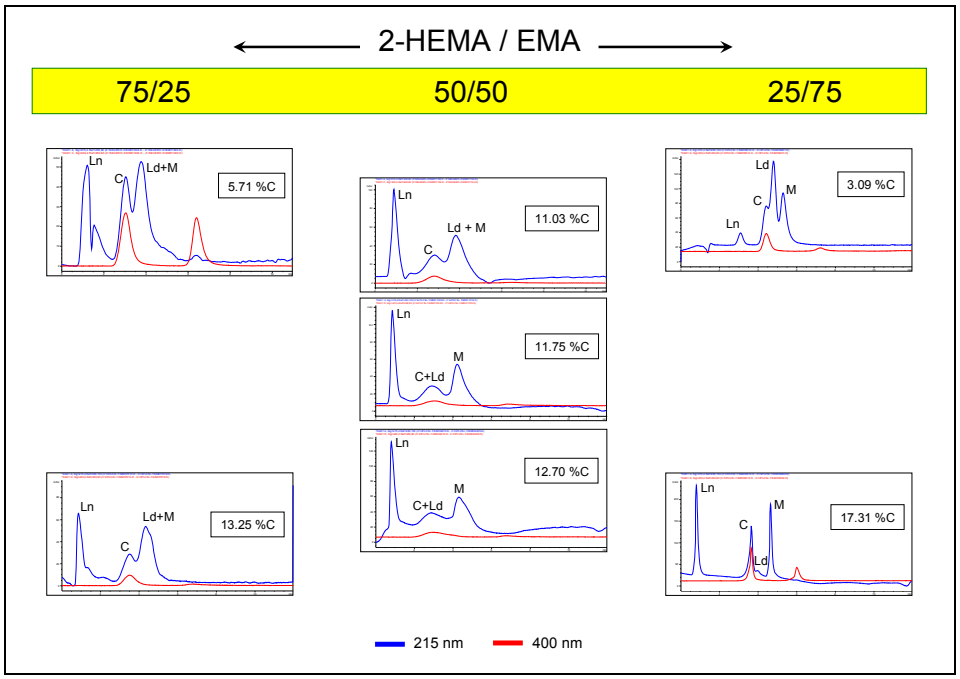

Figure 72: Elution profiles of LCM-test-mixture for columns coated with different co-monomer-compositions respectively polymer load.

The most hydrophilic phases are the ones coated with the 75/25 (n/n) 2-HEMA/EMA-ratio. Both columns exhibit similar retention times of the proteins, but the chromatographic resolution is much higher for the material with the smaller polymer load of 5.71 %. Lysozyme in its native form (Ln) elutes first. The shoulder in the chromatogram of the column with the higher polymer load respectively the second peak of the column with less polymer load are also lysozyme-related as checked by single component injections. The next peak represents cytochrome C (C) and then myoglobin (M) together with denatured lysozyme (Ld). Nearly half of the lysozyme gets denatured during the chromatographic run. The hem-group of myoglobin elutes last, detected at 400 nm wavelength.

All materials coated with a copolymer consisting of 50/50 (n/n) 2-HEMA/EMA, also referred to as P2HE.-E-coated phases have similar polymer loads, as expressed as variation of the carbon contents ranging from 11.03 % to 12.70 %. Thus, all three columns exhibit nearly identical chromatograms. Lysozyme in the native form (Ln) elutes first, then cytochrome C together with denatured lysozyme (Ld) and then myoglobin in a third, distinct peak. The hem-group of myoglobin is split off and elutes in a broad peak after the rest of the molecule.

A slightly more hydrophobic coating consists of 25/75 (n/n) 2-HEMA/EMA-based copolymer. A coating resulting in 3.09 % carbon content indicates, that only a partial coverage with polymer was achieved, as base silica modified with AZO-initiator yields already 2.70 % carbon content. Therefore, the chromatographic behaviour is mainly influenced by the - hydrophilic - native silica. The small first peak represents lysozyme in its

native form (Ln), while most of lysozyme elutes in the denatured form (Ld) in a distinct peak after cytochrome C (C), although they are only partially separated from each other. Afterwards elutes myoglobin and finally the hem group of myoglobin. The column with the higher polymer load, represented by 17.31 % carbon content shows the best chromatographic resolution for the LCM-.test mixture of all tested columns. First, native lysozyme (Ln) elutes, then cytochrome C and denatured lysozyme is represented by a shoulder of the cytochrome C peak. Then the myoglobin peak appears which is baseline-separated from the peak before and as last peak the hem-group of myoglobin is visible in the detector-signal at 400 nm.

H-vs.-u-curves

The dependence of the chromatographic performance from the linear flow velocity is an important criterion for the evaluation of stationary phases. As a first test, the chromatographic performance by means of plate height was investigated employing uracil, which is usually employed in reversed-phase chromatography as dead time marker. This set of columns was evaluated by M. Stein at laboratory of Dr. M. Schulte, Merck KGaA, Darmstadt. The chromatographic conditions are listed in Table 42 for the testing procedure.

Table 42: Chromatographic conditions for H-vs.-u-curves with uracil as analyte.

column dimension: 125 x 4 mm ID; detection: 254 nm;
@ room temperature; flow rate: 0.2 – 7.0 ml/min;
analytes: uracil
mobile phase: 40 % A: 0,1 % acetic acid in water, pH= 1,8 60 % B: 25 % iso-propanol in water

The results are shown in Figure 73 for the tested columns.

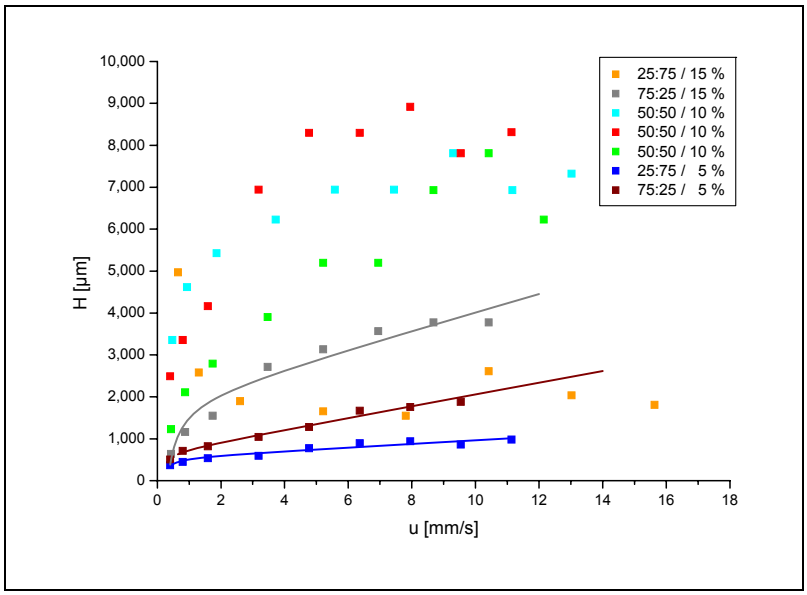

Figure 73: H-vs.-u-plots of columns coated with different co-monomer-compositions respectively polymer load.

Table 43: H-values and C-values of columns coated with different co-monomer-compositions respectively polymer load.

sample	**elemental analysis** % C (w/w)	**Plate Height H** [µm] at 0.2 ml/min	**C-term** [ms] according to Knox
75/25	13.25	642	215.7 ± 46.4
75/25	5.71	507	140.0 ± 10.3
50/50	12.70	2507	-
50/50	11.75	3373	-
50/50	11.03	1224	-
25/75	3.09	373	42.5 ± 8.8
25/75	17.31	1552	-

All columns packed with polymer-coated stationary phases exhibit very poor plate height values in the range between 373 and 1552 µm (see Table 43). This conflicts with a trusting interpretation of the experimental data according to the Knox equation as it implies a very poor packing of the stationary phase. For well packed stationary phases a value between 30 and 75 µm is expected. Furthermore all curves show a buckling at higher flow-rates towards lower plate height values, which is in general an indication for a breakdown of the packing-bed. After the chromatographic evaluation, all columns were opened and a shrinking of the packing bed up to several millimetres was visible.

5.3.3.5 Conclusion

The application of the DoE principle yields valuable information for the further optimization process by a concise set of experiments.

First of all, the experimental data showed a clear dependency between a_s, v_p and the polymer load as represented by the carbon contents of the final product, which is independent from the co-monomer composition. The DoE approach furthermore reveals that the measurement of p_d via nitrogen sorption experiments must be inappropriate.

Furthermore the DoE reveals an unfavourable choice of the experimental parameters as a 10 %-value for the carbon contents should be treated as high value. The lower limit must be guessed to be in the range of 4 %, as a polymer coating of about 3 % shows already the chromatographic behaviour of the uncoated silica. This gives a target carbon contents for the medium value of about 7 %.

The LCM-test-chromatograms are very useful for the evaluation of the separation capabilities towards proteins in gradient elution mode, as the separation depends mostly on surface interactions between analyte and stationary phase. The quality of the packing bed plays only a minor role in this separation process. This is also shown by the excellent agreement of the chromatograms for the three columns packed with the P2HE.-E-coated phases 50/50 (n/n) with similar carbon contents.

All columns exhibit comparable separation capabilities for the LCM-test-mixture, favoring in general polymer coatings with lower carbon contents, although by far the best separation is achieved for the column with the highest carbon contents: the stationary phase coated with the 25/75 (n/n) 2-HEMA/EMA-copolymer resulting in a carbon contents of 17 % resulting in the by far smallest pore volume v_p of 0.04 ml/g and a surface area a_s of only 3 m^2/g. These values indicate that the resulting stationary phase can be regarded as a nonporous packing material, which should exhibit only small loadability and therefore is not the subject for further investigation in this work, although this explains well the sharp peaks.

The second criterion for the optimization of the polymer layer was the copolymer composition by means of which state of hydrophobicity is the most favorable. Therefore, a medium hydrophobic phase with 50/50 (n/n) 2-HEMA/EMA-copolymer (“P2HE.-E-coated phases”) composition was chosen as medium value and only small variations towards more hydrophilic (25/75 (n/n) 2-HEMA/EMA-copolymer) or more hydrophobic (25/75 (n/n) 2-HEMA/EMA-copolymer) coatings. The chromatographic evaluation by the LCM-test-mixture exhibits clear differences between the different phases and recommends the medium hydrophobic phase as best tradeoff between chromatographic resolution and lowest denaturation potential.

To conclude this, further experiments should be performed to optimize the polymer coating based on the P2HE.-E-coated phase with a 50/50 (n/n) monomer composition of 2-HEMA/EMA. An optimum value for the carbon content is expected to be much less then 10 %, which gives the upper target value for polymer coverage as expressed in carbon contents. To gather valid figures for the chromatographic performance in isocratic mode – mainly for the H vs. u-curves of small molecules - a further optimization of the packing procedure has to be performed, which prevents the breakdown of the packing bed.

5.3.4 Variation of the Polymer Load

A polymer coating based on a 50/50 (n/n) monomer composition of 2-HEMA/EMA was chosen for further optimization steps. In this paragraph, the influence of the polymer load as expressed by carbon contents is investigated. As the organic linker already gives 2.76 % carbon content (see Table 26), polymer-coated materials with ca. 5 – 10 % carbon content should be investigated.

5.3.4.1 Synthesis Parameters

Materials with different polymer load where synthesized by variation of the monomer concentration. All other parameters like reaction time, temperature and silica concentration where kept constant as described for the standard polymerization procedure (see Appendix 7.1.3). The experimental parameters are listed in Table 44, as base silica LiChrospher™ WP 300, 15µm (Batch No. ATP107g, Merck KGaA, Darmstadt, Germany) was employed.

Table 44: Elemental analysis and experimental parameters of P2HE.-E-coated silicas for variation of the polymer load and resulting carbon contents.

sample	**Net weight of azo silica** [g]	**Net weight of co-monomer** [g] 2HEMA	EMA	**%C** (w/w)	**%H** (w/w)	**%N** (w/w)
ATP107g	-	-	-	0.13	0.46	< 0.01
C18	-	-	-	4.52	0.80	< 0.01
ATPV 4	2.5	0.167	0.142	4.55	1.02	0.05
ATPV 6	2.5	0.251	0.213	5.82	1.00	0.03
ATPV 9	2.5	0.315	0.286	9.15	1.65	0.04

The results obtained via elemental analysis show the successful synthesis of materials with three polymer coatings represented by a value for the carbon content of 4.55% (ATPV 4), 5.82% (ATPV 6) and 9.15% (ATPV 9). The decrease of the nitrogen content from a value of 0.73 % (see Table 26) for the initiator-coated material down to ~ 0.03 % for the polymer-coated materials is due to the successful decomposition of the initiator groups, which prevent the binding of the polymer onto the surface of the silica.

5.3.4.2 Pore Structural Data by Nitrogen Sorption at 77K

The pore structural data obtained by nitrogen sorption measurements of the bulk materials are listed in Table 45. Figure 74a) shows the adsorption-desorption isotherms of nitrogen at 77 K for the polymer-coated materials. Figure 74b) gives the pore size distribution according to BJH derived from the desorption branch of the isotherm, which gives no indication for an influence of the polymer coating upon the mean pore diameter.

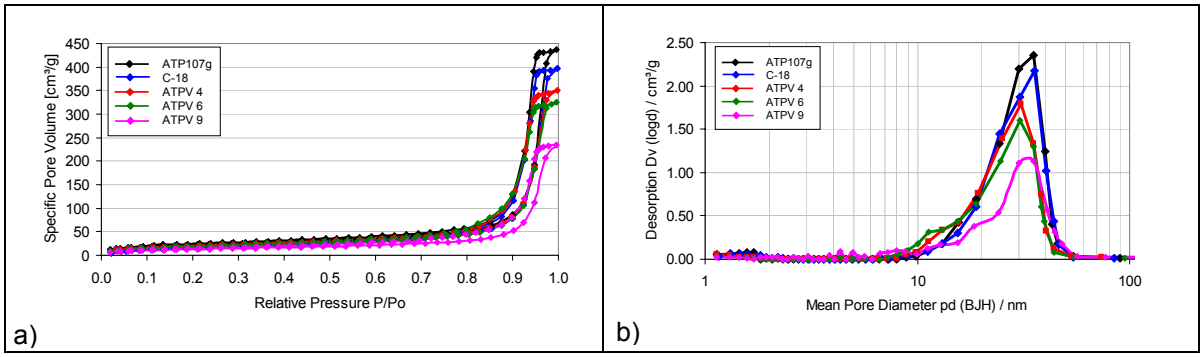

Figure 74: Nitrogen sorption measurements of the initial silica ATP107g, ATPV 4, ATPV 6, ATPV 9 and C18 – a) isotherms and b) pore size distributions.

Table 45: Pore structural data of unmodified silica ATP107g and modified silicas ATPV 4, ATPV 6, ATPV 9 and C18.

Sample	a_S (BET) [m^2g^{-1}]	v_p (G) [ml g^{-1}]	p_d (BJH) [nm]
ATP107g	79	0.701	30.2
C18	66	0.644	30.2
ATPV 4	70	0.565	30.5
ATPV 6	63	0.524	30.3
ATPV 9	46	0.378	30.1

The impact of the polymer coating upon the pore structural parameters derived from nitrogen sorption experiments is best expressed in the figures of the resulting specific pore volume, which decreases with increasing polymer load. The other values are not significantly influenced by the polymer coating, as discussed in 4.4.2.

5.3.4.3 Pore Structural Data by SEC using Polystyrene Standards employing PPM and PNM

Size-exclusion experiments in the inverse size mode are performed with chromatographic columns packed with the polymer-coated stationary phases. The packing of the columns was performed according to the procedure given in the Appendix 7.3.2. Additionally to the normal testing procedure with polystyrene standards in THF, the polymer-coated phases were also investigated with polystyrene standards in Dioxane and DMF to gather information about the swelling of the polymer coating in different mobile phases by their relation upon the resulting pore size distribution (see 4.4). Figure 75a) shows the size-exclusion calibration curves for

the different polymer-coated materials. From these curves, the pore size distribution is derived and shown in Figure 75b). Table 46 lists the pore structural data derived from ISEC-experiments with polystyrene standards in THF, dioxane and DMF.

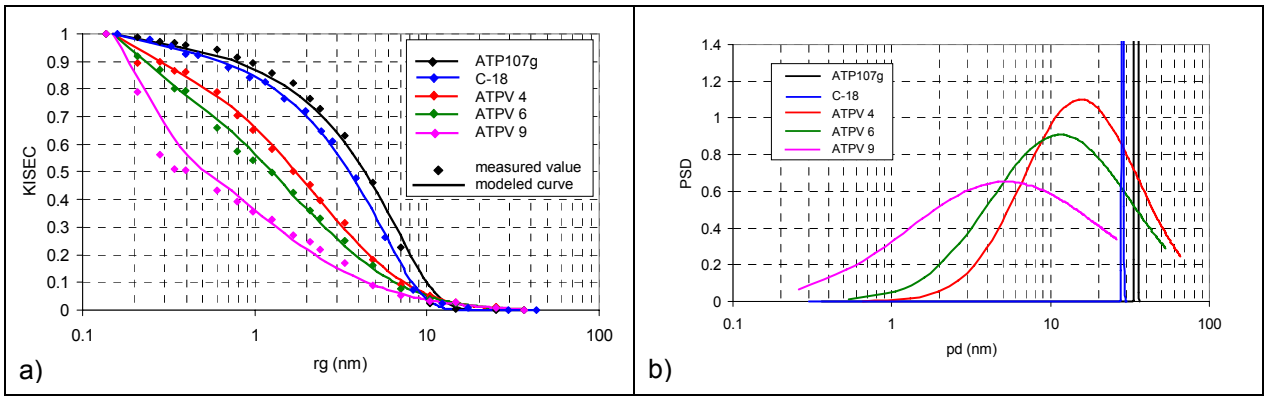

Figure 75: ISEC measurements with THF of unmodified silica ATP107g and modified silicas ATPV 4, ATPV 6, ATPV 9 and C18 – a) calibration plots and b) volume based pore size distribution obtained by PPM.

Table 46: Pore structural data of unmodified silica ATP107g and modified silicas ATPV 4, ATPV 6 and ATPV 9 and C18 applied by PPM.

sample	p_d (BJH) [nm]	$p_{d,v,ave}$ (PPM) [nm] using dioxane rel. polarity[134] 0.164	$p_{d,v,ave}$ (PPM) [nm] using THF rel. polarity[134] 0.207	$p_{d,v,ave}$ (PPM) [nm] using DMF rel. polarity[134] 0.404	n_T (PNM)
ATP107g	30.2	32.0 ± 1.0	34.6 ± 1.0	32.0 ± 0.6	> 10
C18	30.2	-	28.4 ± 0.4	-	> 10
ATPV 4	30.5	10.8 ± 0.6	11.0 ± 0.6	9.8 ± 0.8	> 10
ATPV 6	30.3	6.0 ± 0.8	7.0 ± 0.6	6.6 ± 0.8	8.2
ATPV 9	30.1	2.2 ± 0.6	2.0 ± 0.6	3.0 ± 0.8	3.6

The figures show a strong decrease of the mean pore size of the coated materials with increasing polymer load as expressed in the carbon content of the stationary phase. Furthermore, there is no change in the mean pore diameter between the different solvents. This indicates that the swelling of the polymer layer can be neglected for solvents with a relative polarity range between 0.164 and 0.404, which corresponds to the range of the investigated solvents.

The pore connectivity n_T also decreases with increasing polymer load, starting from an ideal value of 10+ for the polymer-coated material with 4.55 % carbon content, followed by a still acceptable value of 8.2 for the material with 5.82 % carbon content down to a value of only 3.6 for the material with 9.15 % carbon content representing the highest polymer load.

5.3.4.4 Chromatographic Performance: theoretical plate height vs. linear flow velocity

The chromatographic performance by means of theoretical plate height vs. linear flow velocity dependency was determined employing dibutyl phthalate in a water/acetonitrile-

mixture as solvent. To ensure maximum comparability of the obtained values, the solvent was adjusted to generate a retention coefficient in the range of k' = 3 for all the investigated stationary phases, as described in Appendix 7.3.3. Table 47 lists the chromatographic conditions for the investigated stationary phases. As reference and for comparison, columns packed with native silica ATP107g and with a commercially available C18-coated silica (LiChrospher™ WP300 RP18, 15µm, Merck KGaA, Darmstadt, Germany) with 30 nm pore size where also investigated.

Table 47: Chromatographic conditions for testing the theoretical plate height vs. linear flow velocity dependency.

column dimension: 125 x 4 mm ID; injection volume: 5 µl;
detection: 254 nm; @ room temperature;
flow rate: 0.25 – 5.0 ml/min; k'= 3
analytes: uracil, diethyl phthalate, dibutyl phthalate
mobile phase: water/ACN, n-heptane / ethyl acetate

The measured values and the calculated H-vs.-u-curves based on non-linear regression according to the Knox-equation are shown in Figure 76. The curve of the column with the highest polymer load shows a buckling at higher flow rates which indicates a breakdown of the packing bed. The other curves show a normal behaviour, although they show quite high values for the theoretical plate height H even at small flow rates. The values of the nonlinear fit according to the Knox-equation are listed in Table 48. The value for B which represents the molecular diffusion term is not sufficiently supported by the experimental data as the increase at very small flow rates was not covered by the experiments.

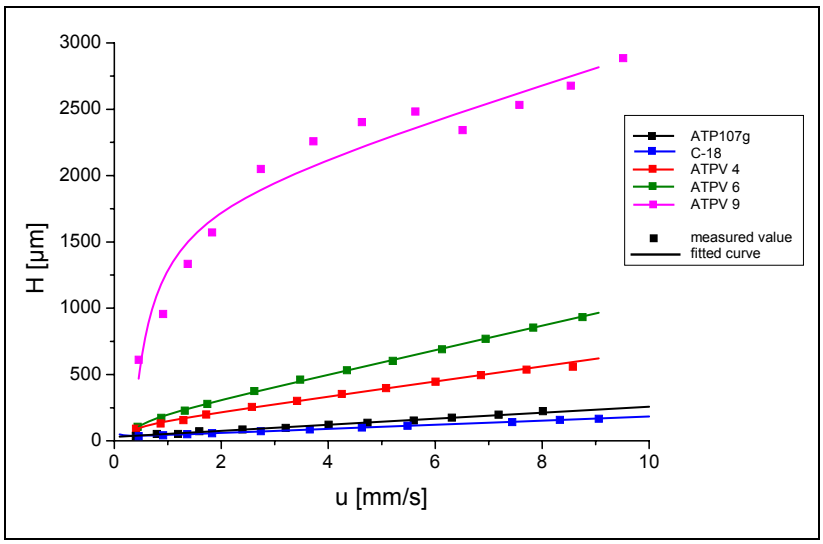

Figure 76: H-vs.-u-plots employing dibutylphthalates of unmodified silica ATP107g and modified silicas ATPV 4, ATPV 6, ATPV 9 and C18.

Table 48: H-values and C-values of unmodified silica ATP107g and modified silicas ATPV 4, ATPV 6, ATPV 9 and C18.

sample	**Plate Height H** [µm] at 0.5 mms^{-1}	**C-term** [ms] according to Knox	**A-term** [$10^{-5}m^{2/3}s^{1/3}$] according to Knox
ATP107g	37.58 ± 1	22.84 ± 0.85	29.56 ± 4.53
C18	35.64 ± 1	15.03 ± 0.18	31.45 ± 1.22
ATPV 4	90.73 ± 1	56.56 ± 1.22	111.12 ± 6.94
ATPV 6	106.59 ± 1	91.51 ± 1.40	140.14 ± 8.16
ATPV 9	610.75 ± 1	121.13 ± 30.56	1787.51 ± 191.55

The curves show clearly that the chromatographic performance improves with smaller polymer load. Although the H-values for the polymer-coated silica still exhibit much higher values than expected for well packed columns, a clear tendency is visible, favouring smaller polymer loads, as the column with the smallest polymer load exhibits the best values of the tested polymer-coated materials. The expected value for the H-value of well packed columns with a mean particle diameter of 15 µm is expected to be somewhere between 30 and 75 µm, which is fulfilled for the columns packed with native silica ATP107g and C18-coated silica. The polymer-coated stationary phases do not meet these requirements. Especially the column packed with the highest polymer load ATPV 9 is by a factor of 20 worse than the expected range. The columns with the materials with lower polymer load exhibit values for the H-value of 90.73 and 106.59 µm, which are at least in the range of the expected values, but still show, that the packing procedure has to be optimized.

The C'-term represents the mass transfer. Again, the figures for the polymer-coated stationary phases exhibit worse values than those obtained for the native silica ATP107g with 22.84 m/s or the C18-coated stationary phase with 15.03 m/s. This is partially due to the not optimized packing procedure of the polymer-coated stationary phase, but can also be explained by the loss of pore volume of the stationary phase, as found by nitrogen sorption experiments, and the decrease of the pore diameter and the pore connectivity, as found by size-exclusion experiments. A value of 121.13 for the stationary phase with the highest polymer load ATPV 9 as expressed in the carbon content of 9.15 %, 91.51 for the material with 5.82 % carbon content ATPV 6 and of 56.56 for the material with 4.55 % carbon content ATPV 4 clearly shows a trend, which favours materials with less polymer load.

5.3.4.5 Chromatographic Evaluation – complex-test-mixture

The chromatographic resolution was tested using a complex-test-mixture consisting of eight components ranging from small molecules up to proteins. The following analytes where employed: Ala-Gly; uracil; angiotensin II; angiotensin I; desmopressin; insulin; albumin; ferritin. As reference, a column packed with C18-modified silica was employed. The chromatographic evaluation was done ingredient elution mode by injection of the single

components to identify the peaks according to their retention times and then injecting the complete test mixture. The chromatographic conditions are listed in Table 49.

Table 49: Chromatographic conditions for an eight component test mixture in gradient elution mode as shown in Figure 77.

column dimension: 125mm x 4mm ID
flow rate: 0.5 ml/min; @ RT;
injection volume: 5 µl;
Figure 77a)
from 100/0 % (v/v) A/B in 60 min to 45/55 % (v/v) A/B;
Figure 77b)
from 100/0 % (v/v) A/B in 60 min to 5/95 % (v/v) A/B;
A: water + 0.1 % TFA;
B: acetonitrile + 0,09 % TFA
Analytes:
1. Ala-Gly; 2. uracil; 3. angII; 4. angI, 5. desmopressin;
6. insulin; 7. albumin; 8. ferritin

The chromatograms are shown in Figure 77.

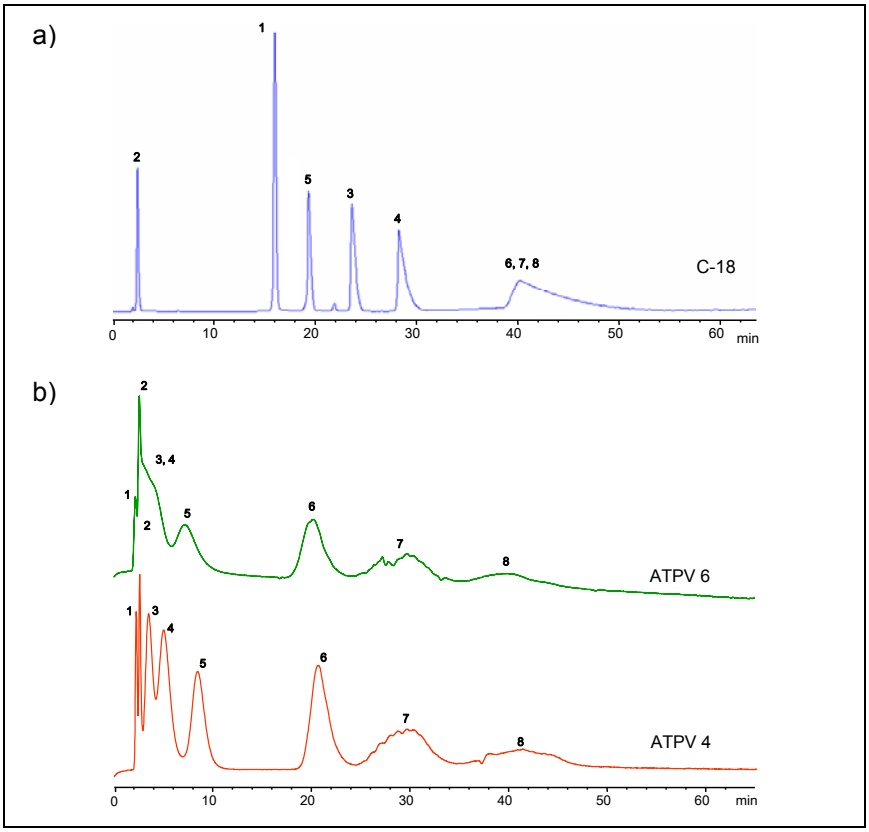

Figure 77: Elution profiles of eight component test mixture applied on columns packed with a) C18-modified silica and b) ATPV 4, ATPV 6.

The chromatograms clearly show, that the chromatographic resolution is increasing with decreasing polymer load. While nearly no separation of the test mixture can be obtained on the stationary phase ATPV 9 with 9.15 % carbon content, a much better separation is observed on the column ATPV 6 with 5.82 % carbon content and the best separation of the polymer-coated materials can be found on the column ATPV 4 with 4.55 % carbon content representing the smallest polymer load. The commercially available column with the C18-modified silica shows by far the best chromatographic resolution of the detected components, although proteins like cytochrome C, insulin, ferritin and albumin cannot be detected – even by injecting the single components, which indicates, that these analytes are bound on the surface of the column and where not eluted by the chosen chromatographic conditions. Furthermore the elution order of the analytes is different for the polymer-coated stationary phases compared to the one obtained on the reference reversed-phase C18-modified silica. An optimization of the packing procedure should lead to much better separations mainly for small molecules.

5.3.4.6 Adsorption Isotherm of Lysozyme

For the possible use of the polymer-coated stationary phase in preparative bioprocess chromatography, the adsorption isotherm towards proteins is very important. As protein lysozyme was used and the adsorption isotherm was gathered by employing the staircase method (see Appendix 7.3.7) of frontal analysis. Therefore in a two-pump HPLC-system was used, where one pump was feeding a solution of 20 g/l lysozyme and the other pure solvent. This allows the successive gathering of the adsorption isotherm for a concentration up to 20 g/l of lysozyme. The chromatographic conditions are given in Table 50.

Table 50: Chromatographic conditions for frontal analysis by the staircase method employing lysozyme as target analyte.

column dimension: 125mm x 4mm ID
conditions:
flow rate: 1 ml/min; @ RT; UV@ 215nm, 300nm
Buffer A: 10mM K2HPO4 solution pH 3.0
Buffer B: 10mM K2HPO4 solution pH 3.0
containing 20 g/l lysozyme

An example chromatogram is shown in Figure 78.

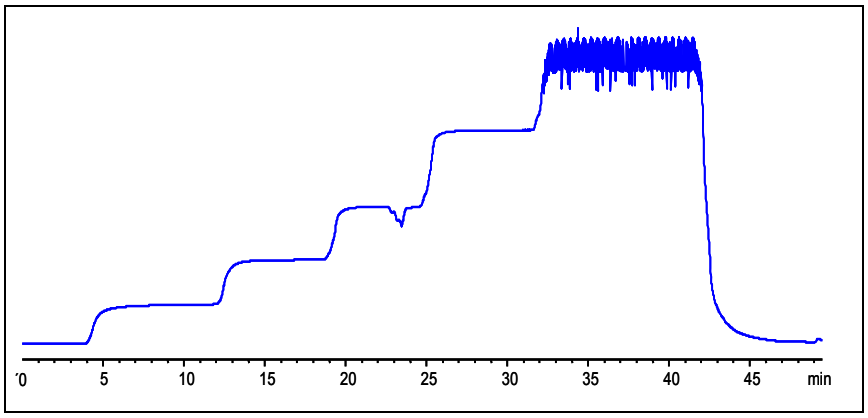

Figure 78: Chromatogram of the evaluation of the adsorption capacity of lysozyme on a column packed with ATPV 9.

The adsorption isotherms were then determined from the inflection points in the chromatograms with the knowledge of the experimental parameters like switching time between the concentrations, the dead time of the machine, the dead time of the column etc. (see Appendix 7.3.7). The resulting adsorption isotherms for lysozyme are shown in Figure 79.

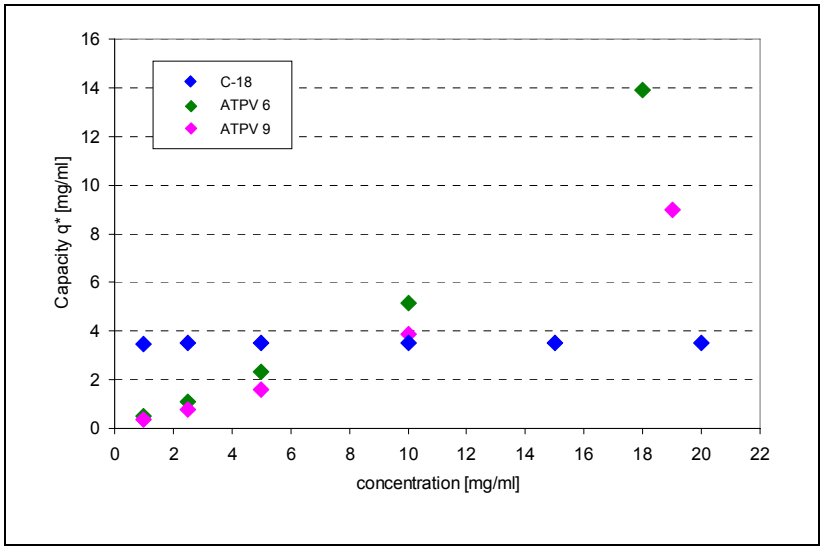

Figure 79: Adsorption isotherms for lysozyme of different stationary phase materials: C18, ATPV 6 and ATPV 9.

The amount of adsorbed lysozyme at the maximum concentration of 20 g/l is listed in Table 51.

Table 51: Amount of adsorbed lysozyme at a concentration of 20 g/l for C18, ATPV 6 and ATPV 9 treated by linear regression. R^2 = coefficient of determination

sample	$q^*_{20g/l}$ [mg/ml]	linearity <R^2>
C18	3.49	0.29
ATPV 6	13.88	0.94
ATPV 9	8.92	0.98

The figures show a very high capacity of the P2HE.-E- coated stationary phases for lysozyme which is still not in saturation even at a concentration of 20 g/l. The reference column with the C18 coated material shows a very high affinity towards lysozyme, which can be observed in reaching the saturation at the first concentration step with a capacity limit of about 3.49 mg/ml. Even the column packed with the highest polymer load ATPV 9 represented by 9.15 % carbon content shows a much higher capacity of 8.92 mg/ml at a concentration of 20 g/l and the column with the medium polymer load ATPV 6 represented by 5.82 % carbon content takes up to 13.88 mg/ml of stationary phase. The column with the smallest polymer load ATPV 4 could not be investigated as it was unwittingly irreversibly loaded with lysozyme during the preparation of the tests. The adsorption isotherms of lysozyme for the polymer-coated stationary phases are still in the linear range with no indication for reaching their capacity limit, as the R^2-value (coefficient of determination) by linear regression is above 0.9 for all materials. Investigation at higher concentrations could not be performed due to limits of the experimental setup. It has to be noted that the desorption-branch of the isotherm could not be obtained from any of the tested columns as the lysozyme could not be removed under the tested chromatographic conditions. Therefore no other tests could be made with columns on which frontal analysis of lysozyme was performed. Again, these experiments favor polymer-coated stationary phases with less polymer load.

5.3.4.7 Conclusion

In general all chromatography-related pore structural values are worsened with increasing polymer load. Size-exclusion experiments detect a strong decrease of the mean pore diameter and pore connectivity values and nitrogen sorption measurements show a decrease of the pore volume with increasing polymer load. Even for the material with the smallest polymer load a mean pore size value of 10 nm is found by size-exclusion experiments, which might be an issue for desired separation of proteins.

The test of chromatographic performance show that mass transfer values benefit much from a small polymer load of the stationary phase, although the poor H-values of the HETP-curves can only partially be explained by the worsening of pore structural values. Some columns show a shrinking of the packing bed, which is not related to a breakdown of the structure of the particle skeleton, but indicates that the packing procedure has to be optimized. Therefore the obtained values would be much enhanced if the packing procedure could be improved.

The chromatographic evaluation in gradient elution mode with a complex-test-mixture shows also an improvement in the chromatographic resolution with decreasing polymer load of the stationary phase. Although none of the polymer-coated stationary materials reach the

chromatographic resolution of the same material coated with hydrophobic C18-groups used as reference, some remarkable differences occur. First of all, the elution order is changed, which indicates a different retardation mechanism. Furthermore polymer-coated stationary phases exhibit a nearly quantitative biorecovery for all tested analytes, while some large probe molecules are not eluted at all from the C18-coated material as they stick on the material.

Remarkably high is the adsorption capacity of up to 16 mg/ml lysozyme for polymer-coated stationary phases as found by frontal analysis, favoring stationary phases with less polymer load. The adsorption isotherm of all investigated polymer-coated materials was in the linear range up to the maximum tested concentration of 20 g/l lysozyme, while the C18-coated reference material reaches its capacity limit of 3.5 mg/ml already at the lowest concentration of lysozyme.

In conclusion all results suggest that an improvement of the material should be based on a reduction of the polymer load, which is only available by changing the amount of anchor-groups, which generate already a carbon contents of 2.7 %, while the minimum achievable carbon contents of the polymer-coated material is 4.5 %.

5.3.5 Reduced Linker Density

All experimental data favour polymer coatings with low polymer load. As the surface bound initiator groups respectively the anchor groups already generate a carbon load of 2.76 % (see Table 17, in 5.2.2.2.2), further reduction of the polymer load can only be achieved by reducing the amount of the anchor groups. Therefore a batch of base silica LiChrospher™ WP 300, 15µm (Batch No. ATP107g, Merck KGaA, Darmstadt, Germany) had to be synthesized with a reduced amount of surface-bound azo-initiator groups to achieve only half of the initial value. In a second step a series of polymer-coated silica materials should be synthesized with target values for the carbon content of 3.60 % (ATPH 3), 4.52 % (ATPH 4) and 5.45 % (ATPH 6).

5.3.5.1 Synthesis Parameters of Silica with a Reduced Amount of Azo-Initiator

The synthesis of the surface bound initiator groups consist of two reaction procedures. First, the silane-groups p-(chloromethyl)phenyltrimethoxysilane have to be bound onto the silica surface and then the synthesis of the azo-initiator group has to be performed. The preparation of silica with a reduced amount of azo-initiator could only be achieved by reducing the amount of silane-groups in the synthesis mixture. In the second step, a quantitative transformation of the silane into azo initiator could only be achieved by using the same amount of educts as in the original procedure (see 7.1.3.3), which was used for the full amount of silanol groups (see 7.1.3.3). A reduction of the amount of 4,4'-Azobis(4-

cyanopentanoic acid) gave only a partial transformation. The reaction parameters are listed in Table 52 and 53.

Table 52: Elemental analysis and experimental parameters of reduced silane modified silica.

sample	**Net weight of initial silica** [g]	**Net weight of silane** [g]	**%C** (w/w)	**%H** (w/w)	**%N** (w/w)
ATPSH 0	13	0.89	0.94	0.38	0.01

Table 53: Elemental analysis and experimental parameters of reduced amount of surface-bound azo-initiator.

sample	**Net weight of silane silica** [g]	**Net weight of azo** [g]	**%C** (w/w)	**%H** (w/w)	**%N** (w/w)
ATPAH 0	13	11.03	1.40	0.31	0.17

The experimental data indicates a complete transition of the silane into surface-bound azo-initiator groups. Furthermore, the example highlights the robustness of the chosen synthesis parameters, which allows a good control and fast adjustment of desired product specifications. The material contains only 1.40 % carbon content of initiator and allows therefore the synthesis of polymer coating with smaller polymer load.

Table 54: Grafting density and surface coverage.

sample	**silica** [µmol/g]	[µmol/m^2]	**Grafting density** in per cent %
ATPSH 0	76.32	0.96	11.94
ATPAH 0	51.60	0.65	8.07

The resulting grafting density of the silane modification of 11.94 % and for the AZO-modified material of 8.07 % represents a still acceptable conversion rate of the silane groups of 68 %, which is quite acceptable as this synthesis procedure is not yet optimized. The values represent the successful reduction of the linker density to half of the original value.

5.3.5.2 Synthesis Parameters of Polymer Modification

Based on the silica with a reduced amount of surface-bound azo-initiator, polymer-coated silica may be produced with less polymer load. Based on the standard synthesis procedure (see 7.1.3.4), well-defined polymer loads where produced by variation of the monomer-concentration. The synthesis parameters and the results of the elemental analysis for the resulting polymer-coated materials are listed in Table 55.

Table 55: Elemental analysis and experimental parameters of P2HE.-E-coated silicas based on silica material with reduced amount of surface-bound azo initiator.

sample	**Net weight of azo silica** [g]	**Net weight of co-monomer** [g] 2HEMA	EMA	**%C** (w/w)	**%H** (w/w)	**%N** (w/w)
ATP107g	-	-	-	0.13	0.46	< 0.01
ATPH 3	2.5	0.085	0.073	3.60	0.58	0.03
ATPH 4	2.5	0.132	0.107	4.52	0.62	0.05
ATPH 6	2.5	0.168	0.150	5.45	0.70	0.06

Based on a silica material with reduced azo-initiator density ATPAH 0, polymer-coated silica materials with 3.60 % (ATPH 3), 4.52 % (ATPH 4) and 5.45 % (ATPH 6) carbon content where successfully synthesized just by adjusting the monomer concentrations of the standard synthesis procedure.

5.3.5.3 Pore Structural Data by Nitrogen Sorption at 77K

Nitrogen sorption measurements at 77 K were performed to gather pore structural data of the materials in bulk phase. The adsorption and desorption isotherms are displayed in Figure 80a) for the polymer-coated silicas as well as for the initial silica ATP107g. The pore size distribution from the desorption branch according to the BJH method is shown in Figure 80b).

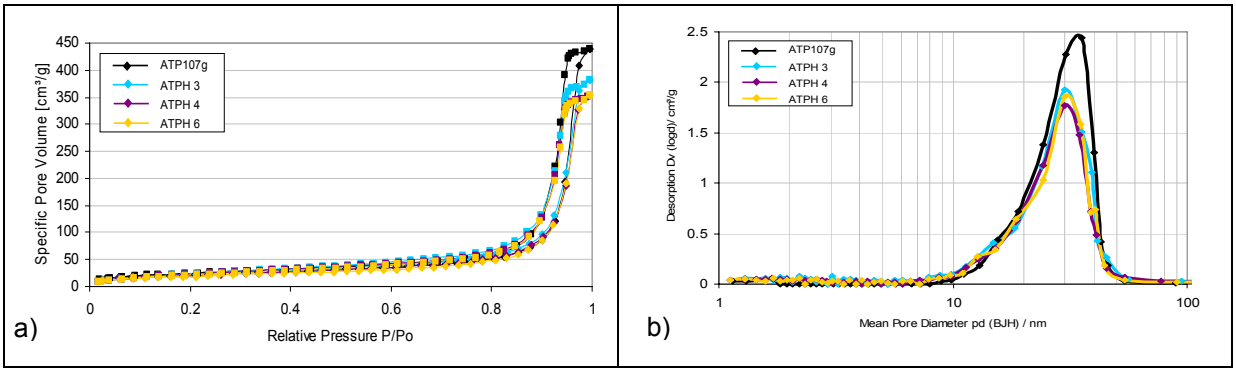

Figure 80: Nitrogen sorption measurements of the initial silica ATP107g, ATPH 3, ATPH 4, ATPH 6 and C18 – a) isotherms and b) pore size distributions.

Table 56 lists the calculated data derived from nitrogen sorption measurements.

Table 56: Pore structural data of unmodified silica ATP107g and modified silicas ATPH 3, ATPH 4, ATPH 6 and C18.

sample	a_S (BET) [m^2g^{-1}]	v_p (G) [ml g^{-1}]	p_d (BJH) [nm]
ATP107g	79	0.701	30.2
ATPH 3	81	0.620	29.9
ATPH 4	74	0.569	29.8
ATPH 6	72	0.571	30.1

The polymer coating procedure affects mainly the value for the specific pore volume of the material. The value decreases by each reaction step slightly, starting from 0.701 ml/g for the initial silica ATP107g, followed by 0.68 ml for the silane-coated silica ATPSH 0, then 0.67 ml/g for the silica with azo-initiator ATPAH 0. The final polymer-coated silicas exhibit values from 0.62 ml/g (ATPH 3), 0.57 ml/g (ATPH 4) and 0.57 ml/g (ATPH 6). These are the same values as polymer-coated silica with the full anchor-density exhibit: the material with 4.55 % carbon content ATPV 4 also has a specific pore volume of 0.57 ml/g.

The specific surface area slightly decreases with increasing polymer load, while the pore size distribution as derived from nitrogen sorption measurements is not affected at all, which is in good agreement with the results obtained for other polymer-coated silica materials.

5.3.5.4 Chromatographic Performance: theoretical plate height vs. linear flow velocity

The theoretical plate height vs. linear flow velocity was tested according to the procedure given in Appendix 7.3.3 employing dibutyl phthalate as analyte water/acetonitrile mixture as solvent. The retention factor was adjusted to a value of k' = 3 for all of the investigated stationary phases, to ensure comparability of the data. The chromatographic conditions are listed in Table 57 for the investigated stationary phases.

Table 57: Chromatographic conditions for testing the theoretical plate height vs. linear flow velocity dependency.

column dimension: 125 x 4 mm ID; injection volume: 5 µl;
detection: 254 nm; @ room temperature;
flow rate: 0.25 – 5.0 ml/min; k'= 3
analytes: uracil, diethyl phthalate, dibutyl phthalate
mobile phase: water/ACN, n-heptane / ethyl acetate

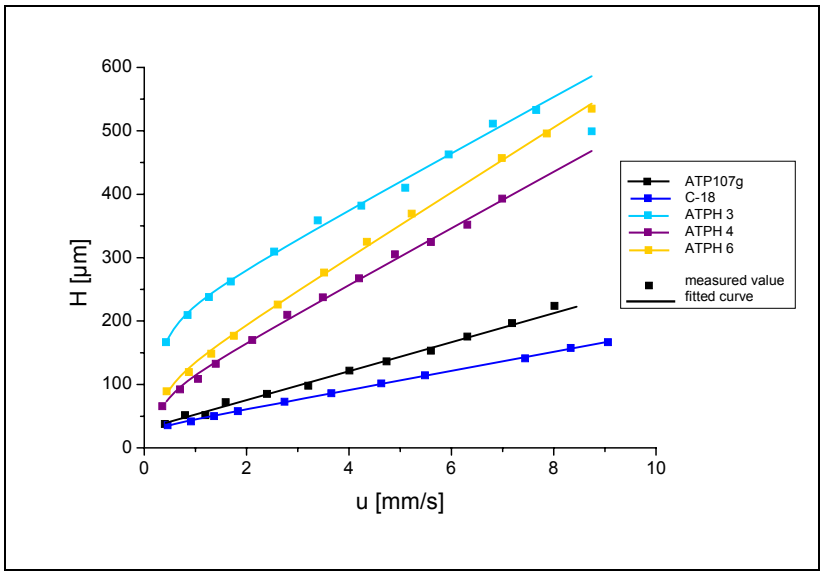

Figure 81: H-vs.-u-plots employing dibutyl phthalates of unmodified silica ATP107g and modified silicas ATPH 3, ATPH 4, ATPH 6 and C18.

Figure 81 displays the corresponding H-vs.-u-values with the calculated curves based on nonlinear regression according to the Knox-equation. The column packed with the material with 3.60 % carbon content ATPH 3, representing the smallest polymer load shows the worst chromatographic performance and the largest discrepancy between the expected and the experimentally measured values. This is due to a bad packing of the stationary phase, which can be especially observed in the improvement of the values at the highest flow rate, indicating a breakdown of the packing bed, which results in a more dense packing bed. The other curves show a normal behaviour, and compared to the columns tested before slightly better values for the theoretical plate height H at small flow rates, which are still quite high. The results obtained by nonlinear fitting of the curve based on the Knox-equation are displayed in Table 58. The molecular diffusion term is not sufficiently supported by the experimental setup, as no experiments at very small flow rates were performed.

Table 58: H-values and C-values of unmodified silica ATP107g and modified silicas ATPH 3, ATPH 4, ATPH 6 and C18.

sample	**Plate Height H** [µm] at 0.5 mms^{-1}	**C-term** [ms] according to Knox	**A-term** [$10^{-5}m^{2/3}s^{1/3}$] according to Knox
ATP107g	37.58 ± 1	22.84 ± 0.85	29.56 ± 4.53
C18	35.64 ± 1	15.03 ± 0.18	31.45 ± 1.22
ATPH 3	166.67 ± 1	44.02 ± 1.54	204.27 ± 8.77
ATPH 4	65.82 ± 1	44.32 ± 1.47	82.37 ± 6.89
ATPH 6	89.37 ± 1	50.94 ± 0.95	99.70 ± 6.02

The plate height H [µm] is related to the inhomogeneity of the packing bed due to a bad packing procedure or broad particle size distribution. For a well packed column a value of 2-5

times of the mean particle size is expected[144], which in this case would be a value between 30-75 µm. This value is almost reached by the column packed with the material with 4.52 % carbon content ATPH 4, which exhibits a value of 65.82 µm, followed by the column packed with the highest polymer load 5.45 % carbon content ATPH 6 which shows a minimum plate height of 89.37 µm. Completely out of this range is the column packed with the smallest polymer load 3.60 % carbon content ATPH 3 with a value of 166.67 µm, indicating a bad packing procedure. The column packed with C18-coated silica or with the unmodified material ATP107g show nearly ideal values of ca. 40 µm representing an optimum packing.

The mass transfer is represented by the C'-term in the Knox-equation. It describes the worsening of the chromatographic performance with increasing flow of the eluent at higher flow rates. Again, the values for the polymer-coated stationary phases are worse than those obtained for the unmodified silica ATP107g with 22.84 ms or the C18-coated stationary phase with 15.03 ms. The value increase with increasing polymer load, starting from 44.02 ms for ATPH 3 by a carbon content of 3.60 %, which is remarkable as it is obtained by a not well-packed column. Also 44.32 ms is found by the column packed with a polymer-coated silica ATPH 4 with 4.52 % carbon content and a slightly worse mass transfer value of 50.94 ms is found for the material with the highest polymer load with 5.45 % carbon content for ATPH 6.

5.3.5.5 Adsorption Isotherm of Lysozyme

The adsorption isotherm of lysozyme was investigated by employing the stair-case method of frontal analysis chromatography. As maximum concentration of 20 g/l lysozyme could be applied by the chromatographic equipment, giving the upper limit for the isotherm. In Table 59 the chromatographic conditions are given. Gathering of the desorption-branch of the isotherm was not possible, as no desorption of lysozyme could be observed by the chosen chromatographic conditions. Furthermore, only the adsorption isotherm of the column packed with the material with 3.60 % carbon content ATPH 3 could be evaluated, due to a failure of the chromatographic equipment while processing the columns packed with the materials with the higher polymer load. As lysozyme could not be removed by standard cleaning procedures, the columns could not be further investigated afterwards.

[144] K.K. Unger, E. Weber, A Guide to Practical HPLC, GIT VERLAG GmbH 1999

Table 59: Chromatographic conditions for frontal analysis by the staircase method employing lysozyme as target analyte.

column dimension: 125mm x 4mm ID
conditions:
flow rate: 1 ml/min; @ RT; UV@ 215nm, 300nm
Buffer A: 10mM K2HPO4 solution pH 3.0
Buffer B: 10mM K2HPO4 solution pH 3.0
containing 20 g/l lysozyme

The experimental data of the adsorption isotherms was gathered by the procedure described in 3.4.2 and Appendix 7.3.7 from the chromatogram. The Data points are displayed in Figure 82.

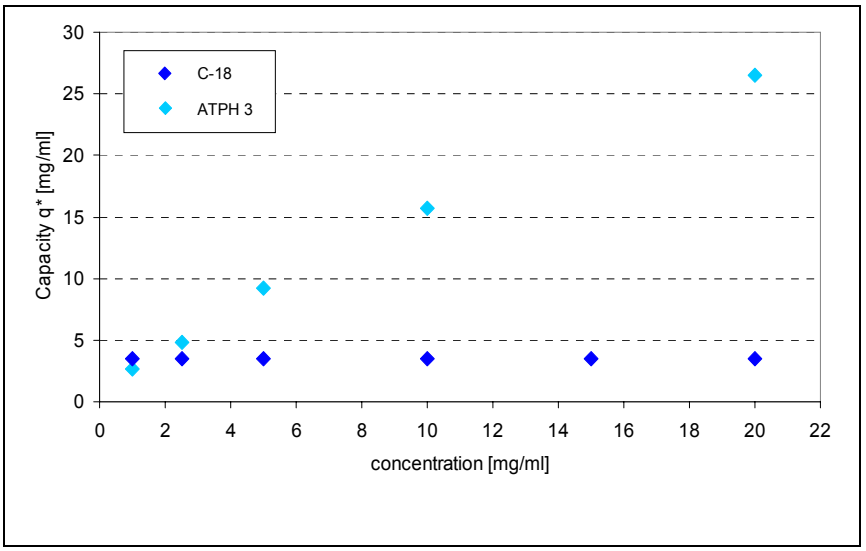

Figure 82: Adsorption isotherms for lysozyme of different stationary phase materials: C18, ATPH 3.

The results of the data treatment by linear regression are listed in Table 60.

Table 60: Amount of adsorbed lysozyme at a concentration of 20 g/l for C18 and ATPH 3 treated by linear regression. R^2 = coefficient of determination

sample	**$q^*_{20g/l}$** [mg/ml]	linearity <R^2>
C18	3.49	0.29
ATPH 3	28.10	0.96

The investigated polymer-coated silica ATPH 3 exhibits a very high adsorption capacity towards lysozyme. The confidence value of the linear regression show a very good value of 96 % indicating, that the adsorption is still in the linear range of the isotherm. The value of 20.0 g lysozyme per l of stationary phase is very high and even better than the values obtained in the experiments before. Unfortunately no direct comparison between the values

obtained by the materials coated with full linker density and this value, which is based on a reduced density of the anchor groups between the polymer coating and the silica surface, can be made. The experiments based on polymer-coated silica with full linker density anticipate an increase of lysozyme capacity by decreasing the polymer content. As only two values at 4.55 % carbon content ATPV 4 and 5.82 % carbon content ATPV 6 were measured, no prediction can be made for the expected value of a comparable stationary phase with 3.60 % carbon. Therefore no information about the influence of the reduction of the anchor groups can be deduced.

5.3.5.6 Conclusion

The synthesis of azo-coated silica with a reduced amount of anchor groups to half of the initial value was performed by distinct reduction of the concentration of silane in the first synthesis step. This allowed the controlled synthesis of polymer-coated silica with carbon contents of 3.2; 4.5 and 5.5 % C. Nitrogen sorption measurements detect a decrease of the pore volume value and specific surface area with increasing polymer load.

Mass transfer values of polymer-coated stationary phases increase in general with decreasing polymer-load, which is also true in the case for polymer-coated materials with a reduced amount of anchor-groups. So far, the best mass-transfer values are obtained of the tested polymer-coated materials corresponding with the lowest polymer load of these phases. Anyway, the mass-transfer values are still by a factor of 2 worse than native or C18-coated materials. Compared to polymer-coated silica with full anchor-group density, there is an indication for an extra effect due to the reduction of the anchor groups. The sample with reduced anchor-group density ATPH 4 features a mass-transfer value, that is one third better than the one of sample ATPV 4 with full anchor-group density, although both materials have nearly the same carbon contents.

The adsorption isotherm was only measured for the material with the smallest polymer load; therefore no general tendency can be deduced. Anyway, the material exhibits a very high adsorption capacity towards lysozyme of 27 mg/ml at the maximum concentration of 20 /l lysozyme, being still in the linear range.

The improvement of the mass-transfer for materials with a smaller concentration of anchor groups is not fully explained by the reduced amount of polymer, but may also be due to an increase in the flexibility of the polymer coating. A high amount of cross-linker was used for the synthesis of the polymer-layer, resulting in a very rigid coating which didn't show any noticeable swelling effect as seen in 4.4. This will be verified in the next chapter by producing a polymer coating with a reduced amount of cross-linker or with inserted flexible spacer molecules like OMA.

5.3.6 Variation of the Rigidity of the Polymer Coating

The rigidity of the polymer coating may affect the chromatographic behavior as inelastic polymer particles may block the pore system of the stationary phase. The introduction of flexibility can be achieved by either reduction of cross-linker density in the polymer network or by introduction of flexible spacers into the polymer network. The lowering of the cross-linker density will increase the mean length of the linear polymer chains between the nodes, which is the cause for the flexibility and swellability of the polymer network. Thus, by lowering the density of cross-linker in the polymer layer, the flexibility of the polymer network can be increased. The introduction of OMA as a molecule with flexible spacer functionality into the polymer network will have a similar effect. As base silica LiChrospher™ WP 300, 15 µm (Batch No. ATP107g, Merck KGaA, Darmstadt, Germany) was employed.

5.3.6.1 Synthesis Parameters

The synthesis of a polymer coating with lower cross-linker density was performed by using a modified standard synthesis procedure with reduced cross-linker concentration of 1% (n/n) EDMA in the synthesis mixture, resulting in ATPH 4.V. For best comparison of the results, as silica source ATP107g with the reduced anchor group density ATPAH 0 was used as base material for the polymer coating. The synthesis conditions and the results of the elemental analysis of the final product are given in Table 61.

Table 61: Elemental analysis and experimental parameters of the initial silica ATP107g and of the polymer-coated silica ATPH 4.V with reduced cross-linker density.

sample	**Net weight of azo silica** [g]	**Net weight of co-monomer** [g] 2HEMA	EMA	**Net weight of** EDMA [g]	**%C** (w/w)	**%H** (w/w)	**%N** (w/w)
ATP107g	-	-	-	-	0.13	0.46	< 0.01
ATPH 4.V	2.5	0.122	0.101	0.0038	3.48	0.54	0.08

The introduction of flexible spacer molecules into the polymer coating was performed by using OMA as a co-monomer. A modified standard synthesis procedure was used, where 1 % (n/n) or respectively 10 % (n/n) of OMA was added to the synthesis mixture, resulting in ATPH 4.O and ATPH 4.O1. The synthesis conditions and the results of the elemental analysis of the final product are presented in Table 62.

Table 62: Elemental analysis and experimental parameters of the initial silica ATP107g and of the polymer-coated silica ATPH 4.O and ATPH 4.O1 containing OMA.

sample	**Net weight of azo silica** [g]	**Net weight of co-monomer** [g] 2HEMA	EMA	**Net weight of** OMA [g]	**%C** (w/w)	**%H** (w/w)	**%N** (w/w)
ATP107g	-	-	-	-	0.13	0.46	< 0.01
ATPH 4.O	2.5	0.128	0.106	0.049	3.56	0.75	0.09
ATPH 4.O1	2.5	0.130	0.110	0.446	3.98	0.63	0.08

5.3.6.2 Pore Structural Data by Nitrogen Sorption at 77K

The isotherms from nitrogen sorption measurements at 77 K of the polymer-coated materials in bulk are shown in Figure 83a).

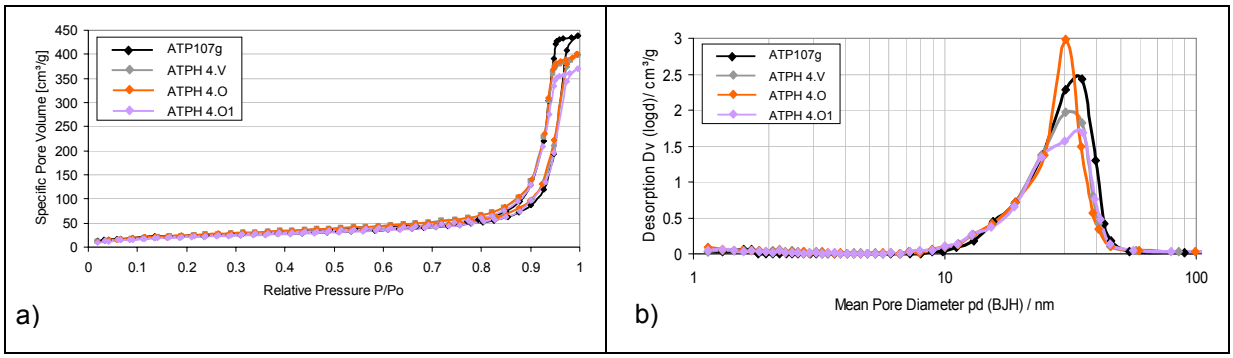

Figure 83: Nitrogen sorption measurements of the initial silica ATP107g, ATPH 4.V, ATPH 4.O and ATPH 4.O1 – a) isotherms and b) pore size distributions.

The results of the data treatment are displayed in Table 63.

Table 63: Pore structural data of unmodified silica ATP107g and modified silicas ATPH 4.V, ATPH 4.O and ATPH 4.O1.

sample	a_S (BET) [m^2g^{-1}]	v_p (G) [ml g^{-1}]	p_d (BJH) [nm]
ATP107g	79	0.701	30.2
ATPH 4.V	84	0.679	30.3
ATPH 4.O	83	0.642	30.1
ATPH 4.O1	74	0.594	24.2

The isotherms of the polymer-coated materials differ only slightly from the one of the uncoated material ATP107g. With increasing polymer load as expressed by carbon contents, the pore volume decreases. The material with 1 % (n/n) cross-linker (ATPH 4.V, 3.48 % carbon content) has the highest value of 0.68 ml/g, followed by the material with 1 % (n/n) OMA (ATPH 4.O, 3.56 % carbon) with 0.64 ml/g and finally the material with 10 % (n/n) OMA (ATPH 4.O1, 3.98 % carbon) shows 0.59 ml/g, while the uncoated material shows a value of 0.70 ml/g. The value for the material with reduced cross-linker exhibits the same decrease as the former investigated materials, while the material containing OMA exhibits a much stronger decrease than expected by the carbon contents.

The specific surface area values according to BET are not affected significantly by the polymer coating procedure and the same is true for the values obtained by BJH-method for the pore size distributions with the exception of the value for the material with the polymer coating containing 10 % (n/n) OMA. This value is significantly decreased from 30.2 nm (ATP107g) to 24.2 nm for the coated material.

5.3.6.3 Pore Structural Data by SEC using Polystyrene Standards employing PPM

The gathering of pore structural data of packed chromatographic columns was performed by size-exclusion chromatography in inverse mode. The measurements were performed employing a set of polystyrene standards in THF as eluent according to the procedure given in Appendix 7.3.4. Figure 84a) shows the size-exclusion calibration curves for the polymer-coated materials. The corresponding pore size distributions as derived from the experimental data are shown in Figure 84b) and displayed as characteristic data in Table 64.

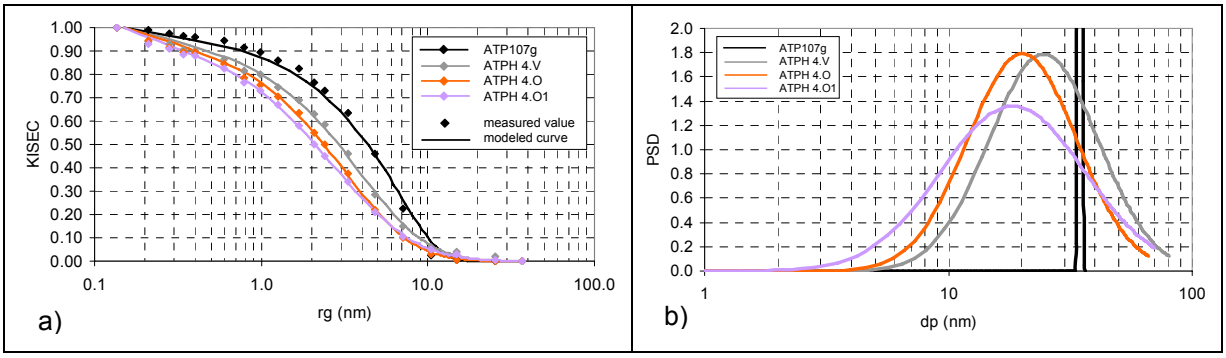

Figure 84: ISEC measurements with THF of unmodified silica ATP107g and modified silicas ATPH 4.V, ATPH 4.O and ATPH 4.O1 – a) calibration plots and b) volume based pore size distribution obtained by PPM.

Table 64: Pore structural data of unmodified silica ATP107g and modified silicas ATPH 4.V, ATPH 4.O and ATPH 4.O1 applied by PPM.

sample	p_d (BJH) [nm]	$p_{d,ave}$ (PPM) by volume [nm]	σ_{pd} by volume [nm]
ATP107g	30.2	34.6	1.0
ATPH 4.V	30.2	21.6	0.8
ATPH 4.O	30.2	17.6	0.4
ATPH 4.O1	24.2	14.6	0.4

The figures indicate a decrease of the mean pore size diameter with increasing carbon contents of the polymer-coated material. The polymer-coated materials exhibit the highest pore size value by inverse size-exclusion chromatography method of all investigated materials. The column packed with the polymer-coated material with 1 % (n/n) cross-linker (containing 3.48 % carbon content) exhibits the largest value of 21.6 nm, followed by the material coated with 1 % (n/n) OMA (containing 3.56 % carbon content) with a value of 17.6 nm. The silica coated with 10 % (n/n) OMA (containing 3.98 % carbon content) exhibits a mean pore radius of 14.6 nm and a broader pore size distribution than the other materials.

The detected pore size values are all in the acceptable range for most separation tasks in HPLC, which is most often performed with stationary phase materials with a mean pore diameter of ca. 10 nm. The measurements show further a very high impact of the polymer coating upon the mean pore size value.

5.3.6.4 Chromatographic Performance: theoretical plate height vs. linear flow velocity

The theoretical plate height vs. linear flow velocity was tested according to the procedure given in Appendix 7.3.3 employing dibutyl phthalate as analyte and water/acetonitrile-mixture as mobile phase. The retention factor was adjusted to a value of k' = 3 for all of the investigated stationary phases, to ensure best comparability of the data. The chromatographic conditions are listed in Table 65 for the investigated stationary phases. The column packed with the material coated with 10 % (n/n) OMA was not investigated because it was unusable after frontal analysis measurements.

Table 65: Chromatographic conditions for testing the theoretical plate height vs. linear flow velocity dependency.

column dimension: 125 x 4 mm ID; injection volume: 5 µl;
detection: 254 nm; @ room temperature;
flow rate: 0.25 – 5.0 ml/min; k'= 3
analytes: uracil, diethyl phthalate, dibutyl phthalate
mobile phase: water/ACN, n-heptane / ethyl acetate

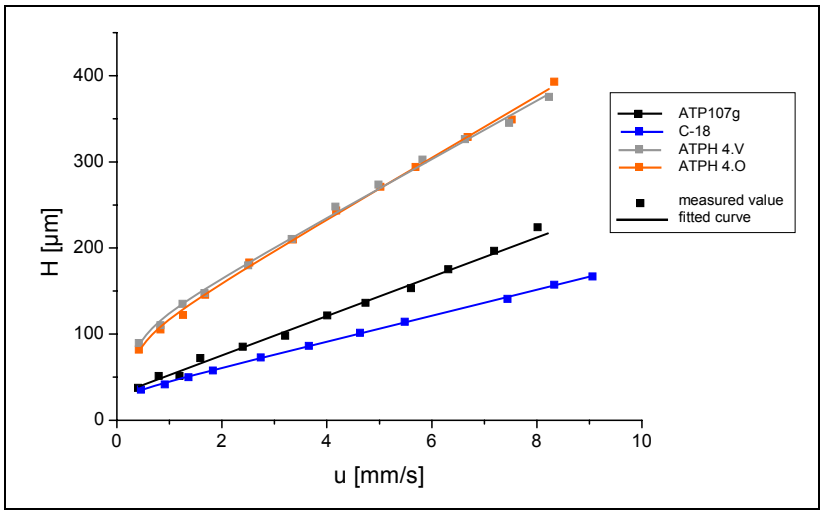

Figure 85: H-vs.-u-plots employing dibutyl phthalates of unmodified silica ATP107g and modified silicas ATPH 4.V, ATPH 4.O1 and C18.

Figure 85 displays the corresponding H-vs.-u-values and the calculated curves based on nonlinear regression according to the Knox-equation. Both of the columns packed with polymer-coated materials exhibit nearly identical behaviours. All curves show a normal behaviour with no indication for a breakdown of the packing bed at higher flow rates. The results obtained b nonlinear fitting of the curves based on the Knox-equation are shown in Table 66. The molecular diffusion term B is not sufficiently supported by the experimental data, as no experiments at very small flow rates were performed.

Table 66: H-values and C-values of unmodified silica ATP107g and modified silicas ATPH 4.V, ATPH 4.O and C18.

sample	**Plate Height H** [µm] at 0.5 mms^{-1}	**C-term** [ms] according to Knox	**A-term** [$10^{-5}m^{2/3}s^{1/3}$] according to Knox
ATP107g	37.58 ± 1	22.84 ± 0.85	29.56 ± 4.53
C18	35.64 ± 1	15.03 ± 0.18	31.45 ± 1.22
ATPH 4.V	89.61 ± 1	33.63 ± 0.87	103.42 ± 5.33
ATPH 4.O	82.13 ± 1	35.52 ± 0.83	93.66 ± 5.06

The H-value is related to the inhomogeneity of the packing bed. The ideally expected value of 30-75 µm for well-packed columns with 15 µm particles is not reached by the columns packed with polymer-coated materials, but a value of 89.61 µm for the material coated with 1 % (n/n) cross-linker ATPH 4.V and 82.13 µm for the material with 1 % (n/n) OMA ATPH 4.O is not so far away from these expectations, but still much worse than the value of 37.58 µm obtained for the uncoated material ATP107g, representing the reference value for this packing material.

The mass transfer is represented by the C-term of the Knox-equation. The values of 33.63 ms for the material with 1 % (n/n) cross-linker ATPH 4.V and 35.52 ms for the material with 1 % OMA (n/n) ATPH 4.O represents the best values obtained for polymer-coated materials based on the ATP107g silica source, although unmodified silica with 22.84 ms exhibits a much better mass transfer.

5.3.6.5 Adsorption Isotherm of Lysozyme

The staircase method of frontal analysis chromatography was employed for accessing the adsorption isotherm of lysozyme. The measurements were performed as described in Appendix 7.3.7 until a maximum concentration of lysozyme of 20 g/l was reached, representing the upper limit of the adsorption isotherm, while the desorption branch could not be investigated, as no desorption of lysozyme could be observed under the chromatographic conditions. The chromatographic conditions are listed in Table 67.

Table 67: Chromatographic conditions for frontal analysis by the staircase method employing lysozyme as target analyte.

column dimension: 125mm x 4mm ID
conditions:
flow rate: 1 ml/min; @ RT; UV@ 215nm, 300nm
Buffer A: 10mM K2HPO4 solution pH 3.0
Buffer B: 10mM K2HPO4 solution pH 3.0
containing 20 g/l Lysozyme

The data points of the adsorption isotherms were gathered by the procedure described in Appendix 7.3.7 from the chromatogram and are displayed in Figure 86.

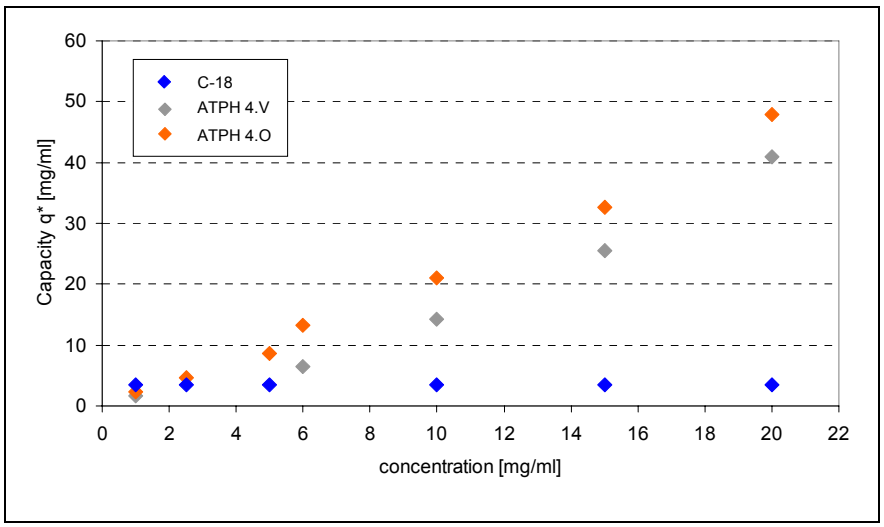

Figure 86: Adsorption isotherms for lysozyme of different stationary phase materials: C18, ATPH 4.V and ATPH 4.O.

The results of the data treatment by linear regression are listed in Table 68.

Table 68: Amount of adsorbed lysozyme at a concentration of 20 g/l for C18, ATPH 4.V and ATPH 4.O treated by linear regression. R^2 = coefficient of determination

sample	$q^*_{20g/l}$ [mg/ml]	linearity <R^2>
C18	3.49	0.29
ATPH 4.V	36.34	0.94
ATPH 4.O	45.25	0.99

The investigated polymer-coated stationary phases exhibit a very high adsorption capacity towards lysozyme. The material coated with 1 % (n/n) cross-linker takes up to 41.0 mg/ml of lysozyme at the maximum concentration of 20 mg/l. The adsorption isotherm does not show any indication for reaching the maximum capacity, while it shows still a linear behavior which can be seen as a confidence value from linear regression of 94 %. The column packed with the material where the polymer coating contains 1 % (n/n) OMA takes 45.25mg/ml of lysozyme at the maximum concentration of 20 mg/ml. The isotherm is in the linear range which can be deduced by a confidence value of 99 % by linear regression with no indication for being in the range of reaching the maximum capacity.

Both materials possess very similar carbon contents of 3.48 % for the coating with 1 % (n/n) cross-linker ATPH 4.V and 3.56 % for the coating containing 1 % (n/n) OMA ATPH 4.O, representing the lowest carbon contents of all investigated materials. Nevertheless, this only partially explains the high capacity of these coatings towards lysozyme. A material with a very similar carbon content of 3.60 % for ATPH 3 but with full linker density 10% (n/n) was investigated in 5.3.5.5, which exhibits with a value of 20.0 mg/ml lysozyme at the maximum

concentration only less than half of the binding capacity compared with the materials containing more flexible polymer coatings ATPH 4.V and ATPH 4.O. This highlights the extra improvement onto the binding capacity via the introduction of flexibility into the polymer coating.

5.3.6.6 Conclusion

All chromatographic properties benefit much from the reduction of the rigidity of the polymer layer. The pore structural values derived by nitrogen sorption measurements showed the usual dependency between carbon load and specific pore volume, which is decreasing with increasing polymer load. Size-exclusion experiments reveal that the mean pore size of the polymer coated materials reaches values between 14.6 to 21.6 nm, which are in an acceptable range for the desired separation of biopolymers.

This allows a further improved mass-transfer values of these polymer-coated stationary phases, although the obtained values are still worse than those of native or C18-coated silica. Although no indication for a breakdown of the packing bed was found during the measurements, the bad H-values indicate that these values may be increased much, if the packing procedure could be improved.

Frontal analysis exhibits a very high adsorption capacity of the stationary phases for lysozyme of 41 g/ml respectively 48 g/ml, being in the linear range up to the maximum tested concentration of 20 g/l. This corresponds with the increased pore size value, giving access for lysozyme to a higher volume fraction. The higher adsorption capacity for lysozyme of the OMA-containing stationary phase in comparison with the stationary phase with a reduced amount of cross-linker may be due to the large hydrophobic interaction of the C18-group in the OMA-monomer.

The reduced rigidity of the polymer layer leads primarily to a smaller reduction of the pore size value of the polymer coated stationary phase, improving much their chromatographic properties. Very remarkable is the high adsorption capacity towards lysozyme as showcase protein, which is in the linear range over the whole tested capacity array. A further improvement of the polymer-coated stationary phase should therefore be based upon changing the silica source to a material with larger pores.

5.4 Variation of the Silica Support Material

In the previous chapters, all investigations about the optimization of the polymer layer were based upon the coating of a particulate silica source originating from one single batch with a particle size of about 15 µm and a mean pore diameter of 30 nm. In this chapter, the influence of the silica skeleton upon the chromatographic behaviour of the polymer-coated

materials is subject of interest. Therefore, different silica sources were coated with a polymer layer consisting of 50/50 (n/n) 2HEMA/EMA monomer and 10 % (n/n) of cross-linker. The properties of the silica sources were varied mainly by two different aspects: first of all, the influence of the pore system of the base silica was investigated by comparing four different chromatographic particulate silica materials ranging from approximately 15 nm up to 100 nm pore diameter, keeping the particle size at the same level of about 15 µm. Secondly, the nature of the skeleton type was investigated by comparing a polymer-coated particulate silica and a monolithic silica source.

5.4.1 Polymer Modification of Base Silicas with Varying Pore Sizes

The variation of the pore size was performed by selecting four so-called “wide-porous” chromatographic bulk media as base materials for the polymer coating. These materials are typically used for the chromatographic evaluation of large molecules like biopolymers. As reference material ATP107g with a mean particle diameter of 15 µm was employed, which is sold under the brand name LiChrospher™ WP 300 (Batch No. ATP107g, Merck KGaA, Darmstadt, Germany). The next materials are Nucleosil 300-10 and Nucleosil 1000-10 with a mean particle diameter of 10 µm, produced by Macherey-Nagel, Düren, Germany, which are commercially available. The last material in this comparison is Kromasil 300 Å with a slightly different mean particle diameter of 16 µm, which was kindly provided by the manufacturer EKA Chemicals AB, Bohus, Sweden.

5.4.1.1 Synthesis Parameters

The coating was performed by the synthesis procedure as described in Appendix 7.1.3 which involves a multiple-step reaction pathway. After the rehydroxylation of the silica, p-(chloromethyl)phenyltrimethoxysilane is covalently attached onto the surface of the material in the first reaction step. The next reaction step involves the coupling of the azo initiator onto the silane. The coating procedure is finalized by the polymerization reaction which is performed as the last reaction step. The polymerization procedures were performed by a standard procedure involving 2 mmol of monomer in the polymerization mixture. In Table 69 are listed the parameters for each of the reaction steps of the materials together with the results by elemental analysis of the products.

Table 69: Elemental analysis and experimental parameters of silane modification on four different particulate silicas.

sample	**Net weight of initial silica** [g]	**Net weight of silane** [g]	**%C** (w/w)	**%H** (w/w)	**%N** (w/w)
ATPSV 0	10	1.23	1.44	0.77	< 0.01
KRSV 300	14	2.51	1.04	0.45	< 0.05
NUSV 300	10	1.36	1.55	0.11	0.05
NUSV 1000	14	0.53	0.38	0.04	0.03

Table 70: Elemental analysis and experimental parameters of azo modification on four different particulate silicas.

sample	**Net weight of silane silica** [g]	**Net weight of azo** [g]	**%C** (w/w)	**%H** (w/w)	**%N** (w/w)
ATPAV 0	10	8.43	2.76	0.43	0.73
KRAV 300	14	11.97	2.10	0.38	0.63
NUAV 300	10	8.51	1.88	0.13	0.21
NUAV 1000	14	2.64	0.73	0.07	0.13

Table 71: Elemental analysis and experimental parameters of P2HE.-E-coated four different particulate silicas.

sample	**Net weight of azo silica** [g]	**Net weight of co-monomer** [g] 2HEMA	EMA	**%C** (w/w)	**%H** (w/w)	**%N** (w/w)
ATPV 4	2.5	0.167	0.142	4.55	1.02	0.05
KRV 300	2.5	0.173	0.144	4.52	0.62	0.05
NUV 300	2.5	0.137	0.110	4.99	0.52	0.04
NUV 1000	2.5	0.131	0.103	3.20	0.45	0.05

The final polymer-coated materials with the exception of NUV 1000 show all very comparable results for the carbon contents as obtained from elemental analysis, ranging from 4.52 % to 4.99 %. This is especially remarkable as no adjustment or optimization for the different silica sources was made, highlighting the good reproducibility of the synthesis procedure. The characterization of the bulk products was performed with carefully washed and dried samples. NUV 1000 show a much lower carbon content of only 3.20 %, but this is due to the much lower surface area and reduced pore volume of this material (see 5.4.1.2).

5.4.1.2 Pore Structural Data by Nitrogen Sorption at 77K

Nitrogen sorption measurements at 77 K were performed on bulk materials of the native silica source as well as of samples from each of the reaction steps until the final polymer-coated materials. The isotherms of the nitrogen sorption measurements are displayed in Figure 87 while the results from the data treatment are listed in Table 72.

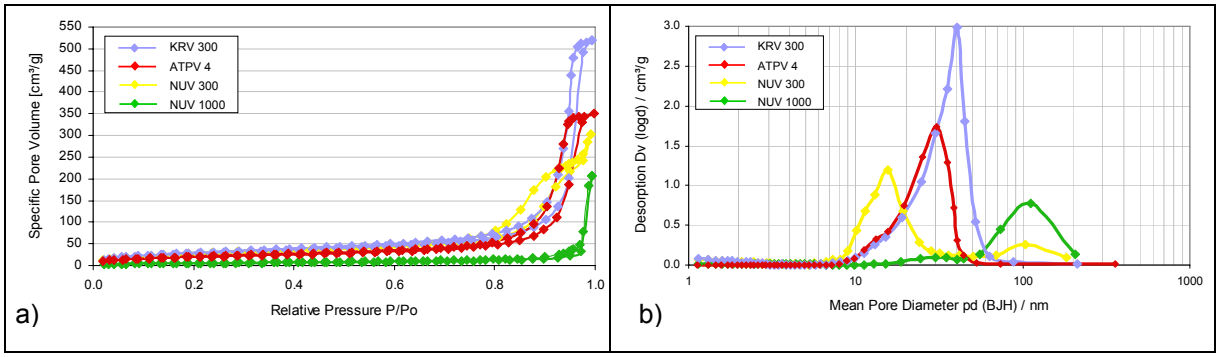

Figure 87: Nitrogen sorption measurements of ATPV 4, KRV 300, NUV 300 and NUV 1000 – a) isotherms and b) pore size distributions.

Table 72: Pore structural data of modified silicas ATPV 4, KRV 300, NUV 300 and NUV 1000 and their unmodified base materials.

sample	a_S (BET) [m^2g^{-1}]	v_p (G) [ml g^{-1}]	p_d (BJH) [nm]
ATP107g	79	0.701	30.2
ATPV 4	70	0.565	30.5
Kromasil 300	108	0.983	40.9
KRV 300	99	0.827	40.0
Nucleosil 300-10	91	0.622	15.7
NUV 300	92	0.488	15.6
Nucleosil 1000-10	21	0.163	110.0
NUV 1000	19	0.325	105.0

In general, the isotherms of each particular material do not change much from step to step of the polymer coating process. The values obtained by nitrogen sorption measurements for the Nucleosil 1000-10 silica are near the upper limit of the method and must be used with precaution. This material was therefore also examined by mercury intrusion porosimetry, which is presented later (see 5.4.1.3).

Again, all materials exhibit a decrease of the pore volume with each reaction step, while the mean pore size of the material and the BET surface area is not changed significantly for nearly all of the materials. Just the materials with the largest pores - NUV 1000 and KRV 300 - show a decrease in the mean pore size value in the course of the coating process, but the original pore system is still visible in the pore size distribution by BJH, with additional smaller pores, which contribute disproportionately high to the overall distribution because the large pores are on the upper working area of the nitrogen sorption method.

5.4.1.3 Pore Structural Data by Mercury Intrusion Porosimetry

The pore size distribution derived from nitrogen sorption measurements by BJH-method of the materials Nucleosil 300-10 and Nucleosil 1000-10 exhibited pores in the range of 110 nm, which is in the upper detection limit for this method. Therefore these materials where also investigated by mercury intrusion porosimetry, enabling the characterization of pores between ca. 20 µm and 3.5 nm. Both materials where investigated as native and polymer-coated bulk media. Figure 88a) show the mercury intrusion curves for the native (Nucleosil 300-10, Nucleosil 1000-10) and polymer-coated (NUV 300, NUV 1000) materials. The corresponding pore size distributions are displayed in Figure 88b).

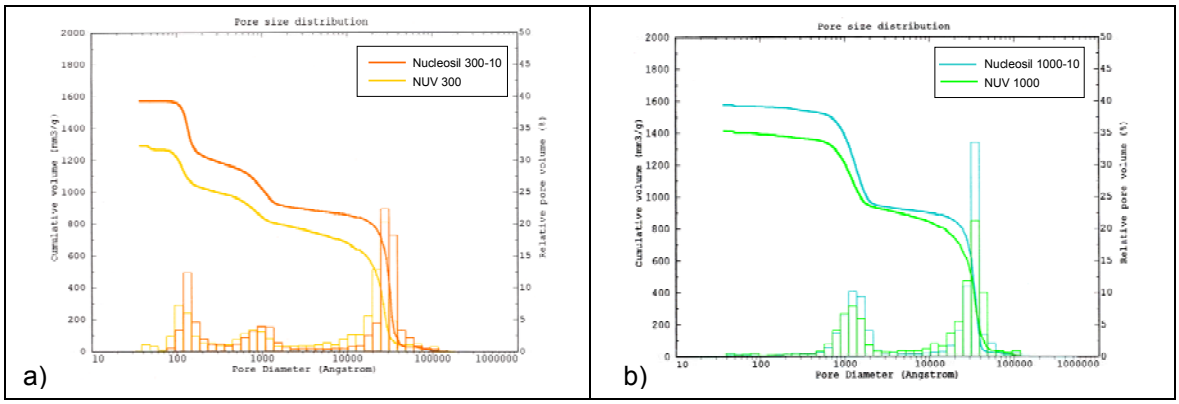

Figure 88: Mercury intrusion measurements with the mercury intrusion curves and the pore size distributions of a) Nucleosil 300-10 and the polymer-coated NUV 300 and b) Nucleosil 1000-10 and the polymer-coated NUV 1000.

Table 73 lists the characteristic data from mercury intrusion method in comparison with the values derived from the nitrogen sorption method.

Table 73: Characteristic data by mercury intrusion porosimetry for unmodified and polymer modified Nucleosil materials.

sample	v_P > 2000 nm [$ml g^{-1}$]	d_{P1} [nm]	d_{P2} [nm]
Nucleosil 300-10	0.6659	13	95
NUV 300	0.5040	11	90
Nucleosil 1000-10	0.6109	-	133
NUV 1000	0.4708	-	122

Mercury intrusion unveils a bimodal pore size distribution of the native Nucleosil 300-10 material, providing half of the pore volume of 0.67 ml/g by very large pores of 95 nm. The second pore system has a medium pore diameter of 15 nm and corresponds with the findings of the nitrogen sorption measurements.

Polymer-coated NUV 300 shows a reduced pore volume of 0.50 ml/g, which is 76 % of the original value. Furthermore, slightly narrower pores are detected, the larger pores show a mean pore size of 90 nm and the smaller pores exhibit a value of 12 nm. Unlike the one of the native material, the mercury intrusion curve of the polymer-coated material shows a breakdown of the material at high pressure, which is visible in the small steep decrease ca. 5 nm, which ends in an x-axis-parallel course. This corresponds to a pressure of 2.5 Kbar. While this is not visible in the native material, and assuming that the rigidity of the silica skeleton is not touched by the polymer coating procedure, this must be a breakdown of a polymer layer, which is of course not as rigid as the silica skeleton. The mercury intrusion method furthermore show a much broader intraparticle space of the polymer-coated material, which is visible as a less x-axis-parallel course of the curve at over 200 nm and a less steep decrease at 3000 nm.

Native Nucleosil 1000-10 materials shows only one discrete pore system with a mean pore diameter of 133 nm and a pore volume of 0.61 ml/g. Furthermore, a breakdown of the material is detected at a pressure of 2.5 Kbar which corresponds to a probed pore size of about 5 nm.

The polymer coating procedure reduces the pore volume of NUV 1000 detected by mercury intrusion to 0.47 ml/g which is 77 % of the initial value. The mean pore size is reduced to 122 nm with a slightly broader pore size distribution. Again, the intraparticle space of the polymer-coated material is less defined than the one of the original material. The breakdown of the material at a pressure of 2.5 Kbar is also detected in the intrusion curve of the native silica and is not large enough to discriminate if there is an extra effect or a breakdown of the polymer layer.

5.4.1.4 Pore Structural Data by SEC using Polystyrene Standards employing PPM

Size-exclusion chromatography in the inverse mode was employed to gather characteristic data of the pore system in chromatographic columns employing a set of polystyrene standards in THF. With this method it is possible to probe the pore system of polymer-coated materials in the swollen state of the polymer layer. Therefore the final polymer-coated materials as well as the unmodified materials were packed in chromatographic columns with an internal diameter of 4.0 mm and a length of 125 mm. The size-exclusion calibration curves of the tested materials are shown in Figure 89a). The corresponding pore size distributions as derived from the experimental data by data treatment are shown in Figure 89b).

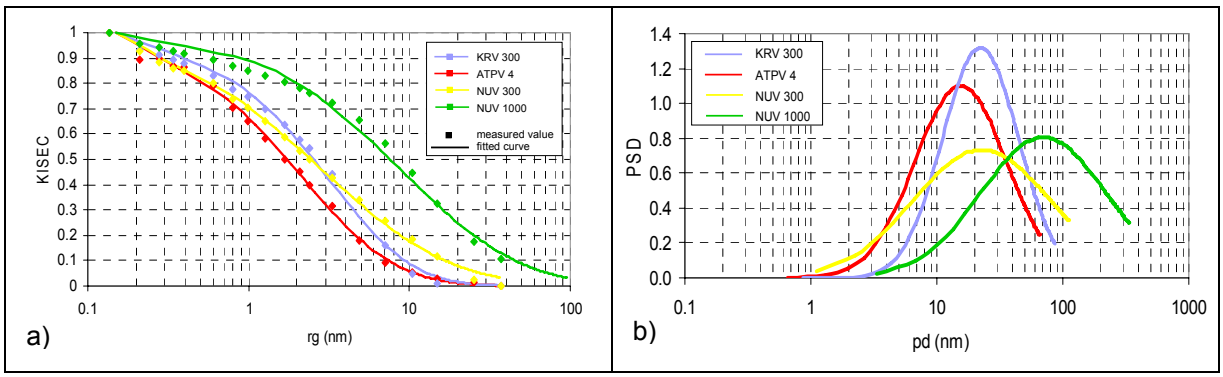

Figure 89: ISEC measurements with THF of modified silicas ATPV 4, KRV 300, NUV 300 and NUV 1000 and their unmodified base materials – a) calibration plots and b) volume based pore size distribution obtained by PPM.

Table 74 shows the exact figures of the data treatment from nitrogen sorption experiments.

Table 74: Pore structural data of modified silicas ATPV 4, KRV 300, NUV 300 and NUV 1000 and their unmodified base materials applied by PPM.

sample	p_d (BJH) [nm]	$p_{d,ave}$ (PPM) by volume [nm]	σ_{pd} by volume [nm]
ATP107g	30.2	34.6	1.0
ATPV 4	30.5	11.0	0.6
Kromasil 300Å	40.9	39.0	0.6
KRV 300	40.0	17.4	1.0
Nucleosil 300-10	15.7	32.4	1.8
NUV 300	15.6	10.4	0.8
Nucleosil 1000-10	110.0	134.4	5.8
NUV 1000	105.0	36.6	4.6

First of all, the mean pore diameter values for the native materials derived from size-exclusion experiments correlate very well with the data obtained by nitrogen sorption experiments and by mercury intrusion porosimetry – with the exception of the Nucleosil 300-10 material. This material has a bimodal pore size distribution with one maximum at around 15 nm and another at around 100 nm, which is in the upper working range of the nitrogen sorption may explains the different results between these two methods, as the larger pores contribute less to the mean pore diameter in nitrogen sorption measurements. Although Nucleosil 300-10 shows a larger mean pore diameter in size-exclusion experiments with a value of 32.4 nm, the material still represents the smallest pore system of the tested materials, followed by a value of 34.6 nm for ATP107g, then 39.0 nm of the material Kromasil 300Å and the largest value is achieved by Nucleosil 1000-10 with 134.4 nm.

Secondly, the figures of the polymer-coated materials differ quite a lot between the data gathered by nitrogen sorption and size-exclusion experiments. In general, all experimental data by size-exclusion experiments show a stricture of the pore system due the polymer coating, as all polymer-coated materials show a much smaller mean pore diameter than the uncoated materials. The mean pore diameter is reduced to a value between 30 to 44 % of the initial value, which is remarkable, as the polymer coating is represented by a carbon load of only between 3.20 % and 4.99 %. The polymer-coated materials exhibit also in size-exclusion experiments the same order for the mean pore size as for the native materials. The smallest resulting mean pore size is detected for the NUV 300 material with a value of 10.4 nm, followed by ATPV 4 with 11.0 nm, then a value of 17.4 nm is detected for KRV 300 and the largest resulting pore size is found for NUV 1000 by 36.6 nm.

Although the difference between the mean pore size of polymer-coated NUV 300 and ATPV 4 is only small, the size-exclusion experiments show unveil an exceptionally wide pore size distribution for the polymer-coated NUV 300 material, with even a large fraction of very small pores. Especially the last finding is disadvantageous for the use of the material as

stationary phase in liquid chromatography, favoring the ATPV 4 much more than expected by just regarding the small difference in their mean pore size.

By focusing on the mean pore size values, all materials feature pore size values, which are in the acceptable range for the separation of small molecules, covering most separations tasks in HPLC. Only the pore size distribution of the polymer-coated NUV 300 shows an unfavorable behavior with a huge pore size distribution containing even large number of much smaller pores. Polymer-coated NUV 1000 exhibits a mean pore diameter which is in the range of so-called wide-pore stationary phases which are applicable for the separation of large molecules like proteins and other biopolymers.

5.4.1.5 Chromatographic Performance: theoretical plate height vs. linear flow velocity

Dibutyl phthalate in water/acetonitrile-mixture as solvent was employed to gather information of theoretical plate height vs. linear flow dependency of the materials towards small molecules. The chromatographic tests were performed on materials packed in chromatographic columns as described in the section before. A retention factor k´ of about 3 was generated for all the tested stationary phases by adjusting the water/acetonitrile ratio according to the procedure given in Appendix 7.3.3 to ensure best comparability of the data. The details of the chromatographic conditions are listed in Table 75 for the columns packed with native and polymer-coated stationary phases.

Table 75: Chromatographic conditions for testing the theoretical plate height vs. linear flow velocity dependency.

column dimension: 125 x 4 mm ID; injection volume: 5 µl;
detection: 254 nm; @ room temperature;
flow rate: 0.25 – 5.0 ml/min; k'= 3
analytes: uracil, diethyl phthalate, dibutyl phthalate
mobile phase: water/ACN, n-heptane / ethyl acetate

The results from the chromatographic evaluation are displayed in Figure 90 as data points, while the lines correspond to the fitted curves as derived by non-linear regression according to the Knox-equation. Please note that the data range of the H-values for the column packed with uncoated Nucleosil 1000-10 is from 540 µm up to 5700 µm, therefore only a few data points of this column are displayed. All curves show a normal behaviour, although the expected increase of the H-value at very small flow rates is not covered by the experimental data points. Therefore, the B-term of the Knox equation is not sufficiently supported by the experimental data. The fitting quality is in all cases very good with R^2-

values of larger than 0.99. All values derived from experimental data by non-linear fit according to the Knox-equation are displayed in Table 76.

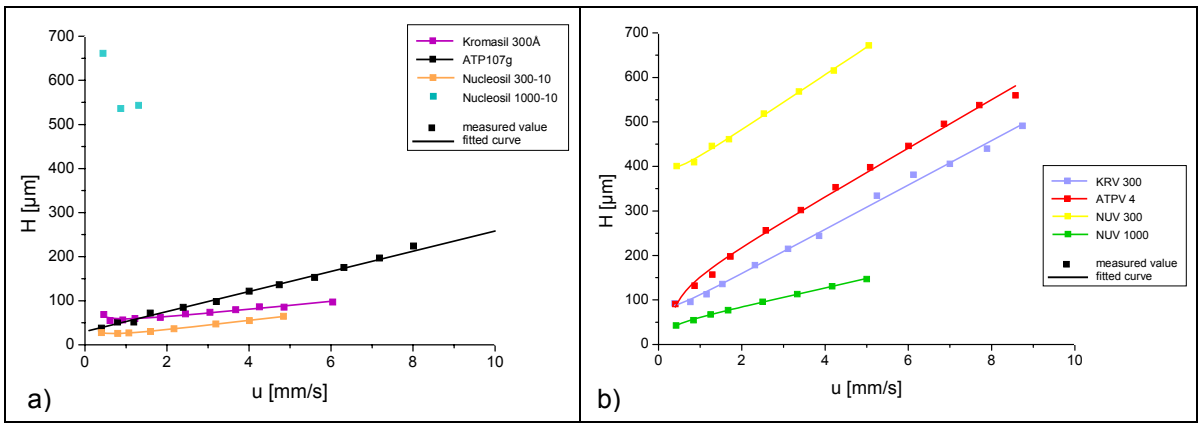

Figure 90: H-vs.-u-plots employing dibutyl phthalates of a) unmodified base materials ATP107g, Kromasil 300Å, Nucleosil 300-10 and Nucleosil 1000-10 and b) modified silicas ATPV 4, KRV 300, NUV 300 and NUV 1000.

Table 76: H-values and C-values of modified silicas ATPV 4, KRV 300, NUV 300 and NUV 1000 and their unmodified base materials.

sample	**Plate Height H** [µm] at 0.5 mms^{-1}	**C-term** [ms] according to Knox	**A-term** [$10^{-5}m^{2/3}s^{1/3}$] according to Knox
ATP107g	37.58 ± 1	22.84 ± 0.85	29.56 ± 4.53
ATPV 4	90.73 ± 1	56.56 ± 1.22	111.12 ± 6.94
Kromasil 300Å	54.94 ± 1	9.31 ± 1.03	41.34 ± 4.72
KRV 300	95.57 ± 1	50.01 ± 1.40	57.42 ± 8.81
Nucleosil 300-10	25.87 ± 1	10.97 ± 0.18	10.18 ± 0.70
NUV 300	400.64 ± 1	62.45 ± 1.79	354.30 ± 7.30
Nucleosil 1000-10	661.38 ± 1	-	-
NUV 1000	42.87 ± 1	20.84 ± 0.39	44.82 ± 1.59

With the exception of the column packed with unmodified Nucleosil 1000-10, all columns packed with the uncoated materials are in the expected range for well packed chromatographic columns, exhibiting values for the H-value of at least 2 to 5 times of their mean particle size. For ATP107g a value of 37.58 µm is reached, while at least 30-75 µm is expected for the mean particle size of 15 µm. Nucleosil 300-10 has a mean particle size of 10 µm, which shifts the expected range down to 20-50 µm, while actually an excellent value of 25.87 µm for the H-value is calculated. The column packed with uncoated Kromasil 300Å exhibits a value of 54.94 µm fulfilling the requirements of 32-78 µm for the particle size of 16 µm. The column packed with native Nucleosil 1000-10 is completely out of the expected range which may be an indication for a bad packing procedure but may also due to the material itself, which has a very small surface area and is not a standard packing material for HPLC.

Furthermore, the materials exhibit excellent mass transfer values, which are represented in the C'-term of the Knox equation. The best mass transfer is found for Kromasil 300Å with 9.31 ms, followed by a value of 10.97 ms for Nucleosil 300-10 and finally ATP107g features a value of 22.84 ms.

In general, all characteristic values are worsened by the polymer coating procedure – with the exception of polymer-coated NUV 1000. The worst polymer-coated material in this comparison is based on NUV 300, which is also the material with the smallest initial pore size in this comparison with an H-value of 400.64 µm and a mass transfer value of 62.45 ms. Polymer-coated ATPV 4 features much better values with 90.73 µm for the H-value and 56.56 ms as C-term. Polymer-coated KRV 300 is based on a silica skeleton with even larger pores and results in an H-value of 95.57 µm and a mass transfer term of 50.01 ms. Finally, the best values are found for the polymer-coated NUV 1000 with an H-value of 42.87 µm and an excellent mass transfer value of 20.84 ms. These values are fully in the expected range of a 10 µm packing material and even can compete with commercial packing media.

The experimental data of this paragraph clearly indicate that the chromatographic properties of the polymer-coated materials are strongly depending on the pore size of the initial silica. The chromatographic performance benefits much from increasing the pore size of the skeleton.

5.4.1.6 Conclusion

All native silica materials, although originating from three different manufacturers, where successfully modified with azo-initiator, enabling to produce materials with very similar polymer loads represented by a carbon content from 3.20 % to 4.99 % C as of elemental analysis. The materials differed mainly in their pore structural values as to mention the specific pore volume and mean pore size. The polymer layer decreases the specific pore volume value to 76-90 % of all materials, except Kromasil 300Å, which was only reduced to 94 % of the initial value of 0.88 ml/g, representing the highest value in this study. The mean pore size value of the materials ranges from 16 to 122 nm, exceeding the capabilities of the nitrogen sorption method, therefore some materials where determined additionally by mercury intrusion. Nucleosil 300 possesses a bimodal pore size distribution with very large pores in the range of 100 nm, being on the upper detection limit of this method, explaining the difference between the pore size value derived by nitrogen sorption and size exclusion experiments. All other native materials show a good agreement of the pore size values derived from nitrogen sorption measurements, mercury intrusion porosimetry and size exclusion experiments. Again, size exclusion chromatography in the inverse mode is the only method, which generates valid data for the polymer-coated materials. The measurements show a strong decrease of the mean pore size value by the polymer coating, resulting in the

same order as of the native materials, ranging from 10 nm to 37 nm with much broader pore size distributions.

Mass-transfer of the native silica materials depends on the mean particle diameter and also benefits from a small high specific pore volume, as Kromasil 300 with a mean particle diameter of 16 µm and the highest specific pore volume shows by far the best C-term value according to Knox with 9.31 ms. Nucleosil 300 has the smallest particle diameter of 10 µm and exhibits a C-value of 10.97 ms, followed by ATP107g with 15 µm particle size, giving a C-value of 21.93 ms, while the Nucleosil 1000 sample is completely out of the range, maybe due to a bad packing of the column.

Polymer modified materials show a completely different behavior. NUV 1000 with the smallest specific pore volume in this study shows the best chromatographic performance of all polymer-coated materials with a C-value of 20.84 ms, followed by KRV 300 with 50.01 ms, then follows ATPV 4 with 56.56 ms and finally NUV 300 with a C-value of 62.45 ms. The order of the mass-transfer of the polymer-coated materials is therefore related to the pore size value, as NUV 1000 shows also the by far biggest mean pore size value of the tested polymer-coated materials.

So far, the major criticism of the polymer-coated materials was the poor chromatographic behavior by means of poor theoretical plate height and bad mass-transfer. NUV 1000 shows that there is an excellent chance to overcome this problem by using silica with extra large pores as skeleton for the polymer coating. Although a not optimized standard coating procedure was used, nearly competitive values by means of chromatographic performance in the range of commercial stationary phases could be achieved. Increasing the flexibility of the polymer layer in combination with reduced polymer load should further increase these values.

Polymer-coated stationary phases based on extra large-pore silica skeleton will be a very interesting subject for further investigations and may be promising materials for the separation of proteins in both analytical and preparative chromatography.

5.4.2 Polymer Modification of Monolithic Base Silica

Stationary phases based on monolithic silica are very promising materials, as they offer excellent resolution with high theoretical plate numbers in combination with low backpressure and excellent mass-transfer-values. In contrast with particulate materials, all modification procedures have to be performed in-column. In a previous work, monolithic columns were already successfully coated with poly(methacrylates) by a physisorption process employing a self-developed synthesis procedure.[33] Although they showed promising properties by means of low denaturation potential towards proteins in combination with good chromatographic

resolution of proteins, physisorbed materials lack of thermal and chemical stability. In this work, monolithic silica materials were coated with poly(methacrylates) employing a chemisorption procedure shown above to generate stable poly(methacrylate) coated monolithic stationary phases.

The manufacturer Merck KGaA, Darmstadt, Germany provided a series of unmodified monolithic columns (Chromolith™, macropores 2 µm, mesopores 25 nm) for this study with a larger pore diameter than the usually available columns branded as Chromolith™. The columns were all from one single batch, ensuring optimum conditions for the reproducibility of the results.

5.4.2.1 Synthesis Parameters

In contrast with particulate materials, monolithic columns can only be chemically modified in-column (see Appendix 7.1.4). This affects not only the synthesis procedure itself, which requires pumping of the synthesis mixture through the column, but also rules characterization methods, as batch-depending methods like elemental analysis or nitrogen sorption measurements require destroying of the column for taking samples.

The reaction conditions used for the particulate materials were also used for the monolithic columns, only the synthesis procedure had to be modified and the reaction times were increased to enable proper heating up.

The first step was to connect a column containing the synthesis mixture to the monolithic column. Applying pressure on the system starts pumping the synthesis mixture through the monolithic column. After at least 5 times of the dead-volume of the monolithic column is pumped through the system, the pressure is reduced and the monolithic column is removed and sealed with plugs. Then the monolithic column was placed in an oven at the desired reaction temperature for the desired reaction time. After reaction was finished, the monolithic column was cooled down to room temperature and washed by pumping the washing solvents through the column.

The rehydroxylation step was skipped, as the provided monolithic columns were already in a surface-activated state, assuming a silanol-group density of 8 µmol/m^2. Therefore, a standard reaction mixture was employed for the coupling reaction with silane. Table 77 lists the experimental reaction conditions and experimental parameters together with the results of elemental analysis of the silane-coupling step.

Table 77: Elemental analysis and experimental parameters of silane modified silica.

sample	**Net weight of silane** [g]	**%C** (w/w)	**%H** (w/w)	**%N** (w/w)	**Grafting density** in per cent %
CM S0*	3.966	2.87	0.80	< 0.01	15.30

*The reaction-time was 35 hours at RT.

The resulting grafting density of the silane modified monolithic silica of 15.30 % is based on the assumed value for the silanol-group density of 8 µmol/m^2 and correlates quite sufficiently with results obtained for particulate materials.

The next step of the synthesis procedure is the coupling of the AZO-initiator-group onto the silane. This was also performed involving standard concentrations for the reaction mixture. The synthesis parameters and the results of elemental parameters are given in Table 78.

Table 78: Elemental analysis and experimental parameters of surface-bound azo-initiator.

sample	**Net weight of silane** [g]	**%C** (w/w)	**%H** (w/w)	**%N** (w/w)	**Grafting density** in per cent %
CM A0*	3.626	4.62	0.83	0.78	11.50

*The reaction-time was 11 hours at 50 °C.

The resulting grafting density for the AZO-modified material of 11.50 % represents a still acceptable conversion rate of the silane groups of 75 %, which is slightly worse than the 88 % reached for particulate silica, but which is still quite acceptable.

Table 79 lists the reaction conditions and monomer concentration for the polymer modification of the AZO-coated monolithic columns together with the results of elemental analysis.

Table 79: Elemental analysis and experimental parameters of initial monolith CM 25nm and the polymer modified monoliths CM P2HE.-E and CM PEMA.

sample	**Net weight of co-monomer** [g] 2HEMA	EMA	**%C** (w/w)	**%H** (w/w)	**%N** (w/w)
CM 25nm	-		0.40	0.70	< 0.01
CM P2HE.-E*	0.226	0.203	11.10	2.01	0.05
CM PEMA*	0	0.628	10.89	1.98	0.04

*The reaction-time was 6 hours at 90 °C.

The figures show, that the monolithic columns were successfully coated with polymer. Two types of polymer-coatings were produced to generate surface interaction with different hydrophobicities. Sample CM P2HE.-E is less hydrophobic than sample CM PEMA and is comparable with the usual standard coating used for particulate materials. Sample CM 25nm is the unmodified monolithic material.

Both materials have very high polymer loads as expressed in the carbon content value of 11.10 %C respectively 10.89 %C.

5.4.2.2 Pore Structural Data by Nitrogen Sorption at 77K

Nitrogen sorption measurements at 77 K were performed on bulk materials generated by carefully destroying the monolithic columns to ensure that no leftovers of the polymeric

column housing are contaminating the sample. The isotherms of the native sample CM 25nm and the polymer-coated sample CM PEMA are displayed in Figure 91. Table 80 lists the results of the data treatment for both samples.

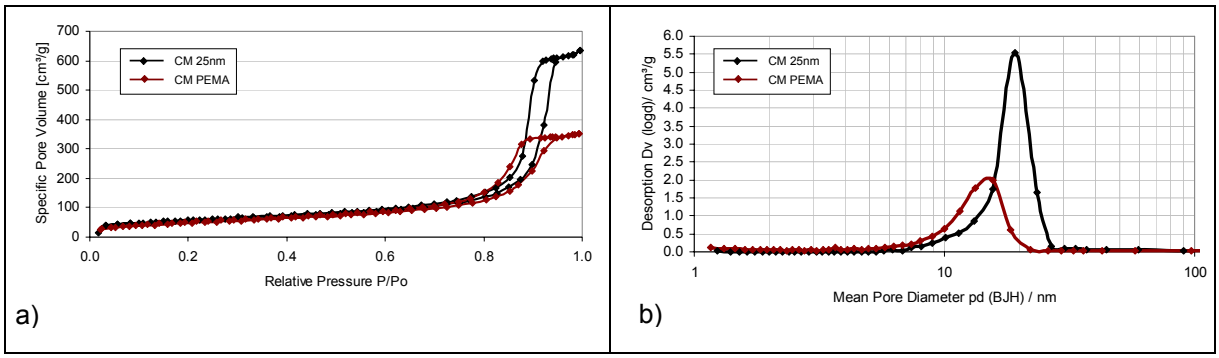

Figure 91: Nitrogen sorption measurements of unmodified monolith CM 25nm and PEMA modified CM PEMA – a) isotherms and b) pore size distributions.

Table 80: Pore structural data of CM 25nm and CM PEMA.

sample	a_S (BET) [m^2g^{-1}]	v_p (G) [ml g^{-1}]	p_d (BJH) [nm]
CM 25nm	197.3	1.009	19.2
CM PEMA	175.7	0.572	13.3

The specific pore volume of the polymer-coated sample is reduced drastically to 57 % of the value from the unmodified silica. The specific surface area according to BET is slightly reduced by 10 % of the initial value. In contrast with the results obtained from other methods, polymer-coated monoliths show a slight decrease in the mean pore size value from 19.2 nm to 13.3 nm derived from the desorption branch of the isotherm to 69 % of the initial value. A closer look to the isotherm shows that this corresponds to a shift of the desorption branch to smaller relative pressure values, while the adsorption branch is slightly shifted towards higher p/p0-values resulting in a bigger adsorption-/desorption-hysteresis between. This is an indication for a hindered pore-filling/emptying of the polymer-coated material, bearing a very high polymer load.

5.4.2.3 Pore Structural data by SEC using Polystyrenes Standards employing PPM and PNM

Size-exclusion chromatography in the inverse mode was employed to gather pore structural data of native and polymer-coated monolithic columns employing a set of polystyrene standards in THF. In contrast to nitrogen sorption experiments, this method allows the pore system characterization of polymer-coated stationary phases in swollen state. The monolithic columns had an internal diameter of 4.6 mm and a length of 25 mm. Size exclusion calibration curves are shown in Figure 92a). The corresponding pore size distributions from the data treatment based on parallel pore model are shown in Figure 92b).

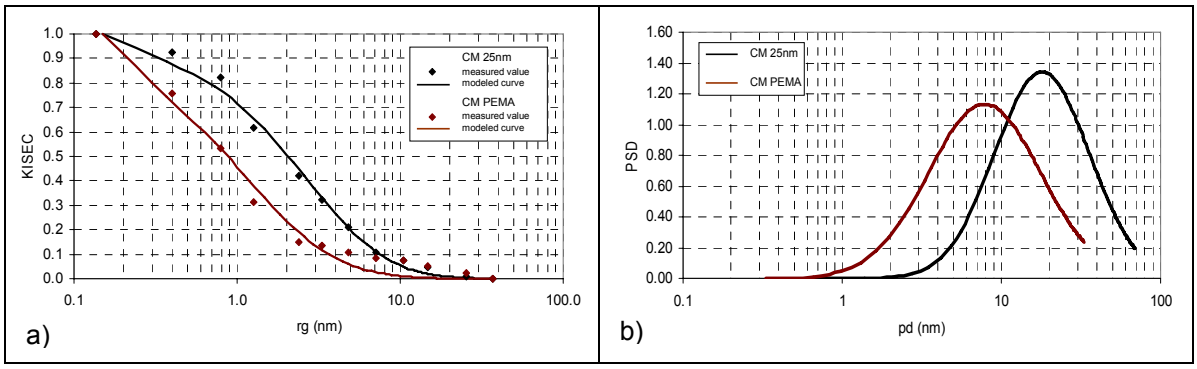

Figure 92: ISEC measurements with THF of unmodified monolith CM 25nm and PEMA modified CM PEMA – a) calibration plots and b) volume based pore size distribution obtained by PPM.

The exact figures derived from data treatment are displayed in Table 81 together with results from nitrogen sorption experiments for comparison. The n_T-values are derived from data treatment employing pore network model.

Table 81: Pore structural data of CM 25nm and CM PEMA applied by PPM.

sample	p_d (BJH) [nm]	$p_{d,ave}$ (PNM) by volume [nm]	σ_{pd} by volume [nm]	n_T (PNM)
CM 25nm	19.2	21.8	1.40	> 10
CM PEMA	13.3	11.0	1.20	> 10

The figures show a strong decrease of the mean pore size value from 21.8 nm from the uncoated monolithic silica CM 25nm down to a value of 1.0 nm for the polymer-coated sample CM PEMA due to the polymer coating procedure. In contrast with the measurements of the particulate polymer-coated silica samples, a very good agreement of the pore size values between nitrogen sorption data (BJH) and size exclusion data (PNM) is found. Although a very high polymer load was applied, and unlike the findings in the case of particulate materials, the pore connectivity value of the polymer coated monolithic sample showed still an ideal value of $n_T > 10$, which is the same as for uncoated monolithic base silica.

5.4.2.4 Chromatographic Evaluation – LCM-test-mixture

The separation capabilities of polymer-coated monolithic columns towards proteins were checked with a test mixture consisting of lysozyme, cytochrome C and myoglobin in gradient mode by reversed phase chromatography. Columns with an inner diameter of 4.6 mm and a length of 25 mm were employed. For comparison, the uncoated monolithic column in its native state was also tested under the same chromatographic conditions as listed in Table 82. Figure 93 shows the chromatograms of the tested columns.

Table 82: Chromatographic conditions for LCM-test-mixture as shown in Figure 93.

column dimension: 25 x 4.6 mm ID
flow rate: 1 ml/min; concentration: 1 mg/ml;
injection volume: 5 µl; detection: 215 nm, 400 nm;
@ room temperature;
from 95/5 % (v/v) A/B in 5 min to 5/95 % (v/v) A/B; with
A: water + 0.1 % TFA,
B: acetonitrile + 0,09 % TFA

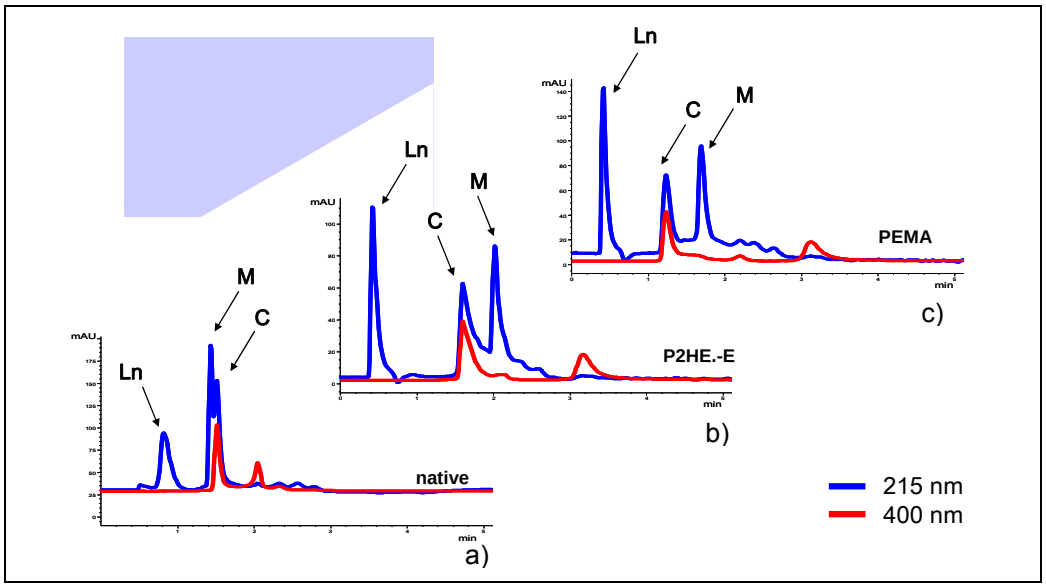

Figure 93: Elution profiles of LCM-test-mixture at different wave lengths applied on monolithical columns CM 25nm (native), CM P2HE.-E and CM PEMA.

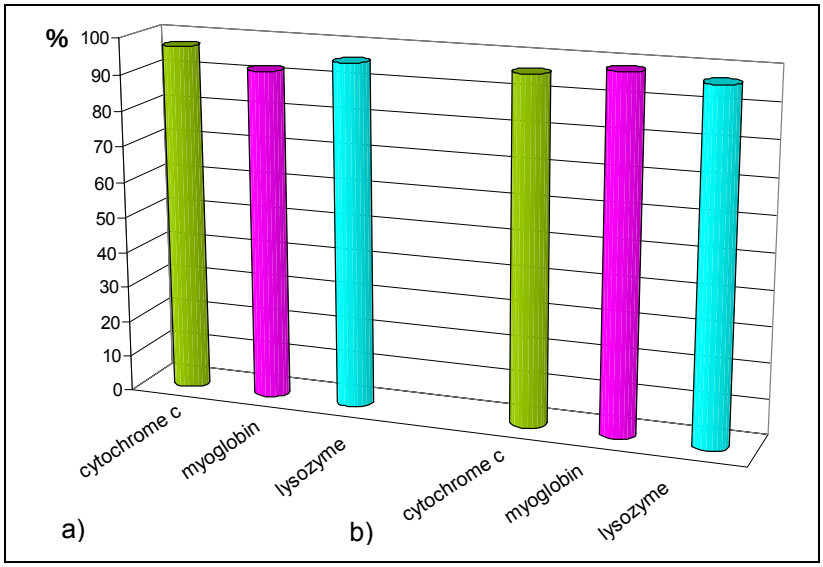

Figure 94: The overall biorecovery of three proteins by a mixture of lysozyme, cytochrome C and myoglobin a) CM P2HE.-E and b) CM PEMA.

Table 83: Biorecovery data of lysozyme, cytochrome C and myoglobin in per cent.

analytes	**biorecovery** in % on P2HE.-E modified column	**biorecovery** in % on PEMA modified column
cytochrome C	97.17	96.08
myoglobin	92.01	98.28
lysozyme	95.76	96.54

Nearly full biorecovery of all proteins could be observed on polymer-coated monolithic materials with values of above 90 %, representing a very good biorecovery of the analytes, with only small variations between the different proteins and columns.

5.4.2.5 Relative Enzymatic Activity Test – Alcohol Dehydrogenase (ADH)

Alcohol dehydrogenase (ADH) was employed as indicator for the biocompatibility of the polymer coated monolithic stationary phases (see 3.3.3.2) by comparing the enzymatic activity of ADH, which was applied to the stationary phase with the activity of ADH, which was only exposed to the stress of the chromatographic equipment as 100 %-reference. The chromatographic conditions are shown in Table 84.

Table 84: Chromatographic conditions for the enzymatic activity test as shown in Figure 95.

HPLC conditions
analyte: ADH; mobile phase: 0.1 M Tris-HCL, pH= 8.8
concentration: 2mg/ml; injection volume: 6 µl
flow rate: 1 ml/min
Collection of Samples
empty column from 0.0-0.7 min = 700 µl
test column from 0.1-0.8 min = 700 µl

The collected ADH was used for catalyzing the decomposition of ethanol with NAD^+ to acetaldehyde and NADH. The reaction (see 3.3.3.2) was followed in a photometer (see Appendix 7.3.6) via the formation of NADH, which exhibits a strong absorption at 366 nm.

Figure 95 represents the formation of NADH after applying ADH samples to the reaction mixture. The samples were collected after the exposure to different stationary phases and the HPLC equipment without a column.

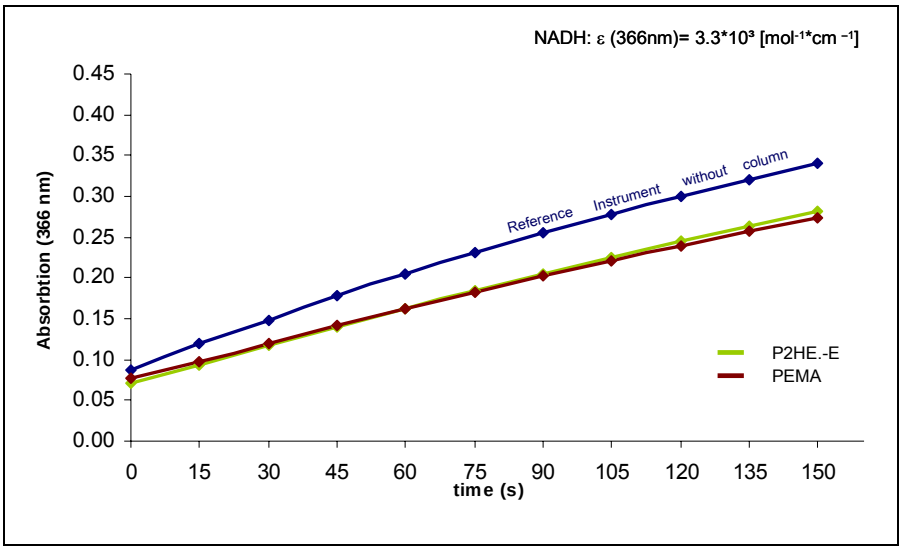

Figure 95: ADH-catalyzed formation of NADH by the application of ADH-samples after passing different stationary phases.

The enzymatic activity for the ADH samples was determined by dividing the slope of the sample-curve with the reference curve and multiplying with 100 %. The results are listed in Figure 96 and the figures are listed in Table 85.

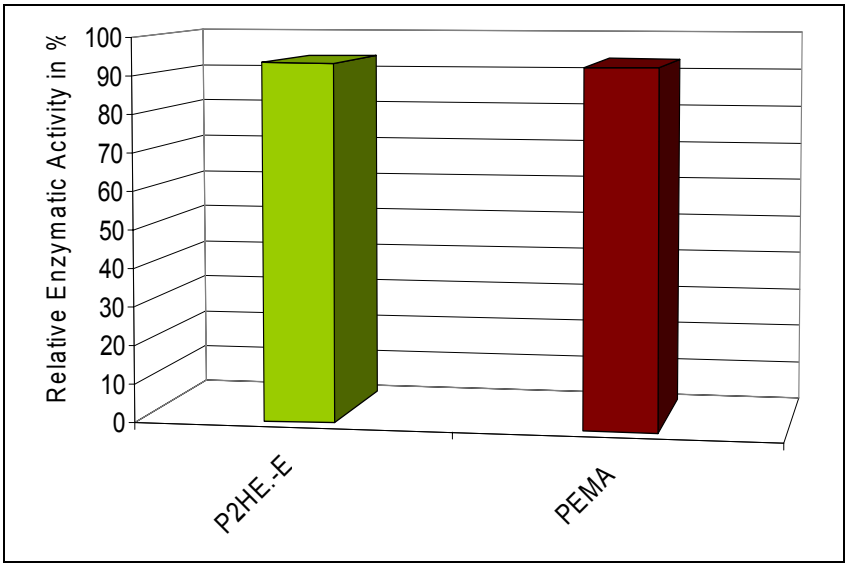

Figure 96: Relative enzymatic activity of ADH in per cent on P2HE.-E and PEMA coated stationary phases.

Table 85: Relative enzymatic activity data of ADH in per cent on P2HE.-E and PEMA coated stationary phases.

sample	P2HE.-E	PEMA
relative enzymatic activity in per cent	93.30	92.80

The contact of ADH with the polymer-coated monolithic stationary phases has only a minor impact upon its enzymatic activity, with nearly identical values of the enzymatic activity

in the range of about 93 % for both of the polymer-coated stationary phases, not favouring a specific phase.

5.4.2.6 Conclusion

Monolithic silica based materials were successfully coated employing a slightly modified standard coating procedure, as the synthesis has to be performed in-column. Although the material exhibits a much higher surface area than the tested particulate materials, the grafting density of the anchor groups exhibited nearly identical values. Although relatively large amounts of polymer were applied by the following polymerization step, as represented in a carbon load of more than 10 %C, polymer-coated monolithic silica showed no worsening of the pore connectivity value. The pore size value was reduced to 11 nm, which is only half of the initial value.

Only short columns were modified in this study, so the chromatographic evaluation was only performed by an LCM-test, which showed very promising results by means of both good separation and high biorecovery of the proteins. All stationary phases left lysozyme in its native state, which further support the findings in the test of the impact of the stationary phases upon the enzymatic activity of ADH, revealing an excellent biocompatibility of the material.

Coating of monolithic materials by an in-column procedure with poly-(methacrylates) is therefore another promising option for the further development of these stationary phases, but further studies should be based on columns of larger dimensions. Reducing the polymer load, increasing the flexibility of the polymer layer and using monolithic materials with larger pores should generate further improvements of the chromatographic properties.

6 DISCUSSION AND OUTLOOK

Case study A: The focus of the first part of case study A was on the assessment of pore structural data by nitrogen sorption at 77 K and by ISEC employing two types of amorphous mesoporous silicas and their pseudomorphically transformed derivatives. Both materials gave ordered MCM-41 type silicas with spherical morphology. The harsh treatment did scarcely change the particle shape as compared to the original materials and also the particle size distribution did not change significantly (s. Table 2). Drastic changes, however, were observed for the pore structural parameters. For LiChrospher Si 60 as initial sample the specific surface area increased from 769 m^2/g to 1,042 m^2/g of the sample MTS1 (s. Table 4). The most notable change was seen at the specific pore volume from 0.896 ml/g to 2.170 ml/g. The average pore diameter as derived from nitrogen sorption measurements was slightly enhanced by 1 nm. From ISEC data using the PPM model a similar increase in the average pore diameter was manifested from 7.8 to 10.4 nm, (s. Table 6). Most importantly, the pore connectivity value n_T calculated by the PNM model remained the same, i.e. a high pore connectivity of $n_T > 10$ resulted after the treatment.

The second probe was a highly porous spherical amorphous silica made by the PES process. Again the particle morphology and the particle size distribution of the sample remained widely unchanged by the transformation process (s. Table 3). Again as seen at LiChropsher Si 60 the specific surface area increased by a factor of more than two (s. Table 5), but the specific pore volume decreased notably from 1.871 ml/g to 1.630 ml/g. Obviously, the initial particle porosity was already so high that stable particles with a higher porosity were not obtained. The results of the assessment of the average pore diameter before and after the treatment remained somewhat complex. While the initial sample exhibited a unimodal distribution with an average pore diameter of 25 nm according to BJH respectively 26 nm derived from NLDFT method (s. Table 5), the treated MTS2 sample showed part of the original pore size and then a bimodal distribution at 3.5 and 6 nm according to BJH, whereas the NLDFT method generates a bimodal distribution with two maxima at 7.0 nm and 8.1 nm, which is typical for the ordered MCM-41 type of material. The ISEC data showed a reduction of the average pore diameter from 33 nm to 15 nm, while the pore connectivity slightly increased by the treatment from 9 to > 10 (s. Table 7).

Most interesting were the results of the theoretical plate height vs. linear flow velocity curves obtained on the two pairs of native silicas in the normal phase mode (s. Fig. 27 and 28). While all pore structural values were changed in the course of the pseudomorphical transformation process, the conversion from an amorphous into a more ordered bulk structure did not significantly alter the column performance characteristics after the material was packed in chromatographic columns. Only the pore connectivity values were unchanged

by the pseudomorphical treatment, highlighting the importance of the pore connectivity as key parameter for the evaluation of stationary phases.

The group of F. Fajula with A. Galarneau and co-workers from CNRS, Montpellier, France expanded these studies and published a number of papers.[19,21,22,117]

The second part of Case Study A dealt with a series of well characterized silica of Kromasil type, supplied by EKA Chemicals AB, Bohus, Sweden. All the samples were C18 functionalized (s. Table 11) and slightly differed in the specific pore volume and in the average pore diameter. All probes gave a high pore connectivity of > 10 calculated from ISEC curves applying the PNM model (s. Table 12). The experimentally measured plate height linear velocity curves showed slight deviations in the C-Term regime. The calculated C-Term values, representing the mass transfer resistance decreased with increasing specific pore volume (s. Fig. 35).

The third part of Case Study A is a comparison of a series of poly(methacrylate)-coated silicas with increasing polymer load being characterized by nitrogen sorption as well as by ISEC. The latter was performed employing three solvents differing in polarity: dioxane, tetrahydrofuran and dimethylformamide to check for possible swelling properties of the polymer layer. While nitrogen sorption showed only the expected decrease of the specific pore volume and the specific surface area with increasing polymer load of the sample, no change in the average pore diameter of the samples was detected by this method (s. Table 15).

Average pore diameter values derived from ISEC measurements by PPM model showed the expected drastic decrease and also a notably diminishing of the pore connectivity with increasing polymer load (s. Table 16). There was nearly no difference seen among the values for the three solvents, which allows one to conclude that changes in the swelling of the polymer layer at least under these conditions are negligible.

Case study B: For a better understanding the following scheme complies with the scheme of the workflow on pages 73 and 74 summarizing the most important results of Case Study B:

Action	Results
Assessment of the basics of the synthesis	
Selecting the way of binding the initiator group to the silica surface	P-(chloromethyl) phenyltrimethoxysilane was subjected to reaction with a rehydroxylated silica (LiChrosper Si 300) and subsequently the azo-initiator group (ACPA) was bonded (Fig. 43)

Polymer bonding aspects and kinetics of the polymerization procedure	The azo-initiator grafted silica was reacted with a methacrylate monomer/co-monomer mixture in presence of EDMA as cross-linker (Fig 46). The kinetic studies of the polymerization step showed that an optimum control of the polymer load could be achieved by selecting a constant reaction time of 120 min and variation of the concentration of a co-monomer of 2-hydroxy-ethylmethacrylate and ethylmethacrylate (Fig 50)
Reproducibility of the synthesis	The reproducibility of the single consecutive reaction steps was assured, showing an overall standard deviation of the carbon content of +/- 2 %
Up scaling of the synthesis procedure	The batch size of the synthesis procedure could be varied from 0.2 g up to 130 g
Transfer of the recipe to other brands of silicas	The standard procedure was transferred to Kromasil 300 from Eka Chemicals AB, Bohus, Sweden, and Nucleosil 300-1000, Macherey-Nagel, Düren, Germany, with good results
Optimization of the reaction composition, reaction route and reaction conditions with respect to enhanced column performance, maintenance of bioactivity and biorecovery	
Adjustment of the hydrophobicity of polymer layer	Various methacrylate monomers and co-monomer compositions with increasing hydrophobicity were tested: 2HEMA, 2HE-E, EMA and OMA (Fig. 59). A co-monomer mixture of 2HE-E was best suited with regard to a low denaturation potential for proteins and with respect to high biorecovery
Variation of the polymer load	The polymer load was varied between 4.5 and 9.2 % w/w. The column performance and chromatographic resolution was increasing with decreasing polymer load.
Adjustment of the linker density	The concentration of surface bound azo-initiator groups was reduced by 50 %. This allowed to synthesize materials with a polymer load between 3.6 and 5.5 % C w/w. Although the chromatographic properties were enhanced and a very high adsorption capacity towards lysozyme was detected, the performance was not satisfactory,

Variation of the rigidity of the polymer layer	Lowering of the rigidity of the polymer layer was performed by introducing OMA with long flexible n-alkyl chains as co-monomer and also by reduction of the cross-linker density. This further enhanced the chromatographic properties, although the expectations were not reached.
Variation of the silica support material	
Extending the range of mesoporous silicas to other brands and including macroporous silicas	In addition to LiChrospher Si300, the polymer coating procedure could be applied to Kromasil 300, Nucleosil 300 and macroporous Nucleosil 1000. The polymer coated Nucleosil 1000 showed by far the best chromatographic performance of all coated materials, reaching even the expectations of commercial materials (Table 76).
Can the recipe developed for particles also be transferred to silica monoliths?	Applying an in-column coating process, silica monoliths with 22 nm average pore diameter could be successfully coated.

Chemisorbed poly(methacrylate) based polymer coatings possess a high potential for further investigations and development to achieve an supplementary stationary phase for reversed phase separation of proteins and peptides with different properties than the usual silanized materials. Promising results by means of good biocompatibility, high capacity and chromatographic performance are presented in this work, giving direction for future development of these polymer coated materials. Furthermore a protocol was developed to use inverse size-exclusion chromatography as a very valuable tool for the development of stationary phases, probing the pore system as ‘real-life’ method in contact with the mobile phase, showing a very strong decrease of the mean pore size with increasing polymer load. The excellent chromatographic performance of polymer-coated macroporous silica indicates the promising potential of these phases for further development, which should be based on as less polymer load as possible. Additionally, reducing the rigidity of the polymer coating would further improve the chromatographic properties. As the method could also be successfully applied on monolithic silica materials by an in-column procedure, development is not limited to the coating of particulate materials in bulk, but allows even the coating of stationary phases in the packed column.

7 APPENDIX

7.1 Synthesis Procedures

7.1.1 Preparation of Highly Porous Silica Beads: the Polyethoxysiloxane (PES) Process[7,125]

7.1.1.1 Preparation of Polyethoxy Siloxane (PES)

Polyethoxy siloxane (PES) was prepared by hydrolytic polycondensation of prepolymerised tetraethoxysilane, labelled as TES 40 (Merck, KGaA, Germany). 1300 g TES 40 are poured into a clean and dry 2 l round bottom flask and 280 g ethanol (99.7 – 100 %, Merck KGaA, Germany) is added while stirring at 800 rpm with a Teflon covered magnetic stirring bar. When the mixture of TES 40 and ethanol is mixed homogeneously, 60.0 g of 0.1 mol/l hydrochloric acid (Titrisol, Merck KGaA, Germany) is added over a period of 10 – 12 min using a dropping funnel in order to initiate the condensation. After stirring for another 30 min, the 2 l round bottom flask is connected to a rotary evaporator system from Büchi Labortechnik AG, Switzerland, which consists of a Rotavapor R-124, a Vacuum Controller B-720, an Oil bath B-485, and a Vacuum System B-172. A temperature of 140°C is applied in order to remove the ethanol, and the vacuum is reduced to 50 mbar. The system is kept at 50 mbar (Δp = 1mbar) and 140 °C for 2 h before leading a nitrogen stream (not a continuous stream, but such that single bubbles are formed) through the PES for 14-18 h at a temperature of 140°C. After that the PES is bottled and stored.

This standard procedure gives PES with a viscosity of 75 mPa*s. By changing the amount of hydrochloric acid, PES of various viscosities can be produced. The viscosity is increasing with increasing the amount of hydrochloric acid. The cone and plate technique was used for the viscosity measurements. The cones and plates are available in different size diameters (2-6 cm) and different angles (0.5-4 degrees) depending on the viscosity to be measured. To measure the dynamic viscosity of PES in the range of 30-100 mPa*s the combination of 4 cm cone diameter and an angle of 1 degree is used. The measurements were carried out using Carri-Med CSL 500 Rheometer, Leatherhead, Great Britain.

7.1.1.2 Preparation of Silica Hydrogel Beads

In the conversion of PES into silica hydrogel beads, 550 ml PES and 33 g dimethylformamide (DMF) (99%, Merck KGaA, Germany) and various amounts of cyclohexane (99%, Merck KGaA, Germany) are mixed in a 2000 ml beaker. In order to increase the pore volume, higher amounts of cyclohexane should be added. Therefore, four syntheses were carried out, adding 150, 300, 450 and 600 ml cyclohexane, respectively, to the PES/DMF mixture. Then 2700 ml of deionized water and 1500 ml iso-propanol (p.a.,

Merck KGaA, Germany) are mixed in a 5 l flask. 3000 ml of the prepared water/iso-propanol solution is poured into a new 5 l flask, and the PES/DMF/cyclohexane mixture is added. A stainless steel stirrer is adjusted to the flask, a drilled stopper including a funnel is connected, and finally the stirrer is attached to a drilling jig. The stirrer engine (FL-RD 20 V 1, Fluid, Lörrach, Germany) is switched on and the revolution rate is increased from 330 rpm up to 1500 ± 5 rpm. The mixture is emulsified for 5 min and then 250 ml of ammonia (25%, Merck KGaA, Germany) is added at once. After 30 min of stirring at the same speed, the suspension is poured into a 10 l glass beaker and is allowed to sediment for 24 h. After 24 h the supernatant dispersion is decanted and the residue is suspended in 8 l of deionized water. Again, the particles are allowed to sediment for 24 h. This last step is repeated once.

After the third sedimentation, the supernatant dispersion is decanted and the residue is suspended in 2 l of deionized water. Afterwards, the suspension is filtered using a porcelain Buechner funnel (diameter: 270 mm) with a round filter paper and washed with 3 l of deionized water at room temperature and with 2 l of methanol (p.a., Merck KGaA, Germany).

7.1.1.3 Preparation of Silica Xerogel Beads

A heatable magnetic stirrer, an electronic contact thermometer and a teflon covered stirring shaft are used to age the native silica. The native silica has been dried in a vacuum oven for 24 h at 140°C using < 20 mbar vacuum. For each gram of dry native silica 10 ml of deionized water and 0.1 ml of ammonia (25 %) is taken. 150 g of the silica hydrogel particles is suspended in 1500 ml of deionized water in a 2 l round bottom flask by adding the particles into the water under stirring using the electronic stirrer at room temperature. Then 15 ml ammonia (25%, Merck KGaA, Germany) is added using a graduated cylinder (40 ml). After that the suspension is heated to 70°C (contact thermometer: 70°C; heat able magnetic stirrer: 250°C). In order to maintain a pH of 7.0 – 7.5 it is necessary to heat the suspension for 8 h at 70°C. Finally, the suspension is filtered once more using a porcelain Buechner funnel (diameter: 270 mm) with a round filter paper and washed with 5 l of deionized water at room temperature, then with 2 l of iso-propanol (p.a., Merck KGaA, Germany), and finally with 1 l of methanol (p.a., Merck KGaA, Germany). Finally, the silica hydrogel is dried for at least 4 h at 150°C in a vacuum oven (< 20 mbar) in order to convert it into a xerogel.

7.1.1.4 Calcination of Silica Xerogel Beads

The dry silica is evenly distributed in a porcelain dish (o.d. = 20 cm), which is placed in a furnace and calcined according to the following temperature program:

Heat-up time:	1 °C/min to 650 °C
Calcination time:	300 min at 650 °C
Cooling down time:	to RT, about 20 h

7.1.2 Preparation of Large Mesostructured Micelle Templated Silica (MTS)

MCM-41 samples were synthesized according to the pseudomorphic synthesis procedure described previously by Martin et al.[19]. This method utilizes an isomorphic transformation of pre-formed silica grains and allows a complete retention of the morphology. In a typical synthesis, mesoporous silica spheres are exposed to hydrothermal treatment under basic conditions in the presence of surfactants used for conventional MCM-41 type materials synthesis (CTAB). The reactions were performed in a steel autoclave with the proportions 1:0.25:0.1:20 SiO_2/NaOH/CTAB/H_2O. Reactants were added under stirring, and the mixture was mechanically stirred (400 rpm) for half an hour at room temperature and put at 388 K for 20 h. The resulting solids were recovered by filtration, washed with water, and dried at 353 K overnight. Materials were then calcined under air flow at 823 K for 8 h.

7.1.3 Polymer Modification of Particulate Silica

7.1.3.1 Silica Surface Activation

The last synthesis step of chromatographic silica is the calcination step, in which the material is heated up to 650 °C to remove organic residues from the synthesis like porogens and solvents. This procedure also fully removes physisorbed water and water from surface silanol groups is also split off, leaving the silica surface in a chemically inactive state. Rehydroxylation (scheme see Figure 97) is the reversal of this reaction and allows the preparation of silica with controlled activity of silanol groups on the surface[145].

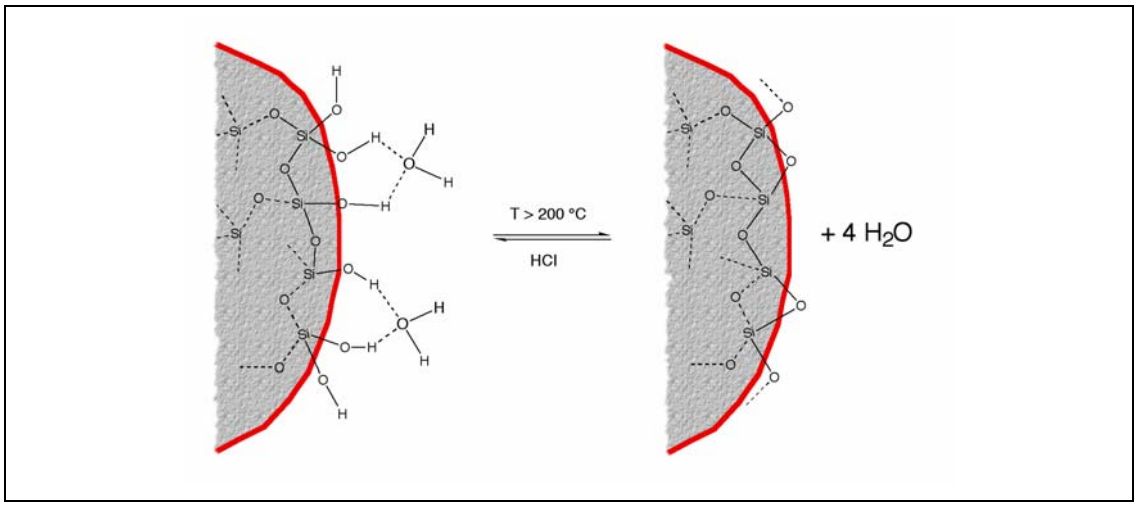

Figure 97: Schematic illustration of the dehydroxylation and decomposition of siloxane-bonds during rehydroxylation.

Standard procedure

[145] C. du Fresne von Hohenesche, V. Ehwald, K.K. Unger, J.Chromatogr.A 1025 (2004) 177-187

400 ml of deionized water (University of Mainz, Germany) is poured into a 1000 ml three-neck round-bottom flask equipped with a Dimroth-condenser, and 400 ml of hydrochloric acid (37 %, Fisher Chemicals, UK) is added. Then 135 g of the calcined silica material is added in small portions while stirring at 500 rpm with a Teflon covered magnetic stirring bar. The flask is then placed into an oil-bath (electronic-thermometer: 150 °C; heater: 200 °C) and the solution is heated using a RCT basic IKAMAG® magnetic stirrer. The mixture is then refluxed at 150 °C and 500 rpm stirring speed for approximately 12 hours. After 12 hours the oil bath is removed and the suspension is allowed to cool down for approximately 30 min. The silica is filtered in a glass filter funnel (Robu® Borosilicat 3.3 Por.-4, Robu Glasgeräte, Hattert, Germany) and washed neutral (check with pH-paper) with 10 l of deionized water. Afterwards the silica is washed with 300 ml of methanol. Finally, the silica is dried in a vacuum oven (Vacutherm, Heraeus, Hanau, Germany) at 150 °C, 12 hPa for 15 hours using a porcelain-dish.

7.1.3.2 Binding of p-(chloromethyl)phenyltrimethoxysilane onto the silica surface

Standard procedure

In a 100 ml three-neck round-bottom flask 25 ml of dry tetrahydrofuran is added. Then 10 g of calcined silica material is added in small portions into tetrahydrofuran while stirring at 500 rpm with a teflon covered magnetic stirring bar. The whole system is then flushed with dry nitrogen. According to the number of silanol groups on the silica surface (8 µmol/m²) the appropriate amount of p-(chloromethyl)phenyltrimethoxysilane (5 mmol, 1.23 g) is added to the mixture. The three-neck round-bottom flask is then sealed with plugs and kept under stirring with 500 rpm for approximately 24 hours[146] at room temperature. Then the silica is filtered by a glass filter funnel (Robu® Borosilicat 3.3 Por.-4, Robu Glasgeräte, Hattert, Germany) and washed with 100 ml of tetrahydrofuran and 50 ml of methanol. Finally, the silica is dried in a vacuum oven (Vacutherm, Heraeus, Hanau, Germany) at 40 °C, 12 hPa for 15 hours using a porcelain-dish.

7.1.3.3 Binding of 4,4'-Azobis(4-cyanopentanoic acid) onto the silanized silica surface

Standard procedure

In a 100 ml three-neck round-bottom flask equipped with a Dimroth-condenser 40 ml of dry toluene is added. Then 10 g of the silanized silica material is suspended in small portions in toluene while stirring at 500 rpm with a teflon covered magnetic stirring bar. The whole system is then flushed with dry nitrogen. A mixture of 4,4'-azobis(4-cyanopentanoic acid) (30 mmol, 8.43 g) and α-picolin (50 mmol, 4.65 g) in 10 ml dry toluene is then added to the

[146] Extension of the reaction-time to 48 hours has no influence on the result.

mixture in the three-neck round-bottom flask. The flask is placed into an oil-bath (electronic-thermometer: 50 °C; heater: 100 °C). The solution is heated for approximately 5 hours at 50 °C using an RCT basic IKAMAG® magnetic stirrer. After 5 hours the oil bath is removed and the suspension is allowed to cool down. The silica is filtered in a glass filter funnel (Robu® Borosilicat 3.3 Por.-4, Robu Glasgeräte, Hattert, Germany) and washed with 100 ml of toluene and 50 ml of methanol. Finally, the silica is dried in a vacuum oven (Vacutherm, Heraeus, Hanau, Germany) at 40 °C, 12 hPa for 15 hours using a porcelain-dish.

7.1.3.4 Polymerization step

Standard procedure

In a 50 ml two-neck round-bottom flask equipped with a Dimroth-condenser 10 ml of dry toluene is added. Then 2.0 g of azo-modified silica material is suspended in toluene while stirring at 500 rpm with a teflon-covered magnetic stirring bar. The whole system is then flushed with dry nitrogen. A mixture of a co-monomer of 2-hydroxy-ethylmethacrylate (1.02 mmol, 0.13 g) and ethyl methacrylate (0.98 mmol, 0.11 g) and as cross-linker EDMA (0.20 mmol, 0.04 g) is then added to the mixture in the two-neck round-bottom flask. The flask is placed into an oil-bath (electronic-thermometer: 90 °C; heater: 150 °C). The solution is heated for approximately 2 hours at 90 °C using an RCT basic IKAMAG® magnetic stirrer. After 2 hours the oil bath is removed and the silica is filtered in a glass filter funnel (Robu® Borosilicat 3.3 Por.-4, Robu Glasgeräte, Hattert, Germany) and washed with 60 ml of toluene and 30 ml of methanol. Finally, the silica is dried in a vacuum oven (Vacutherm, Heraeus, Hanau, Germany) at 40°C, 12 hPa for 15 hours using a porcelain-dish.

7.1.4 Polymer Modification of Monolithical Silica

Figure 98 shows the instrumental set-up for the in-column modification of the monolithical silica with polymer.

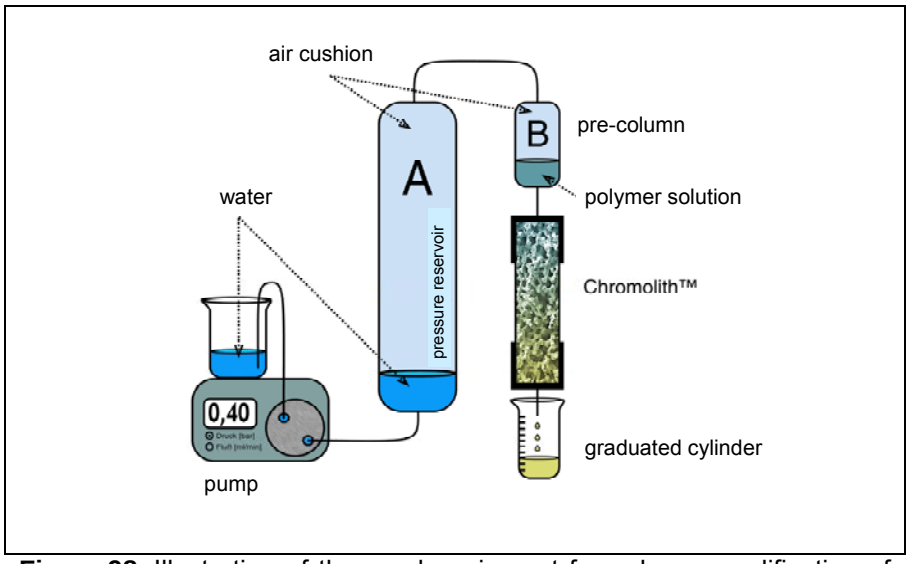

Figure 98: Illustration of the used equipment for polymer modification of CM P2HE.-E and CM PEMA.

7.2 Characterization Methods

7.2.1 Particle Size Distribution (PSD)

The mean particle size and the particle size distribution is one of the key factors of stationary phases for HPLC as it is directly related to the quality of the packing bed and the chromatographic performance. Laser diffraction allows the determination of PSD according to the Mie-theory with Fraunhofer approximation independent of the nature of the particles. A suspension of particles passes a monochromatic laser beam. While the diffraction of particles is directly related to their particle size, the particle size distribution can be deduced from the angle-resolved intensity distribution. A set of CCD-detectors is employed to scan the whole angle range of distracted light during the measurement, generating the angle-resolved intensity distribution.

Equipment

The measurements were carried out using a CILAS 1064 L (CILAS, Orléans, France) at Merck KGaA, Darmstadt, Germany. The instrument allows the determination of particle sizes between 0.04 - 500 µm. For the measurement 100 mg of sample are suspended in deionized water employing an ultrasonic bath for 5 minutes. It was checked with an optical microscope before the measurement, to ensure that the suspension is free of agglomerates, as they may clog the instrument. Then the sample was filled in the sample compartment; ultrasonic

treated for 30 s and then pumped through the sample cell with a peristaltic pump for 20 s. The data treatment was performed with the software supplied with the machine.

7.2.2 Elemental Analysis (EA)

Elemental analysis was employed for the characterization of chemically modified chromatographic silica particles, as the base silica material should only contain silica and oxygen. A catalytic burning process of sample material is employed for the quantification of carbon, nitrogen and hydrogen, which arise in the case of chromatographic silica from organic compounds of the surface coating. The emerged gases – CO_2, H_2O, NO_2 – are determined gravimetrically to quantify the proportional content of carbon, hydrogen and nitrogen as weight percentage of the overall sample mass.

The theoretical layer thickness of a polymer coating can be calculated from elemental analysis results by the following procedure: the carbon content of the polymer coating $\mathbf{C_{pol}}$ is derived by subtracting the carbon content of the pure and uncoated silica $\mathbf{C_{sil}}$ from the carbon content of the polymer-coated sample **C** as obtained as weight-% by elemental analysis:

$$C_{pol} = C - C_{pol} \quad [49]$$

Hence the mass of polymer m_{pol} can be derived by dividing this value with the carbon content as mass-% of the polymer C_{PM}:

$$m_{pol} = (C_{pol} / C_{PM}) * 10^{-2} \quad [50]$$

Dividing m_{pol} by the density d of the polymer layer gives the volume V_{pol}:

$$V_{pol} = m_{pol} / d \quad [51]$$

The surface area a_s of the silica is determined by nitrogen sorption experiments of the uncoated silica. Dividing V_{pol} with a_s gives the theoretical thickness of the polymer layer δ:

$$\delta = V_{pol} / a_s \quad [52]$$

Equipment

The measurements were carried out at the institute of organic chemistry, University of Mainz, using a CHN-rapid analyzer at 1,273 K (Fa. Heraeus, Hanau, Germany).

7.2.3 Scanning Electron Microscopy (SEM)

Scanning electron microscopy (SEM) was used to characterize the morphology of the samples. Due to the fact that silica particles are non-conductive materials, they had to be covered with a conductive coating by a sputtering process. Bal-Tec SCD 050 sputtering equipment was employed after putting the samples on a sample holder with an adhesive carbon foil. The distance between the sample holder and gold target was 5 cm. After

reaching high vacuum ($5*10^{-5}$ Torr), the sample chamber was flushed with argon and repeated 5 times. The sputtering process was then carried out in with a current of 30 mA for 70 seconds.

Equipment

The scanning electron micrographs were obtained using a Zeiss DSM 962 scanning electron microscope (Zeiss, Jena, Germany) at the institute for pathology of Johannes Gutenberg-University, Mainz.

7.2.4 Transmission Electron Microscopy (TEM)

Sample preparation

The embedding epoxy resin consisting of five components (elemental analysis via EDX: 97.0%C, 2.5%O, 0.5% Cl) was purchased from Fluka Chemie AG (Buchs, Switzerland). Copper and gold grids, both with 300 mesh, were obtained from Bal-Tec (Witten/ Ruhr, Germany). For the staining procedure $RuCl_3$ and sodium hypochloride were bought from Fluka Chemie AG (Seelze, Germany) and Merck KGaA (Darmstadt, Germany). Film material respectively. Carbon coated grids have been produced by tarnishing MICA with carbon, floating in water and subsequent transfer onto copper grids. Quantifoil consists of a polymer coating with a hole diameter of 2 µm. The polymer is composed exclusively of 93.5 % C, H and 6.1 % O with a C/O ratio of about 18.

Preparation of the modified silica particles for TEM measurements were carried out using a two step method:

- Staining the particles with RuO_4 steam for 30 min.
- Embedding in epoxy resin and subsequent ultramicrotomy cuts at room temperature into 40 nm slices.

After embedding the material in epoxy resin, 40 nm thick slices were cut using ultramicrotomy at room temperature and transferred onto copper grids coated with Quantifoil. Ultramicrotomed samples exhibited a strong charging in the electron beam. Therefore, the slices were prepared not on raw grids but on coated ones. Quantifoil in contrast to a homogeneous carbon film provides defined holes to carry out elemental analysis without underlying support material.

Equipment

Ultra thin slices were produced at the laboratory of Ute Kolb (Physical Chemistry, Johannes Gutenberg University Mainz, Germany) using a FC 4 Ultramicrotom (C. Reichert Optische Werke AG, Vienna, Austria) equipped with a 2.5-2.9° mm diamond knife (Delaware Diamond Knife, Wilmington, Canada). Transmission Electron Microscopy measurements were carried out with a Philips EM 420 at 120 kV and with a FEI Tecnai F30 ST at 300 kV (FEI,

Eindhoven) equipped with a field emission gun, a scanning unit with a high angular annular dark field detector (HAADF) and an energy dispersive x-ray spectroscope (EDX) (EDAX, Tilburg, The Netherlands) with an ultra thin polymer window and Si/Li detector. Spectra have been taken at 300 kV with a beam size of approx. 1 mm and a dispersion of 5 eV.[147]

7.2.5 Nitrogen Sorption Measurements (N_2)

Equipment

The nitrogen adsorption and desorption measurements were performed on an Autosorb-6 (Quantachrome, Odelzhausen, Germany) sorptometer. The equipment needs at least 10 m² of sample to produce reliable data. Unmodified silica was outgassed at 150 °C for 10 h and modified silica was outgassed at 40 °C for 10 h in high vacuum (0.003 Torr) to remove physically adsorbed compounds, such as water. The dead-volume of the sorptometer is automatically determined with helium at each measurement. The measurements of the isotherms were carried out at 77 K in fluid nitrogen.

7.2.6 Mercury Porosimetry

Mercury intrusion measurements were performed to determine materials with pore sizes larger than 50 nm, as nitrogen sorption measurements give unreliable results for pores above this range, as condensation of nitrogen occurs at relative pressures near $p/p_0 = 1$.

Equipment

The mercury intrusion measurements were performed on a Pascal Series Mercury Porosimeter from Carlo Erba Instruments at Merck KGaA, Darmstadt, Germany.

7.2.7 Differential Thermogravimetric Analysis (TGA/DTA)

Thermo gravimetric analysis (TGA) is the time- and temperature-resolved determination of mass loss during the heating of a sample material. Silica based materials used in chromatography exhibit only a few processes showing a mass loss, for example desorption of physisorbed water, de-hydroxylation and decomposition of silanol-groups or decomposition of un-reacted ethoxy-groups and organic porogens as residues from the synthesis procedure. Surface-modified materials show furthermore a mass-loss due to alkyl-groups from the coating in DTA experiments. Although there is an overlap of the temperature range of some of these processes, the set-up of DTA-experiments may be optimized by applying varying heating rates for special tasks like the determination of physisorbed water, the concentration of silanol -groups or the carbon-contents of modified materials.

A microbalance holds two sample holders, which are placed in a controllable heating device, each equipped with a temperature sensor. One of the sample holders is filled with the sample material and the other is left empty and used as reference. With this set-up two

different experiments can be performed. Recording the mass-loss vs. the temperature of the empty cell is the thermo-gravimetric measurement. The differential thermal analysis (DTA) is gathering information by comparison of the temperature between the empty cell and the sample-containing cell. DTA is able to track chemical reactions or changes in of the material composition as positive (exothermic) or negative (endothermic) temperature differences between the sample-containing cell and the reference cell.

The TGA/DTA-measurements were performed by heating ca. 10 mg of sample material at a heating rate of 5 or 10 K/min from room temperature up to 1.000 °C. The time-resolved mass-loss is collected with the temperature signals of the sample cell and the reference. Afterwards the mass signal and DTA-signal are normalized by subtraction with the signal of an empty sample cell and assigned to the effective temperature.

Equipment

The differential thermo gravimetric measurements were performed on a thermo gravimetric balance L81 (Fa. Linseis, Selb, Germany). A heating rate of 5 K/min or 10 K / min under air from 25 °C to 1.000 °C was chosen. Controller, evaluation and data treatment were carried out on MS-Windows-based Linseis Thermal Analysis software Version 2.18 from Fa. Linseis, Selb, Germany.

7.3 Analytical Part

7.3.1 Size Classification of Materials

In general, the synthesis of silica particles is providing materials with a broad particle size distribution. Some sort of sieving processes have to be employed for the application of these materials in chromatography, as a narrow particle size distribution is an important requirement for the production of well-packed stationary phases and the performance of the chromatographic column. As long as enough material is available, typically starting from a batch of more than 100 g of silica, the material can be classified in an air classifier. The quality of this wind-sieving process is depending on the exact knowledge of different parameters like particle size distribution, particle shape, specific weight of the sample etc. - and of the operating experience of the expert running the equipment.

Equipment

The classifying of the silica materials were carried out on an air classifier Alpine 100 Turboplex® Ultrafine Classifier (Alpine Process Technology Ltd., Cheshire, UK) at laboratory Dr. E. Hauck; Fa. Merck KGaA, Darmstadt, Germany.

7.3.2 Packing of Stainless Steel Columns

The packing of chromatographic columns is usually performed with the slurry method[147], where the stationary phase is first suspended in a suitable solvent mixture and then pumped through the chromatographic column, which is equipped with a sieve at the end with a smaller diameter than the particles.

The following procedure describes the standard packing procedure of adsorbents into stainless steel columns with a length of 125 mm and an inner diameter of 4 mm. The slurry for unmodified silica is prepared by suspending 1.6 g of the dry adsorbent in 30 ml of a solvent mixture consisting of 20 % (v) deionized water (University of Mainz, Institute of Chemistry, Germany) and 80 % (v) methanol (Fisher Scientific, UK). Polymer-coated silica is suspended in a mixture of 25 % (v) acetonitrile (Fisher Scientific, UK) and 75 % deionized water (University of Mainz, Institute of Chemistry, Germany). The suspension was stabilized using an ultrasonic bath for at least 10 min. One end of the column is closed with a frit and the other end is connected to a packing device, which was built in the laboratory of Dr. Schulte, Merck KGaA, Darmstadt, Germany. The slurry is poured into the vessel of the packing device, and additional solvent mixture is added until the vessel is full. The vessel is tightly closed with a metal cap, and the solvent is pressed through the column by using a pneumatic pump (Knauer), which is able to generate a constant pressure. When solvent starts running out of the hose connected to the packing device, there are no more bubbles inside the device, and then the hose is closed. The pressure is then increased up to 300 bar and is kept constant until approximately 100 ml of the solvent has passed the column (in general about twice the volume of the vessel). Then the pressure is reduced, the column is disconnected from the packing device, and the open end is closed by a second frit. Nylon plugs finally seal both ends of the column.

Table 86: Parameters of the employed packing procedures.

sample	**average particle diameter** [µm]	**column dimension** [mm/mm]	**slurry** ratio (v/v) in %	
LiChrospher™ Si 60	10.8	125 x 4	80:20	MeOH/H_2O
MTS1	10.4	125 x 4	80:20	MeOH/H_2O
HP Silica 30nm	8.9	125 x 4	80:20	MeOH/H_2O
MTS2	8.7	125 x 4	80:20	MeOH/H_2O
ATP107g	15.0**	125 x 4	80:20	MeOH/H_2O
C18	15.0**	125 x 4	iso-propanol	
Kromasil 300	16.0*	125 x 4	80:20	MeOH/H_2O
Nucleosil 300	10***	125 x 4	80:20	MeOH/H_2O
Nucleosil 1000	10***	125 x 4	80:20	MeOH/H_2O
ATPSV 0	15.0	125 x 4	25:75	ACN/H_2O
ATPAV 0	15.0	125 x 4	25:75	ACN/H_2O
ATPV 4	15.0	125 x 4	25:75	ACN/H_2O

[147] J.L. Fausnaugh, E. Pfannkoch, S. Gupta, F.E. Regnier, Anal.Biochem. 137 (1984) 464

ATPV 6	15.0	125 x 4	25:75	ACN/H_2O
ATPV 9	15.0	125 x 4	25:75	ACN/H_2O
ATPSH 0	15.0	125 x 4	25:75	ACN/H_2O
ATPAH 0	15.0	125 x 4	25:75	ACN/H_2O
ATPH 3	15.0	125 x 4	25:75	ACN/H_2O
ATPH 4	15.0	125 x 4	25:75	ACN/H_2O
ATPH 6	15.0	125 x 4	25:75	ACN/H_2O
ATPH 4.V	15.0	125 x 4	25:75	ACN/H_2O
ATPH 4.O	15.0	125 x 4	25:75	ACN/H_2O
ATPH 4.O1	15.0	125 x 4	25:75	ACN/H_2O
KRV 300	16.0	125 x 4	25:75	ACN/H_2O
NUV 300	10	125 x 4	25:75	ACN/H_2O
NUV 1000	10	125 x 4	25:75	ACN/H_2O

* as specified by manufacturer EKA Chemicals AB, Bohus, Sweden.

** as specified by manufacturer Merck KGaA, Darmstadt, Germany.

*** as specified by manufacturer Macherey-Nagel, Düren, Germany.

7.3.3 Assessment of the Chromatographic Performance - theoretical plate height vs. linear flow velocity

The chromatographic performance is expressed by the theoretical plate height at a given linear velocity of the mobile phase. The measurements were performed on an HP 1090 HPLC instrument (Agilent Technologies, Waldbronn, Germany) using diethyl phthalate (Fluka Chemie AG, Seelze, Germany) and dibutyl phthalate (Fluka Chemie AG, Seelze, Germany) as analytes, while toluene (ACROS, Geel, Belgium) acted as dead time marker. A mixture of n-heptane (ACROS, Geel, Belgium) and dioxane (ACROS, Geel, Belgium) was used as mobile phase for unmodified silica and a mixture of water (Fisher Scientific, UK) and acetonitrile (Fisher Scientific, UK) was employed for modified silica. The analytes, as well as the dead time marker, are prepared with a concentration of 0.33 mg/ml in the mobile phase. The adsorbents were packed into stainless steel columns of 125 mm length and an inner diameter of 4 mm. The measurements were performed by injecting 1 µl of sample at a flow rate ranging between 0.1 and 5.0 ml/min. To ensure reproducibility of the measurement, the measurements were repeated three times at a constant flow rate. Then the measurement was performed increasing the flow rate stepwise as follows: 0.1 - 0.25 - 0.5 - 1.0 - 1.5 - 2.0 - 2.5 - 3.0 - 3.5 - 4.0 – 4.5 – 5.0 ml/min. A diode array detector used was at an absorption wavelength of 254 nm. To ensure best comparability of the results, the retention coefficient k for dibutyl phthalate was adjusted to a value of ≈3 for each tested stationary phase by variation of the n-heptane/dioxane ratio respectively the water/acetonitrile ratio of the mobile phase, as listed in Table 87.

Table 87: Parameters of the employed packing procedures.

sample	column dimension [mm/mm]	mobile phase ratio (v/v) in %	
LiChrospher™ Si 60	125 x 4	92:8	n-heptane/dioxane
MTS1	125 x 4	95:5	n-heptane/dioxane
HP Silica 30nm	125 x 4	99:1	n-heptane/dioxane
MTS2	125 x 4	96:4	n-heptane/dioxane
C18-3	150 x 4.6	20:80	ACN/H_2O
C18-5	150 x 4.6	23:77	ACN/H_2O
C18-6	150 x 4.6	19:81	ACN/H_2O
C18-7	150 x 4.6	22:78	ACN/H_2O
C18-10	150 x 4.6	22:78	ACN/H_2O
ATP107g	125 x 4	97:3	n-heptane/ethyl acetat
C18	125 x 4	40:60	ACN/H_2O
ATPV 4	125 x 4	65:35	ACN/H_2O
ATPV 6	125 x 4	65:35	ACN/H_2O
ATPV 9	125 x 4	63:37	ACN/H_2O
ATPH 3	125 x 4	67:33	ACN/H_2O
ATPH 4	125 x 4	65:35	ACN/H_2O
ATPH 6	125 x 4	65:35	ACN/H_2O
ATPH 4.V	125 x 4	67:33	ACN/H_2O
ATPH 4.O	125 x 4	67:33	ACN/H_2O
KRV 300	125 x 4	65:35	ACN/H_2O
NUV 300	125 x 4	67:33	ACN/H_2O
NUV 1000	125 x 4	70:30	ACN/H_2O

7.3.4 Assessment of Calibration Curves using Polystyrene Standards in Inverse Size-Exclusion Chromatography (ISEC)

Size-exclusion chromatography in the inverse mode using polystyrene standards was performed on an HP 1090 HPLC instrument (Agilent Technologies, Waldbronn, Germany). The sample materials were packed in chromatographic columns with a length l of 125 mm and an inner diameter ID of 4.0 mm by the packing procedure described above. As mobile phase tetrahydrofuran (THF), dioxane and dimethylformamide (DMF) (Fisher Scientific, HPLC grade) was used, which was degassed under Helium stream for ca. 1 min in a 500 ml bottle connected to the instrument. After connecting the chromatographic column to the instrument it is conditioned with the mobile phase for approximately 1 hour at a flow rate of 0.2 ml/min. Polystyrene standards (PSS Polymer Standards Service GmbH, Mainz, Germany) of different molecular weight, as well as the dead-time-marker benzene (Merck, KGaA, Darmstadt), are prepared with a concentration of 1 mg/ml in THF and put in 2 ml vials, which are the placed in the autosampler of the HPLC system. The measurements were performed by injecting 1 µl sample at a flow rate f_R of 0.2 ml/min. A diode array detector at the absorption wavelength of 254 nm was employed for THF and dioxane. DMF has a strong absorption in the same range, therefore a refractive index detector (Shodex RI-71) was used instead, which was coupled to the machine using an A/D-converter HP A/D 35900E (Agilent

Technologies, Waldbronn, Germany). Each measurement is repeated three times in order to ensure best reproducibility.

An MS Excel Sheet was employed for the determination of K_{ISEC} as first step of the data evaluation and to extract the information needed for the data treatment by molecular modeling. The following values are extracted from the chromatograms.

As retention time $t_{Ri,average}$ for the particular polystyrene the average of the peak maximum of the polystyrene peak of three reruns T_{Ri1} / T_{Ri2} / T_{Ri3} for a given polystyrene sample **i** is used:

$$t_{Ri,\ average}\ [min] = (t_{R,1} + t_{R,2} + t_{R,3})/3\ [min] \quad [53]$$

Multiplication of the value with the flow rate gives the elution volume V_{Ri} of polystyrene sample i:

$$V_{Ri}\ [ml] = t_{Ri,\ average}\ [min] * f_R\ [ml/min] \quad [54]$$

The dead time t_0 of the HPLC instrument was determined as the retention time of the dead-time marker of the system without a column. Multiplying with the flow rate gives the dead volume of the machine V_{0m}:

$$V_{0m}\ [ml] = t_0\ [min] * f_R\ [ml/min] \quad [55]$$

The total column porosity V_C is determined as difference between the elution volume of the dead-time marker V_{R0} and V_{0m}:

$$V_C\ [ml] = V_{R0}\ [ml] - V_{0m}\ [ml] \quad [56]$$

The pore volume of the stationary phase V_P is the difference between V_{R0} and the elution volume of the largest polymer V_{Rmax}:

$$V_P\ [ml] = V_{R0}\ [ml] - V_{Rmax}\ [ml] \quad [57]$$

This allows the determination of the retention coefficient $K_{ISEC}(i)$ for a polystyrene i by dividing the difference between its elution volume V_{Ri} and V_{Rmax} with V_P:

$$K_{ISEC}(i) = (V_{Ri}\ [ml] - V_{Rmax}\ [ml]) / V_P\ [ml] \quad [58]$$

$K_{ISEC}(i)$ of the dead-time marker has therefore a value of 1.

The radius of gyration r_{gi} of the polymer i sample depends on the kind of polymer and the solvent and is calculated from its mean molecular weight M_{Wi} by the following equation:

$$r_{gi} = a\ M_{Wi}\ \hat{}\ b \quad [59]$$

a and b are empirical parameters and can be found[92]. In the case of polystyrenes in THF a values for a = 0.0271 and b = 0.5089 were used. This enables the plotting of the experimental size-exclusion data points, where $K_{ISEC}(i)$ is plotted against r_{gi} of all polymers.

The theoretical size-exclusion curve is based on the pore size distribution curve, which is generated by further data treatment employing specialized software solutions. A limited number of experimental data was treated with a self-developed modeling program by B. A. Grimes, which is based on a pore network model giving values for the pore size distribution and pore connectivity n_T. This method is based on a large number of computer-generated Monte-Carlo simulations of the pore system, where the "best-guess" is taken as result and therefore uses a large amount of computation time. The other experiments were analyzed by commercial software PSS Porocheck 1.0 (Polymer Standards Service, Mainz, Germany) based on a parallel pore model, generating values for pore size distribution only.

The following table gives the specific data of the employed polystyrenes.

Table 88: Polydispersities of Polystyrenes from Polymer Standards Service, Mainz, Germany.

M_p	M_w	M_n	**PDI** (M_w/ M_n)
162	162	162	1.00
266	266	266	1.00
370	370	370	1.00
376	484	435	1.11
890	972	869	1.12
1,620	1,560	1,500	1.06
2,280	2,250	2,140	1.05
3,420	3,470	3,280	1.06
5,440	5,610	5,270	1.06
8,400	8,100	7,800	1.05
10,400	10,300	10,000	1.03
18,100	17,900	17,300	1.03
34,800	34,000	32,700	1.04
67,500	65,000	64,000	1.02
130,000	125,000	120,000	1.04
246,000	226,000	214,000	1.06
579,000	564,000	545,000	1.03
1,090,000	1,070,000	1,010,000	1.06
2,570,000	2,530,000	2,420,000	1.04
4,307,000	5,423,000	3,810,000	1.42
10,100,000	11,100,000	9,250,000	1.20
24,800,000	23,300,000	17,900,000	1.30

M_p is the molecular mass associated with the peak, M_w and M_n are the mass-average and number-average molecular masses. PDI is the polydispersity value. Data supplied by producer.

7.3.5 Biorecovery

The overall biorecovery of proteins on the reversed phase HPLC system was determined by comparing the total peak areas generated by a mixture of three proteins using either the polymer-coated columns or no column at all. The test mixture contained the proteins lysozyme from chicken egg white, cytochrome C from bovine heart and myoglobin from horse heart at a total concentration of 1 mg/ml. 5 µl of the mixture diluted by a factor of 10 were injected and pumped through the tubing and detector, using 5 % acetonitrile (0.1 % TFA) in water (0.09 % TFA) approximating the reversed phase elution conditions. The area of the resulting single peak multiplied by a factor of ten was compared to the total peak area of the non-diluted separated mixture. The peak area was calculated as the sum over all single peak areas determined by manual integration.[35]

7.3.6 Relative Enzymatic Activity Test

The impact of the contact of an enzyme with a stationary phase upon its biological activity can be used to monitor the denaturation potential of a stationary phase. This is performed by comparing the enzymatic activity of an ADH-sample which was applied to the stationary phase in a chromatographic run with built-in column with the activity of an ADH-sample which was exposed to just the stress of the chromatographic equipment. As the measurement was carried out to compare the denaturation potential of different stationary phases packed in columns with the same dimension, it is sufficient to determine the relative enzymatic activity by using the activity of the ADH-sample of the empty machine as 100 %-value.

Before the measurement, appropriate conditions for the ADH-catalyzed formation of NADH have to be defined, as the enzymatic activity of the employed ADH may vary to a large extend depending on the source. A solution of 2 mg/ml ADH in 0.1 M Tris-HCl (pH = 8.8) was prepared. A disposable cuvette was filled with 1 ml of a solution of NAD+ in ethanol and then 10 µl of the ADH-solution was added and stirred with a spatula in a reproducible manner. The ADH-catalyzed reaction of NAD+ to NADH was then followed by the absorption of NADH at 366 nm at a temperature of 25 °C in the photometer for 5 minutes. A sufficient linearity of the absorption curve is obtained, if the confidence coefficient R^2 by linear regression is higher than 0.9. In most cases, the amount of ADH-solution has to be reduced until this condition is reached. This procedure has to be repeated for every measurement series, as the enzymatic activity of the ADH is decreasing by aging procedures. This amount is then used as injection volume for the HPLC-treatment. The sample collection time of the ADH-solution in the HPLC experiment was determined from the DAD-online signal at a wavelength of 215 nm.

The determination of the enzymatic activity was then performed by injecting the appropriate amount of ADH-solution into the HPLC-instrument without a column at a flowrate of 1 ml/min and 700 µl of sample was collected (0.0 - 0.7 min) behind the detector cell into a cuvette. Then 300 µl of NAD+-solution in ethanol were added, stirred with a clean spatula and placed into the photometer where the reaction was followed for 5 minutes at a wavelength of 366 nm. The slope of the absorption curve by linear regression is the reference value R or the 100 %-value for the relative enzymatic activity.

Performing the similar experiment with built-in chromatographic column gives the value for the enzymatic activity of ADH after close contact with the stationary phase. In this case, 700 µl of sample material was collected from 0.1 - 0.8 minutes. The relative enzymatic activity EA_{rel} is then derived by dividing the slope of the absorption curve of the stationary phase S by R in percentage:

$$EA_{rel} = S/R * 100\ \% \qquad [60]$$

Equipment

The measurements were carried out at the institute of inorganic chemistry, University of Mainz, using an HP 1090 HPLC instrument (Agilent Technologies, Waldbronn, Germany) and a Beckmann DU 70 Spectrophotometer (Beckmann Fullerton, CA, USA).

Table 89:

HPLC conditions
analyte: ADH; mobile phase: 0.1 M Tris-HCL, pH= 8.8
concentration: 2mg/ml; injection volume: 6 µl
flow rate: 1 ml/min
Collection of Samples
empty column from 0.0-0.7 min = 700 µl
test column from 0.3-1.0 min = 700 µl
Photometer conditions
Temperature: 25 °C
Wavelength: 366 nm; Absorption
Measuring time: 5 min

7.3.7 Adsorption Isotherm

Mass loadability of stationary phases was determined from the adsorption isotherm for lysozyme by frontal analysis employing the stair-case method. The measurements are performed on an HP 1090 HPLC instrument (Agilent Technologies, Waldbronn, Germany) in packed columns with a length l of 125 mm and an inner diameter ID of 4.0 mm, which were packed with sample material by the packing procedure as described above. The diode array detector was set up to track the absorption at wavelengths of 215 nm 300 nm. The absorption at 215 nm is more sensitive and reaches the upper detection limit at a concentration of ca. 10 g/l lysozyme, while the absorption at the less sensitive wavelength of 300 nm was used to track concentration changes at higher concentrations.

Prior to the measurement, the dead volume of the instrument V_{0m}, the total column porosity V_C and the porosity of the stationary phase V_P is determined, as described and performed in size-exclusion experiments. The value for the porosity of the stationary phase was derived from the retention volume of the polymer with M_w = 10,300 D as it shows the same molecular radius as lysozyme. The solvent reservoir of pump A was filled with a solution of 0.01 M KH_2PO_4 (pH 3) in water (HPLC-grade, Merck KGaA, Darmstadt, Germany). The solvent reservoir of pump B was filled with a filtrated solution (SPARTAN 30/0,45 RC Braunrand H; Schleicher & Schuell, Dassel, Germany) of 20 g/l lysozyme from chicken egg white in 0.01 M KH_2PO_4 (pH 3) solution in water. The column is conditioned for 15 minutes with pure solvent A at a flow rate f_R of 1.0 ml/min, which was kept constant for the whole chromatographic run. The measurement starts with switching the mobile phase composition from 0 % B to the first concentration step with 5 % B respectively $c_{lysozyme}$ 1 g/l lysozyme in the mobile phase or switching time t_s = 0. The switch to the next concentration step is performed, when the detector shows that the first plateau is reached, which was typically reached after 5 minutes. Table 90 shows the switching times and the concentration of lysozyme:

Table 90: Switching times and the concentration of lysozyme of the investigated materials.

sample	concentration $c_{lysozyme}$ [mg/ml]					switching time t_s [min]				
C18	1	2.5	5	-	-	0	13	17	-	-
ATPV 6	1	2.5	5	10	18	0	10	17	24	30
ATPV 9	1	2.5	5	10	19	0	6	10	15	20
ATPH 3	1	2.5	5	10	20	0	10	17	23	30
ATPH 4.V	1	6	10	15	20	0	22	30	37	43
ATPH 4.O	1	6	10	15	20	0	22	30	37	43

The adsorption isotherm was generated from the experimental data employing a Microsoft Excel Sheet. From the chromatogram, the inflection points of the "steps" were determined and used as breakthrough-time t_D. Switching time t_S plus dead time of the instrument t_0 and

the dead volume of the column t_C gives the expected value for a non-adsorbing stationary phase t_E. The difference between t_E and t_D gives the extra-volume till breakthrough V_E:

$$V_E\ [ml] = (t_D\ [min] - t_E\ [min])*f_R\ [ml/min] \quad [61]$$

This allows the determination of the amount dq_i adsorbed in this step i with the concentration c_i:

$$dq_i\ [mg] = V_E\ [ml] *c_i\ [mg/ml] \quad [62]$$

As the stationary phase has already adsorbed from the concentration step before dq_{i-1}, the total amount adsorbed q_i is given as the sum of dq_{i-1} and dq_i:

$$q_i\ [mg] = dq_{i-1}\ [mg] + dq_i\ [mg] \quad [63]$$

Division of q_i by the volume of the stationary phase V_p gives finally the reduced amount adsorbed q_i*, also referred to as capacity of the stationary phase at the concentration i:

$$q_i^*\ [mg/ml] = q_i\ [mg] / V_P\ [ml] \quad [64]$$

This allows the plotting of the experimental adsorption isotherm as q_i* vs. c_i. Data treatment was performed as first approximation by linear regression to check if for the linearity of the adsorption curve. If the stationary phase show a confidence coefficient R^2 by linear regression higher than 0.95, no further data treatment has to be performed as the curve can considered to be in the linear range. If R^2 is below 0.95 non-linear regression according to the Langmuir adsorption models has to be performed, which was not necessary for all of the investigated polymer-coated stationary phases.

7.4 List of chemicals

Mobile Phase:

acetonitrile, 99.9%, HPLC grade	Fisher Scientific, UK
dimethylformamide, 99.9%, HPLC grade	Fisher Scientific, UK
dioxane, 99.9%, HPLC grade	ACROS, Geel, Belgium
ethyl acetate, 99.9%, HPLC grade	ACROS, Geel, Belgium
iso-propanol, 99.9%, HPLC grade	ACROS, Geel, Belgium
methanol, 99.9%, HPLC grade	Merck KGaA, Darmstadt, Germany
n-heptane, 99.9%, HPLC grade	ACROS, Geel, Belgium
tetrahydrofuran, 99.9%, HPLC grade	Fisher Scientific, UK
toluene, 99.9%, HPLC grade	ACROS, Geel, Belgium
water, HPLC grade	Merck KGaA, Darmstadt, Germany
	Fisher Scientific, UK
di-potassiumhydrogenphosphate	Fluka Chemie AG, Seelze, Germany

Synthesis:

ammonia, 25%	Merck KGaA, Darmstadt, Germany
α-picolin	Fluka Chemie AG, Seelze, Germany
4,4'-Azobis(4-cyanopentanoic acid)	Fluka Chemie AG, Seelze, Germany
cyclohexane, 99%	Merck KGaA, Darmstadt, Germany
dimethylformamide, 99%	Merck KGaA, Darmstadt, Germany
ethanol	Merck KGaA, Darmstadt, Germany
etyl methacrylate acid	Merck KGaA, Darmstadt, Germany
ethylenglycol dimethacrylate	Merck KGaA, Darmstadt, Germany
hydrochloric acid, 37%	Fisher Scientific, UK
2-hydroxy-ethylmethacrylate acid	Merck KGaA, Darmstadt, Germany
iso-propanol, p.a.	Merck KGaA, Darmstadt, Germany
methanol, p.a.	Merck KGaA, Darmstadt, Germany
	Fisher Scientific, UK
octadecylmethacrylate-methylmethacrylate-copolymer	Merck KGaA, Darmstadt, Germany
PES	Merck KGaA, Darmstadt, Germany
p-(chloromethyl)phenyltrimethoxysilane	ABCR, Karlsruhe, Germany
Sodiumhypochloride	Merck KGaA, Darmstadt, Germany

	Fluka Chemie AG, Seelze, Germany
TES 40	Merck KGaA, Darmstadt, Germany
tetrahydrofuran, p.a.	ACROS, Geel, Belgium
titrisol	Merck KGaA, Darmstadt, Germany
toluene, p.a.	ACROS, Geel, Belgium
water, deionized	University of Mainz, Germany

Probe Molecules:

alcoholdehydrogenase	Fluka Chemie AG, Seelze, Germany
benzene	Merck KGaA, Darmstadt, Germany
cytochrome C, from bovine heart	Fluka Chemie AG, Seelze, Germany
dibutyl phthalate	Fluka Chemie AG, Seelze, Germany
diethyl phthalate	Fluka Chemie AG, Seelze, Germany
lysozyme, from chicken egg white	Fluka Chemie AG, Seelze, Germany
myoglobin, horse heart	Fluka Chemie AG, Seelze, Germany
polystyrene standards	PSS Standards, Mainz, Germany
toluene	Merck KGaA, Darmstadt, Germany
trifluoroacidicacid	Merck KGaA, Darmstadt, Germany
uracil	ACROS, Geel, Belgium

7.5 List of figures

7.6 List of tables

7.7 List of Abbreviations and Symbols

A	Eddy diffusion in the Knox equation
ADH	alcohol dehydrogenase
AngI	angiotensin I
AngII	angiotensin II
a_s	specific surface area according to BET
B	molecular diffusion in the Knox equation
BET	Brunauer-Emmett-Teller theory for specific surface area determination from nitrogen sorption data
BJH	Barrett-Joyner-Halenda method for deriving mean pore size distribution from nitrogen sorption data
C	mass transfer resistance in the Knox equation
CCD	Charge Coupled Device
CTAB	cetyltrimethylammonium bromide
C18	n-octadecyl bonded silica phase
DMF	dimethyl formamide
DOE	design of experiments
d_p	average particle diameter
DTA	differential thermo analysis
EA	elemental analysis
ECP	elution by a characteristic point
EDMA	ethylene glycol dimethacrylate
EDX	Energy Dispersive X-ray Spectroscopy
EMA	ethyl methacrylate acid
G	Gurwitsch method to receive specific pore volume from nitrogen sorption data
GPC	gel permeation chromatography
H	theoretical plate height referring to one probe molecule
HETP	the height equivalent of a theoretical plate H
HPLC	high performance liquid chromatography
2-HEMA	2-hydroxy ethyl methacrylate acid
ISEC	inverse size-exclusion chromatography
K_{SEC}	exclusion coefficient
LCM	lysozyme, cytochrome C, myoglobin test-mixture
MAC	maximum acceptable concentration
MCM	mobile composition of matter

MeOH	methanol
MTS	Micelle-Templated Silicas
Mw	molecular weight
M41S	The family of mesoporous materials introduced by Mobil Oil.
N	Avocadro number
nm	nano meter; 1nm = 10Å
NP	normal phase
n_T	pore connectivity
OMA	octadecylmethacrylate-methylmethacrylate-comonomer
p	pressure
p_d	average pore size distribution according to BJH
PEEK	polyetheretherketones
PES	polyethoxysiloxane
PNM	Pore Network Model
PPM	Parallel Pore Model
PSD	particle size distribution
PSD	particle size distribution
q_{max}	maximum loading capacity
r_g	radius of gyration
r_K	Kelvin radius
RP	reversed phase
RT	room temperature
R^2	coefficient of determination
SEM	scaning electron microscopy
STEM	transmission electron microscopy in scaning mode
TEM	transmission electron microscopy
TES	tetraethoxysiloxane
TEOS	tetraethyl orthosilicate
TGA	thermogravimetric analysis
THF	tetrahydrofuran
Tris	tris(hydroxymethyl)aminomethane
t_m	dead-time
TMB	1,3,5-trimethyl benzene
t_R	retention-time
u	linear flow velocity
v_p	specific pore volume according to Gurwitsch